PLATELETS AND AGING IN CORONARY ARTERY DISEASE IN MICE

INVESTIGATING THE POTENTIAL EFFECTS OF PLATELET INHIBITION AND AGING ON CORONARY ARTERY DISEASE DEVELOPMENT IN MICE.

By SAMUEL KWANGHO LEE, BMSc (Honours), MSc

A Thesis Submitted to the School of Graduate Studies in Partial Fulfillment of the Requirements for the Degree Doctor of Philosophy.

McMaster University

McMaster University DOCTOR OF PHILOSOPHY (2022) Hamilton, Ontario

(Biochemistry and Biomedical Sciences)

TITLE:	INVESTIGATING THE POTENTIAL EFFECTS OF PLATELET INHIBITION AND AGING ON CORONARY ARTERY DISEASE DEVELOPMENT IN MICE.
AUTHOR:	Samuel Kwangho Lee, BMSc (Honors), MSc
SUPERVISOR:	Dr. Bernardo Trigatti
NUMBER OF PAGES:	xvi, 270

Abstract

Coronary artery disease (CAD) is one of the leading causes of mortality worldwide, and is driven by atherosclerosis development that can lead to occlusive thrombus formation and myocardial infarction. Platelets are known to contribute to atherosclerosis development and thrombosis. Scavenger receptor class B type 1 (SR-B1) deficiency in apolipoprotein E (ApoE) knockout or low-density lipoprotein receptor (LDLR) knockout mice results in occlusive coronary artery atherosclerosis, platelet accumulation in atherosclerotic coronary arteries, and myocardial fibrosis.

In this thesis, we examine the effects of genetically inactivating neurobeachin-like 2 (NBEAL2), which has a prominent role in platelet function, on CAD development in SR-B1/ApoE double knockout mice. NBEAL2 deficiency in SR-B1/ApoE double knockout mice reduced aortic sinus and coronary artery atherosclerosis and platelet accumulation in atherosclerotic coronary arteries, but increased myocardial fibrosis levels and reduced survival. NBEAL2 deficiency in SR-B1/ApoE double knockout mice reduced neutrophil granularity and the proportion of myeloperoxidase-positive neutrophils in the myocardium, which may in part contribute to the increased myocardial fibrosis levels.

Protease-activated receptor 4 (PAR4) also has a prominent role in platelet function. By using a novel pepducin (RAG8), we examine the effects of pharmacological inhibition of PAR4 on CAD development in high-fat, high-cholesterol, cholate (HFCC) diet-fed SR-B1/LDLR double knockout mice. RAG8 treatment did not alter aortic sinus atherosclerosis levels, but reduced coronary

artery atherosclerosis, platelet accumulation in atherosclerotic coronary arteries, and myocardial fibrosis. These protective effects are not dependent on changes in circulating lipids, cytokines, and immune cells, but may be due to reduced vascular cell adhesion 1 (VCAM-1) protein expression in coronary arteries.

We also examine the effects of aging on CAD development in HFCC diet-fed SR-B1 single KO mice. Older age in SR-B1 single KO mice did not alter susceptibility to HFCC diet-induced aortic sinus atherosclerosis, but increased susceptibility to HFCC diet-induced coronary artery atherosclerosis, platelet accumulation in atherosclerotic coronary arteries, and myocardial fibrosis. Older-aged SR-B1 KO mice exhibited reduced survival when fed the HFCC diet. These age-dependent changes are not driven by changes in plasma lipids, but likely driven by a combination of increased VCAM-1 protein levels in coronary arteries and circulating cytokines and neutrophils.

This thesis demonstrates the potential effects of platelet inhibition and aging on CAD development in mice, and demonstrates that SR-B1 single KO mice may be a versatile and useful diet-inducible mouse model for atherosclerosis studies. Moreover, this thesis highlights the importance of analyzing atherosclerosis at multiple sites and utilizing mice that develop CAD and myocardial fibrosis when investigating the effects of interventions on atherosclerosis and/or CAD development.

Acknowledgements

The work presented in this thesis and the progress I made as a researcher would not have been possible without the support and guidance from my supervisor, Dr. Bernardo (Dino) Trigatti. Dino was very patient and understanding throughout my PhD studies, and continuously challenged me to become a better researcher and science communicator. His tremendous work ethic, knowledge, and care has led me to where I am today, and I would not have been able to complete this thesis without him. I will surely take many of the skills I have learned under his supervision and apply them to the next chapters of my life. I would also like to give a big thanks to my supervisory committee, Dr. Peter Gross and Dr. Ishac Nazy, for all of their wisdom, insight, and constructive feedback during my PhD studies. This thesis would certainly not have been possible without all of their help and guidance. Moreover, I would like to thank my collaborators, Dr. Walter Kahr (Toronto SickKids Research Institute) and Dr. Rithwik Ramachandran (Western University), for their contributions to the work presented in this thesis.

During the past 5 years of my PhD, I have been tremendously lucky to work in such a dynamic lab environment filled with many unbelievable former and current colleagues (too many to name). I am extremely thankful for all of the help and support I have received from various people in the lab, and for all of the fun moments we had throughout the years. A big thank you to everyone else at TaARI that have made the last 5 years unforgettable. Thank you to all of my friends outside of the lab who have been there for me the last 5 years. Despite much of

the last 5 years being occupied with my PhD work, I have been able to spend a lot of quality time with you all, which kept me refreshed and provided much needed breaks.

I would also like to give a big thanks to my family, especially my parents. Their constant love and support and all of the sacrifices they have made for me have shaped me to be who I am today, and I would not be where I am without them. Last, but not least, I would like to give unending thanks to my wife, Lydia. You have been there for me from day 1 of my PhD studies, and I am extremely grateful for all of the love and support you have given me, especially during the stressful times. Thank you for all of the times you have cooked delicious meals for me (and still do), otherwise I would have likely been quite unhealthy and perhaps on track to developing coronary artery disease. Thank you for always challenging me to become a better person and keeping me grounded during the difficult times. You have been an unending source of love and support, and this journey would be non-existent without you.

I am extremely blessed and grateful to have been surrounded by so many loving and supporting people, and none of the success I have achieved would have been possible without them. I am excited for the next chapter of my life, and looking forward to all of the happiness and hardships that will come along the way. Thank you to everyone who has been on this journey with me, and for those who will continue to be on the journey with me ahead!

- Sam -

Table of Contents

List of Figures and Tables

List of Abbreviations

ABCA1	ATP-binding cassette A1
ABCG1	ATP-binding cassette G1
ADP	adenosine diphosphate
ApoE	apolipoprotein E
ARC	arthrogryposis, renal dysfunction and cholestasis
ARM	armadillo-like
BEACH	beige and Chediak-Higashi
CAD	coronary artery disease
CCL	c-c chemokine ligand
CCR	c-c chemokine receptor
CD	cluster of differentiation
CD40L	cluster of differentiation 40 ligand
CE	cholesterol ester
ConA	concanavalin-A
CK-MB	creatine kinase myocardial band
CXCL12	c-x-c motif chemokine ligand 12
CX3CR1	CX3C chemokine receptor 1
D4D	domain 4-deficient
eNOS	endothelial nitric oxide synthase
GAPDH	glyceraldehyde 3-phosphate dehydrogenase
GP	glycoprotein

GPCR	G-protein-coupled receptor
GPS	gray platelet syndrome
HDL	high-density lipoprotein
HFCC	high-fat, high-cholesterol, cholate
HMG-CoAR	3-hydroxy-3-methyl-glutaryl-coenzyme A reductase
ICAM-1	intercellular adhesion molecule 1
IL	interleukin
IR	ischemia-reperfusion
LAD	left anterior descending
LDL	low-density lipoprotein
LDLR	low-density lipoprotein receptor
Ly6C	lymphocyte antigen 6 complex locus C
Ly6G	lymphocyte antigen 6 complex locus G
MAPK	mitogen-activated protein kinase
MCP-1	monocyte chemoattractant protein 1
MPO	myeloperoxidase
NBEAL1	neurobeachin-like 1
NBEAL2	neurobeachin-like 2
NETs	neutrophil extracellular traps
NK	natural killer
oxLDL	oxidized low-density lipoprotein
PAR	protease-activated receptor

PCSK9	proprotein convertase subtilisin/kexin type 9
PDGF	platelet-derived growth factor
PF4	platelet factor 4
PH	pleckstrin homology
PI3K	phosphatidylinositol-3-kinase
PKC	protein kinase C
PLA_2	phospholipase A_2
PLCβ	phospholipase C beta
PSGL-1	p-selectin glycoprotein ligand-1
RCT	reverse cholesterol transport
ROS	reactive oxygen species
SR-B1	scavenger receptor class B type 1
SREBP2	sterol regulatory element-binding protein 2
TF	tissue factor
TGF-β1	transforming growth factor beta 1
TNFα	tumour necrosis factor alpha
TSP-1	thrombospondin-1
TXA_2	thromboxane A_2
VCAM-1	vascular cell adhesion molecule 1
VEGF	vascular endothelial growth factor
VLDL	very-low-density lipoprotein
vWF	von Willebrand factor

Chapter 1: General Introduction

1.1 Coronary Artery Disease

Coronary artery disease (CAD) is the most common type of cardiovascular disease and is one of the leading causes of mortality worldwide, accounting for more than 9 million deaths annually (Tryfonos et al., 2019). Major risk factors of CAD development include smoking, diabetes mellitus, hypertension, and hypercholesterolemia (Hajar, 2017). An important independent risk factor of CAD is aging, as the risk of developing CAD and associated mortality increases significantly with older age. In particular, older age (especially over 65 years of age) is associated with increased chronic systemic inflammation, altered hematopoiesis (the formation and production of blood cellular components), loss of arterial elasticity resulting in increased arterial stiffness and subsequent hypertension, and increased expression of pro-inflammatory molecules on vessels (Head et al., 2017; Tyrrell & Goldstein, 2021; Wang & Bennett, 2012). Together, these altered processes can increase the susceptibility and/or progression of CAD development. CAD is characterized by the build-up of cholesterol-rich plaques in the walls of coronary arteries in a process called atherosclerosis, and plaque disruption can result in the formation of an occlusive thrombus and myocardial infarction that can be fatal (Tabas et al., 2015). Since atherosclerosis is a major underlying cause of cardiovascular diseases, many efforts have been focused on understanding the mechanisms associated with atherosclerosis development in order to treat and/or prevent cardiovascular disease.

1.2 Atherosclerosis Overview

1.2.1 Atherosclerosis Initiation

Atherosclerosis is a complex disease characterized by the build up of plaque (consisting primarily of cholesterol-laden, macrophage-derived foam cells, smooth muscle cells, and other inflammatory cells) in artery walls that are driven by many different factors (Hansson & Hermansson, 2011). Endothelial cell dysfunction/activation is an important initiating factor for atherosclerosis development (Davignon & Ganz, 2004; Weber et al., 2008), which preferentially occurs at arterial regions where endothelial cells experience non-laminar blood flow and low shear stress (Chatzizisis et al., 2007). In these regions, endothelial cells are more prone to activation and also experience increased permeability to atherogenic low-density lipoprotein (LDL) particles that become retained and accumulate in the sub-endothelial space (Armstrong et al., 2015; Chatzizisis et al., 2007; Huang et al., 2019). The LDL particles get oxidized in the artery wall by reactive oxygen species (ROS), resulting in oxidized (ox) LDL (oxLDL) particles that stimulate endothelial cells to secrete pro-inflammatory mediators and induce the expression of cell surface adhesion molecules (Fatkhullina et al., 2016; Lusis, 2000; Madamanchi et al., 2005). Upon endothelial cell activation, P- and E-selectins are highly expressed at the cell surface and mediate the initial tethering and rolling of monocytes on the endothelium (Galkina & Ley, 2007). Firm adhesion and trans-endothelial migration of monocytes are mediated by endothelial integrins such as intercellular adhesion molecule 1 (ICAM-1) and vascular cell adhesion

molecule 1 (VCAM-1) (Galkina & Ley, 2007). In the sub-endothelial space, monocytes differentiate into macrophages and phagocytose oxLDL, resulting in the formation of cholesterol-engorged macrophage foam cells (Fatkhullina et al., 2016; Kzhyshkowska et al., 2012; Lusis, 2000; Madamanchi et al., 2005). Accumulation of foam cells results in a fatty streak, and a fatty streak is a hallmark of early stage atherosclerosis and the earliest visible lesion (Crowther, 2005).

1.2.2 The Role of Platelets in the Early Stages of Atherosclerosis

The role of platelets in atherosclerosis development in mice has been demonstrated. In one study, Massberg and colleagues showed via intravital microscopy that platelets adhered to the carotid artery endothelium in apolipoprotein E (ApoE) knockout (KO) mice (an athero-susceptible mouse model) prior to atherosclerosis development (Massberg et al., 2002). They also observed that platelet adhesion to the endothelium preceded leukocyte infiltration into plaques, and blocking platelet adhesion in ApoE KO mice reduced atherosclerosis in the aortic sinus and proximal coronary arteries (Massberg et al., 2002). A different study found that injecting activated platelets, but not P-selectin-deficient activated platelets or resting platelets, in ApoE KO mice increased leukocyte adhesion on the endothelium of carotid arteries and significantly increased lesion size in the aorta (Huo et al., 2003).

Platelets do not adhere to the vascular endothelial wall under normal, physiological conditions, but adhere to activated endothelium in a multi-step

process (Bakogiannis et al., 2019; Gawaz et al., 2005). The initial contact between platelets and the activated endothelium is mainly mediated by endothelial P-selectins that bind to the platelet glycoprotein (GP) Ib-V-IX (GPIb-V-IX; also called GPIbα) receptor (Gawaz et al., 2005). Von Willebrand factor (vWF) secreted from activated endothelial cells mediates platelet adhesion by binding to platelet GPIbα receptors (Denorme et al., 2019). Adhered platelets become activated and release a variety of pro-inflammatory cytokines and chemokines such as interleukin 1 beta (IL-1β), platelet factor 4 (PF4), c-c chemokine ligand 5 (CCL5), and C-X-C motif chemokine 12 (CXCL12) that promote the attraction, adhesion, and trans-migration of monocytes into the artery wall (Gawaz et al., 2005). Additionally, activated platelets express CD40 ligand (CD40L) that bind to endothelial CD40, resulting in the release of monocyte chemoattractant protein 1 (MCP-1) from endothelial cells to further attract circulating monocytes (Henn et al., 1998). Furthermore, platelet-derived CD40L has been shown to enhance the expression of endothelial cell adhesion receptors such as E-selectin, VCAM-1, and ICAM-1 *in vitro*, all of which mediate the attachment of leukocytes to the artery wall (Henn et al., 1998). Firm platelet adhesion to the endothelium is mediated by activated platelet receptor $\alpha_{IIb}\beta_3$ in a bridging mechanism involving platelet-bound fibrinogen and endothelial receptors $\alpha_v\beta_3$ and ICAM-1 (Bombeli et al., 1998; Gawaz et al., 1997). Firmly adhered platelets function as a bridge between monocytes and endothelial cells through the interactions between platelet P-selectin and monocyte PSGL-1, as well as platelet GPIbα and monocyte Mac-1, ultimately assisting in transmigration of

monocytes into the artery wall which potentiates atherosclerosis development (Huilcaman et al., 2022). A schematic of the role of platelets in the early stages of atherosclerosis is shown in Figure 1.1.

Figure 1.1 – Role of Platelets in the Early Stages of Atherosclerosis.

A. Activated endothelial cells express a variety of molecules involved in adhesion such as P-selectin, CD40, ICAM-1, $\alpha_V\beta_3$, and vWF. Initial platelet-endothelial cell adhesion is mediated by endothelial P-selectins that interact with platelet GPIbα receptors. When platelets adhere to the endothelium, they become activated and release fibrinogen, as well as a variety of pro-inflammatory cytokines and chemokines that further activate endothelial cells to release pro-inflammatory mediators. CD40L on activated platelets also interact with CD40 on endothelial cells and exacerbate inflammation. Firm platelet-endothelial cell adhesion is mediated by interactions between endothelial $\alpha_V\beta_3$ and ICAM-1 with activated platelet $\alpha_{IIb}\beta_3$, bridged by fibrinogen. **B.** Cytokines and chemokines released from adhered and activated platelets attract circulating monocytes. Platelets then act as a bridge between monocytes and endothelial cells through platelet GPIbα-monocyte Mac-1 and platelet P-selectin-monocyte PSGL-1 interactions, which promotes the migration of monocytes into the artery wall. The figure was created using BioRender.

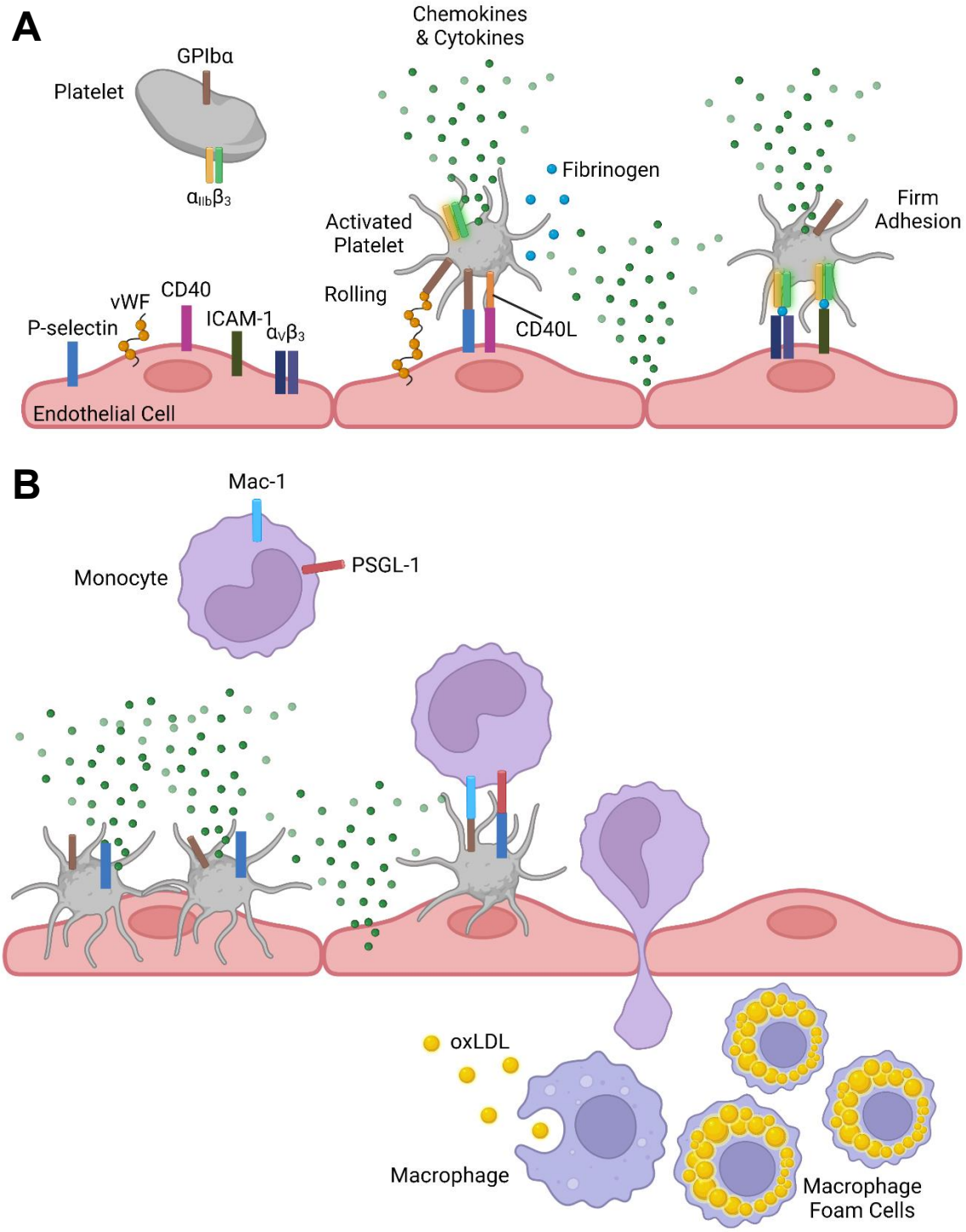
A
Chemokines
& Cytokines
GPIbα
Platelet
αIIbβ3
Fibrinogen
Activated
Platelet
Firm
Adhesion
Rolling
CD40L
vWF
CD40
ICAM-1
αvβ3
P-selectin
Endothelial Cell
B
Mac-1
Monocyte
PSGL-1
oxLDL
Macrophage
Macrophage
Foam Cells

1.2.3 Atherosclerosis Progression

The processes contributing to the initiation of atherosclerotic plaque formation (endothelial cell activation, monocyte recruitment, LDL oxidation, platelet adhesion and activation) continue throughout plaque development and contribute to atherosclerotic plaque progression. In addition, macrophages in the artery wall secrete pro-inflammatory cytokines and chemokines that further attract circulating leukocytes and amplify the inflammatory response in the lesion (Hansson & Libby, 2006; Tabas, 2010). Neutrophils also enter into the artery wall and release granule components such as myeloperoxidase (MPO) that oxidize LDL and enhance foam cell formation (Soehnlein, 2012). Macrophage foam cells undergo apoptosis due to cholesterol overload, and the resulting debris is efficiently cleared by macrophages present in the plaque in a process called efferocytosis (Tabas, 2010). In advanced plaques, efferocytosis becomes impaired, resulting in the accumulation of cell debris and lipids, causing the formation of a lipid-rich necrotic core (Tabas, 2010). Smooth muscle cells also proliferate and migrate from the tunica media to the sub-endothelium, and secrete extracellular matrix proteins such as collagen and elastin fibers, forming a fibrous cap on top of the developing plaque which keeps the atherosclerotic lesion stable (Libby, 2002; Libby et al., 2011).

1.2.4 Plaque Disruption

In advanced plaques, a variety of processes such as inhibition of collagen production by smooth muscle cells, smooth muscle cell death, and secretion of

matrix metalloproteinases by macrophages results in the degradation of the fibrous cap and plaque rupture (Bennett et al., 2016; Libby, 2002). Less commonly, plaques rich in smooth muscle cells and extracellular matrix but lacking a large, lipid-filled necrotic core may undergo plaque erosion (Luo et al., 2021). In ruptured plaques, the local endothelial cells exist but are dysfunctional, whereas in eroded plaques, the local endothelial cells are absent due to apoptosis (Luo et al., 2021). It is also postulated that neutrophils contribute to plaque destabilization by releasing matrix-degrading proteases and large amounts of ROS (Soehnlein, 2012). Both plaque rupture and erosion expose highly pro-thrombotic substances to the flowing bloodstream, which lead to the formation of a thrombus on top of the exposed lesion (Libby, 2009). A schematic of atherosclerotic plaque development in an artery wall is shown in Figure 1.2.

Figure 1.2 – Atherosclerotic Plaque Development.

In regions of endothelial cell dysfunction and/or activation, there is increased permeability to LDL particles that become retained in the sub-endothelial space, and platelets adhere to activated endothelium and release a plethora of pro-inflammatory cytokines and chemokines (1). The LDL particles in the artery wall become oxidized into oxLDL by ROS and also by MPO released from neutrophils, which stimulate endothelial cells to secrete pro-inflammatory cytokines and chemokines and induce the expression of adhesion molecules on the endothelial cell surface. This results in the recruitment, attachment, and migration of circulating monocytes into the artery wall which differentiate into macrophages (2). The macrophages secrete pro-inflammatory cytokines and chemokines to attract more monocytes and amplify inflammation, and phagocytose the oxLDL particles to become macrophage foam cells (3). Eventually, the macrophage foam cells undergo apoptosis, and defective efferocytosis results in the formation of a lipid-rich necrotic core (4). As the lesion progresses, smooth muscle cells are stimulated to proliferate and migrate to the sub-endothelium and secrete substances such as collagen to form a protective fibrous cap overlying the plaque (5). Processes such as smooth muscle cell death and secretion of matrix metalloproteinases by macrophages and neutrophils degrade the fibrous cap, leading to plaque disruption. Pro-thrombotic substances are exposed to the flowing blood, leading to the formation of a thrombus that can occlude the lumen of the artery and cause an ischemic clinical event (6). The figure was created using BioRender.

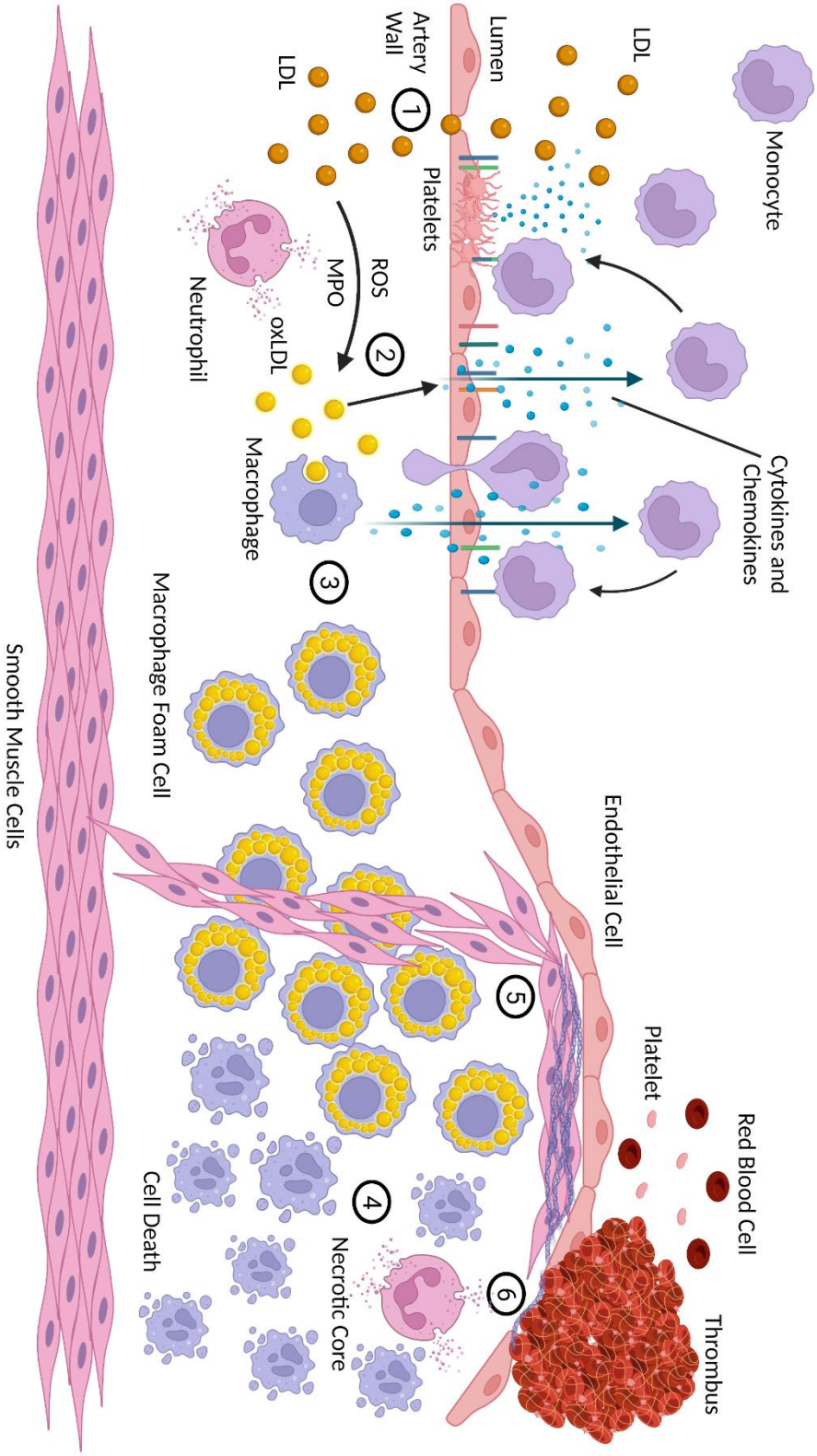
Monocyte
LDL
Lumen
Artery Wall
LDL
1
Platelets
ROS
MPO
Neutrophil
oxLDL
2
Macrophage
Cytokines and Chemokines
3
Macrophage Foam Cell
Endothelial Cell
5
Platelet
Red Blood Cell
Thrombus
4
Cell Death
Necrotic Core
6
Smooth Muscle Cells

1.3 Thrombus Formation

1.3.1 Platelet Adhesion

When potent thrombogenic elements present in the sub-endothelial space such as collagen and collagen-bound vWF are exposed to the flowing blood upon plaque disruption, platelets are initially captured to the vessel wall through the interaction of the platelet GPIbα receptor with collagen-bound vWF (Varga-Szabo et al., 2008). More stable platelet adhesion occurs through the binding of the platelet GPVI receptor to collagen, which triggers intracellular signals that result in platelet integrins shifting to a high-affinity state (Varga-Szabo et al., 2008). Firm platelet adhesion is mediated by high-affinity β1 integrins, such as $\alpha_2\beta_1$ binding to collagen, $\alpha_5\beta_1$ binding to fibronectin, and $\alpha_6\beta_1$ binding to laminin (Varga-Szabo et al., 2008), and results in intracellular signaling that activates platelets and induces platelet $\alpha_{IIb}\beta_3$ receptor activation (Varga-Szabo et al., 2008). Activation of the $\alpha_{IIb}\beta_3$ receptor leads to high-affinity binding to sub-endothelial collagen-bound vWF, resulting in firm platelet adhesion to the vessel wall (Varga-Szabo et al., 2008).

1.3.2 Platelet Activation and Aggregation

Activated platelets undergo shape change and develop multiple filopodia, allowing them to spread over the sub-endothelium and creating a larger surface area for enhanced platelet adhesion and aggregation (Maxwell et al., 2007). Activated platelets release a plethora of agonists from intracellular granules that induce autocrine or paracrine platelet activation (Varga-Szabo et al., 2008).

Platelets contain 3 major granule types: lysosomes, dense granules, and α-granules (Sharda & Flaumenhaft, 2018). Platelet lysosomes, which are few in number and the least studied platelet granules, contain acid hydrolases that may facilitate in thrombus remodeling (Rendu & Brohard-Bohn, 2001). Platelet dense granules contain an abundance of adenosine diphosphate (ADP), which potentiate platelet activation by binding to platelet $P2Y_1$ and $P2Y_{12}$ receptors (Rendu & Brohard-Bohn, 2001). Platelet α-granules are the most abundant platelet granules and their constituents account for the majority of proteins secreted from activated platelets, such as factor XI, PF4, vWF, and fibrinogen (Blair & Flaumenhaft, 2009). Activated platelets also release cytosolic thromboxane A_2 (TXA_2) that binds to platelet thromboxane receptors TPα and TPβ to potentiate platelet activation (Rendu & Brohard-Bohn, 2001).

Platelet aggregation is mainly achieved through platelet $\alpha_{IIb}\beta_3$ linkages, and is indispensable for the formation of stable aggregates (Blair & Flaumenhaft, 2009). The $\alpha_{IIb}\beta_3$ receptors are constitutively present on the surface of platelets, but remain in an inactive form. Once platelets are activated, the $\alpha_{IIb}\beta_3$ receptor binds to collagen-bound vWF and fibrinogen in the sub-endothelium (Blair & Flaumenhaft, 2009). Firm platelet aggregation occurs by the bridging of platelet $\alpha_{IIb}\beta_3$ receptors with fibrinogen and vWF (Blair & Flaumenhaft, 2009). Altogether, platelet adhesion, activation, and aggregation forms an initial platelet plug.

1.3.3 Coagulation

As platelets aggregate, growth and stabilization of the thrombus occurs through a process known as coagulation (Badimon & Vilahur, 2014). Proteins involved in the coagulation cascade circulate in inactive forms, but become activated when the coagulation cascade is activated (Badimon & Vilahur, 2014). The coagulation cascade consists of the intrinsic and the extrinsic pathway, which both lead to a common pathway that interact together and result in the formation of a fibrin mesh that stabilizes the clot (Heestermans et al., 2021).

The intrinsic pathway is initiated when factor XII comes into contact with negatively charged surfaces such as exposed sub-endothelial collagen and polyphosphates that are released from activated platelets. This activates factor XII to factor XIIa, which sequentially activates other coagulation factors, ultimately resulting in factor Xa formation (Heestermans et al., 2021). The extrinsic pathway is initiated when exposed sub-endothelial tissue factor (TF) activates factor VII to factor VIIa (Badimon & Vilahur, 2014; Periayah et al., 2017). Factor VIIa activates factor X into factor Xa and hence, factor Xa is the end product from the activation of both the intrinsic and extrinsic pathways and initiates the common pathway (Periayah et al., 2017). Factor Xa activates prothrombin (factor II) into active thrombin (factor IIa), which is a serine protease that cleaves soluble plasma fibrinogen into insoluble fibrin and also activates factor XIII into factor XIIIa, together creating a mesh that stabilizes the clot (Krishnaswamy, 2013). Additionally, thrombin is the most potent activator of platelets, through activation of protease-

activated receptors (Yun et al., 2016). A schematic of the processes involved in thrombus formation is shown in Figure 1.3.

1.3.4 Myocardial Infarction

When a thrombus occludes coronary arteries and impedes blood flow, downstream ischemia and myocardial infarction can occur (Libby, 2009). Myocardial fibrosis, characterized by excessive deposition of extracellular matrix such as collagen in the cardiac muscle, typically follows myocardial infarction and can lead to abnormal thickening of the ventricular wall, making the cardiac muscle more stiff and less compliant, which can lead to heart failure (Hinderer & Schenke-Layland, 2019). Immune cells such as macrophages and neutrophils are key regulators of cardiac remodeling in response to myocardial infarction, providing pro-inflammatory signals early and reparative signals later on (Duncan et al., 2020; Ma, 2021; Weinberger & Schulz, 2015). For example, macrophages and neutrophils infiltrate the myocardium upon myocardial infarction and phagocytose dead cells and secrete pro-inflammatory mediators that exacerbate inflammation and promote myocardial damage (Duncan et al., 2020; Ma, 2021; Weinberger & Schulz, 2015). In the later stages, macrophages and neutrophils promote wound healing and cardiac regeneration through the secretion of anti-inflammatory cytokines and growth factors, which promote the accumulation of myofibroblasts and collagen deposition (Duncan et al., 2020; Ma, 2021; Weinberger & Schulz, 2015).

Figure 1.3 – Processes of Thrombus Formation.

A. Upon plaque disruption, thrombogenic elements in the sub-endothelial space such as collagen and collagen-bound vWF are exposed to the flowing blood and interact with platelet receptors, resulting in platelet adhesion (1). Platelets become activated and undergo shape change and spread over the sub-endothelium (2). Activated platelets release a plethora of agonists such as ADP, TXA_2 and vWF (3), which activate additional circulating platelets (4). This results in platelet aggregation and forms the initial platelet plug (5). **B.** Next, the initial platelet plug is strengthened by activation of the coagulation cascade. The extrinsic pathway is initiated when factor VII interacts with exposed tissue factor in the sub-endothelium and becomes activated into factor VIIa (1a). The intrinsic pathway is initiated when factor XII interacts with negatively charged surfaces such as sub-endothelium collagen or platelet polyphosphates, resulting in the activation of factor XII to factor XIIa (1b). Both pathways lead to a common pathway, whereby factors Va and Xa act together to activate prothrombin into thrombin (2). Thrombin further activates nearby platelets and potentiates platelet activation, and also cleaves fibrinogen into fibrin (3). Cross-linked fibrin strands act as a firm mesh and trap circulating platelets and red blood cells, resulting in a stable thrombus (4). When the thrombus occludes the lumen of the artery, it can result in myocardial infarction and heart failure. The figure was created using BioRender.

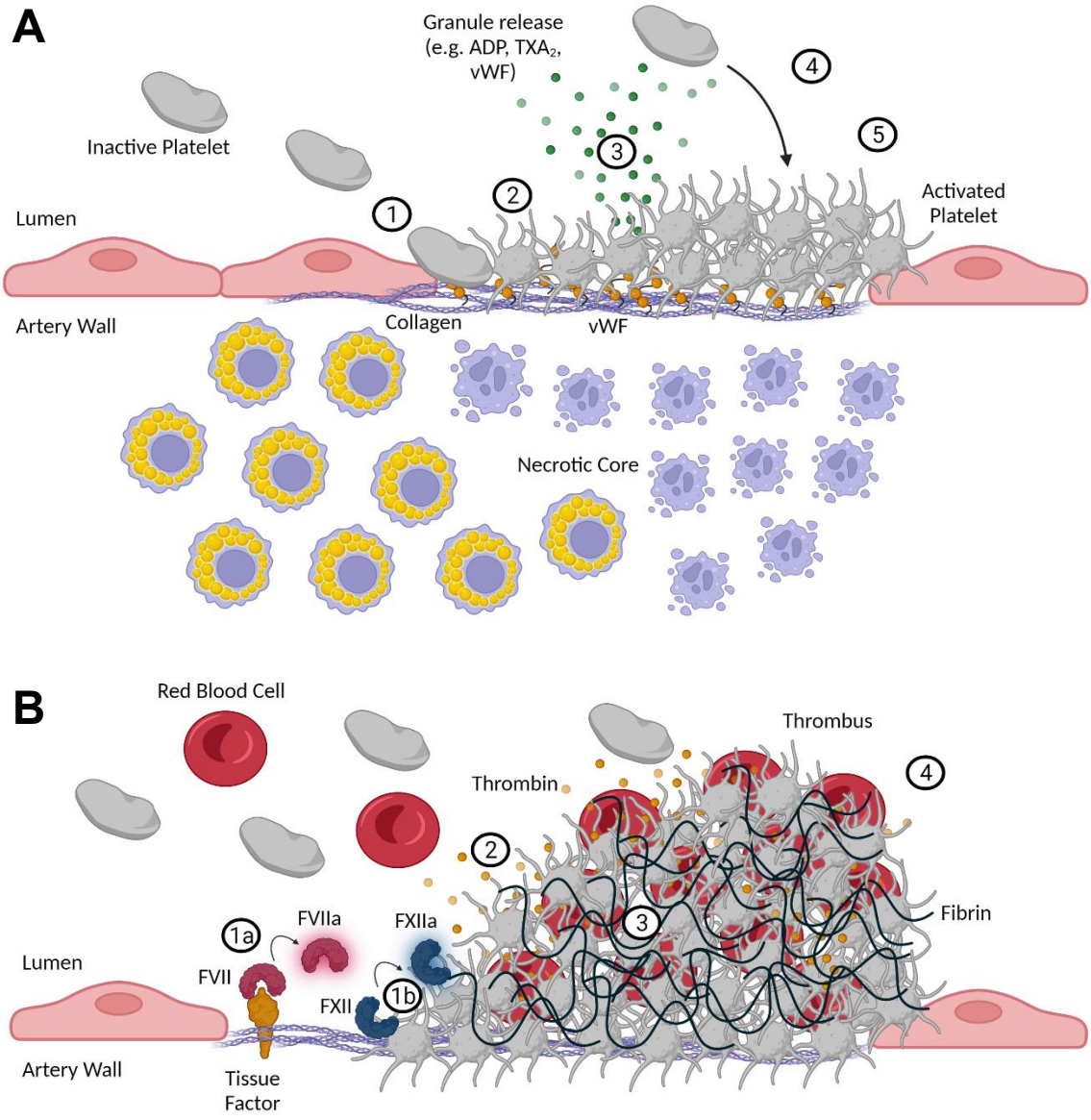
A
Granule release
(e.g. ADP, TXA2,
vWF)
Inactive Platelet
Lumen
Artery Wall
Collagen
vWF
Activated
Platelet
Necrotic Core
B
Red Blood Cell
Thrombus
Thrombin
Fibrin
Lumen
FVII
FVIIa
FXII
FXIIa
Tissue
Factor
Artery Wall

1.4 Conventional Mouse Models of Atherosclerosis

Unlike humans, mice are inherently resistant to the development of atherosclerosis unless they are genetically manipulated (Daugherty, 2002). Mice carry the majority of plasma cholesterol in high-density lipoprotein (HDL) particles, while humans have most of their plasma cholesterol in LDL particles (Daugherty, 2002). HDL protects against while LDL promotes atherosclerosis, likely explaining the inherent protection observed in mice (Assmann & Gotto, 2004). In 1985, Paigen and colleagues fed different strains of mice a high-fat, high-cholesterol, cholate (HFCC) diet (15% fat, 1.25% cholesterol and 0.5% cholic acid) and evaluated atherosclerosis levels (Paigen et al., 1985). The most susceptible strain to atherosclerosis was C57BL/6J, but they developed only mild hypercholesterolemia and small lesions in the aorta with no evidence of fibrous caps even after 14 weeks of diet feeding (Paigen et al., 1985). Therefore, using wild-type mice to study atherosclerosis was very limiting. However, the ability to genetically modify mice became a breakthrough, leading to the generation of the two most frequently used mouse models of atherosclerosis: the ApoE KO and the low-density lipoprotein receptor (LDLR) KO mouse models (Daugherty, 2002).

1.4.1 ApoE KO Mice

ApoE is an apolipoprotein that is present on the surface of chylomicrons, very-low-density lipoproteins (VLDL) and HDL, and is a critical ligand for efficient clearance of these plasma lipoproteins by LDLR and LDLR-related proteins (Lee

et al., 2017). ApoE KO mice exhibit severe hypercholesterolemia, with total plasma cholesterol levels approximately 5-8 times greater than wild-type mice and develop spontaneous atherosclerotic lesions in the proximal aorta by 3 months of age on a normal chow diet (Plump et al., 1992; Zhang et al., 1992). Feeding ApoE KO mice a high-fat, Western-type diet (21% fat, 0.15% cholesterol) exacerbates hypercholesterolemia and lesion development (Nakashima et al., 1994; Plump et al., 1992). However, ApoE KO mice do not develop significant coronary artery atherosclerotic lesions and are largely resistant to the development of unstable atherosclerotic plaques with overlying thrombosis (Getz & Reardon, 2012).

Despite the wide use of ApoE KO mice to study atherosclerosis, there are notable drawbacks. Firstly, the lipid metabolism of ApoE KO mice is not similar to humans, since the majority of plasma cholesterol circulates in VLDL particles rather than LDL particles as observed in humans (Lee et al., 2017). Additionally, ApoE has been shown to have anti-atherogenic effects other than mediating lipoprotein clearance (Lee et al., 2017). Nonetheless, due to the spontaneous and rapid development of atherosclerotic lesions, the ApoE KO mouse model continues to be one of the most widely used mouse models in atherosclerosis research.

1.4.2 LDLR KO Mice

LDLR is a cell-surface receptor that binds to ApoB100 and ApoE on lipoproteins, and is the major receptor responsible for hepatic uptake of plasma LDL cholesterol (Vos et al., 2018). When LDL binds to LDLR at the cell surface,

the LDL-LDLR complex is internalized via clathrin-coated pits and transported to an endosome, where the LDL particle dissociates from the LDLR and the LDL particle is trafficked to the lysosome for degradation, while the LDLR is recycled back to the cell surface for further LDL binding and uptake (Vos et al., 2018). Proprotein convertase subtilisin/kexin type 9 (PCSK9) regulates cell surface LDLR levels, as secreted PCSK9 binds to LDLR and inhibits its endocytic recycling, resulting in lysosomal degradation and increasing plasma LDL levels (Lagace, 2014). LDLR does not have as many functions as ApoE, making it easier to attribute the effects of LDLR KO on atherosclerosis to mainly its effects on lipoprotein uptake and clearance (Getz & Reardon, 2012; Lee et al., 2017).

Compared to ApoE KO mice, LDLR KO mice on a normal chow diet exhibit milder hypercholesterolemia, with only a 2-fold increase in total plasma cholesterol levels compared to wild-type mice (Ishibashi et al., 1993). However, this increase in total plasma cholesterol levels is associated with a 7-9-fold increase in intermediate-density lipoproteins (IDL) and LDL (Ishibashi et al., 1993). The lack of severe hypercholesterolemia is likely due to LDLR-related proteins mediating clearance of ApoB48-containing lipoproteins from circulation (Wouters et al., 2005). LDLR KO mice develop atherosclerotic lesions much more slowly than ApoE KO mice, with lesions beginning to develop at 6-7 months of age (Whitman, 2004). Even up to 22 months of age, LDLR KO mice fed a normal chow diet have been shown to develop only minimal lesions in the aortic root (Moore et al., 2003). Therefore, advanced and extensive lesions are generally not seen in LDLR KO

mice fed a normal chow diet. However, LDLR KO mice fed a HFCC diet for 7 months develop severe hypercholesterolemia, associated with a marked increase in VLDL, IDL, and LDL cholesterol, and exhibit extensive atherosclerosis within the proximal aorta and in some cases, exhibit atherosclerosis in the coronary ostia (Ishibashi et al., 1994). LDLR KO mice fed other atherogenic diets also develop severe hypercholesterolemia and atherosclerotic lesions along the aorta (Lichtman et al., 1999; Tangirala et al., 1995; Whitman, 2004), making the LDLR KO mouse a useful diet-inducible model to study atherosclerosis. However, like ApoE KO mice, LDLR KO mice are largely resistant to the development of occlusive coronary artery atherosclerosis with overlying thrombosis (Braun, Rigotti, et al., 2008; Getz & Reardon, 2012; Gonzalez & Trigatti, 2016; Trigatti & Fuller, 2016).

1.5 Scavenger Receptor Class B Type 1 (SR-B1)

The scavenger receptor class B type 1 (SR-B1) is an HDL receptor that belongs to the class B family of scavenger receptors, which includes CD36 (SR-B2) and lysosomal integral membrane protein-2 (SR-B3) (Krieger, 1999; PrabhuDas et al., 2017; Shen et al., 2018). SR-B1 is encoded by the *SCARB1* gene and is a cell-surface transmembrane receptor containing two transmembrane domains, short intracellular N- and C-termini, and a large extracellular loop that contains multiple N-linked glycosylation sites and cysteine residues that are important for structural integrity and/or function (Krieger, 1999; Shen et al., 2018). The ectodomain of SR-B1 contains an anti-parallel β-barrel core and a hydrophobic

channel that runs through the middle of the receptor (Neculai et al., 2013). These structural features play a critical role in the function of SR-B1-mediated reverse cholesterol transport (RCT) (described below). SR-B1 is broadly expressed in multiple cell types such as macrophages, cardiomyocytes, and endothelial cells, but is most highly expressed in steroidogenic cells of the adrenal gland and ovaries, as well as hepatocytes, making these cell types the major sites for selective lipid uptake (Acton et al., 1994; Krieger, 1999).

1.5.1 The Role of SR-B1 in Reverse Cholesterol Transport

The protective effects of HDL against cardiovascular disease is largely attributed to its role in RCT via SR-B1. The initial step of RCT is the removal of excess cholesterol from macrophage foam cells in atherosclerotic lesions via efflux to lipid-free apolipoprotein A1 (ApoA1; the major apolipoprotein of HDL) mediated by the ATP-binding cassette A1 (ABCA1), followed by efflux of excess cholesterol to mature HDL particles mediated by ATP-binding cassette G1 (ABCG1) and by passive diffusion facilitated by SR-B1 (Phillips, 2014). HDL then carries the excess cholesterol in plasma in the form of cholesterol esters, and transports the cholesterol to hepatocytes for bile acid production or to steroidogenic tissues for steroid production and storage (Krieger, 1999; Phillips, 2014).

Cholesterol ester (CE) uptake from HDL into cells involves a two-step process in which HDL binds to SR-B1, then CEs are transferred from the bound HDL particle into the cell plasma membrane (Krieger, 1999; Rodrigueza et al.,

1999). The binding of HDL to the extracellular domain of SR-B1 is mediated by the interactions of acidic amphipathic α-helices present in ApoA1 with a cluster of basic residues on SR-B1 (Neculai et al., 2013; Williams et al., 2000). Following binding, CEs move down a concentration gradient that exists between the HDL particle (rich in cholesterol) and the plasma membrane through the hydrophobic channel formed by the extracellular domain of SR-B1 (Krieger, 1999; Rodrigueza et al., 1999).

1.5.2 The Effects of SR-B1 Deficiency in Mice

SR-B1 KO mice are viable and have a normal appearance in weight and behaviour. However, relative to wild-type mice, SR-B1 KO mice have significantly increased plasma cholesterol concentrations due to the formation of large ApoA1-containing particles (Rigotti et al., 1997), and exhibit increased ratios of unesterified:total cholesterol in plasma that is exacerbated by high-cholesterol diet feeding (Braun et al., 2003; Van Eck et al., 2003). Cholesterol levels are significantly reduced in the adrenal gland (Rigotti et al., 1997) and gallbladder bile (Trigatti et al., 1999) in SR-B1 KO mice compared to wild-type mice, with the latter supporting findings of hepatic overexpression of SR-B1 resulting in increased biliary cholesterol levels (Kozarsky et al., 1997). SR-B1 is also required for normal oocyte development and female fertility, as female SR-B1 KO mice are infertile (Trigatti et al., 1999). Therefore, SR-B1 plays a key role in regulating plasma HDL cholesterol levels and lipid metabolism in mice.

Interestingly, SR-B1 KO mice exhibit platelet abnormalities due to the accumulation of unesterified cholesterol (Dole et al., 2008; Korporaal et al., 2011; Ma et al., 2010). SR-B1 KO mice exhibit thrombocytopenia and abnormal platelet morphologies such as increased size and unusual multimellar structures (Dole et al., 2008; Korporaal et al., 2011), their platelets circulate in an activated state (Korporaal et al., 2011; Yu et al., 2018), and their platelets exhibit reduced *ex vivo* responsiveness to stimulation by agonists such as ADP (Dole et al., 2008; Korporaal et al., 2011; Ma et al., 2010) and convulxin (Ma et al., 2010), but normal or increased responsiveness to a protease-activated receptor 4 (PAR4) agonist peptide (Dole et al., 2008; Ma et al., 2010). These platelet abnormalities appear to be due to SR-B1 deficiency in non-bone marrow-derived cells rather that platelet SR-B1 deficiency, because when platelets from wild-type mice are transplanted into SR-B1 KO mice, the wild-type platelets exhibit abnormally high cholesterol content, and the mice have reduced platelet counts similar to SR-B1 KO mice (Ma et al., 2010). In contrast, wild-type mice transplanted with SR-B1 KO bone marrow cells have normal platelet counts, suggesting that the thrombocytopenia is induced by the abnormal plasma cholesterol environment (Ma et al., 2010). SR-B1 KO mice also exhibit increased susceptibility to ferric chloride-induced thrombosis in the left carotid artery (Korporaal et al., 2011). However, it should be noted that endothelial integrity and repair is thought to be impaired in SR-B1 KO mice (Mineo & Shaul, 2007) which can result in faster platelet adhesion upon injury.

1.6 The Effects of SR-B1 Deficiency on Atherosclerosis in Mice

Although ApoE KO and LDLR KO mice are largely resistant to the development of occlusive coronary artery atherosclerosis and myocardial infarction, SR-B1 deficiency in these mouse models results in occlusive coronary artery atherosclerosis, platelet accumulation in atherosclerotic coronary arteries, myocardial infarction, and early death. The effects of SR-B1 deficiency in these athero-susceptible mouse models are described below.

1.6.1 SR-B1/ApoE Double KO Mice

Compared to ApoE single KO mice, SR-B1/ApoE double KO (DKO) mice exhibit significantly increased plasma cholesterol levels (mainly in VLDL-sized particles) (Trigatti et al., 1999) and have an abnormally high ratio of unesterified:total cholesterol, suggesting lipoprotein structural abnormalities (Braun et al., 2003). These mice develop extensive atherosclerotic plaques in the aortic sinus by 5 weeks of age on a normal chow diet (Trigatti et al., 1999), and develop spontaneous occlusive coronary artery atherosclerosis that is associated with cardiac enlargement, myocardial fibrosis, and impaired heart function (Braun et al., 2002). Moreover, SR-B1/ApoE DKO mice exhibit a reduced lifespan with a 50% mortality at 6 weeks of age on a normal chow diet (Braun et al., 2002). Interestingly, platelets (Yu et al., 2018) and fibrin (Braun et al., 2002) were detected in the plaques in atherosclerotic coronary arteries of SR-B1/ApoE DKO mice, suggesting the possibility of thrombosis on top of atherosclerotic plaques.

Various interventions have been tested on SR-B1/ApoE DKO mice such as the anti-oxidant drug probucol (Braun et al., 2003), anti-oxidant pomegranate extract (Al-Jarallah et al., 2013), and rosuvastatin (Yu et al., 2018), all of which significantly reduced aortic sinus and coronary artery atherosclerosis and myocardial fibrosis levels. Interestingly, rosuvastatin treatment reduced platelet accumulation in atherosclerotic coronary arteries without altering basal platelet activation or circulating platelet counts (Yu et al., 2018). However, the direct cause of reduced platelet accumulation in atherosclerotic coronary arteries is not clear. Overall, SR-B1/ApoE DKO mice can be utilized to elucidate mechanisms associated with CAD, and/or testing of potential therapies for cardiovascular disease.

1.6.2 SR-B1 KO/HypoE and SR-B1/LDLR DKO Mice

Compared to SR-B1/ApoE DKO mice, SR-B1 KO/HypoE mice (express approximately 5% of normal ApoE mRNA levels) have reduced total plasma cholesterol levels by 71%, and do not exhibit early onset of atherosclerosis on a normal chow diet, suggesting that even the low expression level of ApoE is atheroprotective (Zhang et al., 2005). Compared to LDLR single KO mice, SR-B1/LDLR DKO mice on a normal chow diet exhibit increased plasma cholesterol levels mainly attributed to increased cholesterol in abnormally large HDL particles, but on a high-fat, Western-type diet exhibit reduced total plasma cholesterol levels attributed to reduced cholesterol in VLDL, IDL, and LDL particles due to lower rates

of hepatic VLDL synthesis and triglyceride secretion, and reduced plasma ApoB (Covey et al., 2003; Fuller et al., 2014). Similar reductions in plasma ApoB were reported for SR-B1/ApoE DKO mice compared to ApoE single KO mice (Trigatti et al., 1999). SR-B1/LDLR DKO mice fed the Western-type diet for 2-3 months exhibit a significant increase in atherosclerosis levels in the aorta and aortic sinus compared to LDLR KO mice (Covey et al., 2003; Fuller et al., 2014), and also exhibit evidence of coronary artery atherosclerosis but without signs of myocardial fibrosis or early death (Fuller et al., 2014).

When SR-B1 KO/HypoE (Zhang et al., 2005) and SR-B1/LDLR DKO (Fuller et al., 2014) mice are fed a HFCC diet for 4 or 3.5 weeks, respectively, they exhibit exacerbated hypercholesterolemia, extensive aortic sinus and occlusive coronary artery atherosclerosis, myocardial fibrosis, and cardiomegaly. Moreover, SR-B1 KO/HypoE mice (Zhang et al., 2005) and SR-B1/LDLR DKO mice (Fuller et al., 2014) exhibit reduced survival with a 50% mortality of approximately 32 days or 3.5 weeks, respectively, after initiation of HFCC diet feeding. HFCC diet-fed SR-B1 KO/HypoE mice also exhibit cardiac dysfunction (Zhang et al., 2005). A separate study demonstrated that HFCC diet-fed SR-B1 KO/HypoE mice exhibit a large number of atherosclerotic coronary arteries with evidence of thrombi, and treatment of these mice with aspirin, an inhibitor of platelet function, extended their survival, reduced the extent of myocardial infarction, and reduced the number of thrombi in atherosclerotic coronary arteries (Hermann et al., 2016). HFCC diet-fed SR-B1/LDLR DKO mice also have evidence of platelet accumulation in

atherosclerotic coronary arteries, along with increased levels of circulating cytokines, monocytosis, and higher endothelial VCAM-1 and ICAM-1 protein expression levels in the coronary arteries compared to LDLR single KO mice (Fuller et al., 2014). Overall, both SR-B1 KO/HypoE and SR-B1/LDLR DKO mice are diet-inducible mouse models of coronary artery atherosclerosis and myocardial fibrosis, allowing for the control of the age of onset, duration, and severity of CAD.

1.6.3 SR-B1 Single KO Mice

SR-B1 single KO mice exhibit aortic sinus atherosclerosis when fed a high-fat, Western-type diet (Hildebrand et al., 2010; Van Eck et al., 2003) or a high-fat, high-cholesterol diet (Harder et al., 2007) for a prolonged period of time, but the lesions are not extensive. However, SR-B1 KO mice fed a HFCC diet for 11 weeks have significantly larger atherosclerotic plaques in the aortic sinus compared to wild-type mice (Huby et al., 2006). Moreover, mice with liver-specific deletion of SR-B1 have significantly greater levels of aortic sinus atherosclerosis compared to wild-type mice (Huby et al., 2006), whereas hepatic over-expression of SR-B1 in transgenic mice limits the development of atherosclerosis in different mouse models (Arai et al., 1999; Kozarsky et al., 1997; Ueda et al., 2000). Interestingly, protection against atherosclerosis does not appear to be mediated by SR-B1 in endothelial cells, as SR-B1 in endothelial cells has been shown to mediate LDL transcytosis into arteries (Armstrong et al., 2015; Huang et al., 2019). To elaborate, ApoE KO mice with endothelial cell-specific KO of SR-B1 fed a high-fat diet for 8

weeks have markedly reduced atherosclerosis in the aorta and aortic sinus compared to control mice. This is regardless of mouse gender, and similar findings were also seen in mice with LDLR deficiency (Huang et al., 2019), suggesting that SR-B1 on endothelial cells plays a role in the initiation and progression of atherosclerosis development. Nonetheless, since whole-body SR-B1 KO in mice results in increased atherosclerosis levels, the atherogenic role of SR-B1 in endothelial cells does not outweigh the protective effects of SR-B1 against atherosclerosis in other cell types.

Despite their susceptibility to diet-induced atherosclerosis, SR-B1 single KO mice are not routinely used, and there are a lack of studies extensively characterizing coronary artery atherosclerosis development in SR-B1 single KO mice. This is surprising since SR-B1 deficiency in mice with atherogenic mutations results in extensive occlusive coronary artery atherosclerosis, myocardial fibrosis and early death. Therefore, it would be interesting to characterize the development of coronary artery atherosclerosis in SR-B1 single KO mice.

1.7 Neurobeachin-like 2 (NBEAL2)

1.7.1 NBEAL2 Structural Domains

NBEAL2 is a large (2754 amino acids, 302 kDa), multi-domain protein that is highly expressed in cells of the hematopoietic system, primarily in megakaryocytes and platelets. NBEAL2 is characterized by the beige and Chediak-Higashi (BEACH) domain, a highly conserved domain that is important for

vesicle trafficking and membrane dynamics (Albers et al., 2011; Gunay-Aygun et al., 2011; Jogl et al., 2002). NBEAL2 also contains armadillo-like (ARM), pleckstrin homology (PH), concanavalin-A-like (ConA-like), and WD40 domains that have different functions (Deppermann, Nurden, et al., 2013). NBEAL2 is one of the least studied BEACH domain-containing proteins, and its function was unknown until studies demonstrated that mutations in the NBEAL2 gene are responsible for causing gray platelet syndrome (GPS) in humans (Albers et al., 2011; Gunay-Aygun et al., 2011; Kahr et al., 2011).

1.7.2 NBEAL2 Mutations: The Cause of Gray Platelet Syndrome

A variety of mutations in the NBEAL2 gene resulting in a loss of function causes a rare, autosomal recessive bleeding disorder known as GPS (Albers et al., 2011; Gunay-Aygun et al., 2011; Kahr et al., 2011). Genetic mutations include missense, nonsense, frameshift, and splicing mutations that are scattered along the gene, with missense mutations (many occurring within the BEACH domain) accounting for a large proportion of etiologic variants identified (Glembotsky et al., 2021; Nurden & Nurden, 2016; Sims et al., 2020).

GPS patients exhibit bleeding diathesis, macrothrombocytopenia, myelofibrosis, and splenomegaly as a consequence of myelofibrosis, and in rare instances, severe hemorrhaging (Nurden & Nurden, 2007). Platelets in GPS patients appear gray and contain large vacuoles, and both megakaryocytes and platelets lack α-granules and their contents (Albers et al., 2011; Breton-Gorius et

al., 1981; Gunay-Aygun et al., 2011; Kahr et al., 2011). Platelets from GPS patients also have impaired ADP, thrombin, and collagen-induced platelet aggregation (Gerrard et al., 1980; Mori et al., 1984), suggesting that α-granules and their contents are essential for proper platelet function. Interestingly, the membrane protein P-selectin is detected along the membrane of the vacuole-like vesicles in platelets of GPS patients (Nurden & Nurden, 2007). A separate study showed that biosynthesized α-granule proteins such as vWF and TSP-1 are absent in platelets from GPS patients, whereas the presence of endocytosed α-granule proteins such as fibrinogen and albumin are less affected (Maynard et al., 2010). Another study showed that vWF in the α-granules of GPS patients have random distribution, suggesting a lack of vWF organization or packaging (Cramer et al., 1985). It became evident that the inherent defect in megakaryocytes and platelets from GPS patients involved the packaging and trafficking of α-granule cargo proteins. GPS patients appear to have normal dense granules, lysosomes, mitochondria, and peroxisomes (Breton-Gorius et al., 1981; Nurden & Nurden, 2007). A schematic of the NBEAL2 protein and its functional domains, along with different missense mutations reported to cause GPS, is shown in Figure 1.4.

Figure 1.4 – NBEAL2 Domains and Missense Mutations Causing Gray Platelet Syndrome.

Schematic of the NBEAL2 protein (2754 amino acids, 302 kDa) and its functional domains: ARM domain (green; 377-504), ConA domain (yellow; 580-730), WD40 domain (blue; 1515-1555), PH domain (red; 1915-2040), BEACH domain (purple; 2053-2345), and WD40 domain repeats (blue; 2463-2722). Marked above the protein schematic are some of the missense mutations associated with causing GPS. Other types of mutations are not shown. The figure was created using BioRender.

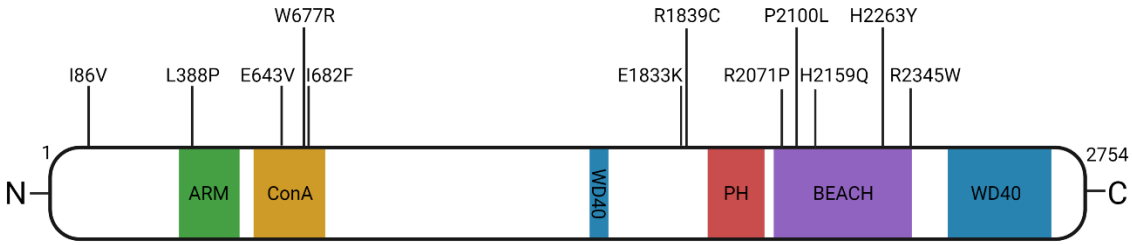

1.7.3 The Role of NBEAL2 in Megakaryocytes and Platelets

Studies have shed light on the role of NBEAL2 in megakaryocytes and platelets. NBEAL2 KO mice recapitulate human GPS, characterized by splenomegaly, macrothrombocytopenia, significantly reduced or absent platelet α-granules, and deficiency in platelet α-granule contents such as vWF, TSP-1 and PF4 (Deppermann, Cherpokova, et al., 2013; Guerrero et al., 2014; Kahr et al., 2013). Interestingly, NBEAL2 KO megakaryocytes display decreased survival, delayed maturation, and decreased proplatelet production, all of which likely explain the thrombocytopenia observed in NBEAL2 KO mice, and NBEAL2 KO megakaryocytes also exhibit abnormal distribution of vWF (Kahr et al., 2013), Platelets from NBEAL2 KO mice have impaired thrombin-induced activation compared to platelets from wild-type mice, and the $\alpha_{IIb}\beta_3$ activation response to ADP is impaired (Kahr et al., 2013). NBEAL2-deficient platelets have impaired adhesion and aggregation on immobilized collagen under flow and a two-fold reduction in phosphatidylserine exposure on the outer surface of platelets upon platelet activation, indicating a defect in coagulant activity (Deppermann, Cherpokova, et al., 2013). Moreover, occlusive thrombus formation following ferric chloride-induced mesenteric arteriole injury is significantly impaired in NBEAL2 KO mice (Deppermann, Cherpokova, et al., 2013), and platelet accumulation in thrombi is reduced in NBEAL2 KO mice compared to wild-type mice following laser-induced injury of cremaster arterioles (Kahr et al., 2013). NBEAL2 KO mice also have significantly prolonged tail bleeding times (Deppermann, Cherpokova, et al.,

2013; Kahr et al., 2013). Altogether, these studies demonstrated that NBEAL2 plays a crucial role in proper platelet function by regulating α-granules.

A recent study has shed light on the role of NBEAL2 in α-granule retention and trafficking (Lo et al., 2018). When comparing the uptake of labeled fibrinogen, wild-type and NBEAL2 KO megakaryocytes did not differ; however, NBEAL2 KO megakaryocytes had reduced fibrinogen retention attributed to rapid loss (Lo et al., 2018). In wild-type megakaryocytes, newly endocytosed fibrinogen moves from Rab (Ras-related protein in brain) 5-associated early endosomes, to Rab7-associated late endosomes, before accumulating in P-selectin-associated α-granules where it is retained (Lo et al., 2018). In contrast, although endocytosed fibrinogen in NBEAL2 KO megakaryocytes associated with Rab5 and Rab7 similar to wild-type megakaryocytes, it did not associate with the P-selectin compartment but rather associated with Rab11 recycling endosomes before being released from the cell (Lo et al., 2018). Endogenously synthesized vWF followed the same pathway out of NBEAL2 KO megakaryocytes (Lo et al., 2018). Interestingly, NBEAL2 co-localized and interacted intracellularly with P-selectin in human megakaryocytes and platelets (Lo et al., 2018). Taken together, NBEAL2 appears to be required for the retention of endogenous and endocytosed proteins by α-granules, which would explain the lack of α-granules and their cargo observed in GPS patients and NBEAL2 KO mice. A schematic of the role of NBEAL2 in α-granule cargo packaging and trafficking is shown in Figure 1.5.

Figure 1.5 – The Role of NBEAL2 in α-Granule Cargo Packaging and Trafficking.

Endocytosed fibrinogen and endogenously synthesized cargo in megakaryocytes (e.g. vWF, PF4 and TSP-1) move from Rab5-associated early endosomes to Rab7-associated late endosomes, then to α-granule precursor vesicles containing membrane-bound P-selectin. NBEAL2 is postulated to localize to α-granules and interact with P-selectin, allowing for normal packaging of α-granule contents and retention of α-granules in the cell. In the absence of NBEAL2, the α-granule cargo is instead trafficked to Rab11-associated recycling endosomes and secreted prematurely, resulting in the empty structures observed in the platelets of NBEAL2 KO mice and GPS patients. The figure was created using BioRender.

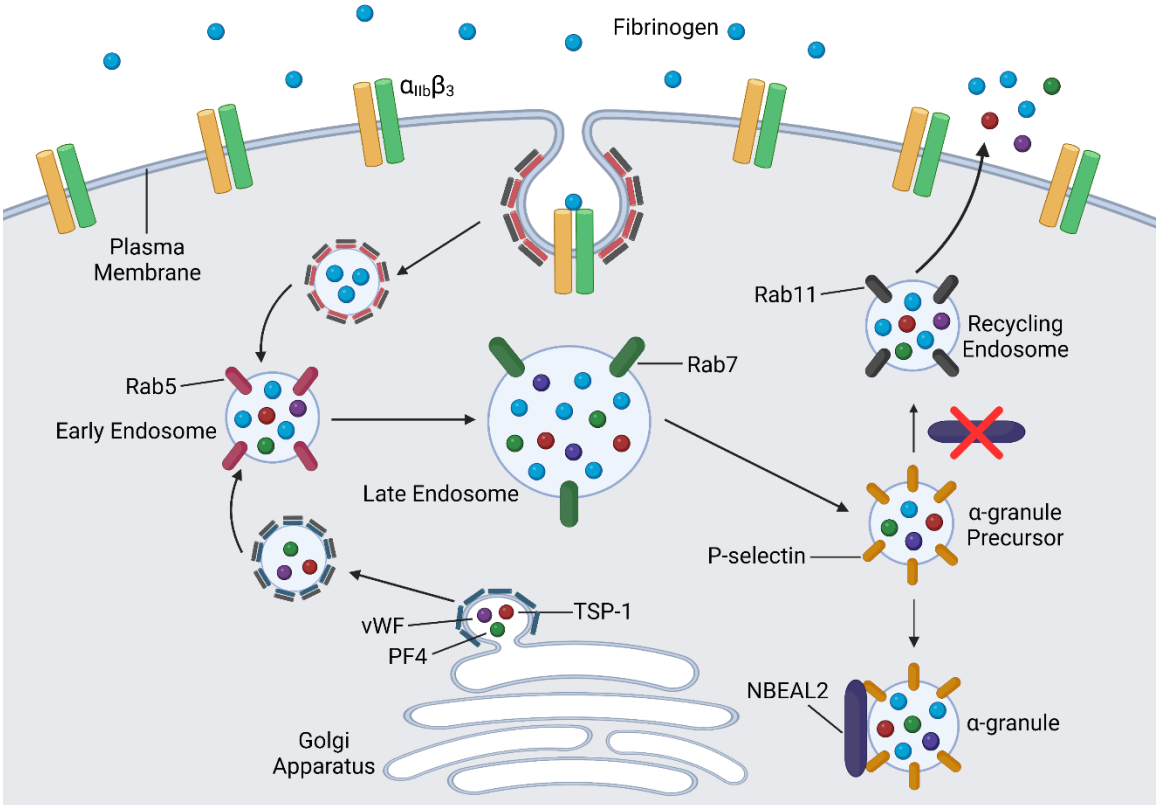

1.7.4 The Role of NBEAL2 in Other Blood Cells

NBEAL2 KO mice have increased levels of circulating neutrophils with reduced granularity (Claushuis et al., 2018; Sowerby et al., 2017), significantly reduced neutrophil granule components such as MPO and elastase (Sowerby et al., 2017), and significantly increased plasma levels of these granule components (Claushuis et al., 2018). Interestingly, a number of GPS patients have been reported to lack neutrophil granules, although this appears to be variable in GPS patients (Aarts et al., 2021; Drouin et al., 2001). Compared to wild-type mice, NBEAL2 KO mice have similar levels of circulating monocytes, but reduced monocyte granularity (but to a lesser extent than the reduced granularity observed in NBEAL2-deficient neutrophils) (Claushuis et al., 2018). Moreover, natural killer (NK) (Sowerby et al., 2017) and mast cells (Drube et al., 2017) in NBEAL2 KO mice have reduced granularity and do not function normally. NBEAL2-deficient mice have increased susceptibility to both bacterial (*Staphylococcus aureus*) and viral (cytomegalovirus) infection, resulting in increased illness and weight loss (Sowerby et al., 2017), and have increased organ damage following induction of pneumosepsis and endotoxemia (Claushuis et al., 2018), suggesting that NBEAL2 plays a role in immunity. Considering the role of NBEAL2 in platelets and a variety of other immune cells, all of which contribute to CAD development, it would be interesting to test the effects of NBEAL2 KO on CAD development in mice.

1.8 Protease-Activated Receptor 4 (PAR4)

Protease-activated receptors (PARs) from a small G-protein-coupled receptor (GPCR) sub-family that have many different functions (French & Hamilton, 2016). Mammals express four PARs (PAR1-4): PAR1 is a high-affinity thrombin receptor, and PAR3 and PAR4 are also activated by thrombin. On the other hand, PAR2 is insensitive to thrombin and activated primarily by trypsin and trypsin-like proteases (French & Hamilton, 2016). PARs are also cleaved by other proteases that lead to unique and irreversible self-activation (French & Hamilton, 2016; Heuberger & Schuepbach, 2019). Many of these proteases are involved in inflammation and coagulation processes and therefore, extensive research has elucidated the role of PARs in thrombosis and cardiovascular diseases (French & Hamilton, 2016). For the focus of this thesis, only PAR4 will be discussed in detail.

1.8.1 PAR4 Structure

PAR4 contains seven transmembrane domains with 3 intracellular and 3 extracellular loops, an intracellular C-terminal tail, an extracellular N-terminal tail, and multiple key structural features that are critical for its activation and function (French & Hamilton, 2016). The extracellular N-terminus contains a hydrophobic signal peptide sequence with a cleavage site in between Ser^{17} and Gly^{18}, and a serine protease cleavage site in between Arg^{47} and Gly^{48} that is essential for activation (French & Hamilton, 2016; Xu et al., 1998). Mutation of Arg^{47} to Ala was shown to render PAR4 unresponsive to thrombin or trypsin (Xu et al., 1998). When

proteolytic cleavage occurs at Arg^{47}/Gly^{48}, a tethered ligand sequence (GYPGQV) is exposed that binds to a three amino acid sequence (CHD) on the second extracellular loop, which results in receptor activation (French & Hamilton, 2016; Xu et al., 1998). Notably, PAR4 lacks a high-affinity thrombin binding domain on the N-terminal tail that reacts with thrombin's exosite I that is present on PAR1 and PAR3. Instead, thrombin's active site interacts with PAR4 on a segment of the N-terminal tail that contains four amino acids (PAPR), and the N-terminal tail also contains an anionic cluster (Asp^{57}, Asp^{59}, Glu^{62}, Asp^{65}) that slows the dissociation rate with thrombin by interacting with cationic residues that border thrombin's exosite I (Jacques & Kuliopulos, 2003). A schematic of the PAR4 structure with key amino acids involved in its activation and function is shown in Figure 1.6.

One notable structural difference between human and mouse PAR4 is the absence of a cysteine residue in human PAR4 that is present in the mouse PAR4 (C368) C-terminus (Ramachandran et al., 2017). C-terminal cysteine residues are common sites of post-translational receptor palmitoylation (covalent lipid attachment) and regulate signaling (Qanbar & Bouvier, 2003), and mutation of glutamine (Q357) to a cysteine in human PAR4 in HEK293 cells has been shown to reduce intracellular calcium signaling (an indicator of GPCR activation) by approximately 50% in response to a PAR4 agonist peptide (AYPGKF-NH_2) (Ramachandran et al., 2017). HEK293 cells expressing a mutant PAR4 receptor with an 8 amino acid deletion flanking the region encompassing Q357 did not even generate a significant calcium signal, and also prevented β-arrestin recruitment

(another indicator of GPCR activation) in response to a PAR4 agonist peptide and thrombin (Ramachandran et al., 2017). Based off of the 8 amino acid (RAGLFQRS) C-terminal motif that appears to regulate calcium signaling and β-arrestin interactions, a novel PAR4 inhibitory peptide has been developed (Ramachandran et al., 2017), which will be described in more detail later in this thesis.

Figure 1.6 – PAR4 Structure.

PAR4 contains seven transmembrane domains, an extracellular N-terminal tail with a signal peptide (yellow), an intracellular C-terminal tail, three intracellular loops, and three extracellular loops. Proteolytic cleavage at Arg^{47}/Gly^{48} (arrow) results in an exposed tethered ligand sequence (GYPGQV; green) that binds to a three amino acid sequence (tethered ligand binding region; CHD; red) on the second extracellular loop. Enhanced thrombin binding occurs through two regions: the thrombin active site binding region (PAPR; purple), and the anionic cluster that interacts with thrombin exosite I (orange). The figure was created using BioRender.

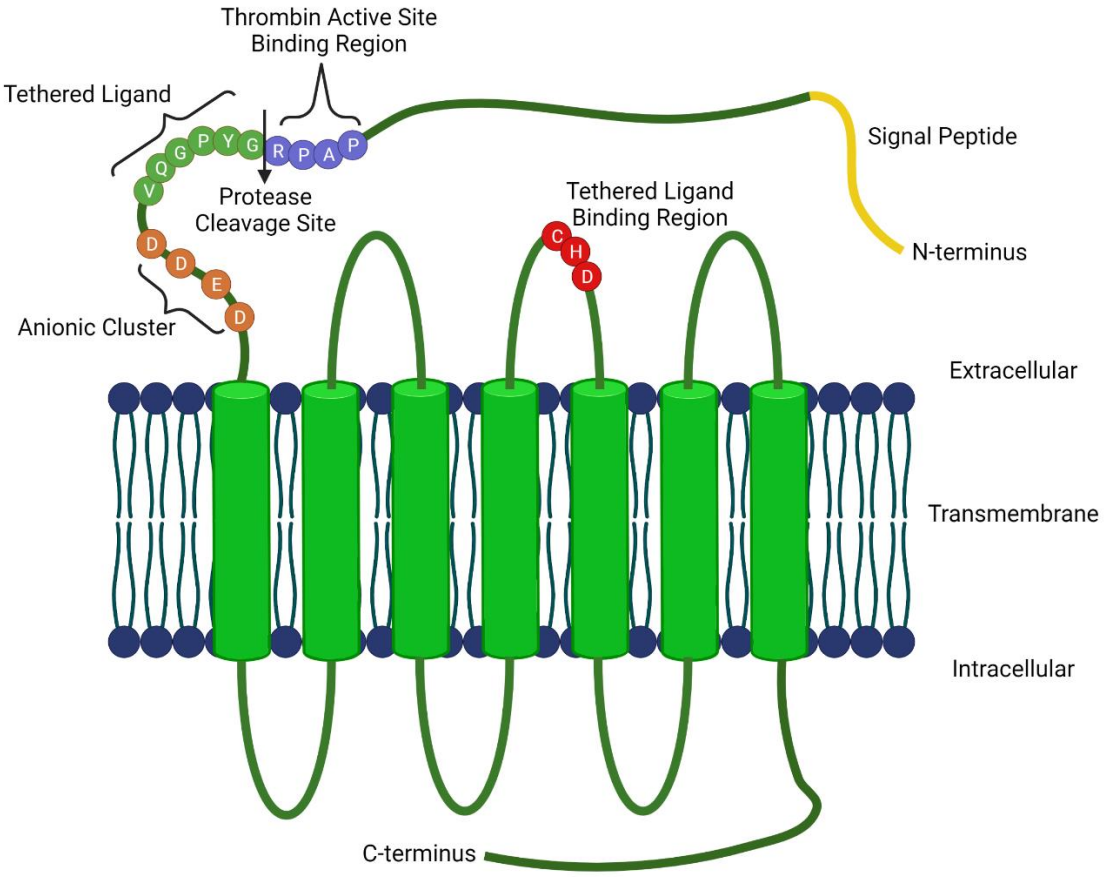

1.8.2 PAR4 Activation and Signaling

Upon activation, PAR4 can couple to the α_q G-protein, which activates the phospholipase C beta (PLCβ) pathway resulting in endoplasmic reticulum (ER) calcium mobilization, which in turn promotes the activity of kinases and phosphatases such as mitogen-activated protein kinase (MAPK), protein kinase C (PKC), phospholipase A_2 (PLA_2), and calpain (Coughlin, 2000; French & Hamilton, 2016). In platelets, the activation of this pathway results in the secretion of platelet granules and integrin receptor activation (Coughlin, 2000, 2005; French & Hamilton, 2016). PAR4 can also couple to the $\alpha_{12/13}$ G-protein, resulting in activation of the Rho pathway, resulting in Rho-dependent cytoskeletal responses and PLC activation (Coughlin, 2000; French & Hamilton, 2016). The activation of this pathway in platelets results in platelet shape change (Debreczeni et al., 2021; French & Hamilton, 2016). PAR4 activation in platelets can also result in β-arrestin recruitment and subsequent phosphatidylinositol-3-kinase (PI3K)-dependent phosphorylation and activation of Akt (a serine/threonine kinase), leading to enhanced fibrinogen binding to the $\alpha_{IIb}\beta_3$ platelet receptor and enhanced platelet activation and aggregation (Li et al., 2011; Ramachandran et al., 2017). Desensitization and signal termination of PAR4, at least in mice, is induced by C-terminal tail phosphorylation via GPCR kinases, resulting in internalization via endocytosis in clathrin-coated pits and degradation in lysosomes (Adams et al., 2011; French & Hamilton, 2016). A schematic of PAR4 activation, signaling, and trafficking in platelets is shown in Figure 1.7.

Figure 1.7 – Platelet PAR4 Activation, Signaling, and Trafficking.

Cleavage at Arg^{47}/Gly^{48} by thrombin (1) exposes a tethered ligand that binds to the orthosteric ligand binding pocket on the second extracellular loop, resulting in PAR4 activation (2). PAR4 coupling to the α_q G-protein activates the PLCβ pathway, leading to ER calcium mobilization that activates a variety of kinases and phosphatases such as MAPK, PKC, PLA_2, and calpain. Coupling to the $\alpha_{12/13}$ G-protein activates the Rho pathway which induces Rho-dependent cytoskeletal responses and PLC activation. β-arrestin recruitment leads to PI3K-dependent activation of Akt (2). Together, these signaling pathways result in different platelet responses. GPCR kinases desensitize PAR4 by phosphorylating the C-terminal tail, which terminates signalling (3). The receptor is internalized via clathrin-coated pits, trafficked to endosomes, and degraded in lysosomes (4). The figure was created using BioRender.

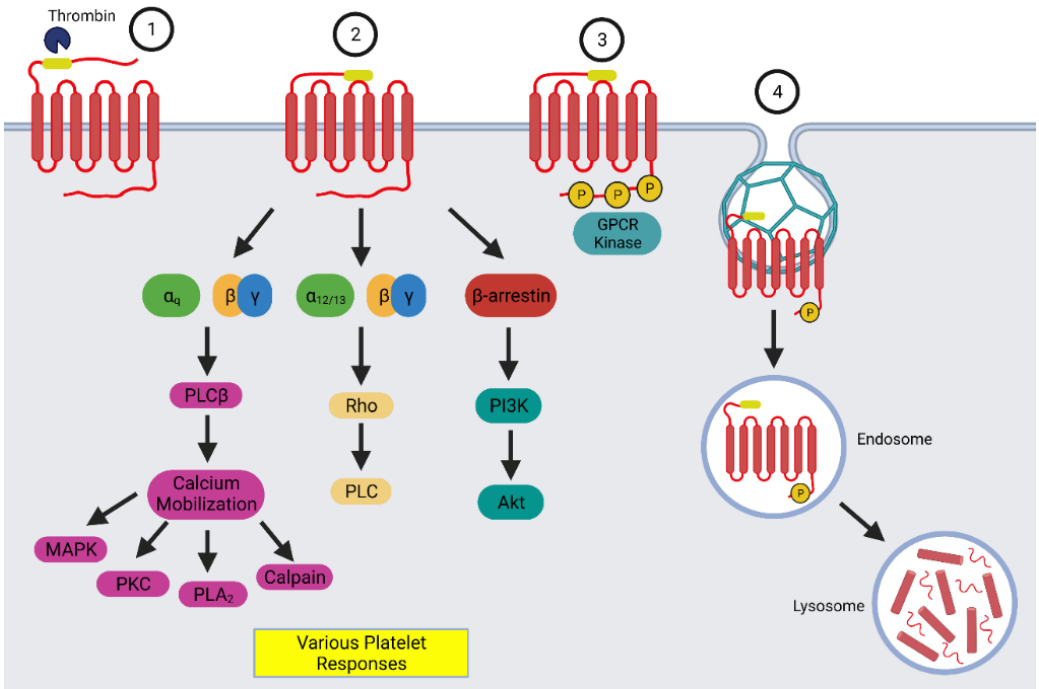

1.8.3 PAR4 Expression Profile

Although PAR4 is broadly expressed in different tissues such as the spleen, pancreas, lung, and skeletal muscle, (Kahn et al., 1998; Xu et al., 1998), research has focused heavily on the function of PAR4 in inflammatory and cardiovascular settings. PAR4 is expressed in key vascular cell types such as platelets (Kahn et al., 1998; Xu et al., 1998), leukocytes (Vergnolle et al., 2002), endothelial cells (Kataoka et al., 2003), smooth muscle cells (Vidwan et al., 2010), and cardiomyocytes (Kolpakov et al., 2020). Platelets are an example of a cell type that has conserved PAR4 expression among different species. For example, human platelets express PAR1 and PAR4, and mouse and rat platelets express PAR3 and PAR4 (Coughlin, 2000; French & Hamilton, 2016). Additionally, endothelial cells in both humans and mice express PAR4, although PAR1 appears to be the major thrombin receptor in both humans and mice (Grimsey & Trejo, 2016; Kataoka et al., 2003). Since PAR4 is expressed on a variety of vascular cell types, the vast majority of PAR4 studies investigated the role of PAR4 in cardiovascular disease.

1.8.4 The Role of PAR4 in Atherosclerosis and Thrombosis

PAR4 is involved in inflammatory processes that drive atherosclerosis, which is not surprising since serine proteases that activate PAR4 such as thrombin and trypsin drive pro-inflammatory processes (French & Hamilton, 2016). For example, a study showed increased leukocyte rolling on endothelium in rat venules following thrombin or PAR4-activating peptide treatment (Vergnolle et al., 2002).

In addition, inflammation has been shown to impact PAR4, such as increased PAR4 expression on isolated human coronary arteries following TNFα treatment (Hamilton et al., 2001), increased PAR4 mRNA and protein levels in isolated rat cardiomyocytes following thrombin and TNFα treatment (Kolpakov et al., 2020), and increased PAR4 mRNA and protein levels in mouse hearts following coronary artery ligation-induced myocardial infarction (Kolpakov et al., 2020).

The effects of PAR4 deficiency on platelets and thrombosis are also well characterized. PAR4 KO mice are normal in appearance, size, and fertility, with no differences in platelet, leukocyte, or erythrocyte counts compared to wild-type mice. However, platelets from PAR4 KO mice do not undergo shape change, mobilize calcium, nor aggregate in response to a PAR4 agonist peptide (AYPGKF) and thrombin (Sambrano et al., 2001). Moreover, PAR4 KO mice (Sambrano et al., 2001) and wild-type mice transplanted with bone marrow from PAR4 KO mice (but not from wild-type mice) (Hamilton et al., 2004) have significantly longer tail bleeding times compared to control mice, and a prolonged time for vessel occlusion upon arterial injury (Lee et al., 2012; Sambrano et al., 2001; Vandendries et al., 2007), suggesting that thrombin-induced platelet activation via PAR4 is necessary for proper platelet activation and function and normal hemostasis. To date, there has been no evidence for spontaneous bleeding in PAR4 KO mice.

However, the role of PAR4 in the development of atherosclerosis is less clear. One study demonstrated that ApoE/PAR4 DKO mice fed a Western diet for 5 or 10 weeks do not exhibit differences in aortic root atherosclerosis levels

compared to control mice, suggesting that thrombin-mediated platelet activation via PAR4 is not required for the early development of atherosclerotic plaques in ApoE KO mice (Hamilton et al., 2009). This finding was in contrast to an abstract that reported reduced aortic root atherosclerosis levels in LDLR/PAR4 DKO mice compared to LDLR single KO mice when fed a high-fat diet infused with angiotensin II for 28 days or when fed a high-fat diet for 12 weeks (Owens et al., 2018). Further studies are needed to elucidate the role of PAR4 in atherosclerotic plaque development. Interestingly, PAR4 KO mice have reduced cardiomyocyte apoptosis, reduced infarct size, and improved functional recovery after acute myocardial infarction (for 2 days) induced by coronary artery ligation compared to wild-type mice (Kolpakov et al., 2020). However, PAR4 KO mice subjected to chronic myocardial infarction (for 7 and 28 days) exhibit impaired cardiac function, increased rates of myocardial rupture, increased mortality, larger infarcts, and delayed neutrophil accumulation which impairs post-myocardial infarction healing (Kolpakov et al., 2020). This study suggests that PAR4 is involved in myocardial infarction, and that short-term administration of PAR4 inhibitors rather than prolonged PAR4 inhibition may be a therapeutic approach to target early inflammation and ischemic injury.

1.8.5 Targeting PAR4 as an Anti-Platelet Approach

The major role of PAR4 in platelets has provided rationale for the development of various pharmacological agents to target PAR4. A diverse set of

PAR4 antagonists inhibit thrombin-induced platelet activation and aggregation, such as peptidomimetics, low molecular weight compounds, and function-blocking antibodies (French & Hamilton, 2016). A highly-selective and reversible PAR4 antagonist that has reached clinical trials is BMS-986120, which has been shown to inhibit *ex vivo* platelet activation, aggregation, and thrombus formation without serious adverse effects (Wilson et al., 2018). A distinct class of inhibitors known as pepducins that target PAR4 have also been developed. Pepducins are unique, cell-penetrating peptides that mimic the region of the target receptor that is thought to bind to G-proteins and block the interactions between the receptor and the effector G-protein (Covic, Gresser, et al., 2002). Pepducins are composed of a peptide corresponding to the target region and conjugated to an N-terminal palmitoylated tail that anchors the peptide to a cell's lipid membrane; the pepducin then flips to the intracellular face of the cell where it exerts its inhibitory effects (Covic, Gresser, et al., 2002). The most characterized anti-PAR4 pepducin is P4pal10 which inhibits approximately 85% of thrombin-induced aggregation of both human and mouse platelets and prolongs tail bleeding times (Covic, Misra, et al., 2002). However, the specificity of P4pal10 remains questionable as it displays a level of cross-reactivity with PAR1 agonist peptide-induced platelet activation (Covic, Misra, et al., 2002).

As previously mentioned, an intracellular PAR4 C-terminal 8 amino acid motif (RAGLFQRS) that regulates calcium signaling and β-arrestin interactions has been identified and based on this motif, a novel PAR4 inhibitory (RAG8) and a control reverse-sequence (SRQ8) pepducin has been developed (Ramachandran

et al., 2017). RAG8 has been shown to inhibit PAR4-dependent calcium signaling and β-arrestin recruitment without affecting PAR2 signaling in HEK-293 cells (Ramachandran et al., 2017). In washed human platelets, RAG8 inhibited platelet aggregation stimulated by a PAR4 agonist peptide but not by a PAR1 agonist peptide, and RAG8, but not SRQ8, inhibited thrombin-induced platelet aggregation (Ramachandran et al., 2017). Moreover, RAG8 treatment, but not SRQ8 treatment, significantly inhibited thrombosis in mice upon ferric chloride-induced femoral artery injury, presumably due to reduced platelet thrombus stabilization, and significantly increased tail bleeding times (Ramachandran et al., 2017). Therefore, the RAG8 pepducin may be an effective tool to probe the *in vivo* function of PAR4.

1.9 Overall Context and Objective

Although platelets play key roles in thrombosis and the initiation and progression of atherosclerosis development, their roles in CAD development are not often examined. As previously mentioned, normal chow-fed SR-B1/ApoE DKO and HFCC diet-fed SR-B1/LDLR DKO mice exhibit occlusive coronary artery atherosclerosis, platelet accumulation in atherosclerotic coronary arteries, and myocardial fibrosis. Moreover, studies have shown that treatment of SR-B1/ApoE DKO mice with rosuvastatin (Yu et al., 2018) or HFCC diet-fed SR-B1 KO/HypoE mice with aspirin reduced platelet accumulation in atherosclerotic coronary arteries (Hermann et al., 2016). Therefore, mouse models that develop coronary artery atherosclerosis and myocardial fibrosis and exhibit platelet accumulation in

atherosclerotic coronary arteries appear to be useful tools for investigating the effects of platelet inhibition on CAD development.

Considering the prominent roles of NBEAL2 and PAR4 in platelet function, they are attractive targets for investigating the potential role of platelets in the development of CAD in mice. Although the role of NBEAL2 in platelet α-granule retention and function is well characterized, studies have not examined the effects of NBEAL2 deficiency and the consequences of impaired α-granule function on atherosclerosis and/or CAD development in mice. Moreover, although studies have examined the effects of PAR4 deficiency on aortic sinus atherosclerosis (Hamilton et al., 2009; Owens et al., 2014) or myocardial infarction induced by coronary artery ligation (Kolpakov et al., 2016, 2020), the effects of PAR4 deficiency on CAD development in mice have not been investigated.

Despite SR-B1 deficiency inducing extensive occlusive coronary artery atherosclerosis and myocardial infarction in mice with ApoE or LDLR deficiency, there is a lack of literature extensively characterizing coronary artery atherosclerosis and myocardial fibrosis in SR-B1 single KO mice. Moreover, although aging is an unavoidable risk factor that predisposes humans to a higher incidence and prevalence of CAD, most basic research studies utilize juvenile or young adult mice to study atherosclerosis, which will not take into account age-related factors that may contribute to CAD development. Studies that have utilized older mice to study atherosclerosis used ApoE KO or LDLR KO mice which develop atherosclerosis spontaneously on a normal chow diet (Dorighello et al.,

2018; Moore et al., 2003; Plump et al., 1992; Zhang et al., 1992). Consequently, findings may just be reflective of the duration in which atherosclerosis develops. Therefore, investigating the effects of older age on the development of CAD in SR-B1 single KO mice may address these issues and potentially provide a novel mouse model to elucidate age-dependent mechanisms associated with CAD.

Taken together, the objectives of this thesis are to examine the effects of NBEAL2 KO and/or PAR4 inhibition on CAD development in mice, and to examine the effects of older age on diet-induced coronary artery atherosclerosis and myocardial fibrosis in SR-B1 single KO mice.

1.10 Hypothesis

We hypothesize that NBEAL2 KO and/or PAR4 inhibition will reduce aortic sinus and coronary artery atherosclerosis, platelet accumulation in atherosclerotic coronary arteries, and myocardial fibrosis in mice, and that SR-B1 single KO mice will develop extensive diet-induced aortic sinus and coronary artery atherosclerosis in an age-dependent manner, with signs of myocardial fibrosis and reduced survival.

1.11 Specific Aims

Aim of Chapter 2

To evaluate the effects of NBEAL2 inactivation on aortic sinus and coronary artery atherosclerosis, platelet accumulation in atherosclerotic coronary arteries, and myocardial fibrosis in SR-B1/ApoE DKO mice.

Aim of Chapter 3

To evaluate the effects of PAR4 inhibition on aortic sinus and coronary artery atherosclerosis, platelet accumulation in atherosclerotic coronary arteries, and myocardial fibrosis in HFCC diet-fed SR-B1/LDLR DKO mice.

Aim of Chapter 4

To evaluate the effects of older age on aortic sinus and coronary artery atherosclerosis, myocardial fibrosis, and survival in atherogenic diet-fed SR-B1 single KO mice.

Chapter 2: Neurobeachin-like 2 Knockout Reduces Aortic Sinus and Coronary Artery Atherosclerosis but Worsens Myocardial Fibrosis in Scavenger Receptor Class B Type 1/Apolipoprotein E Double Knockout Mice.

Author List: Samuel Lee, Peter Gross, Walter H.A. Kahr, and Bernardo L. Trigatti

Foreword

This manuscript examines the effects of NBEAL2 KO on coronary artery disease development in SR-B1/ApoE DKO mice. We demonstrate that NBEAL2 deficiency profoundly increases tail bleeding times in mice. Interestingly, NBEAL2 KO increases plasma cholesterol and PCSK9 levels in SR-B1/ApoE DKO mice. Despite this, NBEAL2/SR-B1/ApoE TKO mice exhibit reduced aortic sinus and coronary artery atherosclerosis compared to SR-B1/ApoE DKO mice, and also have reduced platelet accumulation in atherosclerotic coronary arteries. Surprisingly, despite the reduced coronary artery atherosclerosis burden, NBEAL2/SR-B1/ApoE TKO mice exhibit increased levels of myocardial fibrosis and reduced survival. Moreover, NBEAL2/SR-B1/ApoE TKO mice exhibit increased circulating neutrophil levels and reduced neutrophil granulation, as well as reduced MPO-positive neutrophils in the myocardium compared to SR-B1/ApoE DKO mice.

This manuscript will be submitted for publication by the end of 2022. This manuscript was written by Samuel Lee with guidance from Bernardo L. Trigatti. This project was designed by Samuel Lee and Bernardo L. Trigatti. NBEAL2 KO mice were provided by Peter Gross and Walter H.A. Kahr. All experiments were conducted by Samuel Lee, and all data were analyzed and interpreted by Samuel Lee under the guidance of Bernardo L. Trigatti.

2.1 Abstract

Objective: Scavenger receptor class B type 1 (SR-B1)/Apolipoprotein E (ApoE) double knockout mice exhibit spontaneous development of coronary artery disease (CAD) characterized by occlusive coronary artery atherosclerosis, platelet accumulation in coronary arteries, and myocardial fibrosis. Neurobeachin-like 2 (NBEAL2) knockout in mice results in thrombocytopenia and degranulation of platelet α-granules, resulting in improper platelet function. Although platelets are involved in atherosclerosis development and despite the prominent role of NBEAL2 in platelets, as well as its implications in other blood cells, the role of NBEAL2 on atherosclerosis and CAD in mice has not been tested. Therefore, we tested the effects of NBEAL2 knockout on aortic sinus and coronary artery atherosclerosis, platelet accumulation in atherosclerotic coronary arteries, and myocardial fibrosis in SR-B1/ApoE double knockout mice.

Approach and Results: SR-B1/ApoE double knockout mice and NBEAL2/SR-B1/ApoE triple knockout mice were harvested at 5 weeks of age on a normal chow diet. NBEAL2/SR-B1/ApoE triple knockout mice exhibited increased plasma cholesterol levels and proprotein convertase subtilisin/kexin type 9 levels compared to SR-B1/ApoE double knockout mice. Despite this, NBEAL2/SR-B1/ApoE triple knockout mice exhibited reduced aortic sinus and coronary artery atherosclerosis and reduced platelet accumulation in atherosclerotic coronary arteries. Interestingly, however, NBEAL2/SR-B1/ApoE triple knockout mice

exhibited increased myocardial fibrosis. Moreover, NBEAL2/SR-B1/ApoE triple knockout mice exhibited increased circulating neutrophil levels, reduced neutrophil granulation, and reduced proportion of myeloperoxidase-positive neutrophils in the myocardium compared to SR-B1/ApoE double knockout mice.

Conclusions: Although NBEAL2 knockout in SR-B1/ApoE double knockout mice reduced aortic sinus and coronary artery atherosclerosis and platelet accumulation in atherosclerotic coronary arteries, it increased myocardial fibrosis levels, suggesting that the effects of NBEAL2 knockout on the heart outweigh the benefits to the vasculature. These findings suggest that NBEAL2 plays an important role on the development of CAD, and demonstrates the importance of proper regulation of platelet and neutrophil granulation and function in CAD development.

2.2 Introduction

Coronary artery disease (CAD) continues to be one of the leading causes of mortality worldwide and is characterized by the development of atherosclerosis in the coronary arteries[1]. Atherosclerosis is a chronic inflammatory disease driven by complex interactions between circulating immune cells, lipoproteins, and cells of the artery wall[2]. Mature atherosclerotic plaques become prone to either endothelial cell erosion or rupture, which can lead to platelet activation, aggregation, and the subsequent formation of a thrombus that can completely occlude the lumen of the affected arteries[3]. This process is known as

atherothrombosis and drives ischemic diseases associated with atherosclerosis, such as myocardial infarction, cerebral ischemia, and peripheral vascular disease[4]. Platelets not only play an important role in thrombosis, but are also involved in the early stages of atherosclerosis and accelerate inflammatory processes that promote plaque development[5–8]. Platelets adhere to activated endothelial cells and release pro-inflammatory cytokines such as c-c motif chemokine ligand 5 (CCL5) and c-x-c motif chemokine ligand 12 (CXCL12), facilitating the attraction and firm adhesion of circulating leukocytes to the vascular wall that further exacerbate atherosclerosis[5–7]. Platelet activation induces platelet shape change, granule secretion and aggregation. Platelet α-granules store a vast array of proteins that amplify the activation response and promote thrombus formation and stability upon release[9,10]. The contents in the α-granules include hemostatic and adhesive molecules such as von Willebrand factor (vWF) and fibrinogen, inflammatory peptides such as interleukin-1β (IL-1β) and transforming growth factor-β (TGFβ), and pro-angiogenic factors such as vascular endothelial growth factor (VEGF) and platelet-derived growth factor (PDGF)[9,10]. Insights into platelet granule formation and function have come from investigating mice and patients with secretory granule deficiencies, such as those with Quebec platelet disorder[11,12] and arthrogryposis, renal dysfunction and cholestasis (ARC) syndrome[13–15].

A loss of function mutation of the neurobeachin-like 2 (NBEAL2) gene causes an autosomal recessive bleeding disorder known as gray platelet syndrome (GPS), characterized by macrothrombocytopenia and gray-appearing platelets

with decreased/absent α-granules and α-granule proteins[16–18]. The NBEAL2 gene encodes a multidomain scaffolding protein that is highly expressed in cells of the hematopoietic system[19]. Similar to patients with GPS, NBEAL2 knockout (KO) mice exhibit macrothrombocytopenia and a deficiency of platelet α-granules and their cargo, and their platelets appear pale[20]. NBEAL2 KO bone marrow megakaryocytes have delayed maturation, decreased survival and ploidy, and developmental abnormalities, indicating that NBEAL2 KO has deleterious effects on platelet production[20]. NBEAL2 plays an important role in α-granule cargo trafficking and maturation, and in the absence of NBEAL2, α-granule cargo is trafficked to recycling endosomes and secreted, thereby preventing normal α-granule maturation, and consequently producing the empty structures observed in NBEAL2 KO mouse and human GPS platelets[21]. The lack of α-granules due to NBEAL2 KO results in impaired platelet aggregation, defective platelet adhesion to collagen under flow, and reduced procoagulant activity, thereby impairing hemostasis and thrombosis[22]. NBEAL2 KO mice also exhibit a significantly increased rate of blood loss and cumulative blood loss compared to wild-type mice in experimental tail bleeding assays, clearly pointing to a hemostatic defect in NBEAL2 KO mice[20].

NBEAL2 also plays a role in other blood cells. For example, NBEAL2 KO mice have increased levels of circulating neutrophils, but reduced neutrophil granularity and granule cargo, leading to increased granule components in plasma such as myeloperoxidase (MPO) and elastase[23,24]. Additionally, monocytes[23],

natural killer (NK) cells[24], and mast cells[25] in NBEAL2 KO mice exhibit reduced granularity, indicating the important role of NBEAL2 in granule retention in various cell types. Moreover, NBEAL2-deficient mice have increased susceptibility to bacterial (*Staphylococcus aureus*) and viral (cytomegalovirus) infection with increased illness[24], as well as increased organ damage following pneumosepsis induction[23].

Genetic KO of the HDL receptor, scavenger receptor class B type 1 (SR-B1), in mice containing Apolipoprotein E (ApoE) or low-density lipoprotein receptor (LDLR) KO mutations accelerates spontaneous or diet-induced atherosclerosis development in the aortic sinus and coronary arteries[26–28]. These mice also exhibit platelet accumulation in atherosclerotic coronary arteries and fatal myocardial infarction[26–28]. Mice deficient in SR-B1 exhibit platelet abnormalities associated with increased ratios of unesterified:esterified cholesterol due to impaired HDL-dependent reverse cholesterol transport, leading to the accumulation of unesterified cholesterol in platelets[29–33]. Mice deficient in SR-B1 exhibit thrombocytopenia[29,30,33,34], their platelets appear to circulate in an activated state[29,34], and exhibit increased susceptibility to experimental $FeCl_3$-induced thrombosis[29]. We previously demonstrated that rosuvastatin treatment protected SR-B1/ApoE double KO (DKO) mice against atherosclerosis and attenuated myocardial fibrosis, and interestingly reduced platelet accumulation in atherosclerotic coronary arteries[34]. Another study demonstrated that aspirin treatment in atherogenic diet-fed SR-B1 KO/HypoE mice significantly reduced the

number of thrombi in atherosclerotic coronary arteries and premature deaths, presumably due to aspirin's anti-platelet action[35]. These studies suggest that mouse models that develop coronary artery atherosclerosis, platelet accumulation in coronary arteries, and myocardial fibrosis can be utilized to investigate novel approaches of platelet inhibition and their effects on CAD. Since SR-B1/ApoE DKO mice develop spontaneous aortic sinus and occlusive coronary artery atherosclerosis, platelet accumulation in atherosclerotic coronary arteries and myocardial fibrosis[26,34], and since NBEAL2 has a prominent role in platelets but is also implicated in other blood cells that are involved in CAD development, we tested the effects of NBEAL2 deficiency on the CAD phenotype in these mice.

To investigate the effects of NBEAL2 KO on the CAD phenotype of SR-B1/ApoE DKO mice, we generated NBEAL2/SR-B1/ApoE triple KO (TKO) mice. NBEAL2 KO in SR-B1/ApoE DKO mice increased plasma total and unesterified cholesterol levels and circulating proprotein convertase subtilisin/kexin type 9 (PCSK9) levels. Despite this, NBEAL2 KO in SR-B1/ApoE DKO mice reduced aortic sinus and coronary artery atherosclerosis and reduced platelet accumulation in atherosclerotic coronary arteries. Interestingly, however, NBEAL2 KO in SR-B1/ApoE DKO mice worsened myocardial fibrosis and reduced their survival. Although circulating cytokine levels were not altered, NBEAL2 KO in SR-B1/ApoE DKO mice significantly increased blood neutrophil counts and significantly reduced the granularity of circulating neutrophils. Moreover, NBEAL2/SR-B1/ApoE TKO mice exhibited reduced proportions of MPO-positive neutrophils in the myocardium

compared to SR-B1/ApoE DKO mice, suggesting that NBEAL2 deficiency may lead to dysfunctional neutrophils. This is the first *in vivo* study to demonstrate the effects of NBEAL2 KO on atherosclerosis and CAD in mice, and provides important insights into the role of NBEAL2 in CAD development.

2.3 Materials and Methods

2.3.1 Mice

All procedures involving mice were in accordance with the Canadian Council on Animal Care guidelines and were approved by the McMaster University Animal Research Ethics Board. Female SR-B1/ApoE DKO mice (mixed C57BL/6Jx129 background) were bred to male NBEAL2 single KO mice (C57BL/6J background) and fed normal chow supplemented with 0.5% probucol[36,37] to produce NBEAL2$^{+/-}$/SR-B1$^{+/-}$/ApoE$^{+/-}$ mice. NBEAL2$^{+/-}$/SR-B1$^{+/-}$/ApoE$^{+/-}$ mice fed normal chow were then bred together to generate littermate NBEAL2$^{+/+}$/SR-B1$^{+/-}$/ApoE$^{-/-}$ and NBEAL2$^{-/-}$/SR-B1$^{+/-}$/ApoE$^{-/-}$mice. To generate mice used in this study, NBEAL2$^{+/+}$/SR-B1$^{+/-}$/ApoE$^{-/-}$ mice were bred together to generate littermate ApoE single KO and SR-B1/ApoE DKO mice, whereas NBEAL2$^{-/-}$/SR-B1$^{+/-}$/ApoE$^{-/-}$mice were bred together to generate littermate NBEAL2/ApoE DKO and NBEAL2/SR-B1/ApoE TKO mice. All mice were bred and housed in the David Braley Research Institute Animal Facility at McMaster University and had free access to normal chow (Teklad Global 18% Protein Rodent Diet, 2018, Envigo, Madison, Wisconsin, USA) and water. All experiments were carried out in male mice and selected experiments were

repeated in females where indicated. For survival studies, SR-B1/ApoE DKO mice and NBEAL2/SR-B1/ApoE TKO mice were fed normal chow until they exhibited overt signs of illness, including ruffled coat, hunched posture, labored breathing, and lethargy, at which point they were humanely euthanized. Otherwise, mice used in this study were fed normal chow until 5 weeks of age and fasted for approximately 14 hours, then fully anesthetized with isoflurane-O_2 in an induction chamber followed by continued anaesthesia under a nose comb. While anesthetized, mice were subjected to a tail bleeding assay as described below. Blood was then collected into heparinized Eppendorf tubes via cheek puncture using a lancet. A portion of the blood was used for flow cytometry analysis of blood cells, and the remainder was used to prepare plasma. After blood collection, the mice were then thoracotomized and hearts and vasculature were perfused in situ through the left ventricle with phosphate-buffered saline containing 10 U of heparin/ml. Hearts were then excised and cryoprotected in 30% sucrose for 1-2 hours, then frozen using liquid nitrogen in Shandon Cryomatrix (Thermo Fisher Scientific, 6769006, Ottawa, Ontario, Canada) and stored at -80°C. Livers were rapidly frozen in liquid nitrogen or stored at -80°C in RNAlater (Invitrogen Life Technologies Inc., AM7020, Burlington, Ontario, Canada). Plasma was prepared by centrifugation of blood at 4,000 rpm for 5 minutes in a microcentrifuge at 4°C and stored in -80°C.

2.3.2 Tail Bleeding Assay

As described above, immediately prior to harvesting, mice were anaesthetized under a nose comb using isoflurane-O_2. The tails were transected across the tail vein using a scalpel blade approximately 0.5 cm from the tip, and placed in a cuvette containing 37°C saline. The time taken for the cessation of blood flow was recorded.

2.3.3 Plasma Analysis

Plasma total cholesterol (Cholesterol Infinity, TR13421, Thermo Fisher Scientific, Ottawa, Ontario, Canada), unesterified cholesterol (Free Cholesterol E, Wako Diagnostics, 993-02501, Mountain View, California, USA), HDL cholesterol (not precipitable by phosphotungstate-magnesium salt; HDL Cholesterol E, Wako Diagnostics, 997-01301, Mountain View, California, USA), and triglycerides (L-Type Triglyceride M, Wako Chemicals, 998-02992, Richmond, Virginia, USA) were measured following manufacturers' instructions. Esterified cholesterol levels were calculated as the difference between total cholesterol and unesterified cholesterol measurements, and non-HDL cholesterol levels were calculated as the difference between total cholesterol and HDL cholesterol measurements. Plasma PCSK9 (Mouse Proprotein Convertase 9/PCSK9 Quantikine Kit, R&D Systems, MPC900, Minneapolis, Minnesota, USA), creatine kinase-myocardial band (CK-MB, Mouse Creatine Kinase MB Kit, Novus Biologicals, NBP2-75312, Toronto, Ontario, Canada), interleukin-6 (IL-6) and tumour necrosis factor alpha (TNFα; BioLegend,

431304 and 430904, respectively, San Diego, California, USA) were measured by enzyme linked immunosorbent assay (ELISA) following manufacturer's protocols.

2.3.4 Real Time PCR

Total RNA was extracted from approximately 25 mg of liver tissue that were stored in RNAlater at -80°C (Invitrogen Life Technologies Inc., AM7020, Burlington, Ontario, Canada). RNA was purified using the RNeasy Mini kit (Qiagen Inc., 74101, Toronto, Ontario, Canada), and the RNA concentration was obtained using a Nanodrop ND-8000 spectrophotometer (Thermo Fisher Scientific, Ottawa, Ontario, Canada). cDNA synthesis was performed from 1 µg of total RNA using a QuantiTect reverse transcription kit (Qiagen Inc., 205311, Toronto, Ontario, Canada). Real-time quantitative PCR was performed using a PowerTrack SYBR Green Master Mix (Thermo Fisher Scientific, A46110, Ottawa, Ontario, Canada) in an Applied Biosystems StepOnePlus Real-Time PCR System (Applied Biosystems, Foster City, California, USA). GAPDH was used as the housekeeping gene, and values were compared using the $2^{-\Delta\Delta Ct}$ method[38]. Mouse primer sequences (see Supplementary Table 1) were selected using Pubmed's primer-BLAST. All primers were synthesized by Invitrogen Life Technologies (Burlington, Ontario, Canada).

2.3.5 Histology

For analysis of atherosclerosis in the aortic sinus and coronary arteries, 10 µm-thick transverse cryosections were collected using a cryotome (Shandon

Cryotome Electronic, 77210163GB, Thermo Fisher Scientific, Ottawa, Ontario, Canada) from the middle of the heart to the aortic annulus in 0.3 mm intervals, then in 0.1 mm intervals to the top of the aortic valve leaflets. Lipids in atherosclerotic plaques were detected by oil red O staining, and nuclei were counter-stained with Meyer's hematoxylin. Brightfield images were captured using an Axiovert 200M microscope (Carl Zeiss Canada Ltd., Toronto, Ontario, Canada). For aortic sinus atherosclerosis analyses, the cross-sectional areas of atherosclerotic plaques for a series of sections (100 μm apart) with each of the 3 valve leaflets covering a distance of 500 μm were measured manually in a blinded manner using AxioVision software, and plotted vs. distance and plaque volume (area under the curve) was calculated using GraphPad Prism. Atherosclerosis in coronary arteries were evaluated in a blinded manner by counting coronary arteries with different levels of occlusion in 7 sections (which covers a distance of 1800 μm) prior to reaching the aortic annulus. Coronary arteries were scored as either 0% occluded (non-atherosclerotic - no raised atherosclerotic plaque), <50% occluded, >50% occluded, or 100% (fully) occluded.

Myocardial fibrosis was detected by Masson's trichrome staining (Sigma-Aldrich, Oakville, Ontario, Canada), which stains collagen-rich fibrotic tissue blue/purple, and healthy myocardium red/pink. Images for 1 transverse cryosection per mouse at approximately 900 μm below the aortic annulus were captured using an Olympus BX41 microscope with a DP72 camera (Olympus Canada Inc., Richmond Hill, Ontario, Canada). The percentage of myocardial fibrosis was

measured manually in a blinded manner using the outline function in ImageJ software as the proportion of fibrotic staining to the total area of the cross-section.

2.3.6 Immunofluorescence

Platelets were detected using a rat anti-mouse CD41 antibody (BD Biosciences, 553847, Mississauga, Ontario, Canada) and AlexaFluor 488 goat anti-rat secondary antibody (Invitrogen**,** A-11006, Waltham, Massachusetts, USA). Neutrophils were stained with a rat anti-mouse Ly6G antibody (BD Biosciences, 551459, Mississauga, Ontario, Canada) and AlexaFluor 488 goat anti-rat secondary antibody (Invitrogen**,** A-11006, Waltham, Massachusetts, USA). To detect MPO, the same heart sections were then co-stained with a mouse anti-mouse MPO antibody (Novus Biologicals, NBP1-51148, Toronto, Ontario, Canada) using a mouse-on-mouse immunodetection kit (Vector Laboratories, BMK-2202, Burlington, Ontario, Canada), and a streptavidin conjugated with AlexaFluor 594 (Life Technologies, Burlington, Ontario, Canada). Nuclei were detected with 4', 6'-diamidino-2-phenylindole (DAPI) counterstaining. All fluorescent images were captured using an Olympus BX41 microscope with a DP72 camera (Olympus Canada Inc., Richmond Hill, Ontario, Canada). For analysis of CD41 in coronary arteries, all coronary arteries in 7 sections (which covers a distance of 1800 μm) below the aortic annulus were counted, and the percentage of atherosclerotic coronary arteries with positive CD41 platelet staining was quantified in a blinded manner. For quantification of Ly6G and MPO in cardiac tissue, images for 1

transverse cryosection per mouse at approximately 900 μm below the aortic annulus were captured, and the fluorescence intensity was quantified separately in a blinded manner using ImageJ software. To quantify the percentage of MPO-positive neutrophils, the amount of Ly6G and MPO co-staining fluorescence area (quantified using ImageJ software) was taken as a percentage of the total Ly6G fluorescence area.

2.3.7 Flow Cytometry

Blood was incubated with the following rat anti-mouse antibodies: FITC CD3 (BD Biosciences, 555274, Mississauga, Ontario, Canada), BV510 CD45 (Biolegend, 103138, San Diego, California, USA), PerCP-Cyanine5.5 CD45R (B220) (eBioscience, 45-0452-80, San Diego, California, USA), PE CD11b (M1/70.15) (Thermo Fisher Scientific, RM2805, Ottawa, Ontario, Canada), PE-Cy7 Ly6C (Biolegend, 128018, San Diego, California, USA), PE-Dazzle-594 Ly6G (Biolegend, 127648(BLG), San Diego, California, USA), PE-Cy5 CD4 (BD Biosciences, 553050, Mississauga, Ontario, Canada), PE-Cy7 CD8a (BD Biosciences, 552877, Mississauga, Ontario, Canada), and PE NK1.1 (BD Biosciences, 553165, Mississauga, Ontario, Canada). Next, erythrocytes present in the blood were lysed and samples were fixed with 1x 1-step fix/lyse solution (Thermo Fisher Scientific, 00-5333, Ottawa, Ontario, Canada). Absolute leukocyte counts were determined with the addition of 123count eBeads (Thermo Fisher Scientific, 01-1234-42, Ottawa, Ontario, Canada). Flow cytometry was performed

on a BD FACSCalibur Flow Cytometry system (BD Biosciences, Mississauga, Ontario, Canada), and data were analyzed using FlowJo v10 software.

2.3.8 Statistical Analysis

GraphPad Prism software was used for statistical analyses. For two groups, data were subjected to the Shapiro-Wilk test for normality. Those that passed normality were analyzed by the Student's t-test (2-tailed, unpaired), and those that failed normality were analyzed by the Mann-Whitney Rank Sum test. For multiple groups, data were analyzed by one-way ANOVA with Tukey's Multiple Comparisons Post-Hoc test. Data with two independent variables were analyzed by two-way ANOVA with Sidak's Multiple Comparisons Post-Hoc test. Data are presented as mean ± standard error of the mean. P values <0.05 were considered statistically significant.

2.4 Results

2.4.1 NBEAL2 KO Increased Tail Bleeding Times in Mice

To verify the effects of NBEAL2 KO on hemostasis seen in previous studies[20,22], we performed a tail bleeding assay on SR-B1/ApoE DKO mice and NBEAL2/SR-B1/ApoE TKO mice. Indeed, knocking out NBEAL2 significantly increased tail bleeding times in both male (1183.3 ± 61.3 sec. vs. 327.7 ± 29.1 sec.; $P <0.0001$; Supplementary Figure 2.7) and female (1130.1 ± 76.6 sec. vs. 344.3 ± 39.8 sec.; $P <0.0001$; Supplementary Figure 2.8A) SR-B1/ApoE DKO mice.

Knocking out NBEAL2 in ApoE single KO mice also significantly increased tail bleeding times (1143.3 ± 46.9 sec. vs. 134.5 ± 9.7 sec.; P <0.0001; Supplementary Figure 2.7). SR-B1/ApoE DKO mice exhibited a significant increase in tail bleeding times compared to ApoE single KO mice (327.7 ± 29.1 sec. vs. 134.5 ± 9.7 sec.; P <0.05; Supplementary Figure 2.7), which is consistent with thrombocytopenia reported for mice deficient in SR-B1[29,30,33,34,39]. Nonetheless, the increase in tail bleeding times seen with NBEAL2 deficiency is consistent with previous studies[20,22], and further confirms the prominent role of NBEAL2 in proper platelet function.

2.4.2 NBEAL2 KO Reduced Survival in Male SR-B1/ApoE DKO Mice

We examined whether knocking out NBEAL2 affected the survival of SR-B1/ApoE DKO mice. Male and female SR-B1/ApoE DKO mice had average survival times of 47.6 and 46.5 days respectively, which are consistent with a 50% mortality at 6 weeks of age previously reported for SR-B1/ApoE DKO mice[26]. However, NBEAL2 KO in male SR-B1/ApoE DKO mice reduced survival to an average of 40.3 days (Figure 2.1), whereas NBEAL2 KO did not affect survival of female SR-B1/ApoE DKO mice (average survival of 46.4 days; Supplementary Figure 2.8B). Based on these findings, we focused our analyses on 5-week-old male mice for this study, although selected analyses were also repeated in 5-week-old female mice.

Figure 2.1 – NBEAL2 KO Reduced Survival in Male SR-B1/ApoE DKO Mice. Kaplan-Meier survival curves for SR-B1/ApoE DKO (bolded line) and NBEAL2/SR-B1/ApoE TKO (dotted line) mice (n=14, 9). Mice were monitored until they reached cardiac endpoint, at which point they were humanely euthanized. Data were analyzed by the Mantel-Cox log-rank test. ***P <0.001.

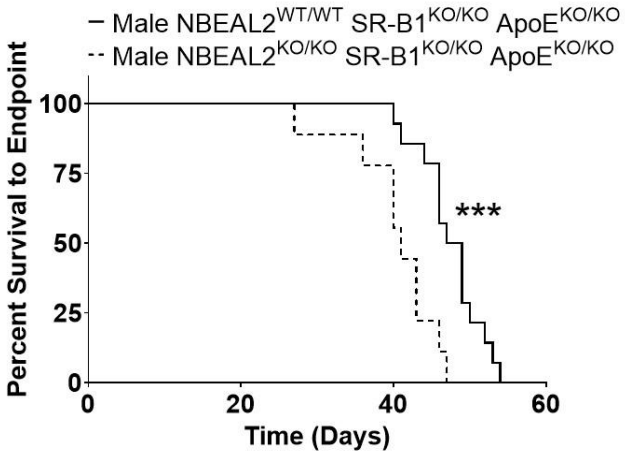

2.4.3 NBEAL2 KO Increased Plasma Total and Unesterified Cholesterol Levels and Circulating PCSK9 Levels in SR-B1/ApoE DKO Mice

Atherosclerosis is driven by inflammation and hypercholesterolemia; SR-B1/ApoE DKO mice exhibited substantially increased plasma IL-6 and TNFα levels compared to control ApoE single KO mice. However, NBEAL2 KO did not alter levels of these cytokines in SR-B1/ApoE DKO mice (Figure 2.2A and B). Since SR-B1/ApoE DKO mice develop hypercholesterolemia, with plasma total cholesterol levels 2-3 fold those of ApoE KO mice (Figure 2.2C)[40], we examined if whole-body deficiency of NBEAL2 had any effects on plasma cholesterol levels in these mice. Surprisingly, NBEAL2 KO increased plasma total and unesterified cholesterol levels but not esterified cholesterol or triglyceride levels in SR-B1/ApoE DKO mice (Figures 2.2C-E and H). These changes were associated with non-HDL but not HDL cholesterol (Figures 2.2F and G). To determine whether other aspects of lipid metabolism may be affected by NBEAL2 deficiency, we evaluated circulating levels of PCSK9, which reduces hepatocyte cell surface LDLR levels and promotes its degradation in lysosomes, which in turn increases plasma LDL cholesterol levels[41]. Interestingly, NBEAL2 KO significantly increased the levels of circulating PCSK9 in SR-B1/ApoE DKO mice (Figure 2.2I). In contrast, no differences in PCSK9 gene expression in the liver (the main source of circulating PCSK9), or in expression of other cholesterol-regulated genes[42] including sterol regulatory element-binding protein 2 (SREBP2), LDLR and 3-hydroxy-3-methyl-glutaryl-coenzyme A reductase (HMG-CoAR) were observed between SR-B1/ApoE DKO and

NBEAL2/SR-B1/ApoE TKO mice (Figures 2.2J-M). These findings suggest that NBEAL2 deficiency impacts PCSK9 protein levels at some post-transcriptional step in SR-B1/ApoE DKO mice and suggest that it has a previously unappreciated effect on plasma lipoprotein cholesterol metabolism. Further research is required to understand the mechanisms by which NBEAL2 KO impacts plasma PCSK9 and lipoprotein cholesterol levels.

Figure 2.2 – NBEAL2 KO Increased Plasma Total and Unesterified Cholesterol Levels and Circulating PCSK9 Levels in SR-B1/ApoE DKO Mice. (A) Plasma interleukin-6 (IL-6) (n=10, 10, 12, 10). (B) Plasma tumour necrosis factor alpha (TNFα) (n=10 per group). (C) Plasma total cholesterol (n=9, 9, 13, 8). (D) Plasma unesterified cholesterol (n=9, 9, 13, 8). (E) Plasma esterified cholesterol (calculated as the difference between total and unesterified cholesterol) (n=9, 9, 13, 8). (F) Plasma HDL cholesterol (n=9, 9, 12, 8). (G) Plasma non-HDL cholesterol (calculated as the difference between total and HDL cholesterol) (n=8, 8, 12, 8). (H) Plasma triglycerides (n=10, 10, 13, 8). (I) Plasma PCSK9 (n=10 per group). RT-PCR analysis of hepatic PCSK9 (J), sterol regulatory element-binding protein 2 (SREBP2) (K), low-density lipoprotein receptor (LDLR) (L), and 3-hydroxy-3-methyl-glutaryl-coenzyme A reductase (HMG-CoAR) (M) transcript levels in male SR-B1/ApoE DKO and NBEAL2/SR-B1/ApoE TKO mice (n=10 per group). Transcript levels are expressed as fold change relative to SR-B1/ApoE DKO mice and were normalized to glyceraldehyde 3-phosphate dehydrogenase (GAPDH) mRNA. Each data point represents an individual mouse. Bars represent means and error bars represent standard errors of the mean. Data in (A) to (I) were analyzed by one-way ANOVA and Tukey's post-hoc test. Data in (J) and (L) passed the normality test and were analyzed by Student's t-test. Data in (K) and (M) did not pass the normality test and were analyzed by Mann-Whitney Rank Sum Test. ns = not statistically significant; *P <0.05, ***P <0.001, ****P <0.0001.

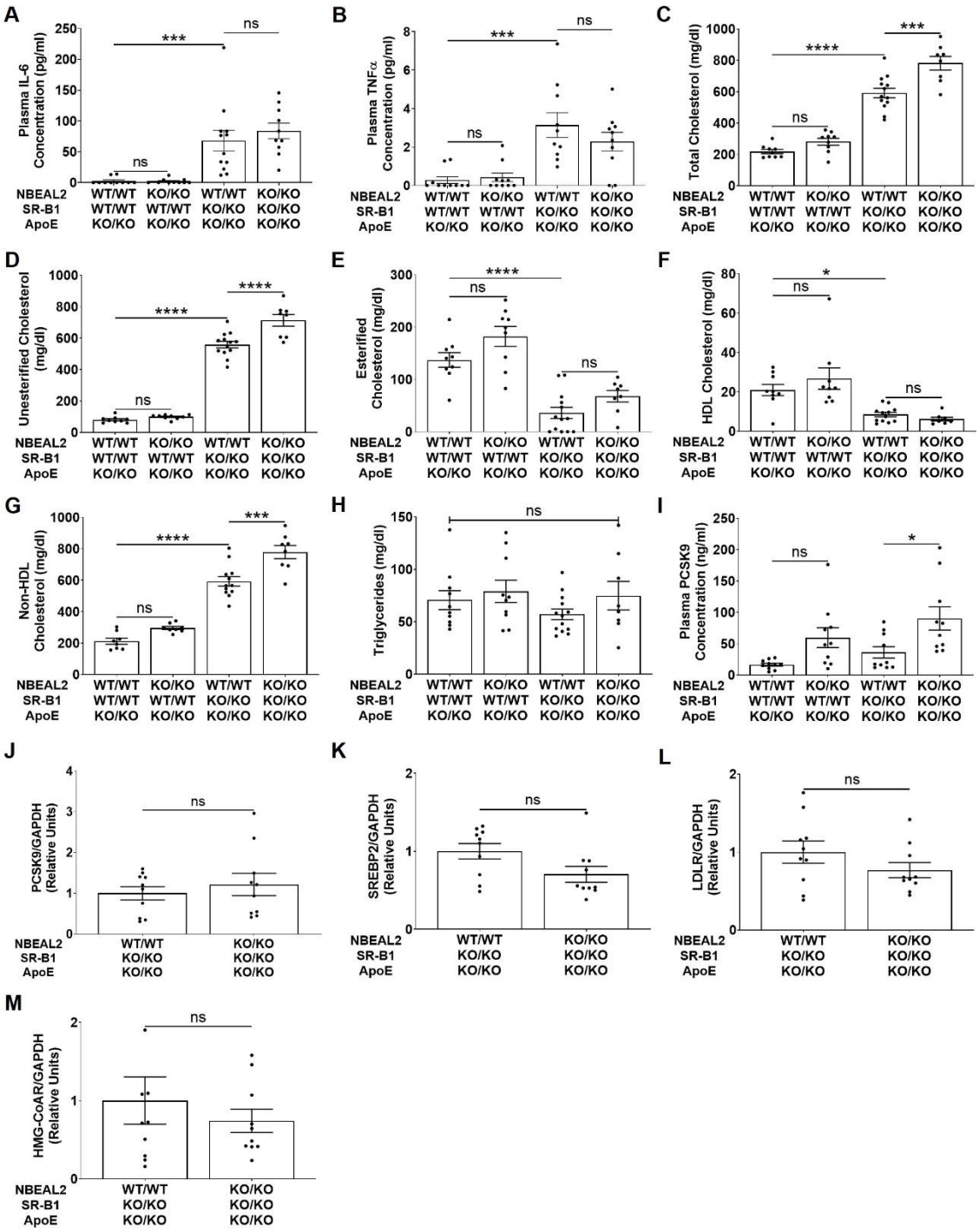
A
Plasma IL-6 Concentration (pg/ml)
B
Plasma TNFα Concentration (pg/ml)
C
Total Cholesterol (mg/dl)
D
Unesterified Cholesterol (mg/dl)
E
Esterified Cholesterol (mg/dl)
F
HDL Cholesterol (mg/dl)
G
Non-HDL Cholesterol (mg/dl)
H
Triglycerides (mg/dl)
I
Plasma PCSK9 Concentration (ng/ml)
J
PCSK9/GAPDH (Relative Units)
K
SREBP2/GAPDH (Relative Units)
L
LDLR/GAPDH (Relative Units)
M
HMG-CoAR/GAPDH (Relative Units)
ns
NBEAL2 WT/WT KO/KO WT/WT KO/KO
SR-B1 WT/WT WT/WT KO/KO KO/KO
ApoE KO/KO KO/KO KO/KO KO/KO

2.4.4 NBEAL2 KO Reduced Aortic Sinus and Coronary Artery Atherosclerosis and Platelet Accumulation in Atherosclerotic Coronary Arteries in SR-B1/ApoE DKO Mice

Since NBEAL2 KO increased plasma cholesterol levels in SR-B1/ApoE DKO mice, we examined whether NBEAL2 KO affected the burden of atherosclerosis in these mice. Consistent with previous reports[26,34,36,43], male and female SR-B1/ApoE DKO mice developed extensive atherosclerosis in the aortic sinus (males, Figures 2.3A, C, E and F and females, Supplementary Figures 2.8C, E and F) and coronary arteries (males, Figures 2.3G-K and females, Supplementary Figure 2.8G) at 5 weeks of age. Interestingly, NBEAL2 KO reduced the levels of atherosclerosis in the aortic sinus of both male ($3.1 \times 10^6 \pm 0.44 \times 10^6$ μm^3 vs. $6.7 \times 10^6 \pm 1.2 \times 10^6$ μm^3; $P < 0.01$; Figures 2.3D-F) and female ($8.2 \times 10^6 \pm 0.99 \times 10^6$ μm^3 vs. $18 \times 10^6 \pm 3.5 \times 10^6$ μm^3; $P < 0.05$; Supplementary Figures 2.8D-F) SR-B1/ApoE DKO mice. Similarly, NBEAL2 KO significantly decreased the proportion of coronary arteries in which the lumen was fully (100%) occluded by atherosclerotic plaque in both male ($6.9 \pm 0.9\%$ vs. $15.5 \pm 2.0\%$; $P < 0.0001$; Figure 2.3K) and female ($7.1 \pm 1.5\%$ vs. $15.1 \pm 1.1\%$; $P < 0.0001$; Supplementary Figure 2.8G) SR-B1/ApoE DKO mice. Corresponding increases were observed in the proportions of coronary arteries lacking atherosclerotic plaques (0% occluded) (Figure 2.3K and Supplementary Figure 2.8G). ApoE single KO and NBEAL2/ApoE DKO mice did not develop atherosclerosis at this age in either the aortic sinus or coronary arteries (Figures 2.3A, B, E, F, and K), as expected. Overall, our data

suggest that NBEAL2 KO reduces atherosclerosis development in both the aortic sinus and coronary arteries of SR-B1/ApoE DKO mice and that this occurs despite the increased plasma cholesterol and PCSK9 levels.

Consistent with our previous work[34], a substantial percentage of atherosclerotic coronary arteries in SR-B1/ApoE DKO mice exhibited CD41 immunostaining (Figures 2.3L and P), suggesting the presence of platelets within atherosclerotic plaques. Since NBEAL2 KO induces thrombocytopenia and improper platelet function[20,21], we sought to determine if NBEAL2 KO in SR-B1/ApoE DKO mice impacted platelet accumulation in atherosclerotic coronary arteries. Interestingly, NBEAL2/SR-B1/ApoE TKO mice had significantly reduced proportions of atherosclerotic coronary arteries that were positive for CD41 staining compared to SR-B1/ApoE DKO mice (59.5 ± 4.0% vs. 78.8 ± 4.0%; $P < 0.01$; Figures 3N and P). Since we only analyzed atherosclerotic coronary arteries and ApoE single KO mice and NBEAL2/ApoE DKO mice did not exhibit evidence of coronary artery atherosclerosis, we only performed CD41 analysis on SR-B1/ApoE DKO and NBEAL2/SR-B1/ApoE TKO mice. Taken together, these data suggest that in addition to reducing the degree of aortic sinus and coronary artery atherosclerosis, NBEAL2 KO reduced platelet accumulation in atherosclerotic coronary arteries in SR-B1/ApoE DKO mice.

Figure 2.3 – NBEAL2 KO Reduced Aortic Sinus and Coronary Artery Atherosclerosis Burden and Platelet Accumulation in Atherosclerotic Coronary Arteries in SR-B1/ApoE DKO Mice. Representative images of oil red O-stained transverse sections of the aortic sinus showing atherosclerotic plaque from ApoE KO (A), NBEAL2/ApoE DKO (B), SR-B1/ApoE DKO (C) and NBEAL2/SR-B1/ApoE TKO (D) mice. Scale bar= 200 μm. (E) Aortic sinus atherosclerotic plaque cross-sectional areas vs. distance and (F) atherosclerotic plaque volumes (areas under the curves of plaque area vs. distance) of ApoE KO (black), NBEAL2/ApoE DKO (red), SR-B1/ApoE DKO (blue) and NBEAL2/SR-B1/ApoE TKO mice (green). Data points in (E) represent means (n=9, 10, 13, 12). Seven sections of each heart were stained with oil red O/hematoxylin, and coronary arteries were scored as either non-atherosclerotic (0%) or containing atherosclerotic plaques that occluded <50%, >50% or 100% of their lumen. (G) to (J) Representative images of coronary arteries for each category are shown. Scale bar= 50 μm. (K) Quantification of coronary arteries in each category (as percentage of total) across seven heart sections (n=10, 10, 13, 12). Representative images of CD41 immunofluorescence (green) and DAPI counterstaining from SR-B1/ApoE DKO (L) and NBEAL2/SR-B1/ApoE TKO (N) mice, with adjacent sections stained with oil red O (M and O). Scale bar= 50 μm. (P) Proportions of atherosclerotic coronary arteries with positive CD41 immunofluorescence staining across seven heart sections for each mouse (n=10 per group). Each data point represents an individual mouse. Bars represent means and error bars represent standard errors

of the mean. Data in (E) and (K) were analyzed by two-way ANOVA with Sidak's multiple comparisons post-hoc test. Data in (F) were analyzed by one-way ANOVA and Tukey's post-hoc test. Data in (P) passed the normality test and were analyzed by Student's t-test. *P <0.05, **P <0.01, ****P <0.0001.

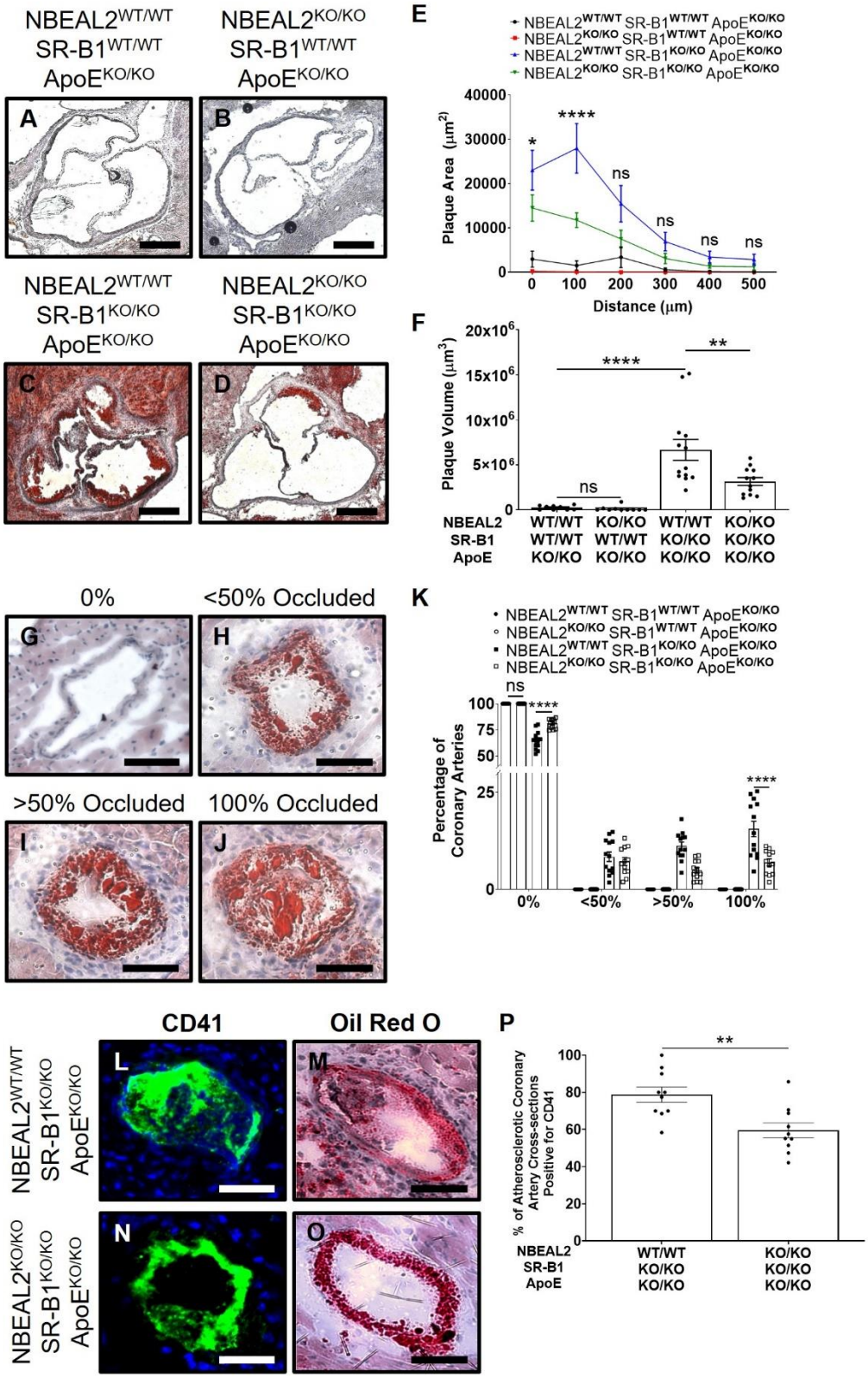
NBEAL2WT/WT SR-B1WT/WT ApoEKO/KO
NBEAL2KO/KO SR-B1WT/WT ApoEKO/KO
NBEAL2WT/WT SR-B1KO/KO ApoEKO/KO
NBEAL2KO/KO SR-B1KO/KO ApoEKO/KO
A
B
C
D
E
Plaque Area (μm2)
Distance (μm)
F
Plaque Volume (μm3)
NBEAL2 WT/WT KO/KO WT/WT KO/KO
SR-B1 WT/WT WT/WT KO/KO KO/KO
ApoE KO/KO KO/KO KO/KO KO/KO
0%
<50% Occluded
>50% Occluded
100% Occluded
G
H
I
J
K
Percentage of Coronary Arteries
CD41
Oil Red O
L
M
N
O
P
% of Atherosclerotic Coronary Artery Cross-sections Positive for CD41

2.4.5 NBEAL2 KO Worsened Myocardial Fibrosis in SR-B1/ApoE DKO Mice Despite Reduced Aortic Sinus and Coronary Artery Atherosclerosis

Since NBEAL2 KO had protective effects against aortic sinus and coronary artery atherosclerosis in SR-B1/ApoE DKO mice, we examined the levels of myocardial fibrosis. ApoE single KO and NBEAL2/ApoE DKO mice at this age exhibited no detectable myocardial fibrosis (Figures 2.4A, B and E). Both male and female SR-B1/ApoE DKO mice exhibited myocardial fibrosis (Figure 4C and Supplementary Figure 2.8H), which is consistent with previous findings of coronary artery atherosclerosis being accompanied by myocardial fibrosis in SR-B1/ApoE DKO mice[26,34]. Surprisingly, however, male NBEAL2/SR-B1/ApoE TKO mice exhibited significantly increased levels of myocardial fibrosis compared to SR-B1/ApoE DKO mice (8.7 ± 2.1% vs. 4.3 ± 0.8%; $P < 0.05$; Figures 2.4D and E), whereas no significant differences in myocardial fibrosis were seen between female NBEAL2/SR-B1/ApoE TKO and SR-B1/ApoE DKO mice (5.6 ± 2.3% vs. 3.7 ± 1.3%; Supplementary Figures 2.8H-J). Heart weight:tibia length ratios and plasma levels of creatine kinase-myocardial band (CK-MB), a circulating marker of myocardial damage, were increased in SR-B1/ApoE DKO and NBEAL2/SR-B1/ApoE TKO mice relative to ApoE single KO and NBEAL2/ApoE DKO mice, but were not different between SR-B1/ApoE DKO and NBEAL2/SR-B1/ApoE TKO mice (Figures 2.4F and G), despite the increased myocardial fibrosis in the latter. There were also no significant differences in heart weight:tibia length ratios

between female SR-B1/ApoE DKO and NBEAL2/SR-B1/ApoE TKO mice (Supplementary Figure 2.8K).

Figure 2.4 – NBEAL2 KO Worsened Myocardial Fibrosis in SR-B1/ApoE DKO Mice. Representative images of Masson's trichrome-stained transverse cryosections of myocardium from ApoE KO (A), NBEAL2/ApoE DKO (B), SR-B1/ApoE DKO (C), and NBEAL2/SR-B1/ApoE TKO (D) mice. Red colored staining indicates undamaged cardiomyocytes, whereas blue/purple colored staining indicates the presence of collagen. Scale bar= 200 μm. (E) Quantification of the percentage of myocardial fibrosis measured by the area of blue staining relative to the cross-sectional area of the heart for one section per mouse (n=9, 9, 11, 10). Each data point represents an individual mouse. Bars represent means and error bars represent standard errors of the mean. (F) Heart weight-to-tibia length ratios (n=18, 21, 26, 25). (G) Plasma CK-MB levels (n=10, 10, 11, 10). All data were analyzed by one-way ANOVA and Tukey's post-hoc test. *P <0.05, **P <0.01.

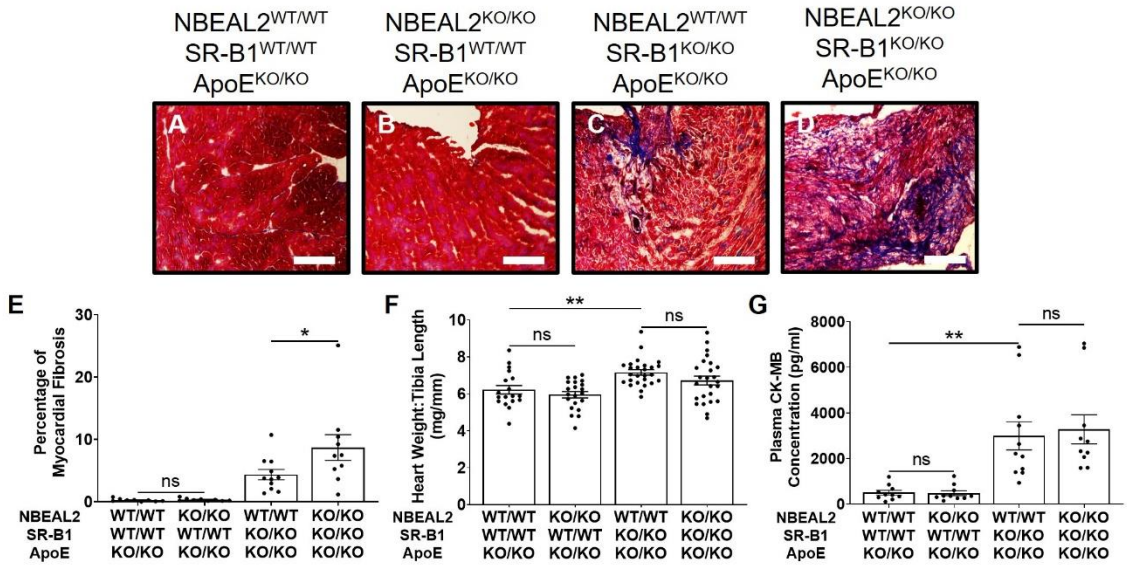

2.4.6 NBEAL2 KO Increased Circulating Neutrophils and Reduced Neutrophil Granularity in SR-B1/ApoE DKO Mice

To investigate the potential mechanisms that might be related to the reduced atherosclerosis or increased myocardial fibrosis in the male NBEAL2/SR-B1/ApoE TKO compared to the SR-B1/ApoE DKO mice, we measured the levels of various circulating blood cells via flow cytometry. Compared to ApoE single KO mice, SR-B1/ApoE DKO mice had an approximate 3-4-fold increase in levels of circulating neutrophils and monocytes (Figures 2.5A and C). Compared to SR-B1/ApoE DKO mice, NBEAL2/SR-B1/ApoE TKO mice exhibited significantly increased levels of neutrophils in blood (858.6 ± 210.7 cells/μL vs. 251.2 ± 25.8 cells/μL; $P < 0.001$; Figure 2.5A) and significantly reduced side scatter (measure of granularity) of neutrophils ($5.8 \times 10^6 \pm 1.5 \times 10^3$ vs. $9.9 \times 10^6 \pm 3.6 \times 10^3$; $P < 0.0001$; Figure 2.5B). The observed increase in blood neutrophil counts and reduced granularity caused by NBEAL2 deficiency is consistent with previous findings[23,24]. One of these studies found that compared to wild-type mice, NBEAL2 KO mice had similar levels of circulating monocytes, but reduced monocyte granularity (albeit to a much lesser extent than the reduced granularity seen in neutrophils)[23]. Likewise, we found that NBEAL2 KO in SR-B1/ApoE DKO mice did not significantly increase circulating monocyte levels (Figure 2.5C). However, NBEAL2 KO did not affect monocyte granularity in SR-B1/ApoE DKO mice, although it significantly reduced monocyte granularity in ApoE single KO mice (Figure 2.5D). NBEAL2 KO resulted in increased circulating $Ly6C^{hi}$ monocytes and reduced $CD4^+$ T-cells in male SR-

B1/ApoE DKO mice, but did not affect other circulating immune cells (Supplementary Figures 2.9A-I). As seen in male mice, NBEAL2 KO in female SR-B1/ApoE DKO mice significantly increased circulating neutrophil levels, reduced neutrophil granularity, and did not affect monocyte granularity (Supplementary Figures 2.10A-B and D); however, NBEAL2 KO increased circulating monocyte levels (Supplementary Figure 2.10C). In female SR-B1/ApoE DKO mice, NBEAL2 deficiency increased circulating Ly6C^{mid} and Ly6C^{hi} monocytes, but did not affect other circulating immune cells (Supplementary Figures 2.10E-M).

Figure 2.5 – NBEAL2 KO Increased Levels of Circulating Neutrophils and Reduced Neutrophil Granularity in SR-B1/ApoE DKO Mice. (A) Blood neutrophils. (B) Neutrophil side scatter. (C) Blood monocytes. (D) Monocyte side scatter. N= 11, 10, 13, 10 for all flow cytometry analyses. Blood was collected into a heparinized tube via cheek puncture using a lancet. Flow cytometry was performed on a BD FACSCalibur Flow Cytometry system, and data were analyzed using FlowJo v10. Granularity of cells were determined by the amount of side scatter (SSC). Each data point represents an individual mouse. Bars represent means and error bars represent standard errors of the mean. All data were analyzed by one-way ANOVA and Tukey's post-hoc. ***P <0.001, ****P <0.0001.

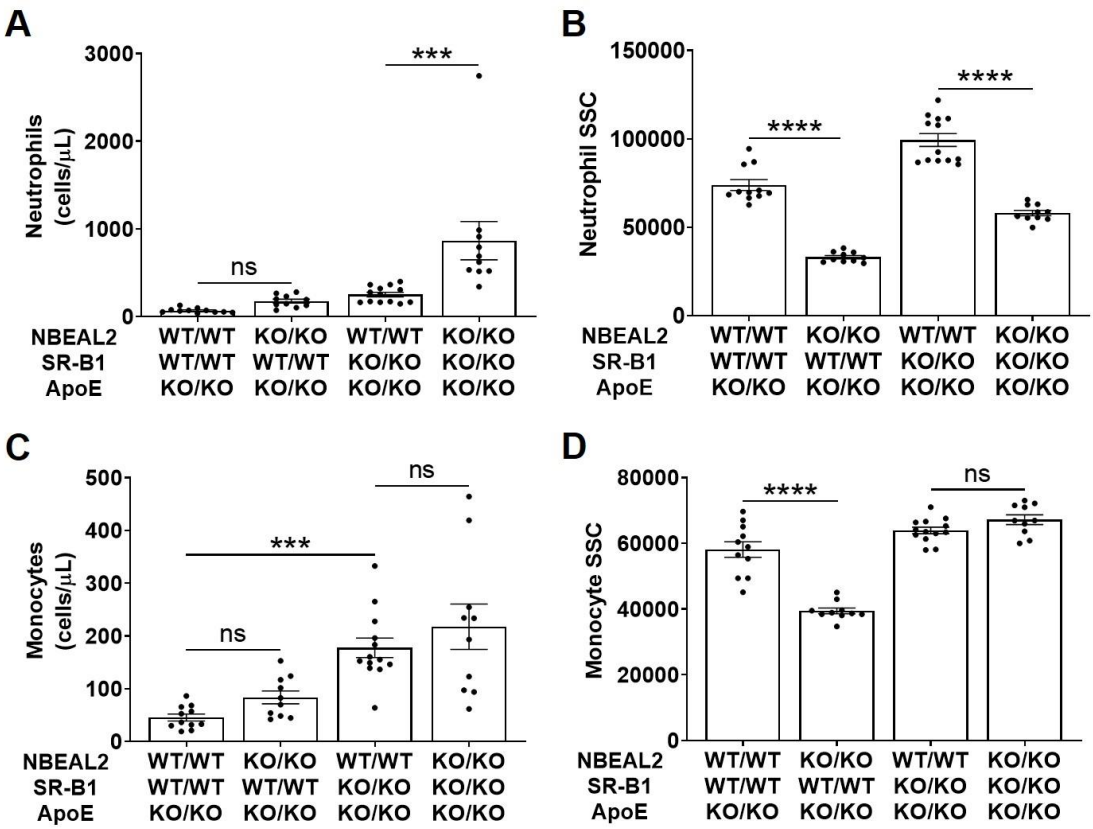

2.4.7 NBEAL2 KO Reduced the Proportion of Myeloperoxidase-Positive Neutrophils in the Myocardium of SR-B1/ApoE DKO Mice

Given the important role of neutrophils in myocardial repair in myocardial infarction and/or ischemia/reperfusion injury[44–46], and the observed effects of NBEAL2 deficiency on neutrophils in SR-B1/ApoE DKO mice, we examined levels of neutrophils and the neutrophil enzyme MPO in heart sections from SR-B1/ApoE DKO and NBEAL2/SR-B1/ApoE TKO mice. Neutrophil abundance (identified by immunofluorescence for Ly6G) in cardiac cross-sections increased substantially in SR-B1/ApoE DKO compared to ApoE single KO samples but was not affected by NBEAL2 KO (Figures 2.6A-D and Q). Co-immunofluorescence staining for MPO, an enzyme stored in neutrophil secretory granules and secreted upon neutrophil activation, revealed corresponding increases in MPO in cardiac cross-sections from SR-B1/ApoE DKO compared to ApoE single KO mice but was also not affected by NBEAL2 KO (Figures 2.6E-H and R). Analysis of co-immunofluorescence for both Ly6G and MPO revealed less co-staining of the two markers in sections from NBEAL2/SR-B1/ApoE TKO compared to SR-B1/ApoE DKO mice (Figures 2.6M-P and S), suggesting that NBEAL2/SR-B1/ApoE TKO mice exhibited reduced MPO-positive neutrophils in the myocardium compared to SR-B1/ApoE DKO mice (25.3 ± 7.0% vs. 42.7 ± 6.8%; $P < 0.05$; Figure 2.6S). Since MPO is normally stored in neutrophil secretory granules, reduction in the proportion of neutrophils positive for MPO appears to be consistent with the observed

reduction in neutrophil granularity and with previous reports of increased levels of neutrophil granular proteins including MPO in plasma of NBEAL2 deficient mice[23,24].

Figure 2.6 – NBEAL2 KO Reduced the Proportion of MPO-Positive Neutrophils in the Myocardium of SR-B1/ApoE DKO Mice. Representative images of transverse cryosections of the myocardium stained with neutrophils via Ly6G (green) (A-D), MPO (red) (E-H) and DAPI (blue) (I-L) by immunofluorescence co-staining. Merged images are shown in (M-P), and MPO-positive neutrophils are detected as yellow. Scale bar= 250 μm. (Q) Quantification of Ly6G fluorescence intensity in the myocardium (n=5, 5, 12, 11). (R) Quantification of MPO fluorescence intensity in the myocardium (n=5, 5, 12, 11). (S) Percentage of MPO-positive neutrophils in the myocardium, taken by the proportion of MPO-positive neutrophils (yellow) to the total amount of neutrophils (green) (n=12, 11). Each data point represents an individual mouse. Bars represent means and error bars represent standard errors of the mean. Data in (Q) and (R) were analyzed by one-way ANOVA and Tukey's post-hoc test. Data in (S) passed the normality test and were analyzed by Student's t-test. *P <0.05.

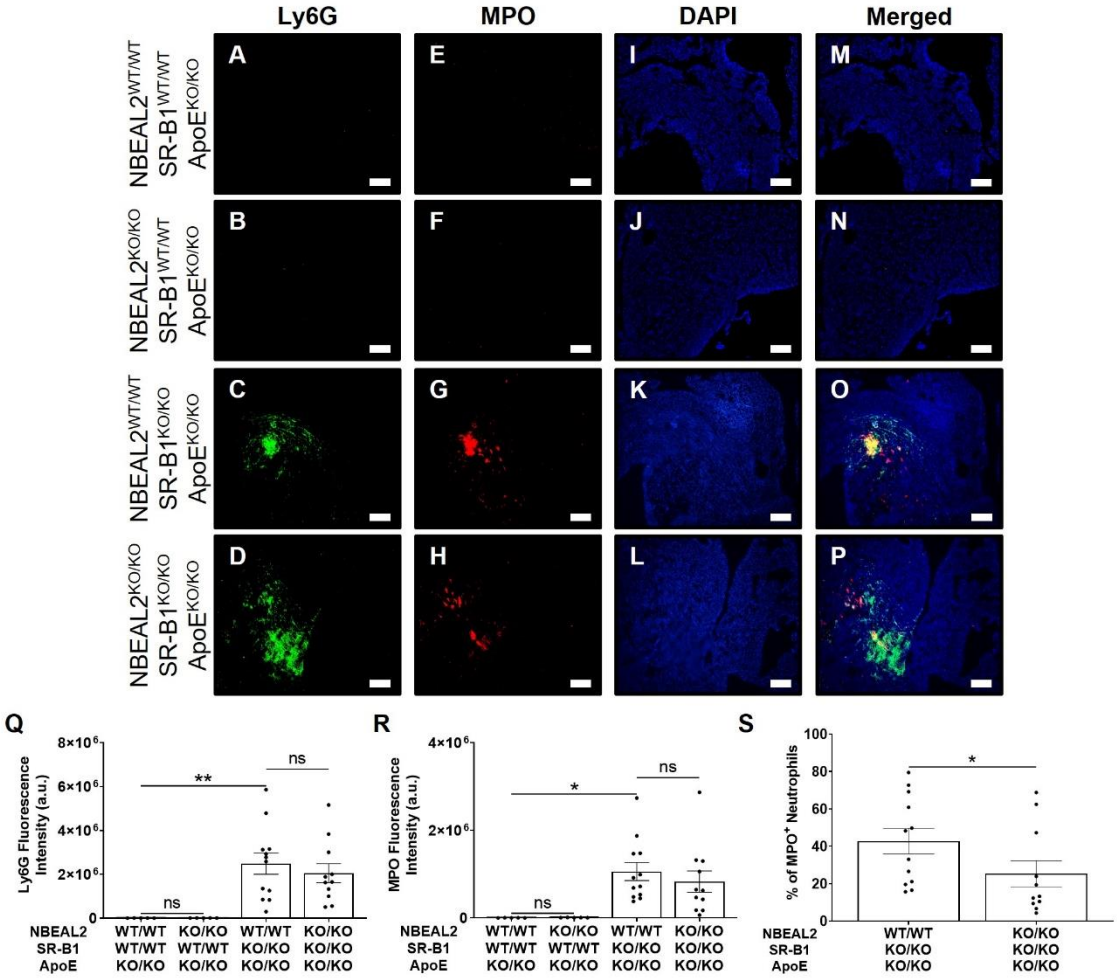
Ly6G
MPO
DAPI
Merged
NBEAL2WT/WT SR-B1WT/WT ApoEKO/KO
NBEAL2KO/KO SR-B1WT/WT ApoEKO/KO
NBEAL2WT/WT SR-B1KO/KO ApoEKO/KO
NBEAL2KO/KO SR-B1KO/KO ApoEKO/KO
A
B
C
D
E
F
G
H
I
J
K
L
M
N
O
P
Q
Ly6G Fluorescence Intensity (a.u.)
8×10^6
6×10^6
4×10^6
2×10^6
0
**
ns
ns
R
MPO Fluorescence Intensity (a.u.)
4×10^6
2×10^6
0
*
ns
ns
S
% of MPO+ Neutrophils
100
80
60
40
20
0
*
NBEAL2
SR-B1
ApoE
WT/WT WT/WT KO/KO
KO/KO WT/WT KO/KO
WT/WT KO/KO KO/KO
KO/KO KO/KO KO/KO

2.5 Discussion

SR-B1/ApoE DKO mice develop aortic sinus and coronary artery atherosclerosis with platelet accumulation in atherosclerotic coronary arteries and myocardial fibrosis by 5 weeks of age when fed a normal chow diet[26,34,36,43]. NBEAL2 deficiency is associated with loss of secretory vesicles in affected cells, including platelet α-granules which are required for proper platelet function[16–18,20–23], and other blood cells such as neutrophils. Neutrophil granules are required for proper neutrophil functions including release of MPO[23,24]. Considering the role of these cells in CAD development, we sought to determine the effects of NBEAL2 knockout on CAD phenotypes in SR-B1/ApoE DKO mice.

Hypercholesterolemia is prominent in SR-B1/ApoE DKO mice and is a major driving force for extensive atherosclerosis development in these mice[40]. Therefore, we wanted to determine whether NBEAL2 KO would have any affects on plasma lipid levels. Surprisingly, NBEAL2/SR-B1/ApoE TKO mice had significantly increased levels of plasma total and unesterified cholesterol levels compared to SR-B1/ApoE DKO mice. We have previously shown that rosuvastatin treatment in SR-B1/ApoE DKO mice increased plasma cholesterol levels, as well as plasma PCSK9 levels[34]. Since PCSK9 increases plasma LDL cholesterol levels[41], we examined whether NBEAL2 KO may be causing an increase in circulating PCSK9 levels in SR-B1/ApoE DKO mice. Compared to SR-B1/ApoE DKO mice, NBEAL2/SR-B1/ApoE TKO mice had increased circulating PCSK9 levels, which likely explains the increase in plasma cholesterol levels. However, it still remains

unclear as to why NBEAL2 deficiency led to increased circulating cholesterol and PCSK9 levels. Interestingly, neurobeachin-like 1 (NBEAL1), which belongs to the same family of proteins as NBEAL2, has been shown to affect cholesterol metabolism by modulating SREBP2 processing and activity and LDLR expression[47]. Low expression of NBEAL1 in primary endothelial cells reduces the expression levels of HMG-CoAR and LDLR and inhibits LDL uptake[47]. Since NBEAL2 is in the same family of proteins as NBEAL1, we wanted to determine whether NBEAL2 KO would also affect the mRNA levels of these genes which are involved in the cholesterol metabolism pathway. However, there were no significant differences in hepatic PCSK9, SREBP2, LDLR, and HMG-CoAR mRNA levels between SR-B1/ApoE DKO and NBEAL2/SR-B1/ApoE TKO mice. This suggests that the increase in plasma cholesterol and PCSK9 levels in NBEAL2/SR-B1/ApoE TKO mice is occurring independently of the transcriptional levels of the genes mentioned. Consistent with a previous report[48], we detected expression of NBEAL2 mRNA in the liver (data not shown). Since PCSK9 is secreted by hepatocytes[49], it is possible that NBEAL2 KO may be dysregulating normal secretion of PCSK9 from hepatocytes in a manner analogous to its effects on the secretion of platelet α-granule and neutrophil granule contents, resulting in an increase in circulating PCSK9 levels and in turn, reducing LDLR surface expression and increasing cholesterol levels. However, further investigation is required to elucidate the factors contributing to the increased circulating PCSK9 and cholesterol levels seen in NBEAL2/SR-B1/ApoE TKO mice.

Despite the increased plasma PCSK9 and plasma cholesterol levels in the NBEAL2/SR-B1/ApoE TKO mice, atherosclerosis in both the aortic sinus and coronary arteries were reduced compared to SR-B1/ApoE DKO mice. This suggests that the reduction in atherosclerosis is independent of the increased circulating cholesterol and PCSK9 levels. Moreover, the reduction in atherosclerosis appears to be independent of changes in circulating cytokine levels, as we observed no effects of NBEAL2 deficiency on circulating IL-6 and TNFα levels. We have previously shown that SR-B1/ApoE DKO mice had a significant proportion of their coronary arteries stain positive for platelets[34], suggesting the possibility of platelet-rich thrombi in the atherosclerotic plaques. Since NBEAL2 KO induces thrombocytopenia and affects proper platelet function in mice[20], we examined whether platelet accumulation in atherosclerotic coronary arteries would be affected. Indeed, NBEAL2 KO significantly reduced the proportion of atherosclerotic coronary arteries that stained positive for platelets in SR-B1/ApoE DKO mice, suggesting that NBEAL2 KO reduces the ability of platelets to accumulate in atherosclerotic plaques. Considering the role of platelets in atherosclerosis development, the reduced accumulation of platelets is likely a factor, at least in coronary arteries, that influences the reduction of atherosclerosis in SR-B1/ApoE DKO mice. However, it is important to point out that in our analysis, we report a reduction in the proportion of platelet-positive *atherosclerotic* coronary arteries, which may reflect reduced accumulation of platelets within pre-existing atherosclerotic plaques in NBEAL2/SR-B1/ApoE TKO mice. Further research is

required to determine the cause-effect relationship between development of atherosclerosis in coronary arteries and platelet accumulation in atherosclerotic coronary arteries.

Surprisingly, despite NBEAL2 KO reducing aortic sinus and coronary artery atherosclerosis in SR-B1/ApoE DKO mice, there was an increase in myocardial fibrosis levels. This was unexpected, as mice that have less coronary artery atherosclerotic burden generally tend to have reduced myocardial fibrosis levels[26,28,34,36,43,50,51]. On the other hand, NBEAL2 KO in female SR-B1/ApoE DKO mice did not increase levels of myocardial fibrosis. These differences may in part explain why NBEAL2 KO in male but not female SR-B1/ApoE DKO mice led to reduced survival. Therefore, female NBEAL2/SR-B1/ApoE TKO mice may be more tolerant to aortic sinus and coronary artery atherosclerosis burden. However, further studies are required to elucidate the mechanisms by which NBEAL2 KO in female SR-B1/ApoE DKO mice results in less profound myocardial fibrosis compared to NBEAL2 KO in male SR-B1/ApoE DKO mice.

To elucidate the mechanisms by which NBEAL2 KO caused increased myocardial fibrosis despite reduced aortic sinus and coronary artery atherosclerosis in male SR-B1/ApoE DKO mice, we examined whether NBEAL2 KO affected blood immune cells in SR-B1/ApoE DKO mice. Consistent with previous reports[23,24], NBEAL2 KO increased blood neutrophil levels, reduced neutrophil granularity, and did not affect blood monocyte levels in SR-B1/ApoE DKO mice. Although one study reported a decrease in monocyte granularity in

NBEAL2 KO mice compared to wild-type mice[23], NBEAL2 KO did not affect monocyte granularity in SR-B1/ApoE DKO mice. Since NBEAL2 KO affected both circulating neutrophil levels and neutrophil granularity in SR-B1/ApoE DKO mice, it is possible that neutrophils, which normally play an important role in the inflammatory response to ischemia/infarction and healing[44–46], may be dysfunctional and influence myocardial fibrosis development. Immunofluorescence co-staining of Ly6G and MPO in the myocardium of SR-B1/ApoE DKO and NBEAL2/SR-B1/ApoE TKO mice revealed no significant differences in either neutrophil or MPO fluorescence intensity. However, since NBEAL2 KO in mice have been shown to have increased MPO in plasma, presumably due to either immature release of MPO or leakage during hematopoiesis[23], we examined whether the proportion of MPO-positive neutrophils were altered in the myocardium of NBEAL2/SR-B1/ApoE TKO mice. Interestingly, NBEAL2/SR-B1/ApoE TKO mice exhibited significantly reduced MPO-positive neutrophils in the myocardium compared to SR-B1/ApoE DKO mice. This suggests that NBEAL2 KO is likely causing dysfunctional regulation of neutrophils and their granular protein release, which may hinder proper myocardial infarction repair in the infarcted myocardium.

Considering the role of NBEAL2 in regulating secretory vesicles and secretion, and the reduced neutrophil granularity seen in NBEAL2/SR-B1/ApoE TKO mice compared to SR-B1/ApoE DKO mice in this study, it is possible that NBEAL2 KO results in a general increase in protein secretion in other unreported cell types such as hepatocytes, which may explain the increased circulating

PCSK9 levels. However, confirming the precise role of NBEAL2 in PCSK9 secretion requires further investigation. Nonetheless, we need to consider the potential effects that increased circulating PCSK9 levels seen in NBEAL2/SR-B1/ApoE TKO mice may have on myocardial fibrosis. A pilot study reported that in patients, circulating PCSK9 levels were associated with reduced left ventricular ejection fraction after myocardial infarction, independent of serum LDL cholesterol levels and statin use[52]. This suggests that circulating PCSK9 may impair cardiac remodelling post-myocardial infarction. An additional study subjected mouse hearts to left coronary artery occlusion and reported a significant increase in PCSK9 protein levels in the zone bordering the infarct area[53]. Inhibition of PCSK9 gene expression and/or function reduced cardiomyocyte autophagy and infarct sizes, independent of circulating LDL cholesterol levels[53]. These findings suggest that PCSK9 may have direct effects on cardiomyocyte survival and heart function. Therefore, the increased circulating PCSK9 may have direct effects on myocardial fibrosis in NBEAL2/SR-B1/ApoE TKO mice. Further experiments are required to determine whether other factors are directly contributing to the increased myocardial fibrosis seen in NBEAL2/SR-B1/ApoE TKO mice compared to SR-B1/ApoE DKO mice.

In conclusion, this is the first *in vivo* study examining the effects of NBEAL2 KO on atherosclerosis in a mouse model that exhibits multiple features of CAD, including coronary artery atherosclerosis, platelet accumulation in atherosclerotic coronary arteries, and myocardial fibrosis. Our findings suggest that although

whole-body deficiency of NBEAL2 may protect against aortic sinus and coronary artery atherosclerosis development, other effects of NBEAL2 deficiency, particularly on the heart, may outweigh those benefits. Our findings also demonstrate the importance of proper platelet and/or neutrophil function and granule retention in cardiovascular disease. Overall, our study provides important insights into the role of NBEAL2 on CAD development in mice, and demonstrates the importance of utilizing a mouse model that not only develops atherosclerosis, but also exhibits features of human CAD, namely myocardial fibrosis, when elucidating mechanisms and/or targeting new pathways that either contribute to and/or reduce CAD development.

2.6 References

1. Ralapanawa U, Sivakanesan R. Epidemiology and the Magnitude of Coronary Artery Disease and Acute Coronary Syndrome: A Narrative Review. *Journal of Epidemiology and Global Health*. 2021;11(2):169–177.
2. Hansson GK, Hermansson A. The immune system in atherosclerosis. *Nature Immunology*. 2011;12(3):204–212.
3. Bentzon JF, Otsuka F, Virmani R, Falk E. Mechanisms of plaque formation and rupture. *Circulation Research*. 2014;114(12):1852–1866.
4. Leys D. Atherothrombosis: a major health burden. *Cerebrovascular Diseases (Basel, Switzerland)*. 2001;11 Suppl 2:1–4.

5. Bakogiannis C, Sachse M, Stamatelopoulos K, Stellos K. Platelet-derived chemokines in inflammation and atherosclerosis. *Cytokine*. 2019;122:154157.
6. Gawaz M, Langer H, May AE. Platelets in inflammation and atherogenesis. *The Journal of Clinical Investigation*. 2005;115(12):3378–3384.
7. Zernecke A, Weber C. Chemokines in atherosclerosis: proceedings resumed. *Arteriosclerosis, Thrombosis, and Vascular Biology*. 2014;34(4):742–750.
8. Massberg S, Brand K, Grüner S, Page S, Müller E, Müller I, Bergmeier W, Richter T, Lorenz M, Konrad I, Nieswandt B, Gawaz M. A critical role of platelet adhesion in the initiation of atherosclerotic lesion formation. *The Journal of Experimental Medicine*. 2002;196(7):887–896.
9. Blair P, Flaumenhaft R. Platelet α–granules: Basic biology and clinical correlates. *Blood reviews*. 2009;23(4):177–189.
10. Coppinger JA, Cagney G, Toomey S, Kislinger T, Belton O, McRedmond JP, Cahill DJ, Emili A, Fitzgerald DJ, Maguire PB. Characterization of the proteins released from activated platelets leads to localization of novel platelet proteins in human atherosclerotic lesions. *Blood*. 2004;103(6):2096–2104.
11. Kahr WH, Zheng S, Sheth PM, Pai M, Cowie A, Bouchard M, Podor TJ, Rivard GE, Hayward CP. Platelets from patients with the Quebec platelet

disorder contain and secrete abnormal amounts of urokinase-type plasminogen activator. *Blood*. 2001;98(2):257–265.

12. Sheth PM, Kahr WHA, Haq MA, Veljkovic DK, Rivard GE, Hayward CPM. Intracellular activation of the fibrinolytic cascade in the Quebec Platelet Disorder. *Thrombosis and Haemostasis*. 2003;90(2):293–298.
13. Benet B, Lainey E, Fenneteau O, Baudouin V, Hurtaud-Roux M-F. [Usefulness of gray platelets observation in ARC syndrome]. *Annales De Biologie Clinique*. 2010;68(4):485–489.
14. Kim SM, Chang HK, Song JW, Koh H, Han SJ, Severance Pediatric Liver Disease Research Group. Agranular platelets as a cardinal feature of ARC syndrome. *Journal of Pediatric Hematology/Oncology*. 2010;32(4):253–258.
15. Gissen P, Johnson CA, Morgan NV, Stapelbroek JM, Forshew T, Cooper WN, McKiernan PJ, Klomp LWJ, Morris AAM, Wraith JE, McClean P, Lynch SA, Thompson RJ, Lo B, Quarrell OW, et al. Mutations in VPS33B, encoding a regulator of SNARE-dependent membrane fusion, cause arthrogryposis-renal dysfunction-cholestasis (ARC) syndrome. *Nature Genetics*. 2004;36(4):400–404.
16. Gunay-Aygun M, Falik-Zaccai TC, Vilboux T, Zivony-Elboum Y, Gumruk F, Cetin M, Khayat M, Boerkoel CF, Kfir N, Huang Y, Maynard D, Dorward H, Berger K, Kleta R, Anikster Y, et al. NBEAL2 is mutated in Gray Platelet Syndrome and is required for biogenesis of platelet alpha-granules. *Nature genetics*. 2011;43(8):732–734.

17. Albers CA, Cvejic A, Favier R, Bouwmans EE, Alessi M-C, Bertone P, Jordan G, Kettleborough RN, Kiddle G, Kostadima M, Read RJ, Sipos B, Sivapalaratnam S, Smethurst PA, Stephens J, et al. Exome sequencing identifies NBEAL2 as the causative gene for Gray Platelet Syndrome. *Nature genetics*. 2011;43(8):735–737.

18. Kahr WHA, Hinckley J, Li L, Schwertz H, Christensen H, Rowley JW, Pluthero FG, Urban D, Fabbro S, Nixon B, Gadzinski R, Storck M, Wang K, Ryu G-Y, Jobe SM, et al. Mutations in NBEAL2, encoding a BEACH protein, cause gray platelet syndrome. *Nature Genetics*. 2011;43(8):738–740.

19. Guerrero JA, Bennett C, van der Weyden L, McKinney H, Chin M, Nurden P, McIntyre Z, Cambridge EL, Estabel J, Wardle-Jones H, Speak AO, Erber WN, Rendon A, Ouwehand WH, Ghevaert C. Gray platelet syndrome: proinflammatory megakaryocytes and α-granule loss cause myelofibrosis and confer metastasis resistance in mice. *Blood*. 2014;124(24):3624–3635.

20. Kahr WHA, Lo RW, Li L, Pluthero FG, Christensen H, Ni R, Vaezzadeh N, Hawkins CE, Weyrich AS, Di Paola J, Landolt-Marticorena C, Gross PL. Abnormal megakaryocyte development and platelet function in Nbeal2−/− mice. *Blood*. 2013;122(19):3349–3358.

21. Lo RW, Li L, Leung R, Pluthero FG, Kahr WHA. NBEAL2 (Neurobeachin-Like 2) Is Required for Retention of Cargo Proteins by α-Granules During

Their Production by Megakaryocytes. *Arteriosclerosis, Thrombosis, and Vascular Biology*. 2018;38(10):2435–2447.

22. Deppermann C, Cherpokova D, Nurden P, Schulz J-N, Thielmann I, Kraft P, Vögtle T, Kleinschnitz C, Dütting S, Krohne G, Eming SA, Nurden AT, Eckes B, Stoll G, Stegner D, et al. Gray platelet syndrome and defective thrombo-inflammation in Nbeal2-deficient mice. *The Journal of Clinical Investigation*. 2013;123(8):3331–3342.
23. Claushuis TAM, de Stoppelaar SF, de Vos AF, Grootemaat AE, van der Wel NN, Roelofs JJTH, Ware J, Van't Veer C, van der Poll T. Nbeal2 Deficiency Increases Organ Damage but Does Not Affect Host Defense During Gram-Negative Pneumonia-Derived Sepsis. *Arteriosclerosis, Thrombosis, and Vascular Biology*. 2018;38(8):1772–1784.
24. Sowerby JM, Thomas DC, Clare S, Espéli M, Guerrero JA, Hoenderdos K, Harcourt K, Marsden M, Abdul-Karim J, Clement M, Antrobus R, Umrania Y, Barton PR, Flint SM, Juss JK, et al. NBEAL2 is required for neutrophil and NK cell function and pathogen defense. *The Journal of Clinical Investigation*. 2017;127(9):3521–3526.
25. Drube S, Grimlowski R, Deppermann C, Fröbel J, Kraft F, Andreas N, Stegner D, Dudeck J, Weber F, Rödiger M, Göpfert C, Drube J, Reich D, Nieswandt B, Dudeck A, et al. The Neurobeachin-like 2 Protein Regulates Mast Cell Homeostasis. *The Journal of Immunology*. 2017;199(8):2948–2957.

26. Braun A, Trigatti BL, Post MJ, Sato K, Simons M, Edelberg JM, Rosenberg RD, Schrenzel M, Krieger M. Loss of SR-BI expression leads to the early onset of occlusive atherosclerotic coronary artery disease, spontaneous myocardial infarctions, severe cardiac dysfunction, and premature death in apolipoprotein E-deficient mice. *Circulation Research*. 2002;90(3):270–276.

27. Zhang S, Picard MH, Vasile E, Zhu Y, Raffai RL, Weisgraber KH, Krieger M. Diet-induced occlusive coronary atherosclerosis, myocardial infarction, cardiac dysfunction, and premature death in scavenger receptor class B type I-deficient, hypomorphic apolipoprotein ER61 mice. *Circulation*. 2005;111(25):3457–3464.

28. Fuller M, Dadoo O, Serkis V, Abutouk D, MacDonald M, Dhingani N, Macri J, Igdoura SA, Trigatti BL. The effects of diet on occlusive coronary artery atherosclerosis and myocardial infarction in scavenger receptor class B, type 1/low-density lipoprotein receptor double knockout mice. *Arteriosclerosis, Thrombosis, and Vascular Biology*. 2014;34(11):2394–2403.

29. Korporaal SJA, Meurs I, Hauer AD, Hildebrand RB, Hoekstra M, Cate HT, Praticò D, Akkerman J-WN, Van Berkel TJC, Kuiper J, Van Eck M. Deletion of the high-density lipoprotein receptor scavenger receptor BI in mice modulates thrombosis susceptibility and indirectly affects platelet function by elevation of plasma free cholesterol. *Arteriosclerosis, Thrombosis, and Vascular Biology*. 2011;31(1):34–42.

30. Ma Y, Ashraf MZ, Podrez EA. Scavenger receptor BI modulates platelet reactivity and thrombosis in dyslipidemia. *Blood*. 2010;116(11):1932–1941.

31. Rigotti A, Trigatti BL, Penman M, Rayburn H, Herz J, Krieger M. A targeted mutation in the murine gene encoding the high density lipoprotein (HDL) receptor scavenger receptor class B type I reveals its key role in HDL metabolism. *Proceedings of the National Academy of Sciences of the United States of America*. 1997;94(23):12610–12615.

32. Van Eck M, Twisk J, Hoekstra M, Van Rij BT, Van der Lans CAC, Bos IST, Kruijt JK, Kuipers F, Van Berkel TJC. Differential effects of scavenger receptor BI deficiency on lipid metabolism in cells of the arterial wall and in the liver. *The Journal of Biological Chemistry*. 2003;278(26):23699–23705.

33. Dole VS, Matuskova J, Vasile E, Yesilaltay A, Bergmeier W, Bernimoulin M, Wagner DD, Krieger M. Thrombocytopenia and platelet abnormalities in high-density lipoprotein receptor-deficient mice. *Arteriosclerosis, Thrombosis, and Vascular Biology*. 2008;28(6):1111–1116.

34. Yu P, Xiong T, Tenedero CB, Lebeau P, Ni R, Macdonald ME, Gross PL, Austin RC, Trigatti BL. Rosuvastatin Reduces Aortic Sinus and Coronary Artery Atherosclerosis in SR-B1 (Scavenger Receptor Class B Type 1)/ApoE (Apolipoprotein E) Double Knockout Mice Independently of Plasma Cholesterol Lowering. *Arteriosclerosis, Thrombosis, and Vascular Biology*. 2018;38(1):26–39.

35. Hermann S, Kuhlmann MT, Starsichova A, Eligehausen S, Schäfers K, Stypmann J, Tiemann K, Levkau B, Schäfers M. Imaging reveals the connection between spontaneous coronary plaque ruptures, atherothrombosis, and myocardial infarctions in HypoE/SRBI2/2 Mice. *Journal of Nuclear Medicine*. 2016;57(9):1420–1427.

36. Braun A, Zhang S, Miettinen HE, Ebrahim S, Holm TM, Vasile E, Post MJ, Yoerger DM, Picard MH, Krieger JL, Andrews NC, Simons M, Krieger M. Probucol prevents early coronary heart disease and death in the high-density lipoprotein receptor SR-BI/apolipoprotein E double knockout mouse. *Proceedings of the National Academy of Sciences of the United States of America*. 2003;100(12):7283–7288.

37. Miettinen HE, Rayburn H, Krieger M. Abnormal lipoprotein metabolism and reversible female infertility in HDL receptor (SR-BI)–deficient mice. *Journal of Clinical Investigation*. 2001;108(11):1717–1722.

38. Livak KJ, Schmittgen TD. Analysis of relative gene expression data using real-time quantitative PCR and the 2(-Delta Delta C(T)) Method. *Methods (San Diego, Calif.)*. 2001;25(4):402–408.

39. Ouweneel AB, Hoekstra M, van der Wel EJ, Schaftenaar FH, Snip OSC, Hassan J, Korporaal SJA, Van Eck M. Hypercholesterolemia impairs megakaryopoiesis and platelet production in scavenger receptor BI knockout mice. *Atherosclerosis*. 2019;282:176–182.

40. Trigatti B, Rayburn H, Viñals M, Braun A, Miettinen H, Penman M, Hertz M, Schrenzel M, Amigo L, Rigotti A, Krieger M. Influence of the high density lipoprotein receptor SR-BI on reproductive and cardiovascular pathophysiology. *Proceedings of the National Academy of Sciences of the United States of America*. 1999;96(16):9322–9327.

41. Benjannet S, Rhainds D, Essalmani R, Mayne J, Wickham L, Jin W, Asselin M-C, Hamelin J, Varret M, Allard D, Trillard M, Abifadel M, Tebon A, Attie AD, Rader DJ, et al. NARC-1/PCSK9 and its natural mutants: zymogen cleavage and effects on the low density lipoprotein (LDL) receptor and LDL cholesterol. *The Journal of Biological Chemistry*. 2004;279(47):48865–48875.

42. Lagace TA. PCSK9 and LDLR degradation: regulatory mechanisms in circulation and in cells. *Current Opinion in Lipidology*. 2014;25(5):387–393.

43. Al-Jarallah A, Igdoura F, Zhang Y, Tenedero CB, White EJ, MacDonald ME, Igdoura SA, Trigatti BL. The effect of pomegranate extract on coronary artery atherosclerosis in SR-BI/APOE double knockout mice. *Atherosclerosis*. 2013;228(1):80–89.

44. Alard J-E, Ortega-Gomez A, Wichapong K, Bongiovanni D, Horckmans M, Megens RTA, Leoni G, Ferraro B, Rossaint J, Paulin N, Ng J, Ippel H, Suylen D, Hinkel R, Blanchet X, et al. Recruitment of classical monocytes can be inhibited by disturbing heteromers of neutrophil HNP1 and platelet CCL5. *Science Translational Medicine*. 2015;7(317):317ra196.

45. Horckmans M, Ring L, Duchene J, Santovito D, Schloss MJ, Drechsler M, Weber C, Soehnlein O, Steffens S. Neutrophils orchestrate post-myocardial infarction healing by polarizing macrophages towards a reparative phenotype. *European Heart Journal*. 2017;38(3):187–197.

46. Marwick JA, Mills R, Kay O, Michail K, Stephen J, Rossi AG, Dransfield I, Hirani N. Neutrophils induce macrophage anti-inflammatory reprogramming by suppressing NF-κB activation. *Cell Death & Disease*. 2018;9(6):665.

47. Bindesbøll C, Aas A, Ogmundsdottir MH, Pankiv S, Reine T, Zoncu R, Simonsen A. NBEAL1 controls SREBP2 processing and cholesterol metabolism and is a susceptibility locus for coronary artery disease. *Scientific Reports*. 2020;10:4528.

48. Tomberg K, Khoriaty R, Westrick RJ, Fairfield HE, Reinholdt LG, Brodsky GL, Davizon-Castillo P, Ginsburg D, Di Paola J. Spontaneous 8bp Deletion in Nbeal2 Recapitulates the Gray Platelet Syndrome in Mice. *PLoS ONE*. 2016;11(3):e0150852.

49. Guo Y-L, Zhang W, Li J-J. PCSK9 and lipid lowering drugs. *Clinica Chimica Acta; International Journal of Clinical Chemistry*. 2014;437:66–71.

50. Karackattu SL, Trigatti B, Krieger M. Hepatic Lipase Deficiency Delays Atherosclerosis, Myocardial Infarction, and Cardiac Dysfunction and Extends Lifespan in SR-BI/Apolipoprotein E Double Knockout Mice. *Arteriosclerosis, Thrombosis, and Vascular Biology*. 2006;26(3):548–554.

51. Gonzalez L, MacDonald ME, Deng YD, Trigatti BL. Hyperglycemia Aggravates Diet-Induced Coronary Artery Disease and Myocardial Infarction in SR-B1-Knockout/ApoE-Hypomorphic Mice. *Frontiers in Physiology*. 2018;9.

52. Miñana G, Núñez J, Bayés-Genís A, Revuelta-López E, Ríos-Navarro C, Núñez E, Chorro FJ, López-Lereu MP, Monmeneu JV, Lupón J, Sanchis J, Bodí V. Role of PCSK9 in the course of ejection fraction change after ST-segment elevation myocardial infarction: a pilot study. *ESC Heart Failure*. 2020;7(1):117–122.

53. Ding Z, Wang X, Liu S, Shahanawaz J, Theus S, Fan Y, Deng X, Zhou S, Mehta JL. Corrigendum to: PCSK9 expression in the ischaemic heart and its relationship to infarct size, cardiac function, and development of autophagy. *Cardiovascular Research*. 2021:cvab353.

2.7 Supplementary Materials

Supplementary Figure 2.7 – NBEAL2 KO Increased Tail Bleeding Times in Male ApoE KO and SR-B1/ApoE DKO Mice. Mice were anesthetized and their tails were transected across the vein approximately 0.5 cm from the tip and placed in a cuvette with warm saline. The time to cessation of bleeding was monitored. Each data point represents an individual mouse (n=15, 21, 19, 16). Bars represent means and error bars represent standard errors of the mean. Data were analyzed by one-way ANOVA and Tukey's post-hoc test. ns = not statistically significant; *P <0.05, ****P <0.0001.

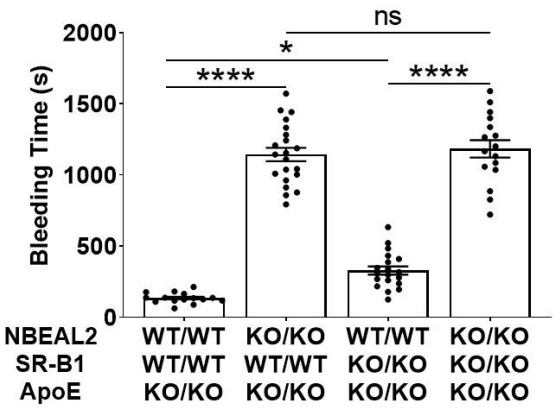

Supplementary Figure 2.8 – The Effects of NBEAL2 KO on Female SR-B1/ApoE DKO Mice. (A) NBEAL2 KO increased tail bleeding times in female SR-B1/ApoE DKO mice. Mice were anesthetized and their tails were transected across the vein approximately 0.5 cm from the tip and placed in a cuvette with warm saline. The time to cessation of bleeding was monitored. NBEAL2 KO did not affect survival in female SR-B1/ApoE DKO mice. (B) Kaplan-Meier survival curves for SR-B1/ApoE DKO (bolded line) and NBEAL2/SR-B1/ApoE TKO (dotted line) mice (n=14, 10). Mice were monitored until they reached cardiac endpoint, at which point they were humanely euthanized. Data were analyzed by the Mantel-Cox log-rank test. NBEAL2 KO reduced aortic sinus and coronary artery atherosclerosis burden in female SR-B1/ApoE DKO mice. Representative images of oil red O-stained transverse sections of the aortic sinus showing atherosclerotic plaque from female SR-B1/ApoE DKO (C) and NBEAL2/SR-B1/ApoE TKO (D) mice. Scale bar= 200 μm. (E) Aortic sinus atherosclerotic plaque cross-sectional areas vs. distance and (F) atherosclerotic plaque volumes (areas under the curves of plaque area vs. distance) of SR-B1/ApoE DKO (red) and NBEAL2/SR-B1/ApoE TKO mice (black). Data points in (E) represent means (n=7, 7). Seven sections of each heart were stained with oil red O/hematoxylin, and coronary arteries were scored as either non-atherosclerotic (0%) or containing atherosclerotic plaques that occluded <50%, >50% or 100% of their lumen. (G) Quantification of coronary arteries in each category (as percentage of total) across seven heart sections (n=7, 7). NBEAL2 KO did not significantly affect myocardial fibrosis in female SR-B1/ApoE DKO mice.

Representative images of Masson's trichrome-stained transverse cryosections of myocardium from female SR-B1/ApoE DKO (H) and NBEAL2/SR-B1/ApoE TKO (I) mice. Red colored staining indicates undamaged cardiomyocytes, whereas blue/purple colored staining indicates the presence of collagen. Scale bar= 200 μm. (J) Quantification of the percentage of myocardial fibrosis measured by the area of blue staining relative to the cross-sectional area of the heart for one section per mouse (n=7, 7). NBEAL2 KO did not alter heart weight-to-tibia length ratios in female SR-B1/ApoE DKO mice. (K) Heart weight-to-tibia length ratios (n=14, 9). Each data point represents an individual mouse. Bars represent means and error bars represent standard errors of the mean. Data in (A), (F), and (K) passed the normality test and were analyzed by Student's t-test. Data in (B) were analyzed by the Mantel-Cox log-rank test. Data in (E) and (G) were analyzed by two-way ANOVA with Sidak's multiple comparisons post-hoc test. Data in (J) did not pass the normality test and were analyzed by Mann-Whitney Rank Sum Test. *P <0.05, **P <0.01, ****P <0.0001.

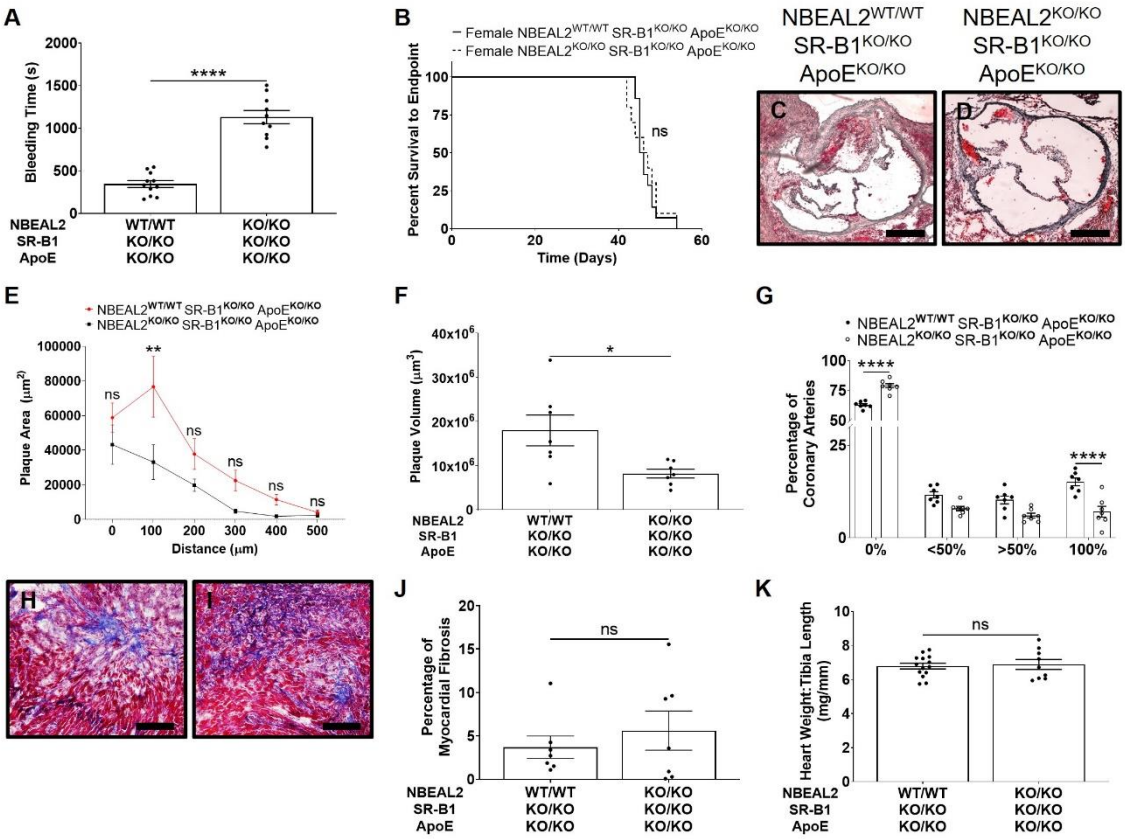
A
Bleeding Time (s)
2000
1500
1000
500
0
****
NBEAL2
SR-B1
ApoE
WT/WT
KO/KO
KO/KO
KO/KO
KO/KO
KO/KO
B
– Female NBEAL2WT/WT SR-B1KO/KO ApoEKO/KO
-- Female NBEAL2KO/KO SR-B1KO/KO ApoEKO/KO
Percent Survival to Endpoint
100
75
50
25
0
ns
0
20
40
60
Time (Days)
NBEAL2WT/WT
SR-B1KO/KO
ApoEKO/KO
NBEAL2KO/KO
SR-B1KO/KO
ApoEKO/KO
C
D
E
NBEAL2WT/WT SR-B1KO/KO ApoEKO/KO
NBEAL2KO/KO SR-B1KO/KO ApoEKO/KO
Plaque Area (μm2)
100000
80000
60000
40000
20000
0
**
ns
ns
ns
ns
ns
0
100
200
300
400
500
Distance (μm)
F
Plaque Volume (μm3)
40x10^6
30x10^6
20x10^6
10x10^6
0
*
NBEAL2
SR-B1
ApoE
WT/WT
KO/KO
KO/KO
KO/KO
KO/KO
KO/KO
G
NBEAL2WT/WT SR-B1KO/KO ApoEKO/KO
NBEAL2KO/KO SR-B1KO/KO ApoEKO/KO
Percentage of Coronary Arteries
100
75
50
25
0
****
****
0%
<50%
>50%
100%
H
I
J
Percentage of Myocardial Fibrosis
20
15
10
5
0
ns
NBEAL2
SR-B1
ApoE
WT/WT
KO/KO
KO/KO
KO/KO
KO/KO
KO/KO
K
Heart Weight:Tibia Length (mg/mm)
10
8
6
4
2
0
ns
NBEAL2
SR-B1
ApoE
WT/WT
KO/KO
KO/KO
KO/KO
KO/KO
KO/KO

Supplementary Figure 2.9 – Flow Cytometry Analysis on Blood Immune Cells in Male Mice. (A) Blood Ly6C^{lo} monocytes. (B) Blood Ly6C^{mid} monocytes. (C) Blood Ly6C^{hi} monocytes. (D) Blood CD4^{+} T-cells. (E) Blood CD8^{+} T-cells. (F) Blood T-cells. (G) Blood B-cells. (H) Blood natural killer (NK) cells. (I) Blood natural killer T (NKT) cells. N= 11, 10, 13, 10 for all flow cytometry analyses. Blood was collected into a heparinized tube via cheek puncture using a lancet. Flow cytometry was performed on a BD FACSCalibur Flow Cytometry system, and data were analyzed using FlowJo v10. Each data point represents an individual mouse. Bars represent means and error bars represent standard errors of the mean. All data were analyzed by one-way ANOVA and Tukey's post-hoc test. *P <0.05, **P <0.01.

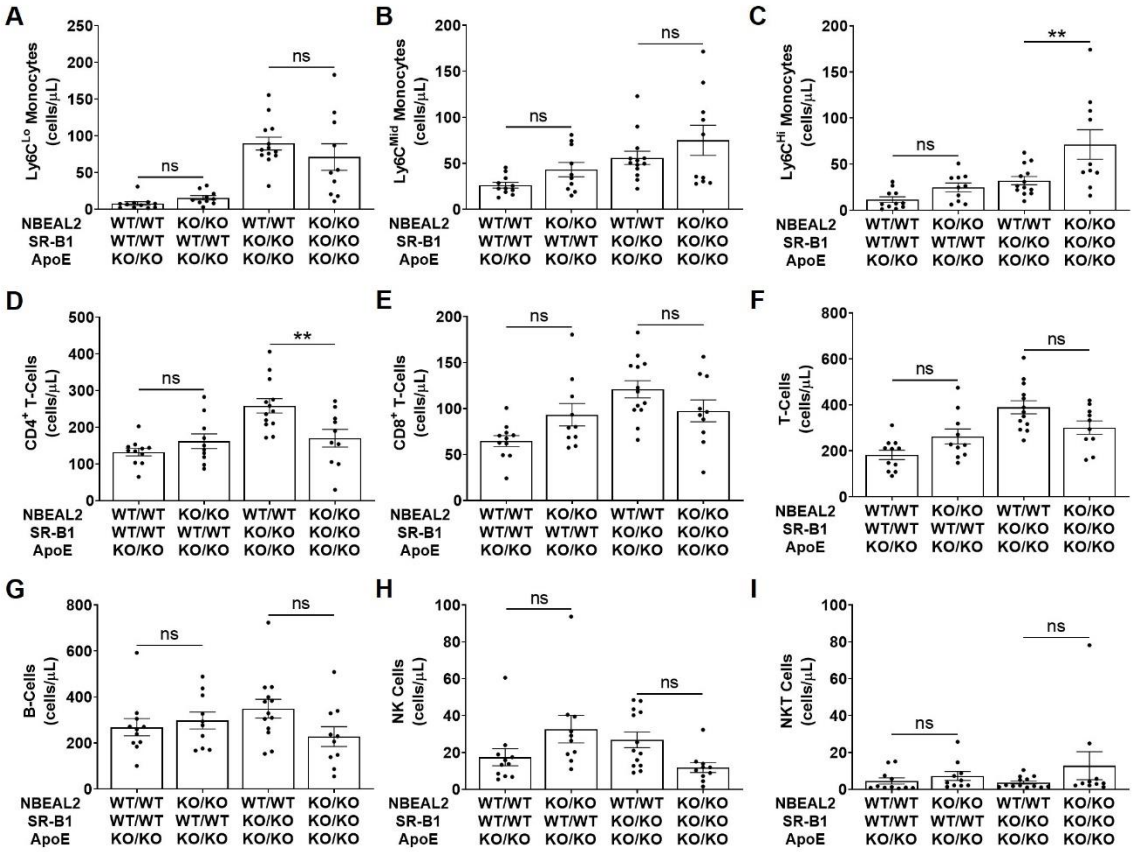

Supplementary Figure 2.10 – Flow Cytometry Analysis on Blood Immune Cells in Female SR-B1/ApoE DKO and NBEAL2/SR-B1/ApoE TKO Mice. (A) Blood neutrophils. (B) Neutrophil side scatter (SSC). (C) Blood monocytes. (D) Monocyte SSC. (E) Blood $Ly6C^{lo}$ monocytes. (F) Blood $Ly6C^{mid}$ monocytes. (G) Blood $Ly6C^{hi}$ monocytes. (H) Blood $CD4^+$ T-cells. (I) Blood $CD8^+$ T-cells. (J) Blood T-cells. (K) Blood B-cells. (L) Blood natural killer (NK) cells. (M) Blood natural killer T (NKT) cells. N= 10, 6 for all flow cytometry analyses. Blood was collected into a heparinized tube via cheek puncture using a lancet. Flow cytometry was performed on a BD FACSCalibur Flow Cytometry system, and data were analyzed using FlowJo v10. Each data point represents an individual mouse. Bars represent means and error bars represent standard errors of the mean. All data passed the normality test and were analyzed by Student's t-test. **P <0.01, ***P <0.001, ****P <0.0001.

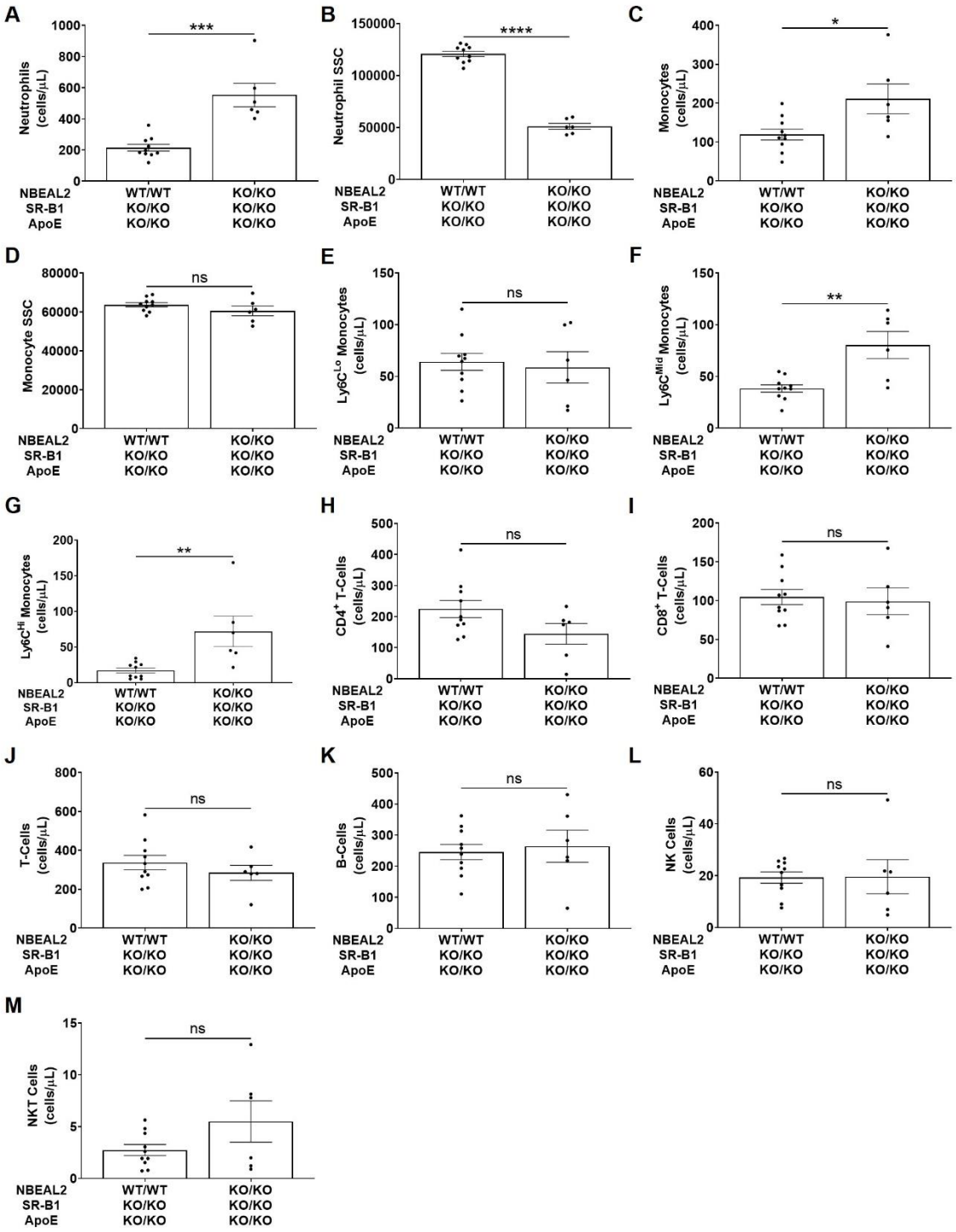
A
Neutrophils (cells/μL)
1000
800
600
400
200
0
***
B
Neutrophil SSC
150000
100000
50000
0
****
C
Monocytes (cells/μL)
400
300
200
100
0
*
D
Monocyte SSC
80000
60000
40000
20000
0
ns
E
Ly6C^Lo Monocytes (cells/μL)
150
100
50
0
ns
F
Ly6C^Mid Monocytes (cells/μL)
150
100
50
0
**
G
Ly6C^Hi Monocytes (cells/μL)
200
150
100
50
0
**
H
CD4+ T-Cells (cells/μL)
500
400
300
200
100
0
ns
I
CD8+ T-Cells (cells/μL)
200
150
100
50
0
ns
J
T-Cells (cells/μL)
800
600
400
200
0
ns
K
B-Cells (cells/μL)
500
400
300
200
100
0
ns
L
NK Cells (cells/μL)
60
40
20
0
ns
M
NKT Cells (cells/μL)
15
10
5
0
ns
NBEAL2 WT/WT KO/KO
SR-B1 KO/KO KO/KO
ApoE KO/KO KO/KO

Supplementary Table 2.1 – Mouse Primers Used for RT-PCR. Primer sequences were selected using PubMed's Primer-BLAST.

Target	Primer	Sequence
GAPDH	Forward	5'-ACCACAGTCCATGCCATCAC-3'
	Reverse	5'-TCCACCACCCTGTTGCTGTA-3'
HMG-CoA Reductase	Forward	5'-GGGAGCATAGGCGGCT-3'
	Reverse	5'-TGCGATGTAGATAGCAGTGACA-3'
LDLR	Forward	5'-TCCAATCAATTCAGCTGTGG-3'
	Reverse	5'-GAGCCATCTAGGCAATCTCG-3'
PCSK9	Forward	5'-TTGCAGCAGCTGGGAACTT-3'
	Reverse	5'-CCGACTGTGATGACCTCTGGA-3'
SREBP2	Forward	5'-GCAGCAACGGGACCATTCT-3'
	Reverse	5'-CCCCATGACTAAGTCCTTCAACT-3'

Chapter 3: Protease-Activated Receptor 4 Inhibition Reduces Coronary Artery Atherosclerosis and Myocardial Fibrosis in Scavenger Receptor Class B Type 1/Low-Density Lipoprotein Receptor Double Knockout Mice.

Author List: Samuel Lee, Rithwik Ramachandran and Bernardo L. Trigatti

Foreword

This manuscript examines the effects of PAR4 inhibition via PAR4 inhibitory pepducin (RAG8) on coronary artery disease development in HFCC diet-fed SR-B1/LDLR DKO mice. We demonstrate that RAG8 treatment increases tail bleeding times in HFCC diet-fed SR-B1/LDLR DKO mice. Although RAG8 treatment does not alter aortic sinus atherosclerosis levels, it reduces the levels of coronary artery atherosclerosis and myocardial fibrosis in HFCC diet-fed SR-B1/LDLR DKO mice. This is independent of changes in circulating lipids, cytokines, and immune cells. However, RAG8 treatment reduces platelet accumulation and VCAM-1 protein levels in coronary arteries in HFCC diet-fed SR-B1/LDLR DKO mice, which may explain the protective effects of RAG8 treatment against coronary artery atherosclerosis and myocardial fibrosis development.

This manuscript has been submitted to the journal of Arteriosclerosis, Thrombosis, and Vascular Biology (ATVB) and is currently under revision. This manuscript was written by Samuel Lee with guidance from Bernardo L. Trigatti. This project was designed by Samuel Lee and Bernardo L. Trigatti. Pepducins

(RAG8 and SRQ8) were provided by Rithwik Ramachandran (Western University). All experiments were conducted by Samuel Lee, and all data were analyzed and interpreted by Samuel Lee under the guidance of Bernardo L. Trigatti.

For simplicity, the main figures only compare HFCC diet-fed SR-B1/LDLR DKO mice treated with either the RAG8 pepducin or the control SRQ8 pepducin. The supplementary figures include HFCC diet-fed LDLR single KO mice and SR-B1/LDLR DKO mice that did not receive any injections (untreated), and serve as control mice. Relevant comparisons are noted in the results section.

3.1 Abstract

Objective: Scavenger receptor class B type 1 (SR-B1)/low-density lipoprotein receptor (LDLR) double knockout mice fed a high-fat, high-cholesterol, cholate (HFCC) diet exhibit coronary artery disease (CAD) characterized by occlusive coronary artery atherosclerosis, platelet accumulation in coronary arteries, and myocardial fibrosis. Platelets are involved in atherosclerosis development, and protease-activated receptor 4 (PAR4) has a prominent role in platelet function. However, the role of PAR4 on CAD development in mice has not been tested. Therefore, we tested the effects of a PAR4 inhibitory pepducin (RAG8) on diet-induced aortic sinus and coronary artery atherosclerosis, platelet accumulation in atherosclerotic coronary arteries, and myocardial fibrosis in SR-B1/LDLR double knockout mice.

Approach and Results: SR-B1/LDLR double knockout mice were fed a HFCC diet and injected daily with 20 mg/kg of either the RAG8 pepducin or a control reverse-sequence pepducin (SRQ8) for 20 days. RAG8-treated mice exhibited increased tail bleeding times compared to control SRQ8-treated mice. Although aortic sinus atherosclerosis levels did not differ, RAG8-treated mice exhibited reduced coronary artery atherosclerosis, platelet accumulation in atherosclerotic coronary arteries, and myocardial fibrosis. These protective effects were not accompanied by changes in circulating lipids, inflammatory cytokines, or immune cells. However, RAG8-treated mice exhibited reduced vascular cell adhesion molecule 1 (VCAM-

1) protein levels in non-atherosclerotic coronary arteries compared to SRQ8-treated mice.

Conclusions: The PAR4 inhibitory RAG8 pepducin reduced coronary artery atherosclerosis and myocardial fibrosis in HFCC diet-fed SR-B1/LDLR double knockout mice. Furthermore, RAG8 reduced VCAM-1 protein levels in non-atherosclerotic coronary arteries and reduced platelet accumulation in atherosclerotic coronary arteries. These findings highlight PAR4 as an attractive target in reducing CAD development, and the use of RAG8 may potentially be beneficial in cardiovascular disease.

3.2 Introduction

Coronary artery disease (CAD) is a common cause of cardiovascular disease and death worldwide[1]. Atherosclerosis, a major cause of CAD, is a chronic inflammatory disease driven by complex interactions between circulating lipoproteins, immune cells, and cells of the artery wall[2]. Activation of arterial endothelial cells, for example caused by non-laminar blood flow or inflammatory cytokines, increases expression of adhesion molecules such as vascular cell adhesion molecule-1 (VCAM-1), mediating adhesion of monocytes and other inflammatory cells which drive atherosclerosis development[3–6]. Mature atherosclerotic plaques can exhibit endothelial cell erosion or, if they exhibit large necrotic cores and thin fibrous caps are prone to rupture; both of which lead to

formation of thrombi which either occlude the lumen of the affected artery or accelerate further atherosclerotic plaque development[7]. The process of thrombosis formation on atherosclerotic plaques is referred to as atherothrombosis and drives ischemic diseases associated with atherosclerosis, including myocardial infarction, ischemic stroke and peripheral vascular disease[8]. Platelets play important roles throughout atherothrombosis development. In early stages, platelets adhere to activated endothelium and release pro-inflammatory chemokines such as c-c motif chemokine ligand 5 and c-x-c motif chemokine ligand 12, facilitating the attraction and firm adhesion of circulating leukocytes to the vascular wall and contributing to inflammatory processes that drive atherosclerosis[9,10]. Additionally, adherent and activated platelets on endothelial cells secrete inflammatory factors such as interleukin-1β (IL-1β) and CD40 ligand (CD40L), leading to endothelial cell activation and subsequent adhesion molecule expression that exacerbate atherosclerosis development[11]. In late stages when plaque rupture or endothelial cell erosion occur, platelets drive thrombus formation to form a stabilized clot[7,12].

Genetic knockout (KO) of the high-density lipoprotein (HDL) receptor, scavenger receptor class B type 1 (SR-B1), in mice containing apolipoprotein E (ApoE) or low-density lipoprotein receptor (LDLR) KO mutations increases spontaneous or diet-induced atherosclerosis development in the aortic sinus and, uniquely among mouse models, in coronary arteries[13–15]. This is accompanied by platelet accumulation in atherosclerotic coronary arteries and fatal myocardial infarction[13–15]. Mice deficient in SR-B1 exhibit impaired HDL-dependent reverse

cholesterol transport and dyslipidemia characterized by increased ratios of unesterified:total cholesterol, which is worsened by high-cholesterol diet feeding[16,17]. These mice exhibit platelet abnormalities associated with the accumulation of unesterified cholesterol in platelets[18–20]. These include thrombocytopenia[18–21] and reduced *ex vivo* responsiveness to stimulation by agonists such as ADP[18–20] and convulxin[18], but normal or increased responsiveness to the protease-activated receptor 4 (PAR4) agonist peptide[18,20]. On the other hand, platelets in SR-B1 deficient mice appear to circulate in an activated state[19,21] and SR-B1 deficient mice exhibit increased susceptibility to experimental $FeCl_3$-induced thrombosis[19]. We previously demonstrated that rosuvastatin protects atherogenic SR-B1/ApoE double KO (DKO) mice against atherosclerosis and attenuates myocardial fibrosis and cardiomegaly. Interestingly, rosuvastatin also reduced platelet accumulation in atherosclerotic coronary arteries of these mice[21]. Treating atherogenic diet-fed SR-B1 KO/HypoE mice with aspirin also significantly reduces the number of thrombi in atherosclerotic coronary arteries, myocardial infarction levels, and premature deaths, presumably due to aspirin's anti-platelet action[22]. These studies demonstrate that platelet accumulation can be reduced in atherosclerotic coronary arteries in mice, which may protect against coronary artery atherosclerosis and/or myocardial infarction development. Since SR-B1/LDLR DKO mice develop diet-inducible occlusive coronary artery atherosclerosis, platelet accumulation in atherosclerotic coronary arteries and myocardial fibrosis[15], and because platelets from SR-B1-deficient

mice remain responsive to PAR4 activation[18–20], we set out to test the effects of PAR4 inhibition on CAD development in SR-B1/LDLR DKO mice.

Thrombin represents a potent stimulus for activation of platelets and does so by activating PARs by proteolytically unmasking an N-terminal motif that acts as a tethered ligand to initiate signaling[23] via G protein- and β-arrestin-mediated pathways[24]. In mice, PAR4 represents the major receptor for thrombin-mediated platelet activation[25,26]. We previously identified an intracellular motif on the PAR4 C-terminus (RAGLFQRS) that coordinately regulates calcium signaling and interaction of the receptor with β-arrestins 1 and 2[27]. Based on this motif, we developed a novel pepducin (a cell-penetrating peptide that interferes with intracellular signaling) (RAG8)[27]. Disrupting the PAR4 calcium/β-arrestin signaling process with RAG8 inhibited platelet aggregation in response to both a PAR4 agonist peptide and thrombin in washed human platelets, and attenuated clot stabilization *in vivo* in mice without affecting signaling from other PARs[27]. Therefore, RAG8 represents a tool for selectively probing the role of PAR4 signaling *in vivo* in mice. Considering the major role of PAR4 in platelets and the involvement of platelets in atherosclerosis and thrombosis, utilizing RAG8 may be a useful approach to examine the effects of PAR4 inhibition on the development of CAD in mice, which has never been investigated previously.

In the current study, we utilized RAG8 to examine the effects of PAR4 inhibition on diet-induced CAD development in SR-B1/LDLR DKO mice. RAG8 treatment did not affect diet-induced atherosclerosis development in the aortic

sinus of SR-B1/LDLR DKO mice. However, RAG8 treatment reduced coronary artery atherosclerosis and myocardial fibrosis without altering circulating lipid, cytokine, or immune cell levels. Interestingly, RAG8 treatment reduced platelet accumulation in atherosclerotic coronary arteries and VCAM-1 protein levels in coronary arteries, which may in part explain the protective effects of PAR4 inhibition against CAD development.

3.3 Materials and Methods

3.3.1 Mice

All procedures involving mice were in accordance with the Canadian Council on Animal Care guidelines and were approved by the McMaster University Animal Research Ethics Board. All mice were on a mixed C57BL/6:129 background. SR-B1/LDLR DKO mice and control LDLR single KO mice were derived from breeders originally provided by Dr. Monty Krieger (Massachusetts Institute of Technology, Cambridge, Massachusetts, USA). Male SR-B1/LDLR DKO mice and female SR-B1$^{+/-}$/LDLR KO mice were bred together to generate littermate SR-B1/LDLR DKO mice, and male and female SR-B1$^{+/+}$/LDLR KO mice were bred together to generate littermate LDLR single KO control mice. All mice were bred and housed in the David Braley Research Institute animal facility at McMaster University and had free access to normal chow (Teklad Global 18% Protein Rodent Diet, 2018, Envigo, Madison, Wisconsin, USA) and water. Only female mice were used in this study.

3.3.2 Pepducin Design and Synthesis

The PAR4 antagonist pepducin, palmitoyl-RAGLFQRS-NH_2 (RAG8), and the control reverse-sequence pepducin, palmitoyl-SRQFLGAR-NH_2 (SRQ8), were custom synthesized by Genscript (Piscataway, New Jersey, USA) using solid-phase synthesis, purified by reverse-phase high-performance liquid chromatography, and verified by mass spectrometry analysis (>95% purity). For injections, the pepducins were prepared at a concentration of 4 mg/ml in 25 mM HEPES, 129 mM NaCl, pH 7.4. The RAG8 pepducin contains an amino terminal palmitic acid and carboxy terminal amino group, making it stable in blood and easily taken up by target cells. On the other hand, the control pepducin has the reverse amino acid sequence as RAG8 that renders it inert towards PAR4 and unable to affect platelet activation and subsequent thrombosis[27].

3.3.3 Diet Induction of Atherosclerosis and Pepducin Injections

At 11 weeks of age, SR-B1/LDLR DKO mice were placed on a high-fat, high-cholesterol, cholate (HFCC) diet (Teklad, TD88051, Envigo, Madison, Wisconsin, USA) containing 15% fat (7.5% from cocoa butter), 1.25% cholesterol and 0.5% sodium cholate[28] for 20 days (SR-B1/LDLR DKO mice exhibit 50% mortality after approximately 24 days of HFCC diet feeding)[15]. SR-B1/LDLR DKO mice received daily subcutaneous injections with 100 µL of either the RAG8 pepducin or the control SRQ8 pepducin (0.4 mg of peptide/20 g mouse/day) beginning at the start and continuing for the duration of HFCC diet feeding. As controls, we included

untreated but HFCC diet-fed SR-B1/LDLR DKO mice and LDLR single KO mice. The mice were monitored on a daily basis throughout the 20 day feeding period. At the end of the 20 day feeding/treatment period, mice were fasted for approximately 14 hours, and fully anesthetized with isoflurane-O_2 in an induction chamber followed by continued anaesthesia under a nose comb. While anesthetized, mice were subjected to a tail bleeding assay as described below. Blood was then collected into heparinized Eppendorf tubes via cheek puncture using a lancet. A portion of the blood was used for flow cytometry analysis of blood cells, and the remainder was used to prepare plasma. After blood collection, the mice were then thoracotomized and hearts and vasculature were perfused in situ through the left ventricle with phosphate-buffered saline containing 10 U of heparin/ml. Hearts were then excised and cryoprotected in 30% sucrose for 1-2 hours, then rapidly frozen using liquid nitrogen in Shandon Cryomatrix (Thermo Fisher Scientific, 6769006, Ottawa, Ontario, Canada) and stored at -80°C. Plasma was prepared by centrifugation of blood at 4,000 rpm for 5 minutes in a microcentrifuge at 4°C and stored in -80°C.

3.3.4 Tail Bleeding Assay

As described above, immediately prior to harvesting, mice were anaesthetized under a nose comb using isoflurane-O_2. The tails were transected across the tail vein using a scalpel blade approximately 0.5 cm from the tip, and

placed in a cuvette containing 37°C saline. The time taken for the cessation of blood flow was recorded.

3.3.5 Histology

For analysis of atherosclerosis in the aortic sinus and coronary arteries, 10 μm-thick transverse cryosections were collected using a cryotome (Shandon Cryotome Electronic, 77210163GB, Thermo Fisher Scientific, Ottawa, Ontario, Canada) from the middle of the heart to the aortic annulus in 0.3 mm intervals, then in 0.1 mm intervals to the top of the aortic valve leaflets. Lipids in atherosclerotic plaques were detected by oil red O staining, and nuclei were counter-stained with Meyer's hematoxylin. Brightfield images were captured using an Axiovert 200M microscope (Carl Zeiss Canada Ltd., Toronto, Ontario, Canada). For aortic sinus atherosclerosis analyses, the cross-sectional areas of atherosclerotic plaques for a series of sections (100 μm apart) with each of the 3 valve leaflets covering a distance of 300 μm were measured manually in a blinded manner using AxioVision software and plotted vs. distance, and plaque volume (area under the curve) was calculated using GraphPad Prism. Atherosclerosis in coronary arteries were evaluated in a blinded manner by counting coronary arteries with different levels of occlusion in 7 sections (which covers a distance of 1800 μm) below the aortic annulus. Coronary arteries were scored as either 0% occluded (non-atherosclerotic - no raised atherosclerotic plaque), <50% occluded, >50% occluded, or 100% (fully) occluded.

Myocardial fibrosis was detected by Masson's trichrome staining (Sigma-Aldrich, Oakville, ON, Canada), which stains collagen-rich fibrotic tissue blue/purple, and healthy myocardium red/pink. Images for 1 transverse cryosection per mouse at approximately 900 μm below the aortic annulus were captured using an Olympus BX41 microscope with a DP72 camera (Olympus Canada Inc., Richmond Hill, Ontario, Canada). The percentage of myocardial fibrosis was measured manually in a blinded manner using the outline function in ImageJ software as a proportion of fibrotic staining to the total area of the cross-section.

3.3.6 Immunofluorescence

Vascular cell adhesion molecule 1 (VCAM-1) was detected using cell-culture supernatants from rat B-lymphocyte hybridoma cells that produce antibodies against mouse VCAM-1 (ATCC, CRL-1909, Manassas, Virginia, USA)[29], and AlexaFluor 594 goat anti-rat secondary antibody (Invitrogen, A-11007, Waltham, Massachusetts, USA). Platelets were detected using a rat anti-mouse CD41 antibody (BD Biosciences, 553847, Mississauga, Ontario, Canada) and AlexaFluor 488 goat anti-rat secondary antibody (Invitrogen, A-11006, Waltham, Massachusetts, USA). Nuclei were detected with 4', 6'-diamidino-2-phenylindole (DAPI) counterstaining. All fluorescent images were captured using an Olympus BX41 microscope with a DP72 camera (Olympus Canada Inc., Richmond Hill, Ontario, Canada). All coronary arteries in 7 sections (which covers a distance of 1800 μm) below the aortic annulus were counted. For VCAM-1 analysis, the

percentage of non-atherosclerotic coronary arteries with positive VCAM-1 staining was quantified in a blinded manner. For CD41 platelet analysis, the percentage of atherosclerotic coronary arteries with positive CD41 platelet staining was quantified in a blinded manner.

3.3.7 Plasma Analysis

Plasma total cholesterol (Cholesterol Infinity, TR13421, Thermo Fisher Scientific, Ottawa, Ontario, Canada), unesterified cholesterol (Free Cholesterol E, Wako Diagnostics, 993-02501, Mountain View, California, USA), HDL cholesterol (not precipitable by phosphotungstate-magnesium salt; HDL Cholesterol E, Wako Diagnostics, 997-01301, Mountain View, California, USA), and triglycerides (L-Type Triglyceride M, Wako Chemicals, 998-02992, Richmond, Virginia, USA) were measured using the indicated commercial assay kits and following manufacturers' instructions. Esterified cholesterol levels were calculated as the difference between total cholesterol and unesterified cholesterol measurements, and non-HDL cholesterol levels were calculated as the difference between total cholesterol and HDL cholesterol measurements. Plasma creatine kinase myocardial band (CK-MB) levels were measured using commercial ELISA kits (Mouse CK-MB ELISA Kit, Novus Biologicals, NBP2-75312, Toronto, Ontario, Canada) and following manufacturer's protocols. Plasma troponin I levels were measured using commercial ELISA kits (Mouse Cardiac Troponin I ELISA Kit, CTNI-1-HSP, Life Diagnostics, West Chester, Pennsylvania, USA) and following manufacturer's

protocols. Plasma interleukin-6 (IL-6) and tumour necrosis factor alpha (TNFα) cytokines were measured using commercial ELISA kits (BioLegend, 431304 and 430904, respectively, San Diego, California, USA) and following manufacturer's protocols. Soluble plasma VCAM-1 and intercellular adhesion molecule 1 (ICAM-1) were measured using commercial ELISA kits (R&D Systems, MVC00 and MIC100, respectively, Minneapolis, Minnesota, USA) and following manufacturer's protocols.

3.3.8 Flow Cytometry

Blood was incubated with the following rat anti-mouse antibodies: FITC CD3 (BD Biosciences, 555274, Mississauga, Ontario, Canada), BV510 CD45 (Biolegend, 103138, San Diego, California, USA), PerCP-Cyanine5.5 CD45R (B220) (eBioscience, 45-0452-80, San Diego, California, USA), PE CD11b (M1/70) (eBioscience, 12-0112-82, San Diego, California, USA), PE-Cy7 Ly6C (Biolegend, 128018, San Diego, California, USA), PE-Dazzle-594 Ly6G (Biolegend, 127648, San Diego, California, USA), PE-Cy5 CD4 (BD Biosciences, 553050, Mississauga, Ontario, Canada), PE-Cy7 CD8a (BD Biosciences, 552877, Mississauga, Ontario, Canada), and PE NK1.1 (BD Biosciences, 553165, Mississauga, Ontario, Canada). Next, erythrocytes present in the blood were lysed and samples were fixed with 1x 1-step fix/lyse solution (Thermo Fisher Scientific, 00-5333, Ottawa, Ontario, Canada). Absolute leukocyte counts were determined with the addition of 123count eBeads (Thermo Fisher Scientific, 01-1234-42, Ottawa, Ontario, Canada). Flow

cytometry was performed on a BD FACSCalibur Flow Cytometry system (BD Biosciences, Mississauga, Ontario, Canada), and data were analyzed using FlowJo v10 software.

3.3.9 Statistical Analysis

GraphPad Prism software was used for statistical analyses. For two groups, data were subjected to the Shapiro-Wilk test for normality. Those that passed normality were analyzed by the Student's t-test (2-tailed, unpaired), and those that failed normality were analyzed by the Mann-Whitney Rank Sum test. For multiple groups, data were analyzed by one-way ANOVA with Tukey's Multiple Comparisons Post-Hoc test. Data with two independent variables were analyzed by two-way ANOVA with Sidak's Multiple Comparisons Post-Hoc test. Data are presented as mean ± standard error of the mean. P values <0.05 were considered statistically significant.

3.4 Results

3.4.1 RAG8 Treatment Increased Tail Bleeding Times in SR-B1/LDLR DKO Mice

To verify RAG8-mediated PAR4 inhibition *in vivo* in SR-B1/LDLR DKO mice, a tail bleeding assay was performed in mice fed an atherogenic HFCC diet and treated for 20 days with daily injections of the RAG8 or control SRQ8 pepducins. Indeed, RAG8-treated SR-B1/LDLR DKO mice exhibited a significant increase in tail bleeding times compared to SR-B1/LDLR DKO mice treated with the inactive

SRQ8 control pepducin (389.8 ± 27.1 sec. v 221.8 ± 27.3 sec.; P <0.001; Figure 3.1). SRQ8 injection itself did not affect tail bleeding times in SR-B1/LDLR DKO mice (compare to Supplementary Figure 3.7A). The RAG8-dependent increase in tail bleeding times is consistent with our previous findings and with previous reports of prolonged tail bleeding times with PAR4 deficiency but not PAR3 deficiency[26,27]. We noticed that untreated SR-B1/LDLR DKO mice exhibited a significant increase in tail bleeding times compared to LDLR KO mice (180.6 ± 4.8 sec. vs. 106.2 ± 6.0 sec.; P <0.0001; Supplementary Figure 3.7A). This appears to be consistent with thrombocytopenia reported for hypercholesterolemic mice deficient in SR-B1[18–21,30]. Nonetheless, the further increase in tail bleeding time resulting from treatment of SR-B1/LDLR DKO mice with the RAG8 pepducin is consistent with a prominent role for PAR4 in platelet function.

Figure 3.1 – RAG8-Treated Mice Exhibited Increased Tail Bleeding Times Compared to SRQ8-Treated Mice. SR-B1/LDLR DKO mice fed the HFCC diet for 20 days were anesthetized and their tails were transected across the vein approximately 0.5 cm from the tip and placed in a cuvette with warm saline. The time to cessation of bleeding was monitored. Each data point represents an individual mouse (n=12, 14). Bars represent means and error bars represent standard errors of the mean. Data passed the normality test and were analyzed by Student's t-test. ***P <0.001.

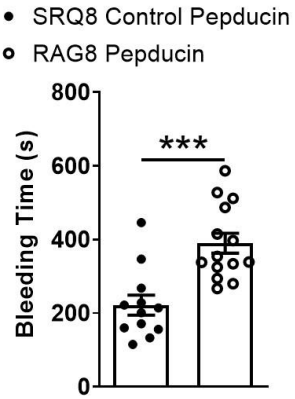

3.4.2 RAG8 Treatment Reduced Diet-Induced Coronary Artery Atherosclerosis Despite Similar Levels of Aortic Sinus Atherosclerosis in SR-B1/LDLR DKO Mice

Consistent with previous findings, HFCC diet feeding resulted in significantly increased atherosclerosis development in the aortic sinuses and coronary arteries of SR-B1/LDLR DKO compared to control HFCC diet-fed LDLR single KO mice (Supplementary Figures 3.7B-F). No significant differences were seen in atherosclerosis levels in either the aortic sinuses or coronary arteries of the HFCC diet fed SR-B1/LDLR DKO mice that were either untreated or had been treated with the SRQ8 inactive control pepducin (compare Figures 3.2A, C and D with Supplementary Figures 3.7C-E; and Figure 3.3E with Supplementary Figure 3.7F).

HFCC diet-fed SR-B1/LDLR DKO mice that had been treated with the RAG8 pepducin exhibited similar levels of aortic sinus atherosclerosis ($2.6 \times 10^7 \pm 0.19 \times 10^7$ μm^3 vs. $2.8 \times 10^7 \pm 0.27 \times 10^7$ μm^3; Figure 3.2), but reduced proportions of atherosclerotic coronary arteries (Figures 3.3A-E) compared to HFCC diet-fed SR-B1/LDLR DKO mice that had been treated with the SRQ8 inactive control pepducin. RAG8-treated SR-B1/LDLR DKO mice exhibited significantly greater proportions of coronary arteries lacking atherosclerotic plaques (0% occluded) (79.9 ± 1.8% vs. 63.2 ± 2.7%; $P < 0.0001$) and significantly lower proportions of coronary artery cross-sections in which the artery lumen was fully occluded by atherosclerotic plaque (9.9 ± 1.4% vs. 24.3 ± 3.2%; $P < 0.0001$; Figures 3.3A-E).

Consistent with previous findings from our lab[15], HFCC diet-fed SR-B1/LDLR DKO mice had increased proportions of non-atherosclerotic coronary

artery cross-sections that stained positive for VCAM-1 compared to HFCC diet-fed LDLR single KO mice (Supplementary Figures 3.7G, I and K). The extent of VCAM-1 staining around the circumference of non-atherosclerotic coronary artery cross-sections also appeared to be greater in HFCC diet-fed SR-B1/LDLR DKO mice compared to HFCC diet-fed LDLR single KO mice (Supplementary Figures 3.7G and I). Treatment of HFCC diet-fed SR-B1/LDLR DKO mice with the inactive SRQ8 control pepducin did not affect the proportion of non-atherosclerotic coronary artery cross-sections that stained positive for VCAM-1, compared to untreated HFCC diet-fed SR-B1/LDLR DKO mice (compare Figures 3.3F and J with Supplementary Figures 3.7I and K). However, treatment of HFCC diet-fed SR-B1/LDLR DKO mice with the PAR4 inhibitory RAG8 pepducin significantly reduced the proportion of non-atherosclerotic coronary artery cross-sections that were positive for VCAM-1 (Figures 3.3H and J). Moreover, the extent of VCAM-1 staining around the circumference of non-atherosclerotic coronary artery cross-sections also appeared to be reduced in HFCC diet-fed SR-B1/LDLR DKO mice treated with the RAG8 pepducin compared to those treated with the SRQ8 control pepducin (Figures 3.3F and H). No differences were however detected in plasma levels of soluble VCAM-1 or ICAM-1 between the RAG8- and SRQ8-treated SR-B1/LDLR DKO mice (Supplementary Figure 3.10).

Figure 3.2 – RAG8 Treatment Did Not Affect HFCC Diet-Induced Atherosclerosis Development in the Aortic Sinus of SR-B1/LDLR DKO Mice. Representative images of oil red O-stained transverse sections of the aortic sinus showing atherosclerotic plaque from (A) control SRQ8-treated and (B) RAG8-treated SR-B1/LDLR DKO mice. Scale bar= 200 μm. (C) Aortic sinus atherosclerotic plaque cross-sectional areas vs. distance and (D) atherosclerotic plaque volumes (areas under the curves of plaque area vs. distance) of HFCC diet-fed SR-B1/LDLR DKO mice treated with control SRQ8 pepducin or RAG8 pepducin. Data points in (C) represent means (n=11, 12). Data in (C) were analyzed by two-way ANOVA with Sidak's multiple comparisons post-hoc test. Each data point in (D) represents an individual mouse (n=11, 12). Bars represent means and error bars represent standard errors of the mean. Data in (D) did not pass the normality test and were analyzed by Mann-Whitney Rank Sum Test. ns = not statistically significant.

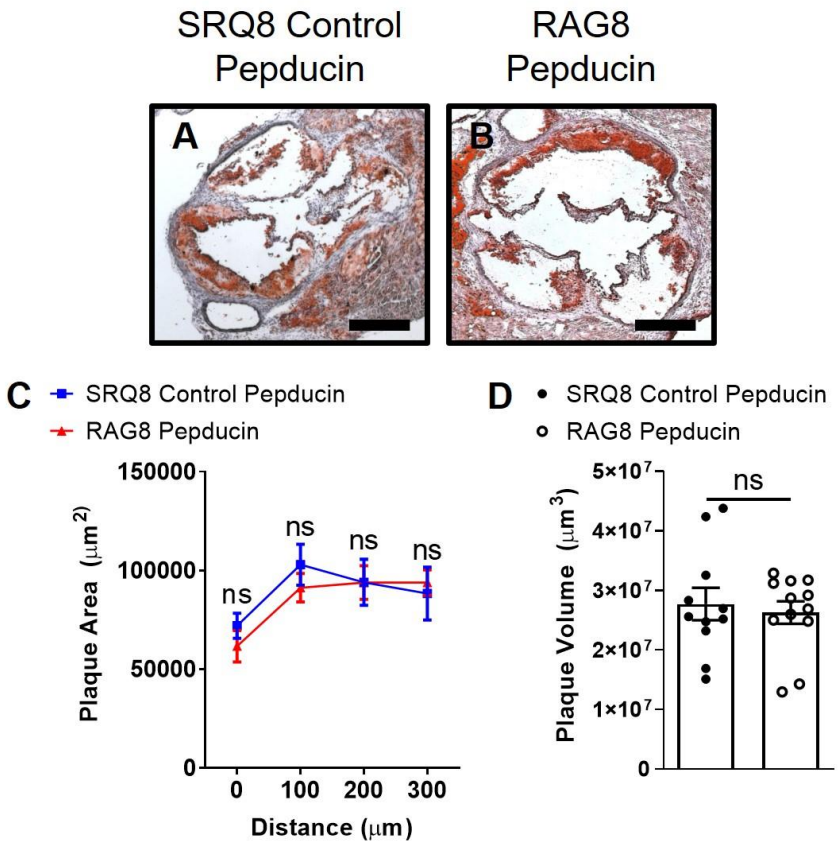
SRQ8 Control Pepducin
RAG8 Pepducin
A
B
C
SRQ8 Control Pepducin
RAG8 Pepducin
Plaque Area (μm2)
150000
100000
50000
0
ns
ns
ns
ns
0
100
200
300
Distance (μm)
D
SRQ8 Control Pepducin
RAG8 Pepducin
Plaque Volume (μm3)
5×10^7
4×10^7
3×10^7
2×10^7
1×10^7
0
ns

Figure 3.3 – RAG8 Treatment Reduced Coronary Artery Atherosclerosis and VCAM-1 Protein Levels in Non-Atherosclerotic Coronary Arteries of HFCC Diet-Fed SR-B1/LDLR DKO Mice. Seven sections of each heart were stained with oil red O/hematoxylin, and coronary arteries were scored as either 0% (non-atherosclerotic) or containing atherosclerotic plaques that occluded <50%, >50% or 100% of their lumen. (A) to (D) Representative images of coronary arteries for each category are shown. Scale bar= 50 μm. (E) Quantification of coronary arteries in each category (as percentage of total) across seven heart sections for each mouse (n=10, 12 mice). Representative fluorescence images of VCAM-1 immunofluorescence (red) and DAPI (blue) nuclear counter-staining in non-atherosclerotic coronary artery sections from (F) control SRQ8-treated and (H) RAG8-treated SR-B1/LDLR DKO mice, with adjacent sections stained with oil red O (G) and (I). Scale bar= 50 μm. (J) Proportions of non-atherosclerotic coronary artery sections with positive VCAM-1 staining across seven heart sections for each mouse (n=10 mice per group). Each data point represents an individual mouse. Bars represent means and error bars represent standard errors of the mean. Data in (E) were analyzed by two-way ANOVA with Sidak's multiple comparisons post-hoc test. Data in (J) passed the normality test and were analyzed by Student's t-test. ***P <0.001, ****P <0.0001.

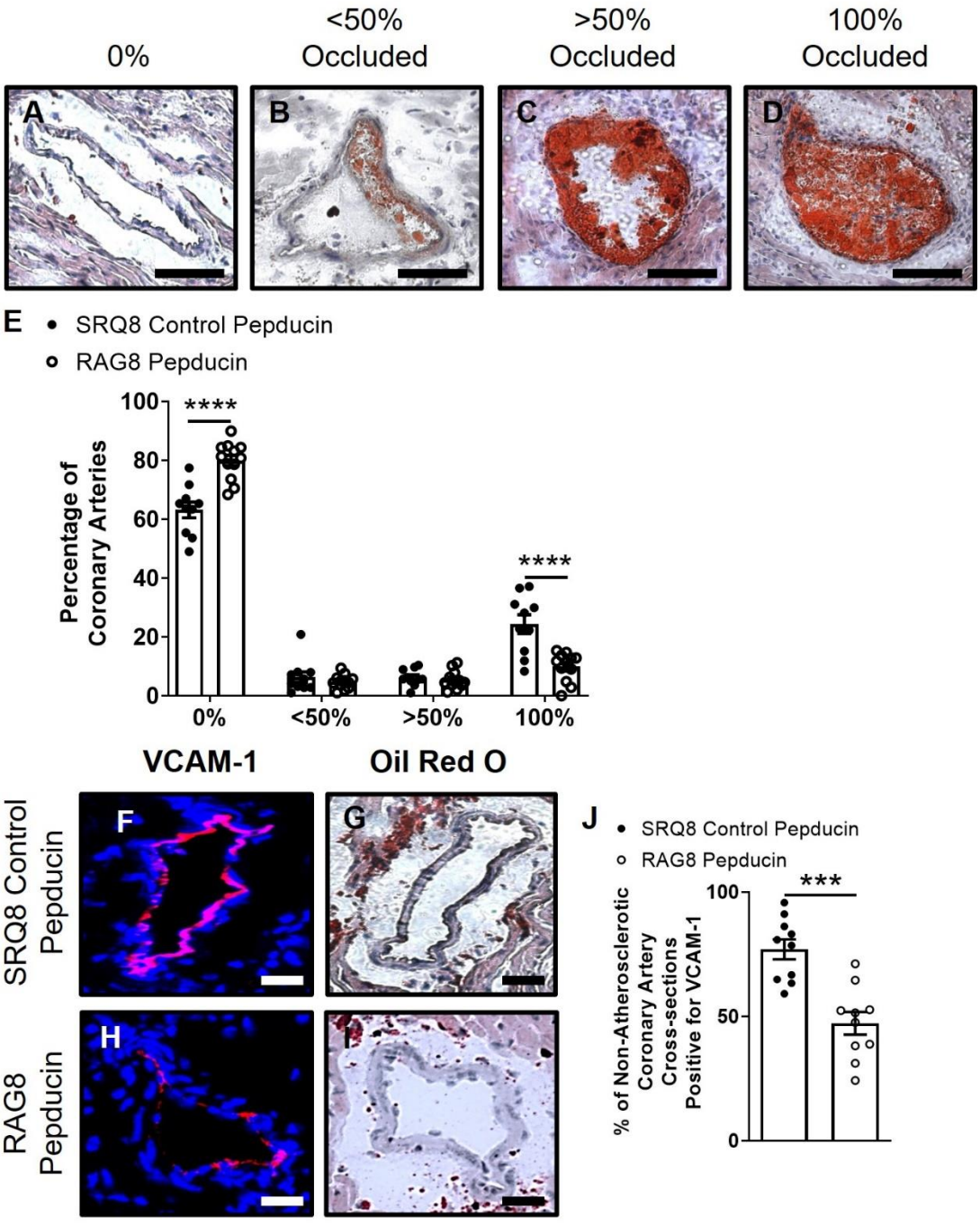
0%
<50% Occluded
>50% Occluded
100% Occluded
A
B
C
D
E
SRQ8 Control Pepducin
RAG8 Pepducin
Percentage of Coronary Arteries
100
80
60
40
20
0
****
****
0%
<50%
>50%
100%
VCAM-1
Oil Red O
SRQ8 Control Pepducin
RAG8 Pepducin
F
G
H
I
J
SRQ8 Control Pepducin
RAG8 Pepducin
% of Non-Atherosclerotic Coronary Artery Cross-sections Positive for VCAM-1
100
50
0
***

3.4.3 RAG8 Treatment Reduced Platelet Accumulation in Atherosclerotic Coronary Arteries in SR-B1/LDLR DKO Mice

Consistent with previous reports, a substantial percentage of atherosclerotic coronary arteries in SR-B1/LDLR DKO mice fed a HFCC diet showed abundant staining for CD41, a marker of platelets[15] (Supplementary Figures 3.7N and P), suggesting that CAD development in these mice may involve thrombus formation in addition to atherosclerosis development. Since the RAG8 pepducin inhibits thrombin-triggered platelet aggregation *in vitro* and attenuates clot stabilization *in vivo*[27], we sought to determine if treatment of the HFCC diet-fed SR-B1/LDLR DKO mice with the RAG8 pepducin impacted platelet accumulation in atherosclerotic coronary arteries. Therefore, we performed CD41 immunostaining and quantified the proportion of atherosclerotic coronary arteries that showed positive CD41 staining across 7 cardiac cross-sections for both the RAG8-treated and the inactive SRQ8 control pepducin-treated HFCC-fed SR-B1/LDLR DKO mice. RAG8-treated SR-B1/LDLR DKO mice had significantly reduced proportions of atherosclerotic coronary arteries that were positive for CD41 staining compared to the SRQ8-treated SR-B1/LDLR DKO mice (29.6 ± 2.5% vs. 52.2 ± 2.5%; $P < 0.0001$; Figure 3.4E), which themselves did not differ significantly from untreated HFCC diet-fed SR-B1/LDLR DKO mice (compare Figure 3.4E with Supplementary Figure 3.7P). Taken together, these data suggest that in addition to reducing the degree of coronary artery atherosclerosis, PAR4 inhibition via RAG8 treatment reduced the

accumulation of platelets in atherosclerotic coronary arteries in HFCC diet-fed SR-B1/LDLR DKO mice.

Figure 3.4 – RAG8 Treatment Reduced Platelet Accumulation in Atherosclerotic Coronary Arteries of HFCC Diet-Fed SR-B1/LDLR DKO Mice. Representative images of CD41 immunofluorescence (green) and DAPI counterstaining from (A) control SRQ8-treated and (B) RAG8-treated SR-B1/LDLR DKO mice, with adjacent sections stained with oil red O (B) and (D). Scale bar= 50 μm. (E) Proportions of atherosclerotic coronary arteries with positive CD41 immunofluorescence staining across seven heart sections for each mouse (n=10 mice per group). Each data point represents an individual mouse. Bars represent means and error bars represent standard errors of the mean. Data in (E) did not pass the normality test and were analyzed by Mann-Whitney Rank Sum Test. ****P <0.0001.

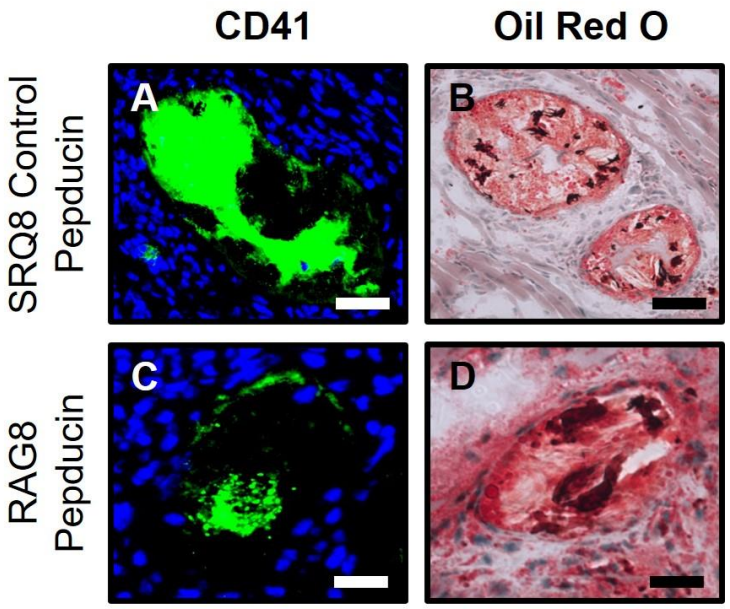
CD41
Oil Red O
SRQ8 Control Pepducin
RAG8 Pepducin
A
B
C
D

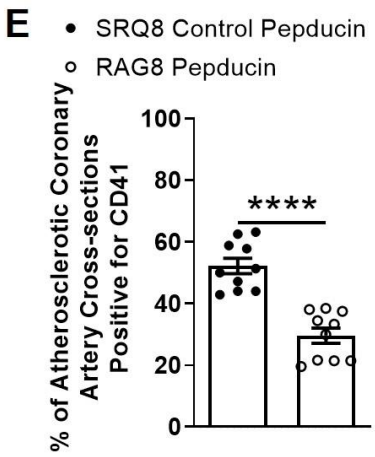
E
SRQ8 Control Pepducin
RAG8 Pepducin
% of Atherosclerotic Coronary Artery Cross-sections Positive for CD41
100
80
60
40
20
0
****

3.4.4 RAG8 Treatment Reduced Myocardial Fibrosis in HFCC Diet-Fed SR-B1/LDLR DKO Mice

Coronary artery atherosclerosis in SR-B1/LDLR DKO mice fed a HFCC diet is accompanied by myocardial fibrosis[15] which can be detected by staining frozen cross-sections of myocardial tissue with Masson's trichrome to differentiate collagen-rich fibrotic regions, which stain blue/purple, from healthy myocardium, which stains red. Untreated HFCC diet-fed SR-B1/LDLR DKO mice in comparison to untreated LDLR single KO mice exhibited increased myocardial fibrosis, increased heart:body weights, and increased plasma levels of cardiac troponin I and creatine kinase (CK)-MB, indicators of myocardial enlargement and damage, respectively (Supplementary Figures 3.8C-F). RAG8-treated HFCC diet-fed SR-B1/LDLR DKO mice had a significant reduction in myocardial fibrosis compared to inactive SRQ8 control pepducin-treated HFCC diet-fed SR-B1/LDLR DKO mice (0.9 ± 0.2% vs. 2.7 ± 0.2%; $P < 0.0001$; Figures 3.5A-C). Despite this, we observed no reductions in either heart:body weight ratios or plasma levels of cardiac troponin I or CK-MB between RAG8-treated and SRQ8-treated SR-B1/LDLR DKO mice fed the HFCC diet (Figures 3.5D-F). Nevertheless, the reduced collagen deposition is consistent with RAG8 treatment leading to at least some attenuation of myocardial damage, likely as a consequence of reduced coronary artery atherosclerosis burden.

Figure 3.5 – RAG8 Treatment Reduced Development of Myocardial Fibrosis in HFCC Diet-Fed SR-B1/LDLR DKO Mice. Representative images of Masson's trichrome-stained transverse cryosections of myocardium from (A) control SRQ8-treated and (B) RAG8-treated SR-B1/LDLR DKO mice. Red colored staining indicates undamaged cardiomyocytes, whereas blue/purple colored staining indicates the presence of collagen. Scale bar= 200 μm. (C) Quantification of the percentage of myocardial fibrosis measured by the area of blue staining relative to the cross-sectional area of the heart for one section per mouse (n=10, 11). (D) Heart-to-body weight ratios (n=15, 17). (E) Plasma troponin I levels (n=8, 8). (F) Plasma creatine kinase myocardial band (CK-MB) levels (n=10, 10). Each data point represents an individual mouse. Bars represent means and error bars represent standard errors of the mean. Data in (C) to (F) passed normality tests and were analyzed by Student's t-test. ****P <0.0001.

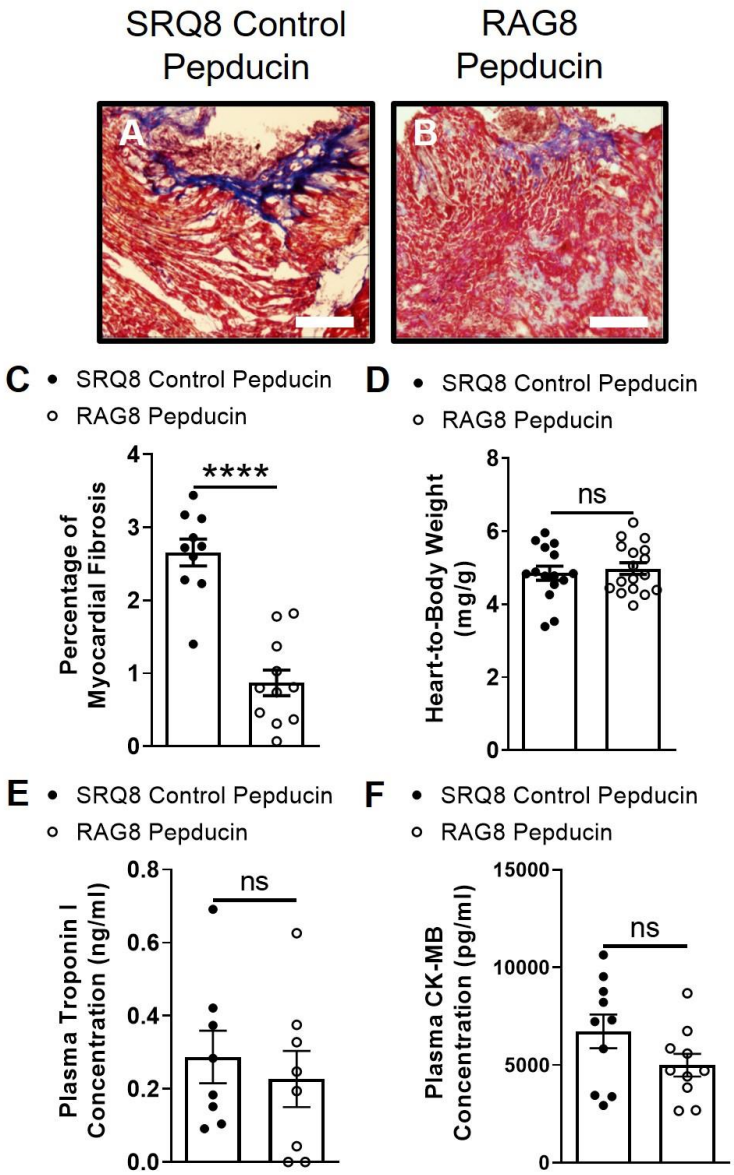
SRQ8 Control Pepducin
RAG8 Pepducin
A
B
C
SRQ8 Control Pepducin
RAG8 Pepducin
Percentage of Myocardial Fibrosis
****
D
SRQ8 Control Pepducin
RAG8 Pepducin
Heart-to-Body Weight (mg/g)
ns
E
SRQ8 Control Pepducin
RAG8 Pepducin
Plasma Troponin I Concentration (ng/ml)
ns
F
SRQ8 Control Pepducin
RAG8 Pepducin
Plasma CK-MB Concentration (pg/ml)
ns

3.4.5 RAG8 Treatment Did Not Affect Circulating Lipid, Cytokine and Immune Cell Levels in HFCC Diet-Fed SR-B1/LDLR DKO Mice

Since hypercholesterolemia is a major contributing factor to the development of atherosclerosis in general and in particular in this mouse model of diet-induced CAD (Supplementary Figures 3.9A-F), we examined whether RAG8 treatment had unanticipated effects on plasma lipid levels in the treated mice. No differences were observed in any of the plasma lipid parameters (total, unesterified, esterified, HDL and non-HDL cholesterol and triglycerides) measured (Figures 3.6A-F), confirming that PAR4 inhibition does not impact plasma lipid levels in this model.

We previously reported increased plasma levels of the pro-inflammatory cytokines TNFα and IL-6 in HFCC diet-fed SR-B1/LDLR DKO mice compared to HFCC diet-fed LDLR single KO mice[15]. Consistent with this, we observed increased IL-6 and a trend to increased TNFα in plasma from the untreated SR-B1/LDLR DKO mice compared to LDLR single KO mice when both were fed the HFCC diet (Supplementary Figures 3.9G-H). However, neither RAG8 pepducin treatment nor SRQ8 control pepducin treatment affected circulating TNFα or IL-6 levels in the HFCC diet-fed SR-B1/LDLR DKO mice (Figures 3.6G-H). Similarly, treatment with the RAG8 pepducin did not affect the elevated blood levels of various leukocytes previously reported in HFCC diet-fed SR-B1/LDLR DKO mice[15] (Supplementary Figure 3.11). Together, these results indicate that the PAR4 inhibitor RAG8 pepducin did not exhibit a general anti-inflammatory effect.

Figure 3.6 – RAG8 Treatment Did Not Affect Plasma Lipid and Cytokine Levels in HFCC Diet-Fed SR-B1/LDLR DKO Mice. (A) Plasma total cholesterol. (B) Plasma unesterified cholesterol. (C) Plasma esterified cholesterol (calculated as the difference between total and unesterified cholesterol). (D) Plasma HDL cholesterol. (E) Plasma non-HDL cholesterol (calculated as the difference between total and HDL cholesterol) (F) Plasma triglycerides. N=9, 8 for all plasma lipid analyses. (G) Plasma tumour necrosis factor alpha (TNFα) (n=9, 8). (H) Plasma interleukin-6 (IL-6) (n=10, 10). Each data point represents an individual mouse. Bars represent means and error bars represent standard errors of the mean. All data passed the normality test and were analyzed by Student's t-test.

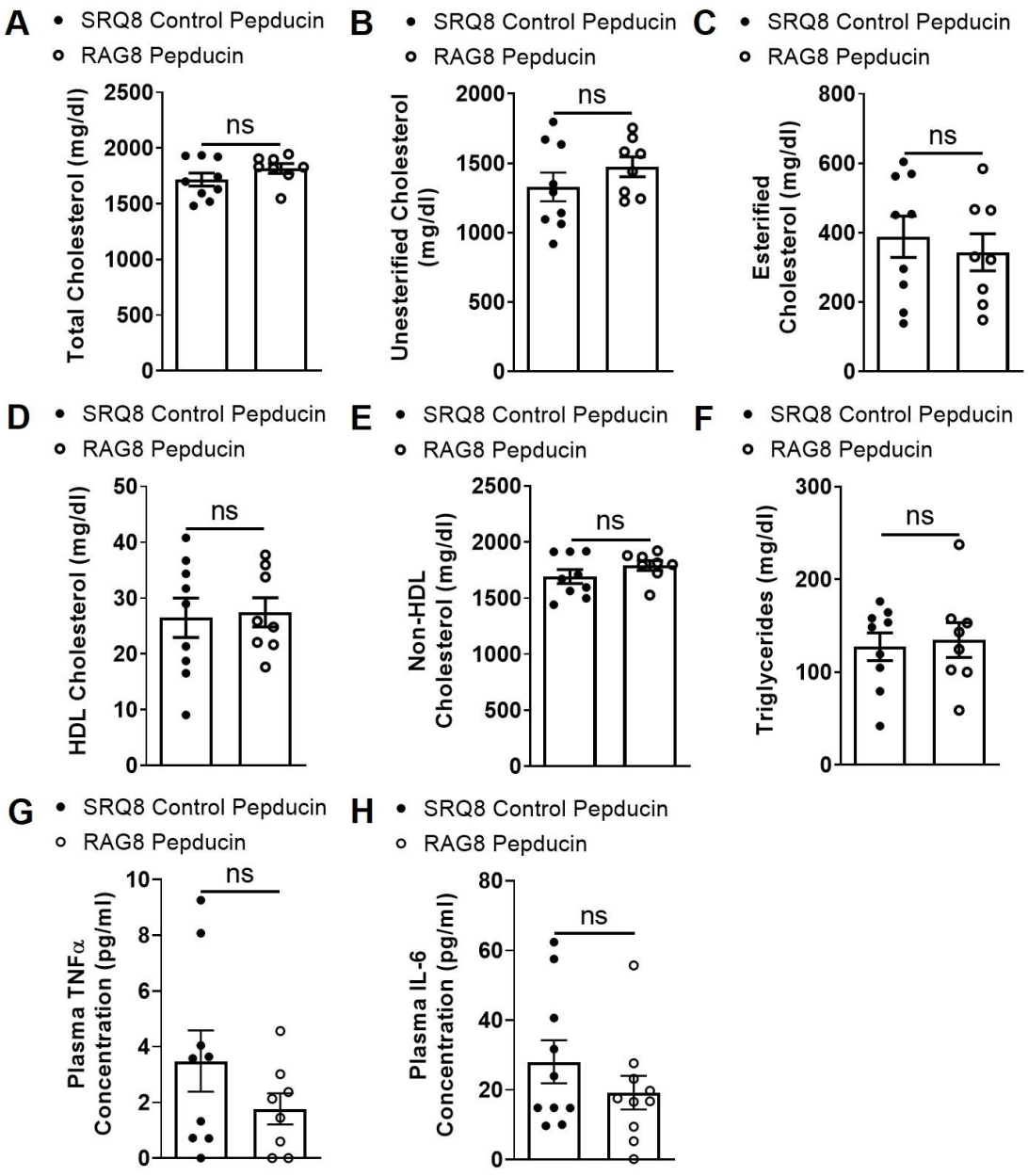
A
SRQ8 Control Pepducin
RAG8 Pepducin
Total Cholesterol (mg/dl)
2500
2000
1500
1000
500
0
ns
B
SRQ8 Control Pepducin
RAG8 Pepducin
Unesterified Cholesterol (mg/dl)
2000
1500
1000
500
0
ns
C
SRQ8 Control Pepducin
RAG8 Pepducin
Esterified Cholesterol (mg/dl)
800
600
400
200
0
ns
D
SRQ8 Control Pepducin
RAG8 Pepducin
HDL Cholesterol (mg/dl)
50
40
30
20
10
0
ns
E
SRQ8 Control Pepducin
RAG8 Pepducin
Non-HDL Cholesterol (mg/dl)
2500
2000
1500
1000
500
0
ns
F
SRQ8 Control Pepducin
RAG8 Pepducin
Triglycerides (mg/dl)
300
200
100
0
ns
G
SRQ8 Control Pepducin
RAG8 Pepducin
Plasma TNFα Concentration (pg/ml)
10
8
6
4
2
0
ns
H
SRQ8 Control Pepducin
RAG8 Pepducin
Plasma IL-6 Concentration (pg/ml)
80
60
40
20
0
ns

3.5 Discussion

Here, we demonstrated that treatment of HFCC diet-fed SR-B1/LDLR DKO mice with the RAG8 pepducin attenuated atherosclerosis development in coronary arteries but not the aortic sinus, VCAM-1 protein levels in coronary arteries, accumulation of platelets in atherosclerotic coronary arteries, and myocardial fibrosis, suggesting a role for PAR4 in these processes. HFCC diet-fed SR-B1/LDLR DKO mice exhibit extensive aortic sinus and coronary artery atherosclerosis, platelet accumulation in atherosclerotic coronary arteries, myocardial infarction, and rapid death with a median survival of 3.5 weeks of HFCC diet feeding[15]. Hypercholesterolemic SR-B1 KO mice exhibit thrombocytopenia[18–20] and consistent with this, we found that HFCC diet-fed SR-B1/LDLR DKO mice exhibited increased tail bleeding times compared to similarly fed LDLR single KO mice. It has also been reported that platelets in hypercholesterolemic SR-B1 KO mice circulate in an activated state, although they remain sensitive to activation by PAR4 agonists[18–20]. These effects appear to be due to increased plasma lipoprotein associated with unesterified cholesterol, leading to increased unesterified cholesterol associated with platelets[18–20]. SR-B1 KO mice have also been reported to be more susceptible to experimental thrombosis[19] and, indeed, we reported that SR-B1 KO mice on different atherogenic backgrounds including LDLR KO exhibit platelet accumulation in atherosclerotic coronary arteries[15,21,31].

Given that platelets from SR-B1 KO mice remain sensitive to PAR4-mediated activation, we set out to test the consequences of inhibiting PAR4 on

CAD development in response to HFCC diet feeding in SR-B1/LDLR DKO mice. RAG8, a pepducin corresponding to an 8 amino acid motif in the C-terminus of PAR4 (but not a control pepducin SRQ8, containing the reverse amino acid sequence), is an effective inhibitor of PAR4-dependent calcium signaling and β-arrestin 1 and 2 recruitment in cultured cells, acts as a PAR4-selective inhibitor of Akt phosphorylation, blocks PAR4-dependent aggregation of human platelets *in vitro*, and attenuates $FeCl_3$-induced arterial thrombus formation and prolongs the time to stable occlusion in a tail bleeding assay in mice[27]. Therefore, we treated HFCC diet-fed SR-B1/LDLR DKO mice with the PAR4 inhibitory RAG8 and inactive control SRQ8 pepducins. Consistent with previously reported results utilizing these pepducins on C57BL/6J mice[27], treatment of HFCC diet-fed SR-B1/LDLR DKO mice with RAG8 but not SRQ8 resulted in increased time to occlusion in a tail bleeding assay, confirming an important role for PAR4 in platelet function in these mice. The increased tail bleeding is likely due to the effects of PAR4 inhibition on platelets rather than on other cell types such as endothelial cells, as mice reconstituted with bone marrow cells from PAR4 KO mice also exhibit increased tail bleeding times compared to control mice[32]. We observed no evidence of spontaneous bleeding in our mice.

We observed lower levels of CD41 staining in atherosclerotic coronary arteries from HFCC diet-fed SR-B1/LDLR DKO mice that had been treated with the RAG8 pepducin as compared to the inactive control SRQ8 pepducin, suggesting that PAR4 inhibition reduced the accumulation of platelets in atherosclerotic

coronary arteries in these mice. This is consistent with the known role for PAR4 in activation of murine platelets and the reported sensitivity of platelets from SR-B1 deficient hypercholesterolemic mice to PAR4 activation[18–20,27].

HFCC diet-fed SR-B1/LDLR DKO mice that had been treated with the RAG8 pepducin exhibited a reduction in the extent of coronary artery atherosclerosis as compared with those treated with the control SRQ8 pepducin, although no differences were observed in atherosclerosis development in the aortic sinus. The lack of protection against aortic sinus atherosclerosis via PAR4 inhibition seen here is consistent with results from a study that analyzed ApoE/PAR4 DKO mice fed a high-fat diet for 10 weeks, in which no changes in aortic sinus atherosclerosis were observed compared to ApoE single KO mice[33]. This suggests that, at least in SR-B1/LDLR DKO mice, the development of atherosclerosis in coronary arteries but not in the aortic sinus is sensitive to PAR4 inhibition. We have previously reported that increased coronary artery atherosclerosis in atherogenic diet-fed SR-B1/LDLR DKO mice (compared to LDLR single KO mice) is accompanied by increased protein levels of VCAM-1 in non-atherosclerotic coronary arteries[15] (also see Supplementary Figures 3.7G, I and K). RAG8 treatment of HFCC diet-fed SR-B1/LDLR DKO mice was accompanied by a reduction in the extent of VCAM-1 immunofluorescence in non-atherosclerotic coronary arteries. VCAM-1 is upregulated in activated endothelium and promotes atherosclerosis by promoting the adhesion of leukocytes on the artery wall[5]. This suggests that PAR4 inhibition may have resulted in reduced coronary artery atherosclerosis at least in part, by

attenuating expression of VCAM-1 in coronary artery endothelium. Whether this is a direct effect of RAG8-mediated inhibition of PAR4 on endothelial cells, or an indirect effect through RAG8-mediated inhibition of PAR4 on platelets is not clear. *In vitro*, inflammatory cytokines such as TNFα are known to upregulate both PAR4[34] and VCAM-1[35,36] in endothelial cells, and thrombin activation of PAR1 has been reported to trigger VCAM-1 expression[37,38], although a direct role for PAR4 in VCAM-1 upregulation has not been described. Activated platelets have also been reported to release factors such as IL-1β and CD40L which trigger endothelial cell activation and upregulation of VCAM-1[11]. The precise mechanism by which PAR4 may be involved and RAG8 attenuated VCAM-1 protein levels in coronary arteries of the HFCC diet-fed SR-B1/LDLR DKO mice remains to be elucidated.

RAG8 treatment of HFCC diet-fed SR-B1/LDLR DKO mice reduced myocardial fibrosis, although no statistically significant reductions in plasma markers of cardiomyocyte damage (cardiac troponin I or CK-MB) or heart:body weight ratios were observed. The reduced cardiac fibrosis may be secondary to reduced coronary artery atherosclerosis, although direct effects of PAR4 inhibition on myocardial fibrosis cannot be ruled out. For example, consistent with our findings, PAR4 KO has been reported to reduce myocardial fibrosis during early stages (2 days) after acute myocardial infarction in a murine coronary artery ligation model; however, PAR4 KO was found to be detrimental at later stages (7 days) as it was associated with impaired resolution of inflammation and myocardial healing[39,40]. Whether prolonged treatment of HFCC diet-fed SR-B1/LDLR DKO

mice with the RAG8 pepducin might similarly exhibit long-term detrimental effects remains to be examined.

Nevertheless, our findings suggest that RAG8-mediated PAR4 inhibition protects against acute CAD by reducing coronary artery atherosclerosis, platelet accumulation in atherosclerotic coronary arteries, and myocardial fibrosis in HFCC diet-fed SR-B1/LDLR DKO mice. These protective effects by RAG8 were not accompanied by changes in circulating lipids, cytokines, or immune cell levels, but are likely driven in part by reduced VCAM-1 protein levels in coronary arteries. Moreover, our study suggests that utilizing RAG8 as a tool to inhibit PAR4 may potentially be beneficial in cardiovascular disease settings. Although RAG8 appears to impair hemostasis in mice, the beneficial effects of reducing coronary artery atherosclerosis and myocardial fibrosis likely outweigh the risk of increased bleeding, especially considering that RAG8-mediated PAR4 inhibition does not induce spontaneous bleeding. We show for the first time that PAR4 inhibition reduces coronary artery atherosclerosis, platelet accumulation in atherosclerotic coronary arteries, and myocardial fibrosis in mice, suggesting that targeting PAR4 appears to be a useful approach in reducing CAD development.

3.6 References

1. Tryfonos A, Green DJ, Dawson EA. Effects of Catheterization on Artery Function and Health: When Should Patients Start Exercising Following

Their Coronary Intervention? *Sports Medicine (Auckland, N.Z.)*. 2019;49(3):397–416.

2. Hansson GK, Hermansson A. The immune system in atherosclerosis. *Nature Immunology*. 2011;12(3):204–212.
3. Galkina E, Ley K. Vascular adhesion molecules in atherosclerosis. *Arteriosclerosis, Thrombosis, and Vascular Biology*. 2007;27(11):2292–2301.
4. Hajra L, Evans AI, Chen M, Hyduk SJ, Collins T, Cybulsky MI. The NF-κB signal transduction pathway in aortic endothelial cells is primed for activation in regions predisposed to atherosclerotic lesion formation. *Proceedings of the National Academy of Sciences of the United States of America*. 2000;97(16):9052–9057.
5. Cybulsky MI, Iiyama K, Li H, Zhu S, Chen M, Iiyama M, Davis V, Gutierrez-Ramos JC, Connelly PW, Milstone DS. A major role for VCAM-1, but not ICAM-1, in early atherosclerosis. *Journal of Clinical Investigation*. 2001;107(10):1255–1262.
6. Ley K, Huo Y. VCAM-1 is critical in atherosclerosis. *Journal of Clinical Investigation*. 2001;107(10):1209–1210.
7. Bentzon JF, Otsuka F, Virmani R, Falk E. Mechanisms of plaque formation and rupture. *Circulation Research*. 2014;114(12):1852–1866.
8. Leys D. Atherothrombosis: A major health burden. In: *Cerebrovascular Diseases*.Vol 11.; 2001:1–4.

9. Zernecke A, Weber C. Chemokines in atherosclerosis: proceedings resumed. *Arteriosclerosis, Thrombosis, and Vascular Biology*. 2014;34(4):742–750.
10. Bakogiannis C, Sachse M, Stamatelopoulos K, Stellos K. Platelet-derived chemokines in inflammation and atherosclerosis. *Cytokine*. 2019;122:154157.
11. Gawaz M, Langer H, May AE. Platelets in inflammation and atherogenesis. *The Journal of Clinical Investigation*. 2005;115(12):3378–3384.
12. Periayah MH, Halim AS, Mat Saad AZ. Mechanism Action of Platelets and Crucial Blood Coagulation Pathways in Hemostasis. *International Journal of Hematology-Oncology and Stem Cell Research*. 2017;11(4):319–327.
13. Braun A, Trigatti BL, Post MJ, Sato K, Simons M, Edelberg JM, Rosenberg RD, Schrenzel M, Krieger M. Loss of SR-BI expression leads to the early onset of occlusive atherosclerotic coronary artery disease, spontaneous myocardial infarctions, severe cardiac dysfunction, and premature death in apolipoprotein E-deficient mice. *Circulation Research*. 2002;90(3):270–276.
14. Zhang S, Picard MH, Vasile E, Zhu Y, Raffai RL, Weisgraber KH, Krieger M. Diet-induced occlusive coronary atherosclerosis, myocardial infarction, cardiac dysfunction, and premature death in scavenger receptor class B

type I-deficient, hypomorphic apolipoprotein ER61 mice. *Circulation*. 2005;111(25):3457–3464.

15. Fuller M, Dadoo O, Serkis V, Abutouk D, MacDonald M, Dhingani N, Macri J, Igdoura SA, Trigatti BL. The effects of diet on occlusive coronary artery atherosclerosis and myocardial infarction in scavenger receptor class B, type 1/low-density lipoprotein receptor double knockout mice. *Arteriosclerosis, Thrombosis, and Vascular Biology*. 2014;34(11):2394–2403.
16. Van Eck M, Twisk J, Hoekstra M, Van Rij BT, Van der Lans CAC, Bos IST, Kruijt JK, Kuipers F, Van Berkel TJC. Differential effects of scavenger receptor BI deficiency on lipid metabolism in cells of the arterial wall and in the liver. *The Journal of Biological Chemistry*. 2003;278(26):23699–23705.
17. Rigotti A, Trigatti BL, Penman M, Rayburn H, Herz J, Krieger M. A targeted mutation in the murine gene encoding the high density lipoprotein (HDL) receptor scavenger receptor class B type I reveals its key role in HDL metabolism. *Proceedings of the National Academy of Sciences of the United States of America*. 1997;94(23):12610–12615.
18. Ma Y, Ashraf MZ, Podrez EA. Scavenger receptor BI modulates platelet reactivity and thrombosis in dyslipidemia. *Blood*. 2010;116(11):1932–1941.
19. Korporaal SJA, Meurs I, Hauer AD, Hildebrand RB, Hoekstra M, Cate HT, Praticò D, Akkerman J-WN, Van Berkel TJC, Kuiper J, Van Eck M. Deletion of the high-density lipoprotein receptor scavenger receptor BI in

mice modulates thrombosis susceptibility and indirectly affects platelet function by elevation of plasma free cholesterol. *Arteriosclerosis, Thrombosis, and Vascular Biology*. 2011;31(1):34–42.

20. Dole VS, Matuskova J, Vasile E, Yesilaltay A, Bergmeier W, Bernimoulin M, Wagner DD, Krieger M. Thrombocytopenia and platelet abnormalities in high-density lipoprotein receptor-deficient mice. *Arteriosclerosis, Thrombosis, and Vascular Biology*. 2008;28(6):1111–1116.
21. Yu P, Xiong T, Tenedero CB, Lebeau P, Ni R, Macdonald ME, Gross PL, Austin RC, Trigatti BL. Rosuvastatin Reduces Aortic Sinus and Coronary Artery Atherosclerosis in SR-B1 (Scavenger Receptor Class B Type 1)/ApoE (Apolipoprotein E) Double Knockout Mice Independently of Plasma Cholesterol Lowering. *Arteriosclerosis, Thrombosis, and Vascular Biology*. 2018;38(1):26–39.
22. Hermann S, Kuhlmann MT, Starsichova A, Eligehausen S, Schäfers K, Stypmann J, Tiemann K, Levkau B, Schäfers M. Imaging reveals the connection between spontaneous coronary plaque ruptures, atherothrombosis, and myocardial infarctions in HypoE/SRBI2/2 Mice. *Journal of Nuclear Medicine*. 2016;57(9):1420–1427.
23. Coughlin SR. Thrombin signalling and protease-activated receptors. *Nature*. 2000;407(6801):258–264.
24. Gieseler F, Ungefroren H, Settmacher U, Hollenberg MD, Kaufmann R. Proteinase-activated receptors (PARs) – focus on receptor-receptor-

interactions and their physiological and pathophysiological impact. *Cell Communication and Signaling : CCS*. 2013;11:86.

25. Sambrano GR, Weiss EJ, Zheng YW, Huang W, Coughlin SR. Role of thrombin signalling in platelets in haemostasis and thrombosis. *Nature*. 2001;413(6851):74–78.
26. Bynagari-Settipalli YS, Cornelissen I, Palmer D, Duong D, Concengco C, Ware J, Coughlin SR. Redundancy and Interaction of Thrombin- and Collagen-Mediated Platelet Activation in Tail Bleeding and Carotid Thrombosis in Mice. *Arteriosclerosis, Thrombosis, and Vascular Biology*. 2014;34(12):2563–2569.
27. Ramachandran R, Mihara K, Thibeault P, Vanderboor CM, Petri B, Saifeddine M, Bouvier M, Hollenberg MD. Targeting a proteinase-activated receptor 4 (PAR4) carboxyl terminal motif to regulate platelet function. *Molecular Pharmacology*. 2017;91(4):287–295.
28. Paigen B, Morrow A, Brandon C, Mitchell D, Holmes P. Variation in susceptibility to atherosclerosis among inbred strains of mice. *Atherosclerosis*. 1985;57(1):65–73.
29. Iiyama K, Hajra L, Iiyama M, Li H, DiChiara M, Medoff BD, Cybulsky MI. Patterns of vascular cell adhesion molecule-1 and intercellular adhesion molecule-1 expression in rabbit and mouse atherosclerotic lesions and at sites predisposed to lesion formation. *Circulation Research*. 1999;85(2):199–207.

30. Ouweneel AB, Hoekstra M, van der Wel EJ, Schaftenaar FH, Snip OSC, Hassan J, Korporaal SJA, Van Eck M. Hypercholesterolemia impairs megakaryopoiesis and platelet production in scavenger receptor BI knockout mice. *Atherosclerosis*. 2019;282:176–182.

31. Gonzalez L, MacDonald ME, Deng YD, Trigatti BL. Hyperglycemia aggravates diet - Induced coronary artery disease and myocardial infarction in SR -B1 -Knockout/ApoE -Hypomorphic mice. *Frontiers in Physiology*. 2018;9:1398.

32. Hamilton JR, Cornelissen I, Coughlin SR. Impaired hemostasis and protection against thrombosis in protease-activated receptor 4-deficient mice is due to lack of thrombin signaling in platelets. *Journal of Thrombosis and Haemostasis*. 2004;2(8):1429–1435.

33. Hamilton JR, Cornelissen I, Mountford JK, Coughlin SR. Atherosclerosis proceeds independently of thrombin-induced platelet activation in ApoE-/- mice. *Atherosclerosis*. 2009;205(2):427–432.

34. Hamilton JR, Frauman AG, Cocks TM. Increased Expression of Protease-Activated Receptor-2 (PAR2) and PAR4 in Human Coronary Artery by Inflammatory Stimuli Unveils Endothelium-Dependent Relaxations to PAR2 and PAR4 Agonists. *Circulation Research*. 2001;89(1):92–98.

35. Cook-Mills JM, Marchese ME, Abdala-Valencia H. Vascular cell adhesion molecule-1 expression and signaling during disease: regulation by reactive

oxygen species and antioxidants. *Antioxidants & Redox Signaling*. 2011;15(6):1607–1638.

36. Zhang F, Yu W, Hargrove JL, Greenspan P, Dean RG, Taylor EW, Hartle DK. Inhibition of TNF-alpha induced ICAM-1, VCAM-1 and E-selectin expression by selenium. *Atherosclerosis*. 2002;161(2):381–386.
37. Rezaie AR. Protease-activated Receptor Signaling by Coagulation Proteases in Endothelial Cells. *Thrombosis and haemostasis*. 2014;112(5):876–882.
38. Minami T, Abid RM, Zhang J, King G, Kodama T, Aird WC. Thrombin stimulation of vascular adhesion molecule-1 in endothelial cells is mediated by protein kinase C (PKC)-δ-NF-κB and PKC-ζ-GATA signaling pathways. *Journal of Biological Chemistry*. 2003;278(9):6976–6984.
39. Kolpakov MA, Guo X, Rafiq K, Vlasenko L, Hooshdaran B, Seqqat R, Wang T, Fan X, Tilley DG, Kostyak JC, Kunapuli SP, Houser SR, Sabri A. Loss of Protease-Activated Receptor 4 Prevents Inflammation Resolution and Predisposes the Heart to Cardiac Rupture after Myocardial Infarction. *Circulation*. 2020:758–775.
40. Kolpakov MA, Rafiq K, Guo X, Hooshdaran B, Wang T, Vlasenko L, Bashkirova YV, Zhang X, Chen X, Iftikhar S, Libonati JR, Kunapuli SP, Sabri A. Protease-activated receptor 4 deficiency offers cardioprotection after acute ischemia reperfusion injury. *Journal of Molecular and Cellular Cardiology*. 2016;90:21–29.

3.7 Supplementary Materials

Supplementary Figure 3.7 – Atherosclerosis and Associated Phenotypes of Untreated LDLR Single KO and Untreated SR-B1/LDLR DKO Mice. (A) Untreated SR-B1/LDLR DKO mice exhibited increased tail bleeding times compared to untreated LDLR single KO mice. Mice were anesthetized and their tails were transected across the vein approximately 0.5 cm from the tip and placed in a cuvette with warm saline. The time to cessation of bleeding was monitored. Each data point represents an individual mouse (n=15, 10). Untreated SR-B1/LDLR DKO mice exhibited increased aortic sinus and coronary artery atherosclerosis compared to untreated LDLR single KO mice. Representative images of oil red O-stained transverse sections of the aortic sinus showing atherosclerotic plaque from (B) untreated LDLR KO and (C) untreated SR-B1/LDLR DKO mice. Scale bar= 200 μm. (D) Aortic sinus atherosclerotic plaque cross-sectional areas vs. distance and (E) atherosclerotic plaque volumes (areas under the curves of plaque area vs. distance) of untreated SR-B1/LDLR DKO mice and untreated LDLR single KO mice. Data points in (D) represent means (n=10, 9). (F) Quantification of coronary arteries in each category (as percentage of total) across seven heart sections per mouse (n=10 mice per group). Untreated SR-B1/LDLR DKO mice exhibited increased VCAM-1 levels in non-atherosclerotic coronary arteries compared to untreated LDLR single KO mice. Representative fluorescence images of VCAM-1 immunofluorescence (red) and DAPI (blue) nuclear counter-staining in non-atherosclerotic coronary artery sections from (G)

untreated LDLR single KO mice and (I) untreated SR-B1/LDLR DKO mice, with adjacent sections stained with oil red O (H) and (J). Scale bar= 50 μm. (K) Proportions of non-atherosclerotic coronary artery sections with positive VCAM-1 staining across seven heart sections for each mouse (n=10 mice per group). Untreated SR-B1/LDLR DKO mice exhibited increased platelet accumulation in atherosclerotic coronary arteries compared to untreated LDLR single KO mice. Representative images of CD41 immunofluorescence (green) and DAPI counterstaining from (L) untreated LDLR single KO mice and (N) untreated SR-B1/LDLR DKO mice, with adjacent sections stained with oil red O (M) and (O). Scale bar= 50 μm. (P) Proportions of atherosclerotic coronary arteries with positive CD41 immunofluorescence staining across seven heart sections for each mouse (n=10 mice per group). Bars represent means and error bars represent standard errors of the mean. Data in (A), (E) and (K) passed the normality test and were analyzed by Student's t-test. Data in (P) did not pass the normality test and were analyzed by Mann-Whitney Rank Sum Test. Data in (D) and (F) were analyzed by two-way ANOVA with Sidak's Multiple Comparisons Post-Hoc test. ****P <0.0001.

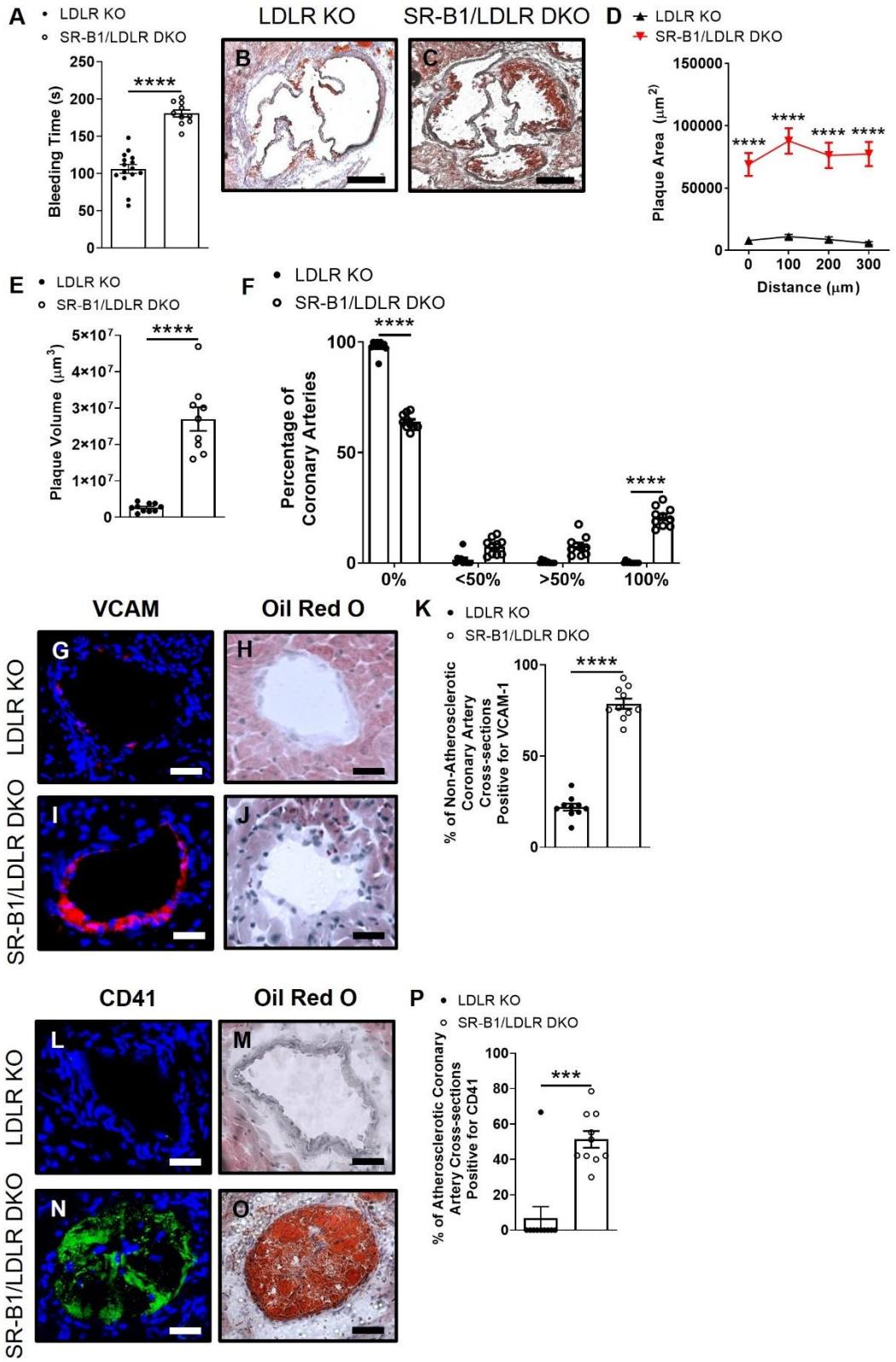
A
LDLR KO
SR-B1/LDLR DKO
Bleeding Time (s)
****
LDLR KO
SR-B1/LDLR DKO
B
C
D
LDLR KO
SR-B1/LDLR DKO
Plaque Area (μm²)
Distance (μm)
E
LDLR KO
SR-B1/LDLR DKO
Plaque Volume (μm³)
F
LDLR KO
SR-B1/LDLR DKO
Percentage of Coronary Arteries
0%
<50%
>50%
100%
VCAM
Oil Red O
LDLR KO
SR-B1/LDLR DKO
G
H
I
J
K
LDLR KO
SR-B1/LDLR DKO
% of Non-Atherosclerotic Coronary Artery Cross-sections Positive for VCAM-1
CD41
Oil Red O
L
M
N
O
P
LDLR KO
SR-B1/LDLR DKO
% of Atherosclerotic Coronary Artery Cross-sections Positive for CD41
***

Supplementary Figure 3.8 – Untreated SR-B1/LDLR DKO Mice Exhibited Increased Myocardial Fibrosis, Heart-to-Body Weight Ratio and Plasma Cardiac Damage Markers Compared to Untreated LDLR Single KO Mice. Representative images of Masson's trichrome-stained transverse cryosections of myocardium from (A) untreated LDLR single KO mice and (B) untreated SR-B1/LDLR DKO mice. Red colored staining indicates undamaged cardiomyocytes, whereas blue/purple colored staining indicates the presence of collagen. Scale bar= 200 μm. (C) Quantification of the percentage of myocardial fibrosis measured by the area of blue staining relative to the cross-sectional area of the heart for one section per mouse (n=10 per group). (D) Heart-to-body weight ratios (n=24, 10). (E) Plasma troponin I levels (n=12, 9). (F) Plasma creatine kinase myocardial band (CK-MB) levels (n=12, 10). Each data point represents an individual mouse. Bars represent means and error bars represent standard errors of the mean. Data in (C) to (E) did not pass the normality test and were analyzed by Mann-Whitney Rank Sum Test. Data in (F) passed the normality test and were analyzed by Student's t-test. **P <0.01, ****P <0.0001.

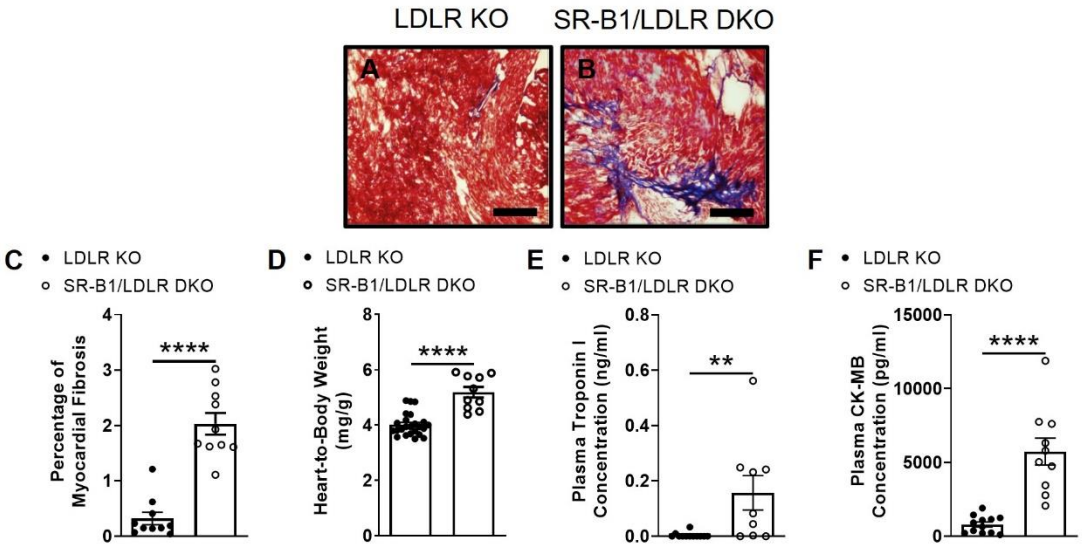
LDLR KO
SR-B1/LDLR DKO
A
B
C
LDLR KO
SR-B1/LDLR DKO
Percentage of Myocardial Fibrosis
****
D
LDLR KO
SR-B1/LDLR DKO
Heart-to-Body Weight (mg/g)
****
E
LDLR KO
SR-B1/LDLR DKO
Plasma Troponin I Concentration (ng/ml)
**
F
LDLR KO
SR-B1/LDLR DKO
Plasma CK-MB Concentration (pg/ml)
****

Supplementary Figure 3.9 – Untreated SR-B1/LDLR DKO Mice Exhibited Increased Plasma Lipid Levels and Circulating IL-6 Levels Compared to Untreated LDLR Single KO Mice. (A) Plasma total cholesterol. (B) Plasma unesterified cholesterol. (C) Plasma esterified cholesterol (calculated as the difference between total and unesterified cholesterol). (D) Plasma HDL cholesterol. (E) Plasma non-HDL cholesterol (calculated as the difference between total and HDL cholesterol) (F) Plasma triglycerides. N=12, 10 for all plasma lipid analyses. (G) Plasma tumour necrosis factor alpha (TNFα) (n=9, 10). (H) Plasma interleukin-6 (IL-6) (n=11, 10). Data in (A), (D), (F) and (H) did not pass the normality test and were analyzed by Mann-Whitney Rank Sum Test. Data in (B), (C), (E) and (G) passed the normality test and were analyzed by Student's t-test. Each data point represents an individual mouse. Bars represent means and error bars represent standard errors of the mean. *P <0.05, ***P <0.001, ****P <0.0001.

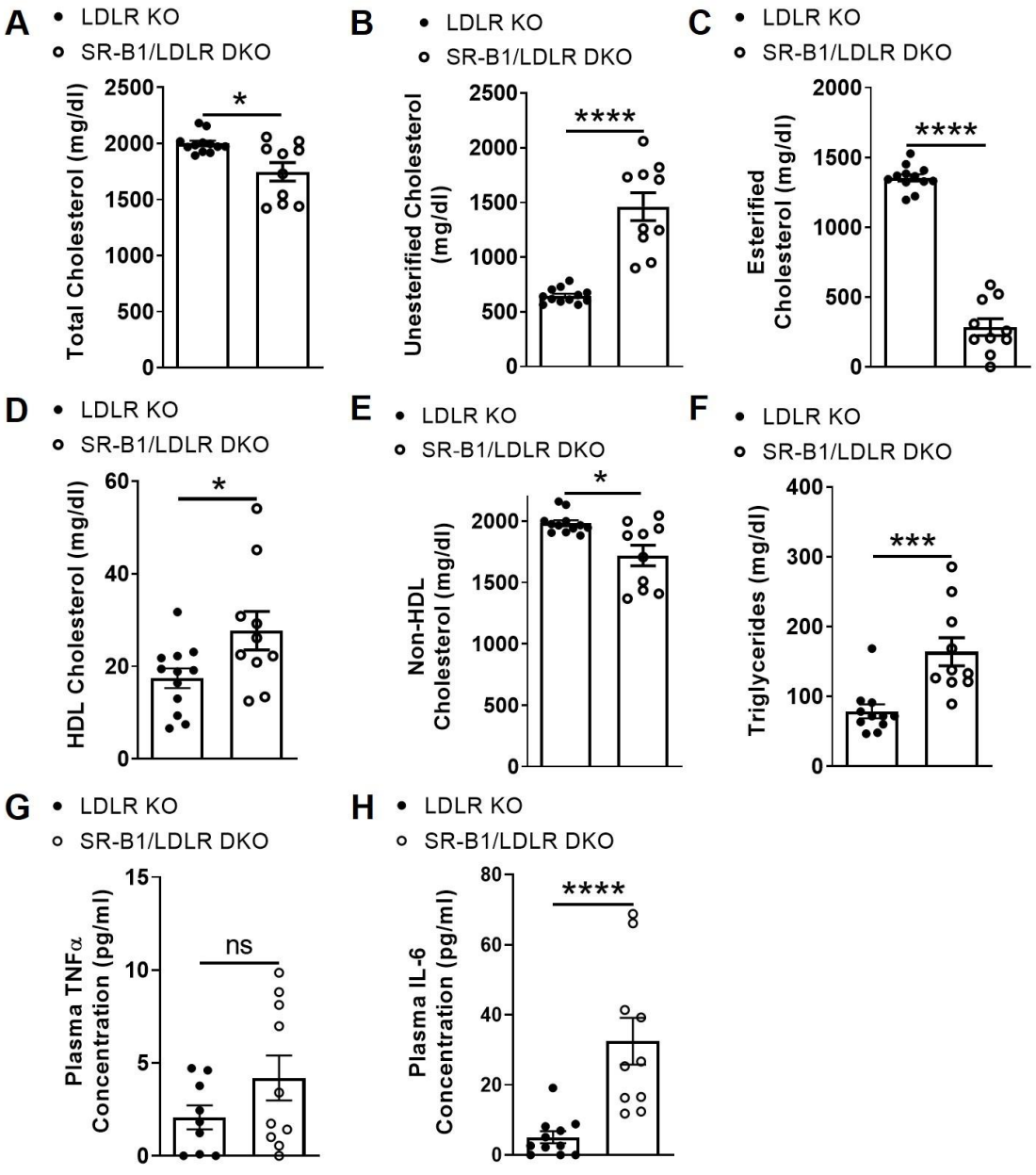
A
LDLR KO
SR-B1/LDLR DKO
Total Cholesterol (mg/dl)
2500
2000
1500
1000
500
0
*
B
LDLR KO
SR-B1/LDLR DKO
Unesterified Cholesterol (mg/dl)
2500
2000
1500
1000
500
0
****
C
LDLR KO
SR-B1/LDLR DKO
Esterified Cholesterol (mg/dl)
2000
1500
1000
500
0
****
D
LDLR KO
SR-B1/LDLR DKO
HDL Cholesterol (mg/dl)
60
40
20
0
*
E
LDLR KO
SR-B1/LDLR DKO
Non-HDL Cholesterol (mg/dl)
2000
1500
1000
500
0
*
F
LDLR KO
SR-B1/LDLR DKO
Triglycerides (mg/dl)
400
300
200
100
0
***
G
LDLR KO
SR-B1/LDLR DKO
Plasma TNFα Concentration (pg/ml)
15
10
5
0
ns
H
LDLR KO
SR-B1/LDLR DKO
Plasma IL-6 Concentration (pg/ml)
80
60
40
20
0
****

Supplementary Figure 3.10 – Soluble VCAM-1 and ICAM-1 Levels of HFCC Diet-Fed LDLR Single KO and SR-B1/LDLR DKO Mice. (A) Soluble VCAM-1. (B) Soluble ICAM-1. Each data point represents an individual mouse (n=8, 8, 9, 9). Bars represent means and error bars represent standard errors of the mean. Data were analyzed by one-way ANOVA and Tukey's post-hoc test. *P <0.05.

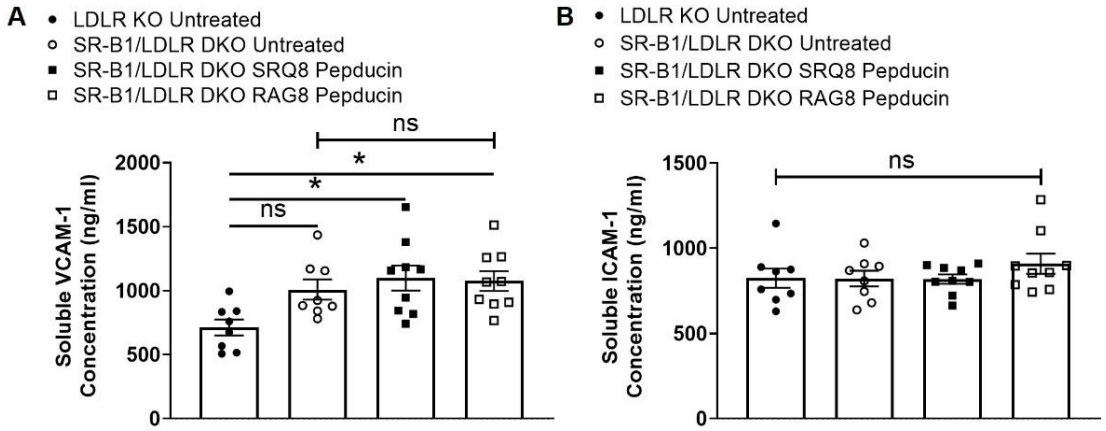

Supplementary Figure 3.11 – Flow Cytometry Analysis on Blood Immune Cells in HFCC Diet-Fed Untreated LDLR Single KO and Treated SR-B1/LDLR DKO Mice. Flow cytometry was performed on a BD FACSCalibur Flow Cytometry system, and data were analyzed using FlowJo v10. Each data point represents an individual mouse (n=9, 5, 5). Bars represent means and error bars represent standard errors of the mean. Data were analyzed by one-way ANOVA and Tukey's post-hoc test. **P <0.01, ***P <0.001, ****P <0.0001.

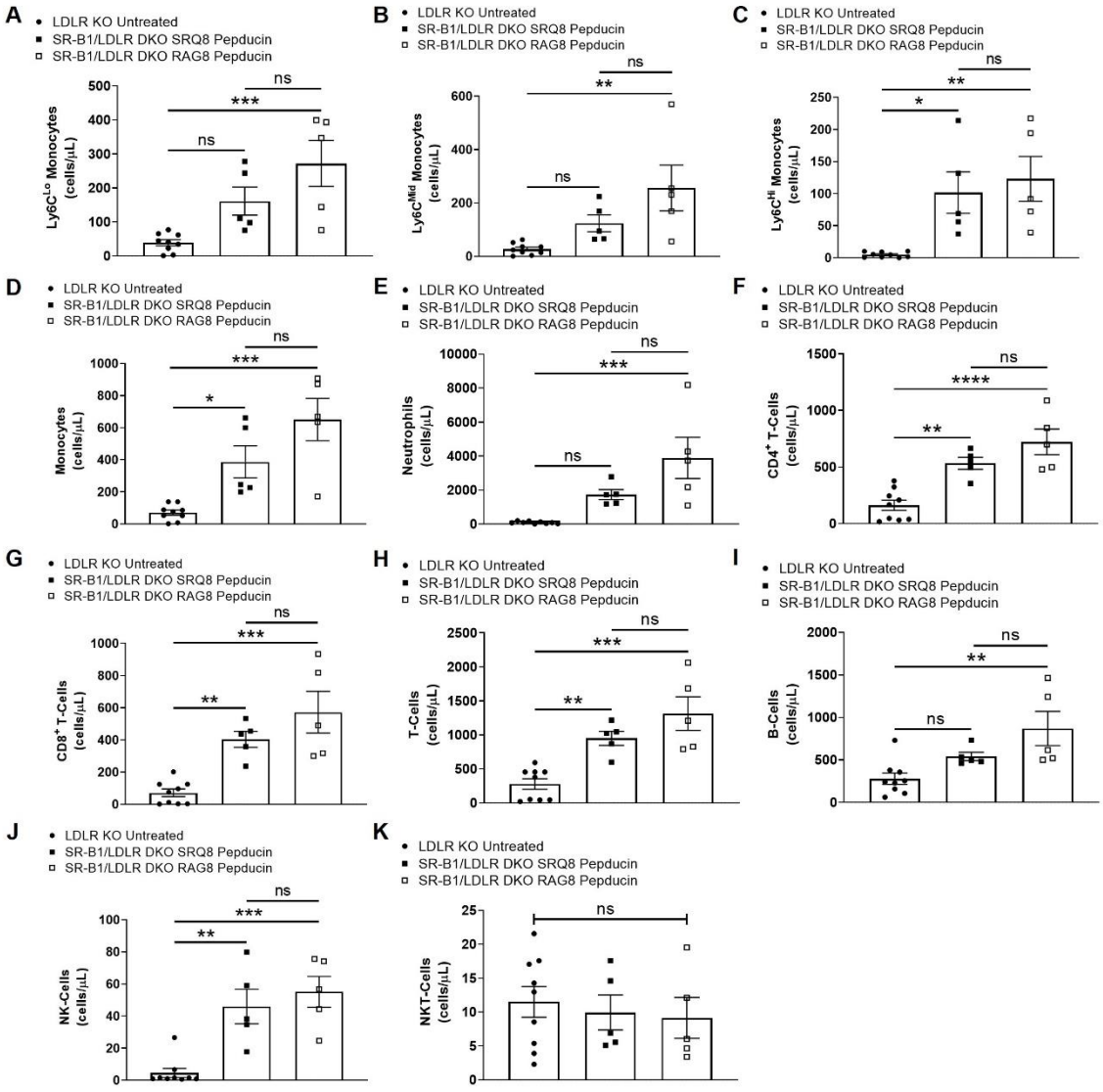
A
B
C
D
E
F
G
H
I
J
K
LDLR KO Untreated
SR-B1/LDLR DKO SRQ8 Pepducin
SR-B1/LDLR DKO RAG8 Pepducin
Ly6C^Lo Monocytes (cells/μL)
Ly6C^Mid Monocytes (cells/μL)
Ly6C^Hi Monocytes (cells/μL)
Monocytes (cells/μL)
Neutrophils (cells/μL)
CD4+ T-Cells (cells/μL)
CD8+ T-Cells (cells/μL)
T-Cells (cells/μL)
B-Cells (cells/μL)
NK-Cells (cells/μL)
NKT-Cells (cells/μL)
ns
*
**
***
****

Chapter 4: Scavenger Receptor Class B Type 1 Knockout Mice Develop Extensive Diet-Induced Coronary Artery Atherosclerosis in an Age-Dependent Manner.

Author List: Samuel Lee and Bernardo L. Trigatti

Foreword

This manuscript examines the effects of aging on CAD development in HFCC diet-fed SR-B1 KO mice. We demonstrate that advanced age in HFCC diet-fed SR-B1 KO mice results in increased coronary artery atherosclerosis, increased platelet accumulation in atherosclerotic coronary arteries, increased myocardial fibrosis, and reduced survival compared to younger HFCC diet-fed SR-B1 KO mice. Our data show that these age-dependent changes do not appear to be driven by changes in plasma lipid levels, but rather likely driven by increased VCAM-1 levels in coronary arteries, increased circulating pro-inflammatory cytokines, and increased circulating neutrophils.

This manuscript will be submitted for publication by the end of 2022. This manuscript was written by Samuel Lee with guidance from Bernardo L. Trigatti. This project was designed by Samuel Lee and Bernardo L. Trigatti. All experiments were conducted by Samuel Lee, and all data were analyzed and interpreted by Samuel Lee under the guidance of Bernardo L. Trigatti.

4.1 Abstract

Objective: Knockout of scavenger receptor class B type 1 (SR-B1) in mice with atherogenic mutations results in the development of coronary artery disease (CAD) characterized by occlusive coronary artery atherosclerosis, platelet accumulation in coronary arteries, myocardial fibrosis, and early death. However, the extent of CAD in SR-B1 single knockout mice has not been examined. Additionally, although age is a major risk factor for CAD in humans, there are a lack of studies examining the effects of age on susceptibility to CAD development in mice. Therefore, we set out to examine the effects of age on susceptibility to diet-induced CAD development in SR-B1 knockout mice.

Approach and Results: SR-B1 KO mice were placed on a high-fat, high-cholesterol, cholate (HFCC) diet for 12 weeks from either 14 weeks of age (26-week-old) or 40 weeks of age (52-week-old). Age- and diet-matched C57BL/6J mice and 40-week-old SR-B1 KO mice maintained on normal chow until 52 weeks of age were included as controls. HFCC diet-fed C57BL/6J and normal chow-fed SR-B1 KO mice developed very minimal to no aortic sinus and coronary artery atherosclerosis. 26- and 52-week-old HFCC diet-fed SR-B1 KO mice exhibited similar plasma cholesterol levels and aortic sinus atherosclerosis. However, 52-week-old SR-B1 KO mice developed increased HFCC diet-induced coronary artery atherosclerosis, increased vascular cell adhesion molecule 1 levels and platelet accumulation in coronary arteries, increased myocardial fibrosis, and reduced survival. This was

accompanied by greater levels of circulating interleukin-6, tumour necrosis factor alpha, and neutrophils.

Conclusions: HFCC diet-fed SR-B1 KO mice develop occlusive coronary artery atherosclerosis and myocardial fibrosis in an age-dependent manner, and exhibit an increased inflammatory state with older age. Therefore, aged SR-B1 KO mice may prove to be an attractive mouse model to analyze age-dependent mechanisms associated with CAD development.

4.2 Introduction

Coronary artery disease (CAD) is the foremost single cause of mortality worldwide driven by atherosclerosis development in the coronary arteries, and its prevalence and mortality significantly increases with aging[1]. Atherosclerosis is a chronic inflammatory disease characterized by the build up of cholesterol-rich plaque in artery walls, driven by complex interactions between circulating immune cells, lipoproteins, and cells of the artery wall[2]. Moreover, endothelial cells of affected regions are activated and express high levels of adhesion molecules such as vascular cell adhesion molecule 1 (VCAM-1), mediating adhesion of inflammatory cells which drive atherosclerosis development[3–6]. Mature atherosclerotic plaques can exhibit endothelial cell erosion or become prone to rupture, which can lead to platelet-rich thrombus formation that can either accelerate atherosclerotic plaque development, or completely occlude the lumen

of the affected artery[7]. Thrombus formation on atherosclerotic plaques is known as atherothrombosis and can cause myocardial infarction, commonly known as heart attack[8].

Conventional mouse models widely used for atherosclerosis research include the apolipoprotein E (ApoE) knockout (KO) and high-fat/high-cholesterol-fed low-density lipoprotein receptor (LDLR) KO mice[9]. These mice are genetically predisposed to hypercholesterolemia. ApoE KO mice develop atherosclerosis spontaneously, and atherosclerosis development is dramatically accelerated by feeding them high-fat and/or high-cholesterol diets[10,11]. Similarly, atherosclerosis in LDLR KO mice is typically triggered by feeding them high-fat and/or high-cholesterol diets[12,13], although there have been reports of spontaneous atherosclerosis development in older-aged LDLR KO mice maintained on normal chow diets[14,15]. Therefore, atherosclerosis develops spontaneously and continuously in both ApoE KO and LDLR KO mice as the mice age, making it difficult to evaluate the effect of aging as a factor in susceptibility to atherosclerosis development. Furthermore, in these mice, atherosclerosis develops in the aortic sinus, the lesser curvature of the aortic arch, and arteries (e.g. brachiocephalic artery) that branch from the aorta, where blood flow is non-laminar. However, coronary arteries in these mice are less susceptible to atherosclerosis development[16].

Genetic KO of scavenger receptor class B type 1 (SR-B1) in mice containing ApoE or LDLR KO mutations results in accelerated spontaneous (SR-B1/ApoE

double KO (DKO)) and high-fat diet-induced (SR-B1/LDLR DKO) atherosclerosis development in the aortic sinus, and triggers the development of occlusive coronary artery atherosclerosis accompanied by fatal myocardial infarction[17–19]. SR-B1 is a high-density lipoprotein (HDL) receptor expressed on the surface of many cell types and mediates HDL-dependent atheroprotective signaling[20,21]. SR-B1 also plays a vital role in a process known as reverse cholesterol transport, in which SR-B1 mediates hepatic selective uptake of HDL-derived cholesterol for biliary secretion[22], and elimination of SR-B1 globally[23] or in the liver[24] results in increased abundance of cholesterol associated with enlarged HDL particles of altered composition and presumably function. It has been shown that high-fat and high-cholesterol diets trigger atherosclerosis development in the aortic sinus of SR-B1 single KO mice[24–27]. However, none of these studies have reported atherosclerosis in coronary arteries of SR-B1 KO mice. Although atherosclerotic CAD is generally a disease in middle- and older-aged individuals and aging is a well-known independent risk factor, most basic research studies using mouse models utilize juvenile or young adult mice. Moreover, those studies that have examined atherosclerosis in aged mice have utilized LDLR and ApoE KO mice which develop atherosclerosis spontaneously[10,11,14,15], making it difficult to separate the effects of age on susceptibility to atherosclerosis from the increased time allowed for atherosclerotic plaques to develop in the older mice. One study has examined the effects of aging on susceptibility to diet-induced atherosclerosis

in C57BL/6J wild-type (WT) mice[28], but these mice do not develop atherosclerosis beyond fatty streaks.

In this study, we examined atherosclerosis development in the aortic sinus and coronary arteries of 26-week-old (w.o) and 52 w.o SR-B1 KO mice that were fed an atherogenic HFCC diet for 12 weeks, along with age-matched control wild-type mice fed the HFCC diet for 12 weeks and 52 w.o SR-B1 KO mice fed only a normal chow diet. There were no significant differences in plasma lipid levels or levels of atherosclerosis in the aortic sinus between HFCC diet-fed 26 w.o and 52 w.o SR-B1 KO mice. In contrast, the HFCC diet-fed 52 w.o SR-B1 KO mice exhibited significantly greater levels of coronary artery atherosclerosis, increased myocardial fibrosis, and reduced survival compared to 26 w.o HFCC diet-fed SR-B1 KO mice. Moreover, HFCC diet-fed 52 w.o SR-B1 KO mice exhibited increased levels of VCAM-1 in non-atherosclerotic coronary arteries, increased platelet accumulation in atherosclerotic coronary arteries, increased levels of circulating interleukin-6 (IL-6) and tumour necrosis factor alpha (TNFα), and increased levels of circulating neutrophils compared to 26 w.o. HFCC diet-fed SR-B1 KO mice. Our data suggest that older-aged SR-B1 KO mice develop increased HFCC diet-induced coronary artery atherosclerosis and myocardial fibrosis, and exhibit an increased HFCC diet-induced inflammatory state compared to younger SR-B1 KO mice, suggesting that advanced age increases susceptibility to coronary artery but not aortic sinus atherosclerosis, likely by modulating inflammatory responses.

4.3 Materials and Methods

4.3.1 Mice

All procedures involving mice were in accordance with the Canadian Council on Animal Care guidelines and were approved by the McMaster University Animal Research Ethics Board. C57BL/6J WT mice were originally purchased from Jackson Labs and bred in-house. SR-B1 KO mice were originally obtained from Dr. Monty Krieger (Massachusetts Institute of Technology, Cambridge, Massachusetts, USA) and crossed >10 times onto a C57BL/6J background in-house. To generate SR-B1 KO mice for experiments, male and female SR-B1 KO breeders were fed a diet consisting of Prolab RMH3000 containing 0.5% probucol (Lab Diet, St. Louis, Missouri, USA). Pups were placed on a normal chow diet (Teklad Global 18% Protein Rodent Diet, 2018, Envigo, Madison, Wisconsin, USA) at weaning. All mice were bred and housed in the David Braley Research Institute Animal Facility at McMaster University and had free access to normal chow (Teklad Global 18% Protein Rodent Diet, 2018, Envigo, Madison, Wisconsin, USA) and water. Female mice were used for this study.

For survival studies, 14 w.o C57BL/6J WT mice and SR-B1 KO mice and 40 w.o C57BL/6J WT mice and SR-B1 KO mice were placed on a HFCC diet (Teklad, TD88051, Envigo, Madison, Wisconsin, USA) containing 15% fat (7.5% from cocoa butter), 1.25% cholesterol and 0.5% sodium cholate[29] for a maximum of 20 weeks, or until they exhibited endpoint symptoms, which included ruffled coat, hunched posture, lethargy, and labored breathing. Control SR-B1 KO mice were

maintained on a normal chow diet for an equivalent period of time. Mice that exhibited endpoint symptoms including ruffled coat, hunched posture, labored breathing, and lethargy or reached the end of the 20 week feeding period were humanely euthanized. Alternatively, mice were harvested after 12 weeks of feeding either the HFCC or control normal chow diets. At the end of the feeding period, mice were fasted for approximately 14 hours, then fully anesthetized with isoflurane-O_2 in an induction chamber followed by continued anaesthesia under a nose comb. While anesthetized, blood was collected into heparinized Eppendorf tubes via cheek puncture using a lancet and used to prepare plasma. For some mice, a portion of the blood was used for flow cytometry analysis of blood cells. After blood collection, the mice were thoracotomized and hearts and vasculature were perfused in situ through the left ventricle with phosphate-buffered saline containing 10 U of heparin/ml. Hearts were then excised and cryoprotected in 30% sucrose for 1-2 hours, then frozen using liquid nitrogen in Shandon Cryomatrix (Thermo Fisher Scientific, 6769006, Ottawa, Ontario, Canada) and stored at -80°C. Plasma was prepared by centrifugation of blood at 4,000 rpm for 5 minutes in a microcentrifuge at 4°C and stored in -80°C.

4.3.2 Histology

For analysis of atherosclerosis in the aortic sinus and coronary arteries, 10 µm-thick transverse cryosections were collected using a cryotome (Shandon Cryotome Electronic, 77210163GB, Thermo Fisher Scientific, Ottawa, Ontario,

Canada) from the middle of the heart to the aortic annulus in 0.3 mm intervals, then in 0.1 mm intervals to the top of the aortic valve leaflets. Lipids in atherosclerotic plaques were detected by oil red O staining, and nuclei were counter-stained with Meyer's hematoxylin. Brightfield images were captured using an Axiovert 200M microscope (Carl Zeiss Canada Ltd., Toronto, Ontario, Canada). For aortic sinus atherosclerosis analyses, the cross-sectional areas of atherosclerotic plaques in the section best represented by three intact valve leaflets were measured manually in a blinded manner using AxioVision software. Atherosclerosis in coronary arteries were evaluated in a blinded manner by counting coronary arteries with different levels of occlusion in 7 sections (which covers a distance of 1800 μm) below the aortic annulus. Coronary arteries were scored as either 0% occluded (non-atherosclerotic - no raised atherosclerotic plaque), <50% occluded, >50% occluded, or 100% (fully) occluded.

Myocardial fibrosis was detected by Masson's trichrome staining (Sigma-Aldrich, Oakville, Ontario, Canada), which stains collagen-rich fibrotic tissue blue/purple, and healthy myocardium red/pink. Images for 1 transverse cryosection per mouse at approximately 900 μm below the aortic annulus were captured using an Olympus BX41 microscope with a DP72 camera (Olympus Canada Inc., Richmond Hill, Ontario, Canada). The percentage of myocardial fibrosis was measured manually in a blinded manner using the outline function in ImageJ software as a proportion of fibrotic staining to the total area of the cross-section.

4.3.3 Immunofluorescence

Vascular cell adhesion molecule 1 (VCAM-1) was detected using cell-culture supernatants from rat B-lymphocyte hybridoma cells that produce antibodies against mouse VCAM-1 (ATCC, CRL-1909, Manassas, Virginia, USA)[31], and AlexaFluor 594 goat anti-rat secondary antibody (Invitrogen, A-11007, Waltham, Massachusetts, USA). Platelets were detected using a rat anti-mouse CD41 antibody (BD Biosciences, 553847, Mississauga, Ontario, Canada) and AlexaFluor 488 goat anti-rat secondary antibody (Invitrogen, A-11006, Waltham, Massachusetts, USA). Nuclei were detected with 4', 6'-diamidino-2-phenylindole (DAPI) counterstaining. All fluorescent images were captured using an Olympus BX41 microscope with a DP72 camara (Olympus Canada Inc., Richmond Hill, Ontario, Canada). All coronary arteries in 7 sections (which covers a distance of 1800 μm) below the aortic annulus were counted. For VCAM-1 analysis, the percentage of non-atherosclerotic coronary arteries with positive VCAM-1 staining was quantified in a blinded manner. For CD41 platelet analysis, the percentage of atherosclerotic coronary arteries with positive CD41 platelet staining was quantified in a blinded manner.

4.3.4 Plasma Analysis

Plasma alanine aminotransferase (ALT) (ALT Colorimetric Assay Kit, Elabscience, E-BC-K235-M, Houston, Texas, USA) and aspartate aminotransferase (AST) (AST Colorimetric Assay Kit, Elabscience, E-BC-K236-M,

Houston, Texas, USA) were measured using the indicated commercial assay kits and following manufacturers' instructions. Plasma total cholesterol (Cholesterol Infinity, TR13421, Thermo Fisher Scientific, Ottawa, Ontario, Canada), unesterified cholesterol (Free Cholesterol E, Wako Diagnostics, 993-02501, Mountain View, California, USA), HDL cholesterol (not precipitable by phosphotungstate-magnesium salt; HDL Cholesterol E, Wako Diagnostics, 997-01301, Mountain View, California, USA), and triglycerides (L-Type Triglyceride M, Wako Chemicals, 998-02992, Richmond, Virginia, USA) were measured using the indicated commercial assay kits and following manufacturers' instructions. Esterified cholesterol levels were calculated as the difference between total cholesterol and unesterified cholesterol measurements, and non-HDL cholesterol levels were calculated as the difference between total cholesterol and HDL cholesterol measurements. Plasma IL-6, TNFα, soluble vascular cell adhesion molecule 1 (sVCAM-1) and soluble intercellular adhesion molecule 1 (sICAM-1) were measured by ELISA (IL-6: catalogue # 431304; TNFα: catalogue #430904, BioLegend, San Diego, California, USA; sVCAM-1: catalogue # MVC00; sICAM-1; catalogue # MVC100, R&D Systems, Minneapolis, Minnesota, USA) following manufacturer's protocols.

4.3.5 Flow Cytometry

Blood was incubated with the following rat anti-mouse antibodies: FITC CD3 (BD Biosciences, 555274, Mississauga, Ontario, Canada), BV510 CD45

(Biolegend, 103138, San Diego, California, USA), PerCP-Cyanine5.5 CD45R (B220) (eBioscience, 45-0452-80, San Diego, California, USA), PE CD11b (M1/70) (eBioscience, 12-0112-82, San Diego, California, USA), PE-Cy7 Ly6C (Biolegend, 128018, San Diego, California, USA), PE-Dazzle-594 Ly6G (Biolegend, 127648, San Diego, California, USA), PE-Cy5 CD4 (BD Biosciences, 553050, Mississauga, Ontario, Canada), PE-Cy7 CD8a (BD Biosciences, 552877, Mississauga, Ontario, Canada), and PE NK1.1 (BD Biosciences, 553165, Mississauga, Ontario, Canada). Next, erythrocytes present in the blood were lysed and samples were fixed with 1x 1-step fix/lyse solution (Thermo Fisher Scientific, 00-5333, Ottawa, Ontario, Canada). Absolute leukocyte counts were determined with the addition of 123count eBeads (Thermo Fisher Scientific, 01-1234-42, Ottawa, Ontario, Canada). Flow cytometry was performed on a BD FACSCalibur Flow Cytometry system (BD Biosciences, Mississauga, Ontario, Canada), and data were analyzed using FlowJo v10 software.

4.3.6 Statistical Analysis

GraphPad Prism software was used for statistical analyses. For two groups, data were subjected to the Shapiro-Wilk test for normality. Those that passed normality were analyzed by the Student's t-test (2-tailed, unpaired), and those that failed normality were analyzed by the Mann-Whitney Rank Sum test. For multiple groups, data were analyzed by one-way ANOVA with Tukey's Multiple Comparisons Post-Hoc test. Data with two independent variables were analyzed

by two-way ANOVA with Sidak's Multiple Comparisons Post-Hoc test. Data are presented as mean ± standard error of the mean. P values <0.05 were considered statistically significant.

4.4 Results

4.4.1 Older Age Increased Diet-Induced Atherosclerosis Development in Coronary Arteries but Not in the Aortic Sinuses of SR-B1 KO Mice

To examine if older age affected the degree of atherosclerotic plaque development, SR-B1 KO mice were either maintained on normal chow until 52 weeks of age, or were fed an HFCC diet for 12 weeks (prior to harvest) and harvested at 52 weeks of age and were compared to SR-B1 KO mice fed an HFCC diet for 12 weeks (prior to harvest) and harvested at 26 weeks of age. SR-B1 KO mice maintained on normal chow until they were 52 weeks of age did not develop much detectable atherosclerotic plaques in their aortic sinus (Figures 4.1C and F). Similarly, control C57BL/6J WT mice harvested at either 26 or 52 weeks of age after having been fed the HFCC diet for 12 weeks exhibited minimal atherosclerotic plaque development in the aortic sinus (Figures 4.1A, B and F). In contrast, when SR-B1 KO mice were fed the HFCC diet for 12 weeks from 14 weeks of age, they developed substantial atherosclerosis in the aortic sinus (Figures 4.1D and F), consistent with previous reports[24]. When SR-B1 KO mice were fed the HFCC diet for 12 weeks from 40 weeks of age, a similar level of atherosclerosis development in the aortic sinus was observed as that in SR-B1-KO mice fed the HFCC diet for

12 weeks from 14 weeks of age (Figures 4.1D-F; 2.6 x 10^5 ± 0.16 x 10^5 μm^2 vs. 2.2 x 10^5 ± 0.15 x 10^5 μm^2), demonstrating that increasing age from 14 to 40 weeks did not alter the susceptibility to HFCC diet-induced atherosclerosis development in the aortic sinus.

When we examined atherosclerotic plaque burden in coronary arteries, we observed virtually no atherosclerosis development in coronary arteries from 52 w.o normal chow-fed SR-B1 KO mice, or in either HFCC diet-fed 26 or 52 w.o C57BL/6J WT mice (Figure 4.1K). However, significant atherosclerosis development was evident in coronary arteries from 26 w.o SR-B1 KO mice that had been fed the HFCC diet for 12 weeks, with 10.4 ± 1.6% of coronary artery cross-sections fully occluded by atherosclerotic plaques and 80.6 ± 1.5% of coronary artery cross-sections lacking atherosclerotic plaques (Figures 4.1G-K). Surprisingly, when we analyzed coronary artery atherosclerosis levels in 52 w.o SR-B1 KO mice fed the HFCC diet for the same length of time but beginning from 40 weeks of age, a substantially higher level of coronary atherosclerosis was detected, with 30.6 ± 1.9% of coronary artery cross sections completely occluded by plaques compared to the 10.4 ± 1.6% detected in 26 w.o SR-B1 KO mice fed the HFCC diet for 12 weeks ($P < 0.0001$; Figures 4.1G-K). In contrast, only 48.5 ± 2.6% of coronary artery cross-sections were devoid of atherosclerotic plaques compared to the 80.6 ± 1.5% detected in 26 w.o. SR-B1 KO mice fed the HFCC diet for 12 weeks ($P < 0.0001$; Figure 4.1K). These data demonstrate that, despite similar susceptibilities to HFCC-diet induced atherosclerosis in the aortic sinus,

older-aged SR-B1 KO mice exhibit increased susceptibility to HFCC-diet induced atherosclerosis development in coronary arteries.

Figure 4.1 – Older Age Increased Diet-Induced Atherosclerosis Development in Coronary Arteries but Not Aortic Sinuses of SR-B1 KO Mice. Representative images of oil red O-stained transverse sections of the aortic sinus showing atherosclerotic plaque from HFCC diet-fed 26 w.o C57BL/6J mice (A), HFCC diet-fed 52 w.o C57BL/6J mice (B), normal chow-fed 52 w.o SR-B1 KO mice (C), HFCC diet-fed 26 w.o SR-B1 KO mice (D), and HFCC diet-fed 52 w.o SR-B1 KO mice (E). Scale bar= 200 μm. (F) Aortic sinus atherosclerotic plaque cross-sectional areas of mice (n=8, 8, 10, 10, 10). Seven sections of each heart were stained with oil red O/hematoxylin, and coronary arteries were scored as either non-atherosclerotic (0%) or containing atherosclerotic plaques that occluded <50%, >50% or 100% of their lumen. (G) to (J) Representative images of coronary arteries for each category are shown. Scale bar= 50 μm. (K) Quantification of coronary arteries in each category (as percentage of total) across seven heart sections (n=8, 8, 10, 10, 10). Each data point represents an individual mouse. Bars represent means and error bars represent standard errors of the mean. Data in (F) were analyzed by one-way ANOVA and Tukey's post-hoc test. Data in (K) were analyzed by two-way ANOVA with Sidak's multiple comparisons post-hoc test. ****P <0.0001.

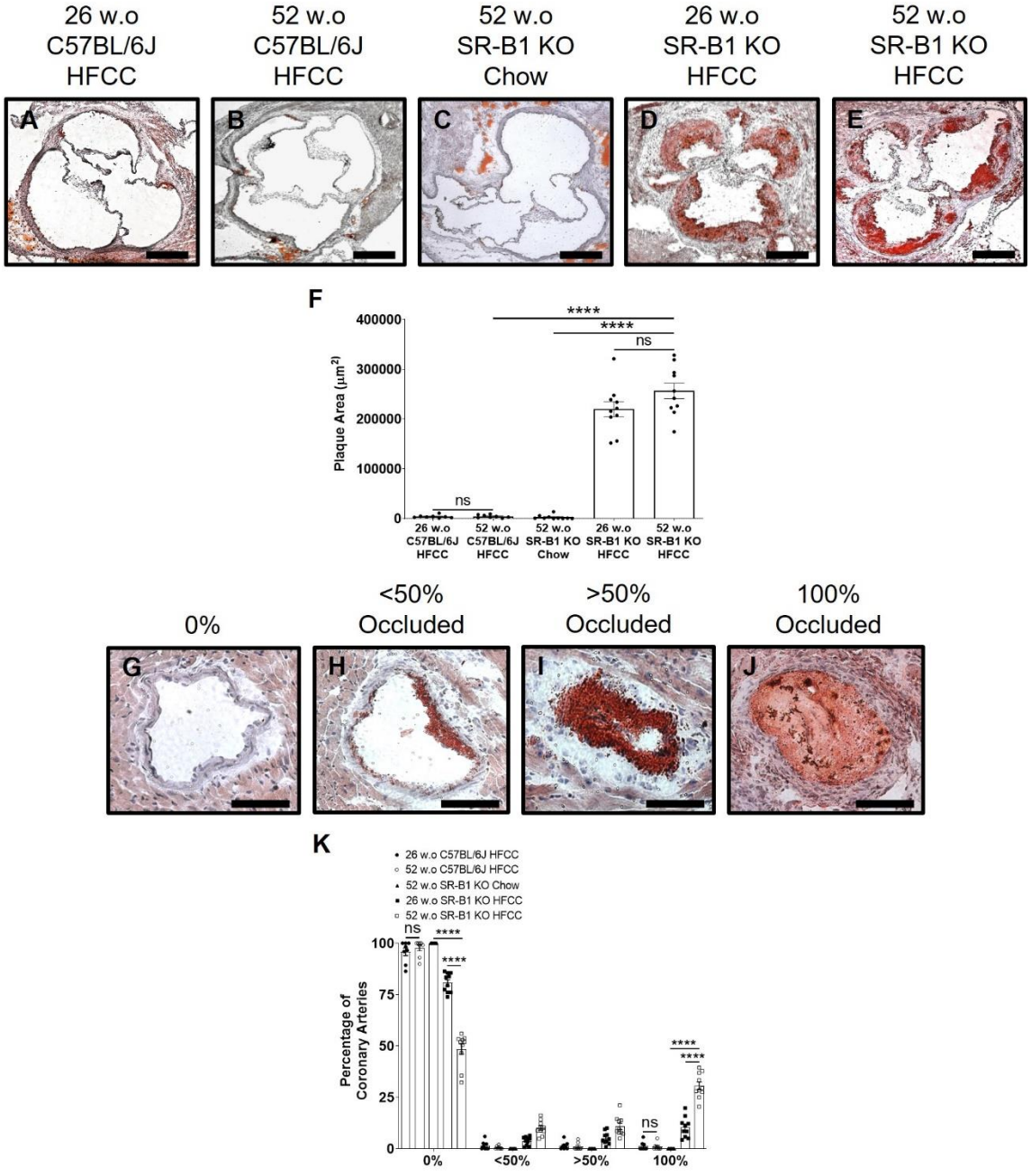
26 w.o C57BL/6J HFCC
52 w.o C57BL/6J HFCC
52 w.o SR-B1 KO Chow
26 w.o SR-B1 KO HFCC
52 w.o SR-B1 KO HFCC
A
B
C
D
E
F
Plaque Area (μm²)
400000
300000
200000
100000
0
****
****
ns
ns
26 w.o C57BL/6J HFCC
52 w.o C57BL/6J HFCC
52 w.o SR-B1 KO Chow
26 w.o SR-B1 KO HFCC
52 w.o SR-B1 KO HFCC
0%
<50% Occluded
>50% Occluded
100% Occluded
G
H
I
J
K
26 w.o C57BL/6J HFCC
52 w.o C57BL/6J HFCC
52 w.o SR-B1 KO Chow
26 w.o SR-B1 KO HFCC
52 w.o SR-B1 KO HFCC
Percentage of Coronary Arteries
100
75
50
25
0
ns
****
****
****
****
ns
0%
<50%
>50%
100%

4.4.2 Older Age Increased Vascular Cell Adhesion Molecule 1 Levels and Platelet Accumulation in Coronary Arteries of HFCC Diet-Fed SR-B1 KO Mice

Analysis of VCAM-1 immunostaining (Figures 4.2A-E) revealed the presence of VCAM-1 in approximately 20% of non-atherosclerotic coronary artery sections from either 26 or 52 w.o C57BL/6J mice fed the HFCC diet for 12 weeks, or from 52 w.o. SR-B1 KO mice that had been maintained on a normal chow diet with a trend towards an increased proportion (31.0 ± 2.1%; P= 0.0594; not statistically significant) of coronary artery cross-sections staining positive for VCAM-1 from 26 w.o SR-B1 KO mice fed the HFCC diet for 12 weeks. However, 52 w.o SR-B1 KO mice that had been fed the HFCC diet for 12 weeks beginning at 40 weeks of age exhibited a substantially increased proportion (69.8 ± 3.9%; P <0.0001; Figure 4.2K) of non-atherosclerotic coronary artery cross-sections that were positive for VCAM-1 and appeared to show a greater extent of VCAM-1 staining around the circumference of the coronary artery cross-sections (Figure 4.2E compared to 4.2D). In contrast, no differences were evident in plasma levels of soluble VCAM-1 or soluble ICAM-1 between 26 w.o and 52 w.o C57BL/6J or SR-B1 KO mice that had been fed the HFCC diet for 12 weeks, although all exhibited elevated levels compared to SR-B1 KO mice maintained on normal chow diet (Supplementary Figures 4.7A and B), suggesting that increased HFCC-diet induction of VCAM-1 levels with advanced age in SR-B1 KO mice might be restricted to coronary artery endothelial cells rather than a general phenomenon.

Previous studies in our lab found evidence of platelet accumulation in

atherosclerotic coronary arteries of SR-B1/ApoE and SR-B1/LDLR DKO mice, which develop spontaneous or HFCC diet-induced coronary artery atherosclerosis, respectively[19,30], suggesting possible thrombus formation and/or contributions of platelets in driving atherosclerosis development in coronary arteries in these mice. We examined if platelets were present in atherosclerotic coronary arteries of HFCC-diet fed SR-B1 KO mice that were either 26 or 52 weeks of age by immunostaining for CD41. We only analyzed coronary arteries from HFCC diet-fed 26 w.o and 52 w.o SR-B1 KO mice, since the HFCC diet-fed C57BL/6J mice and normal chow-fed SR-B1 KO mice developed little to no coronary artery atherosclerosis. CD41 positive staining was detected in atherosclerotic coronary arteries from both 26 and 52 w.o. SR-B1 KO mice that had been fed the HFCC diet for 12 weeks (Figures 4.2L and M), but a higher proportion of atherosclerotic coronary artery cross-sections were positive for CD41 from 52 w.o vs. 26 w.o SR-B1 KO mice after 12 weeks of HFCC diet feeding (60.2 ± 4.3% vs. 37.8 ± 4.1%; $P < 0.01$; Figure 4.2P). This suggests that older-aged SR-B1 KO mice exhibited increased susceptibility to HFCC diet-induced accumulation of platelets in atherosclerotic coronary arteries in addition to a greater degree of atherosclerosis in coronary arteries.

Figure 4.2 – Older Age Increased VCAM-1 Protein Levels in Non-Atherosclerotic Coronary Arteries and Platelet Accumulation in Atherosclerotic Coronary Arteries in HFCC Diet-Fed SR-B1 KO Mice. Representative fluorescence images of VCAM-1 immunofluorescence (red) and DAPI (blue) nuclear counter-staining in non-atherosclerotic coronary artery sections from HFCC diet-fed 26 w.o C57BL/6J mice (A), HFCC diet-fed 52 w.o C57BL/6J mice (B), normal chow-fed 52 w.o SR-B1 KO mice (C), HFCC diet-fed 26 w.o SR-B1 KO mice (D), and HFCC diet-fed 52 w.o SR-B1 KO mice (E), with adjacent sections stained with oil red O (F) to (J). Scale bar= 50 μm. (K) Proportions of non-atherosclerotic coronary artery sections with positive VCAM-1 staining across seven heart sections for each mouse (n=8, 8, 10, 10, 10). Representative images of CD41 immunofluorescence (green) and DAPI counterstaining from HFCC diet-fed 26 w.o SR-B1 KO mice (L), and HFCC diet-fed 52 w.o SR-B1 KO mice (M), with adjacent sections stained with oil red O (N) and (O). (P) Proportions of atherosclerotic coronary arteries with positive CD41 immunofluorescence staining across seven heart sections for each mouse (n=10, 10). Each data point represents an individual mouse. Bars represent means and error bars represent standard errors of the mean. Data in (K) were analyzed by one-way ANOVA and Tukey's post-hoc test. Data in (P) passed the normality test and were analyzed by Student's t-test. **P <0.01, ****P <0.0001.

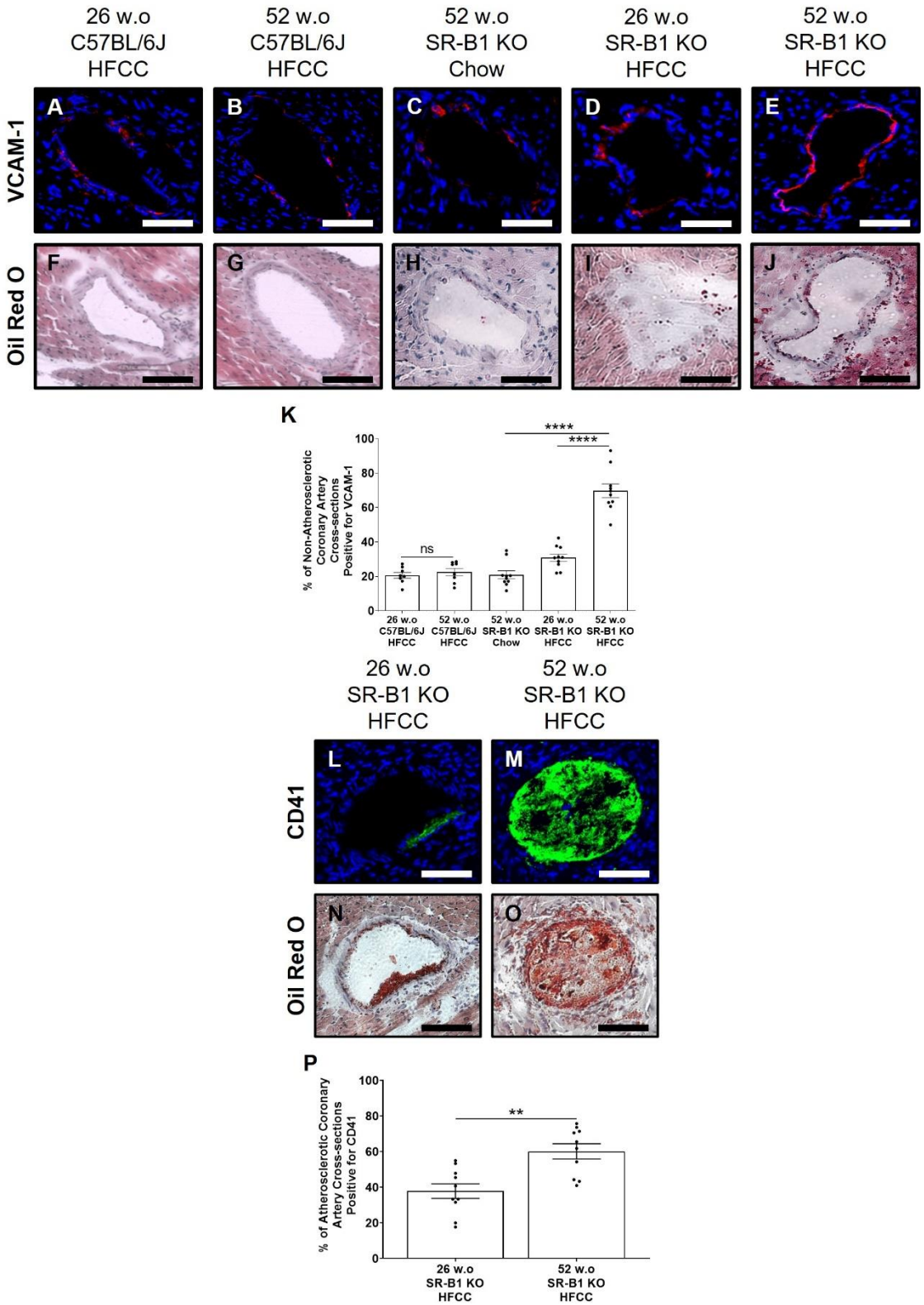
26 w.o C57BL/6J HFCC
52 w.o C57BL/6J HFCC
52 w.o SR-B1 KO Chow
26 w.o SR-B1 KO HFCC
52 w.o SR-B1 KO HFCC
VCAM-1
Oil Red O
A
B
C
D
E
F
G
H
I
J
K
% of Non-Atherosclerotic Coronary Artery Cross-sections Positive for VCAM-1
ns
****
****
26 w.o C57BL/6J HFCC
52 w.o C57BL/6J HFCC
52 w.o SR-B1 KO Chow
26 w.o SR-B1 KO HFCC
52 w.o SR-B1 KO HFCC
26 w.o SR-B1 KO HFCC
52 w.o SR-B1 KO HFCC
CD41
Oil Red O
L
M
N
O
P
% of Atherosclerotic Coronary Artery Cross-sections Positive for CD41
**
26 w.o SR-B1 KO HFCC
52 w.o SR-B1 KO HFCC

4.4.3 Older Age Increased Myocardial Fibrosis and Damage in HFCC Diet-Fed SR-B1 KO Mice

Given the increased levels of occlusive coronary artery atherosclerosis observed in 52 w.o compared to 26 w.o SR-B1 KO mice after 12 weeks of HFCC diet feeding, and previous observations that spontaneous or diet-induced coronary artery atherosclerosis was accompanied by myocardial fibrosis in SR-B1 KO mice containing mutations in other genes predisposing them to either spontaneous or diet-induced atherosclerosis[17–19], we examined the levels of myocardial fibrosis using Masson's trichrome to differentiate collagen-rich fibrotic regions, which stain blue/purple, from healthy myocardium, which stain red/pink. Consistent with the low levels of coronary artery atherosclerosis, HFCC diet-fed C57BL/6J mice (at either 26 or 52 weeks of age) and 52 w.o normal chow-fed SR-B1 KO mice exhibited low levels of myocardial fibrosis (Figures 4.3A-C and F). Levels of myocardial fibrosis tended to be higher in 26 w.o. HFCC-diet fed SR-B1 KO mice than in similarly-aged and fed C57BL/6J or normal chow-fed SR-B1 KO mice (Figures 4.3D and F). The level of myocardial fibrosis was substantially higher, however, in 52 w.o compared to 26 w.o SR-B1 KO mice after 12 weeks of HFCC diet-feeding (3.8% ± 0.2% vs. 1.0% ± 0.2%, $P < 0.0001$; Figure 4.3F), which is consistent with the increased levels of coronary artery atherosclerosis.

We then examined the levels of plasma cardiac troponin I (a marker of myocardial damage), and found that the HFCC diet-fed 52 w.o SR-B1 KO mice had significantly higher levels than all of the other mouse groups which is

consistent with the myocardial fibrosis findings, and were the only group with detectable levels of plasma cardiac troponin I (Figure 4.3G). We also examined heart weight:tibia length ratios, an indicator of myocardial enlargement, and found that there were no differences between 26 w.o and 52 w.o HFCC diet-fed C57BL/6J mice (Figure 4.3H). Although HFCC diet-fed 52 w.o SR-B1 KO mice had increased heart weight:tibia length ratios compared to HFCC diet-fed 26 w.o SR-B1 KO mice, there were no differences in heart weight:tibia length ratios between HFCC diet-fed vs. normal chow-fed 52 w.o SR-B1 KO mice (Figure 4.3H), suggesting a lack of pathological cardiac enlargement in older-aged SR-B1 KO mice.

Figure 4.3 – Older Age Increased Myocardial Fibrosis Levels and Plasma Cardiac Troponin I Levels in HFCC Diet-Fed SR-B1 KO Mice. Representative images of Masson's trichrome-stained transverse cryosections of myocardium from HFCC diet-fed 26 w.o C57BL/6J mice (A), HFCC diet-fed 52 w.o C57BL/6J mice (B), normal chow-fed 52 w.o SR-B1 KO mice (C), HFCC diet-fed 26 w.o SR-B1 KO mice (D), and HFCC diet-fed 52 w.o SR-B1 KO mice (E). Red colored staining indicates undamaged cardiomyocytes, whereas blue/purple colored staining indicates the presence of collagen. Scale bar= 200 μm. (F) Quantification of the percentage of myocardial fibrosis measured by the area of blue staining relative to the cross-sectional area of the heart for one section per mouse (n=8, 8, 9, 10, 10). (G) Plasma cardiac troponin I levels (n=10, 8, 7, 10, 10). (H) Heart weight-to-tibia length ratios (n=24, 15, 13, 22, 21). Each data point represents an individual mouse. Bars represent means and error bars represent standard errors of the mean. Data were analyzed by one-way ANOVA and Tukey's post-hoc test. **P <0.01, ***P <0.001, ****P <0.0001.

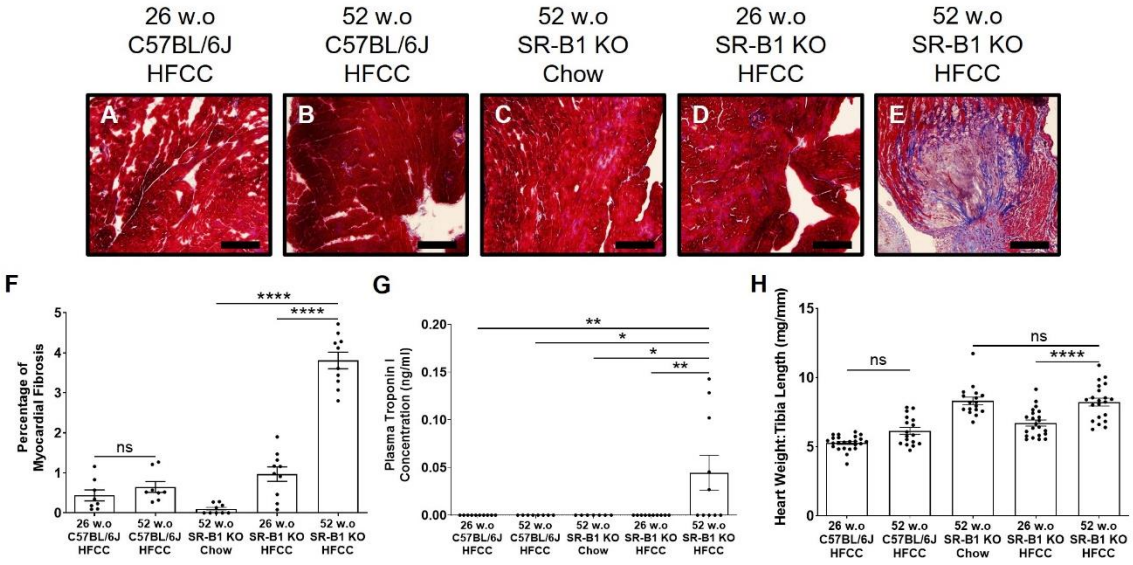
26 w.o C57BL/6J HFCC
52 w.o C57BL/6J HFCC
52 w.o SR-B1 KO Chow
26 w.o SR-B1 KO HFCC
52 w.o SR-B1 KO HFCC
A
B
C
D
E
F
Percentage of Myocardial Fibrosis
ns
****
****
G
Plasma Troponin I Concentration (ng/ml)
**
*
*
**
H
Heart Weight:Tibia Length (mg/mm)
ns
ns
****

4.4.4 Older Age Reduced Survival in HFCC Diet-Fed SR-B1 KO Mice

Given that SR-B1 KO mice with mutations in ApoE or LDLR develop spontaneous or diet-induced occlusive coronary artery atherosclerosis and myocardial fibrosis also die prematurely[17,19], we examined the survival of both young (14 w.o) and older (40 w.o) C57BL/6J control and SR-B1 KO mice fed the HFCC diet (Figures 4.4A and B). The young mice exhibited no mortality when put on the HFCC diet at 14 weeks of age, up to 20 weeks of HFCC diet feeding (Figures 4.4A and B). Although there was some mortality apparent in the older C57BL/6J control group put on the HFCC diet at 40 weeks of age, survival was not statistically significantly different from that of C57BL/6J mice started on the HFCC diet at 14 weeks of age (Figure 4.4A). In contrast, when SR-B1 KO mice were started on the HFCC diet at 40 weeks of age, none of the mice survived beyond 18 weeks of HFCC diet feeding (mean survival of 13.7 ± 1.1 weeks of HFCC diet-feeding; $P < 0.0001$; Figure 4.4B). By comparison, there was no mortality detected in SR-B1 KO mice maintained in parallel on the normal chow diet for an equivalent period of time from 40-60 weeks of age (data not shown). Since C57BL/6J have been shown to develop hepatotoxicity when fed a high-fat diet[32,33], we examined whether older age affected levels of plasma alanine aminotransferase (ALT) and aspartate aminotransferase (AST), both markers of liver damage[34]. An increased trend (that did not reach statistical significance) in circulating ALT and AST levels was observed in 52 w.o C57BL/6J mice fed the HFCC diet for 12 weeks compared to diet-matched 26 w.o C57BL/6J mice (Supplementary Figures 4.8A and B).

Interestingly, there was a significant increase in plasma ALT levels in 52 w.o HFCC diet-fed C57BL/6J mice compared to HFCC diet-fed and normal chow-fed SR-B1 KO mice (Supplementary Figures 4.8A and B).

Figure 4.4 – Older Age Reduced Survival of HFCC Diet-Fed SR-B1 KO Mice.

(A) Kaplan-Meier survival curves for 14-week-old (w.o) C57BL/6J (bolded line) and 40 w.o C57BL/6J (dotted line) mice fed a HFCC diet for up to 20 weeks (n=13, 13). (B) Kaplan-Meier survival curves for 14 w.o SR-B1 KO (bolded line) and 40 w.o SR-B1 KO (dotted line) mice fed a HFCC diet for up to 20 weeks (n=14, 14). Mice were monitored until they reached cardiac endpoint or the end of 20 weeks of diet feeding, at which point they were humanely euthanized. Data were analyzed by the Mantel-Cox log-rank test. ****P <0.0001.

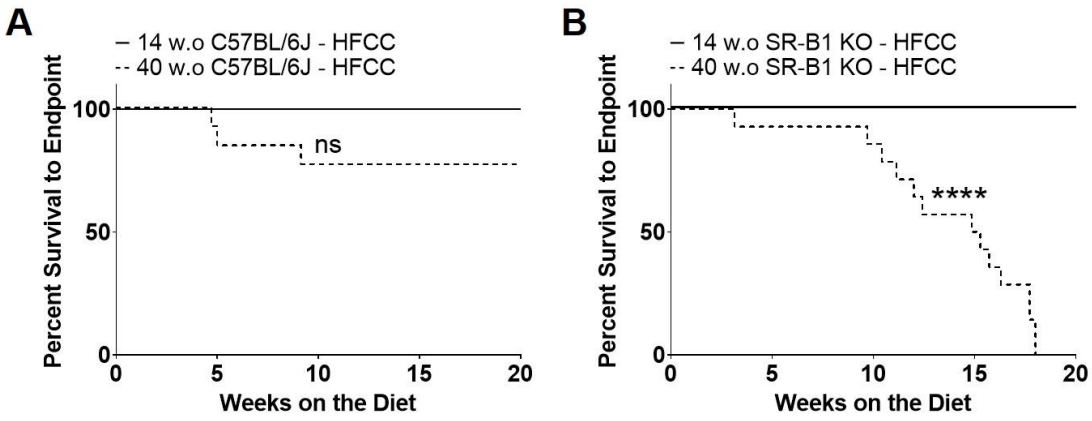

4.4.5 Older Age Affected Plasma Cytokine but Not Lipid Levels in HFCC Diet-Fed SR-B1 KO Mice

Plasma total cholesterol, unesterified cholesterol, esterified cholesterol and non-HDL cholesterol were increased while “HDL cholesterol” (resistant to precipitation by phosphotungstate-magnesium salt) was reduced and triglycerides in plasma were unchanged in HFCC vs. normal chow diet feeding in 52 w.o SR-B1 KO mice (Figures 4.5A-F). Levels of total, unesterified, esterified, and non-HDL cholesterol and triglycerides were increased while HDL (non-precipitable) cholesterol was unchanged in HFCC diet-fed SR-B1 KO mice compared to similarly fed/aged C57BL/6J mice (Figures 4.5A-F). No differences were seen in plasma lipid levels in SR-B1 KO mice fed the HFCC diet for 12 weeks starting at either 14 or 40 weeks of age; similar observations were made for C57BL/6J mice (Figures 4.5A-F), indicating that increased age did not affect plasma levels of these lipids in these mice fed the HFCC diet.

Plasma levels of IL-6 (Figure 4.5G) and TNFα (Figure 4.5H) were also higher in HFCC diet-fed compared to normal chow-fed SR-B1 KO mice at 52 weeks of age, and TNFα levels were statistically higher in 52 w.o HFCC diet-fed SR-B1 KO mice compared to C57BL/6J mice. Unlike plasma lipids, plasma IL-6 and TNFα levels were significantly higher in HFCC diet-fed SR-B1 KO mice (but not C57BL/6J mice) when the mice were fed for 12 weeks beginning at 40 weeks of age compared to 14 weeks of age (Figures 4.5G and H). This suggests that age increased the susceptibility of SR-B1 KO mice to HFCC diet-induced inflammation.

Figure 4.5 – Older Age Did Not Affect Circulating Lipid Levels in HFCC Diet-Fed SR-B1 KO Mice, but Increased Circulating IL-6 and TNFα Levels. (A) Plasma total cholesterol (n=12, 10, 12, 12, 12). (B) Plasma unesterified cholesterol (n=12, 10, 12, 12, 12). (C) Plasma esterified cholesterol (calculated as the difference between total and unesterified cholesterol) (n=12, 10, 12, 12, 12). (D) Plasma HDL cholesterol (n=11, 9, 11, 12, 12). (E) Plasma non-HDL cholesterol (calculated as the difference between total and HDL cholesterol) (n=10, 9, 11, 12, 12) (F) Plasma triglycerides (n=12, 10, 12, 12, 12). (G) Plasma IL-6 (n=12, 9, 13, 11, 13). (H) Plasma TNFα (n=10, 10, 13, 13, 16). Each data point represents an individual mouse. Bars represent means and error bars represent standard errors of the mean. All data were analyzed by one-way ANOVA and Tukey's post-hoc test. *P <0.05, ***P <0.001, ****P <0.0001.

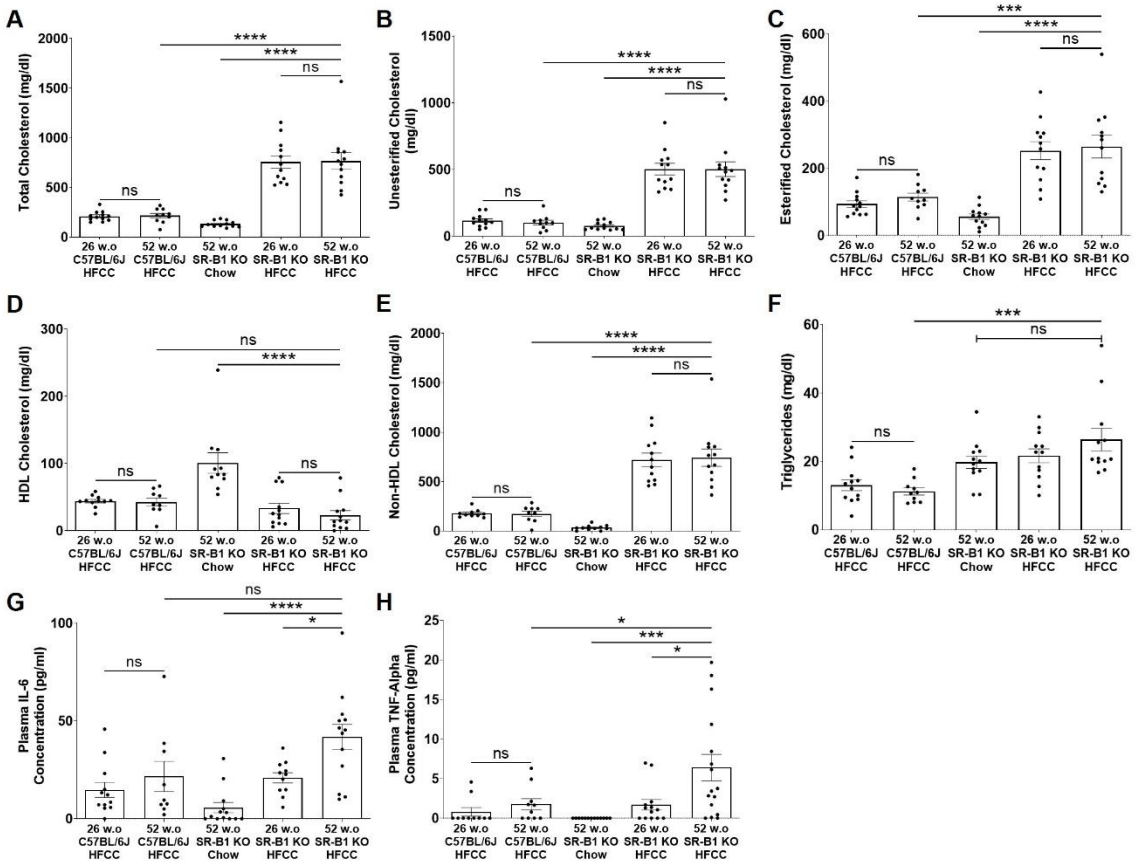
A
Total Cholesterol (mg/dl)
B
Unesterified Cholesterol (mg/dl)
C
Esterified Cholesterol (mg/dl)
D
HDL Cholesterol (mg/dl)
E
Non-HDL Cholesterol (mg/dl)
F
Triglycerides (mg/dl)
G
Plasma IL-6 Concentration (pg/ml)
H
Plasma TNF-Alpha Concentration (pg/ml)
ns
26 w.o C57BL/6J HFCC
52 w.o C57BL/6J HFCC
52 w.o SR-B1 KO Chow
26 w.o SR-B1 KO HFCC
52 w.o SR-B1 KO HFCC

4.4.6 Older Age Increased Circulating Neutrophil Levels in HFCC Diet-Fed SR-B1 KO Mice

Flow cytometry analysis of circulating immune cells revealed that circulating neutrophil levels were substantially elevated in 52 w.o HFCC diet-fed SR-B1 KO mice compared to all other groups of mice (Figure 4.6A). A trend towards increased circulating monocyte levels (that did not reach statistical significance) was also observed in 52 w.o HFCC diet-fed SR-B1 KO mice compared to 26 w.o HFCC diet-fed SR-B1 KO mice, and appeared to be mainly associated with a significant increase in $Ly6C^{mid}$ monocyte levels (Figures 4.6B-E). Moreover, 52 w.o HFCC diet-fed SR-B1 KO mice exhibited significantly greater levels of circulating $Ly6C^{mid}$ monocytes, $Ly6C^{hi}$ monocytes, and total monocytes compared to 52 w.o SR-B1 KO mice maintained on a normal chow diet (Figures 4.6C-E). Circulating $CD4^+$ T-cells were reduced in HFCC diet-fed C57BL/6J and SR-B1 KO mice that were 52 weeks of age compared to 26 weeks of age (Figure 4.6F), whereas there were no differences in circulating $CD8^+$ T-cell levels between similarly aged HFCC diet-fed C57BL/6J and SR-B1 KO mice (Figure 4.6G). There was a trend (that did not reach statistical significance) to lower average levels of circulating total T-cells and B-cells in HFCC diet-fed C57BL/6J and SR-B1 KO mice that were 52 weeks of age compared to 26 weeks of age (Figures 4.6H and I). There were no significant differences in circulating NK cells between 26 w.o and 52 w.o HFCC diet-fed C57BL/6J mice, but there was a decrease in 52 w.o HFCC diet-fed SR-B1 KO mice compared to 26 w.o HFCC diet-fed SR-B1 KO mice (Figure 4.6J). NKT cells tended

to be elevated in 52 w.o HFCC diet-fed SR-B1 KO mice compared to other groups of mice, but this did not reach statistical significance (Figure 4.6K). 52 w.o SR-B1 KO mice maintained on a normal chow diet had the lowest levels of $CD4^+$ T-cells, $CD8^+$ T-cells, total T-cells, B-cells, NK cells and NKT-cells, but did not reach statistical significance compared to 52 w.o HFCC diet-fed SR-B1 KO mice. Overall, advanced age appears to be associated with changes in circulating immune cells in HFCC-diet fed SR-B1 KO mice.

Figure 4.6 – Flow Cytometry Analysis on Blood Immune Cells in HFCC Diet-Fed C57BL/6J and SR-B1 KO Mice and Normal Chow-Fed SR-B1 KO Mice. (A) Blood neutrophils. (B) Blood Ly6C^{lo} monocytes. (C) Blood Ly6C^{mid} monocytes. (D) Blood Ly6C^{hi} monocytes. (E) Blood monocytes. (F) Blood CD4^{+} T-cells. (G) Blood CD8^{+} T-cells. (H) Blood T-cells. (I) Blood B-cells. (J) Blood natural killer (NK) cells. (K) Blood natural killer T (NKT) cells. N= 7, 7, 4, 10, 7 for all flow cytometry analyses. Blood was collected into a heparinized tube via cheek puncture using a lancet. Flow cytometry was performed on a BD FACSCalibur Flow Cytometry system, and data were analyzed using FlowJo v10. Each data point represents an individual mouse. Bars represent means and error bars represent standard errors of the mean. All data were analyzed by one-way ANOVA and Tukey's post-hoc test. *P <0.05, **P <0.01, ****P <0.0001.

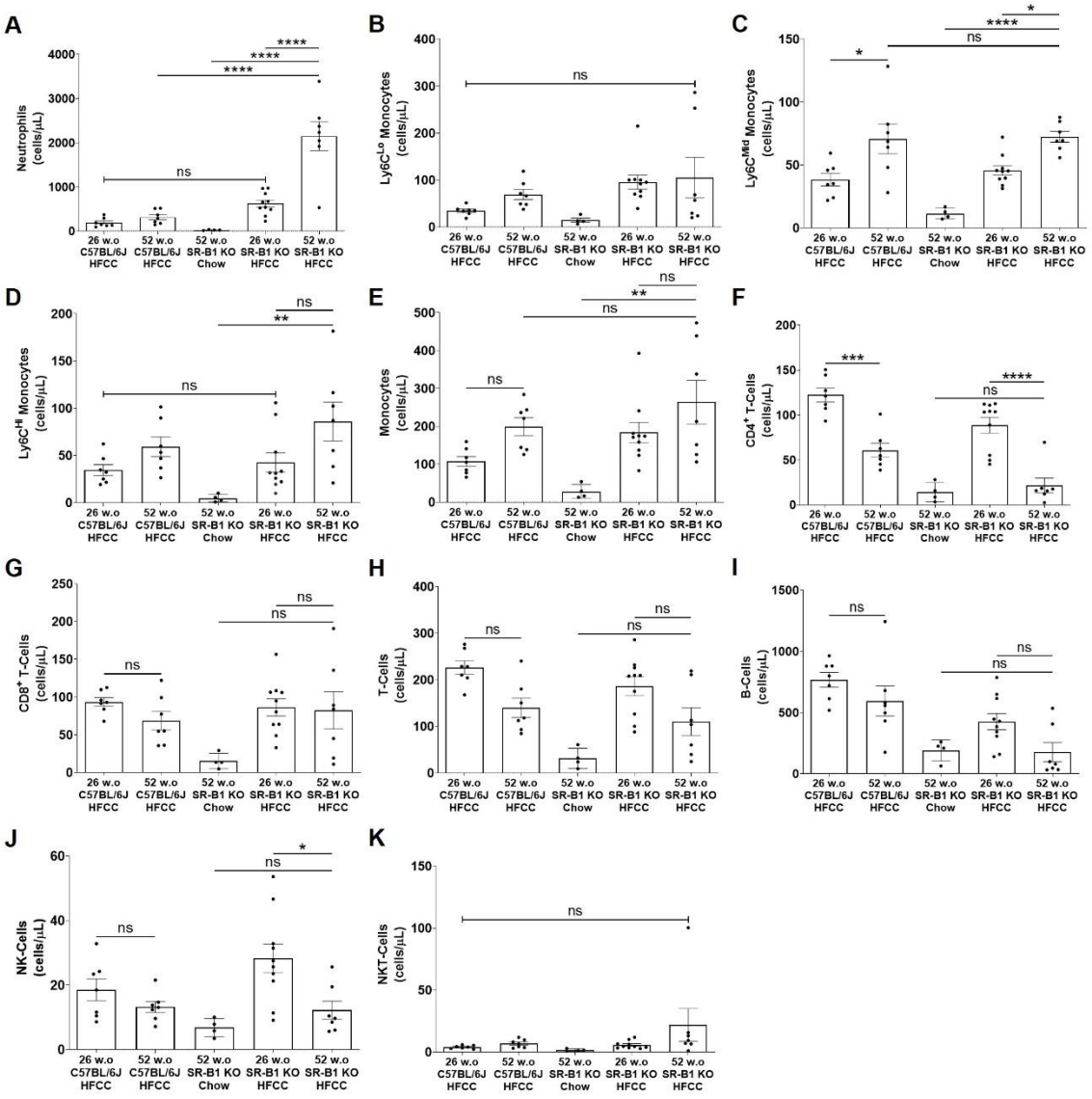
A
Neutrophils (cells/µL)
B
Ly6C^Lo Monocytes (cells/µL)
C
Ly6C^Mid Monocytes (cells/µL)
D
Ly6C^Hi Monocytes (cells/µL)
E
Monocytes (cells/µL)
F
CD4+ T-Cells (cells/µL)
G
CD8+ T-Cells (cells/µL)
H
T-Cells (cells/µL)
I
B-Cells (cells/µL)
J
NK-Cells (cells/µL)
K
NKT-Cells (cells/µL)
26 w.o C57BL/6J HFCC
52 w.o C57BL/6J HFCC
52 w.o SR-B1 KO Chow
26 w.o SR-B1 KO HFCC
52 w.o SR-B1 KO HFCC
ns

4.5 Discussion

Previous studies on the effects of age on atherosclerosis in mouse models have been difficult to interpret because they either used C57BL/6J mice which are resistant to atherosclerosis and only develop early stage fatty streaks when fed a potent atherogenic diet[28], making it difficult to draw conclusions related to development of advanced plaques; or because they have utilized ApoE KO or LDLR KO mice, both of which have been shown to develop atherosclerosis spontaneously with age[10,11,14,15], making it difficult to separate the effects of age on susceptibility to atherosclerosis from the increased time over which plaques develop. Furthermore, these studies used mouse models that develop atherosclerosis in the aortic sinus and did not analyze coronary arteries or outcomes of CAD, namely myocardial fibrosis. In contrast, SR-B1 KO mice fed a normal chow diet do not develop much detectable atherosclerosis in either the aortic sinus or coronary arteries, even at 52 weeks of age, but do develop atherosclerosis in both sites when fed an HFCC diet, making them a good model to test the effects of advanced age on susceptibility to diet-induced atherosclerosis in both the aortic sinus and coronary arteries.

Surprisingly, we found that HFCC diet feeding triggered the same degree of atherosclerosis development in the aortic sinus in young (26 w.o) and older (52 w.o) SR-B1 KO mice, but triggered increased coronary artery atherosclerosis in the older mice. This increase in coronary artery atherosclerosis in older HFCC diet-fed SR-B1 KO mice was associated with increased platelet accumulation in

atherosclerotic coronary arteries, increased myocardial fibrosis and damage, and reduced survival. Our data suggest that the increased susceptibility to diet-induced CAD among older SR-B1 KO mice was not driven by age-dependent changes in plasma lipid levels. Instead, advanced age in HFCC diet-fed SR-B1 KO mice appears to increase cellular and systemic inflammation and increase VCAM-1 levels in coronary arteries. The increased inflammation and VCAM-1 levels in coronary arteries coupled with increased circulating neutrophils and a trend towards increased circulating monocytes likely resulted in increased leukocyte recruitment into the coronary arteries, which likely explain the age-dependent increase in coronary artery atherosclerosis and subsequent myocardial fibrosis and damage and reduced survival in HFCC diet-fed SR-B1 KO mice. Moreover, the increased platelet accumulation in atherosclerotic coronary arteries in older-aged vs. younger-aged HFCC diet-fed SR-B1 KO mice suggest the possibility of increased plaque rupture or erosion and subsequent thrombosis. This may also contribute to the increased myocardial fibrosis and damage and reduced survival seen in the older-aged HFCC diet-fed SR-B1 KO mice. However, we cannot rule out the possibility that platelets may contribute to increased atherosclerosis with older age in HFCC diet-fed SR-B1 KO mice, since platelets are known to contribute to the initiation and progression of atherosclerosis development[35–38].

In summary, HFCC diet-fed SR-B1 KO mice develop occlusive coronary artery atherosclerosis, platelet accumulation in atherosclerotic coronary arteries, and myocardial fibrosis in an age-dependent manner. Whether age impacts CAD

in other mouse models commonly used to study atherosclerosis such as ApoE KO or LDLR KO mice remains to be determined. Nonetheless, we demonstrate that the SR-B1 KO mouse is a useful mouse model whereby atherosclerosis is diet-inducible, making it possible to clearly evaluate the effects of age on susceptibility to atherosclerosis, rather than a reflection of time over which atherosclerosis develops. Moreover, we show that older-aged HFCC diet-fed SR-B1 KO mice are a mouse model that develops extensive atherosclerosis in both the aortic sinus and coronary arteries, as well as outcomes of CAD, namely myocardial fibrosis and reduced survival. Using this unique mouse model has allowed us to demonstrate that advanced age increases the susceptibility of SR-B1 KO mice to diet-induced coronary artery atherosclerosis, which may be driven by increased inflammation, VCAM-1 protein levels in coronary arteries, and circulating neutrophil levels suggesting the involvement of increased leukocyte recruitment to coronary arteries. Use of these mice for age-related studies may allow for further testing of these concepts and the identification of other age-related factors that contribute to the predisposition of CAD.

4.6 References

1. Ralapanawa U, Sivakanesan R. Epidemiology and the Magnitude of Coronary Artery Disease and Acute Coronary Syndrome: A Narrative Review. *Journal of Epidemiology and Global Health*. 2021;11(2):169–177.

2. Hansson GK, Hermansson A. The immune system in atherosclerosis. *Nature Immunology*. 2011;12(3):204–212.

3. Galkina E, Ley K. Vascular adhesion molecules in atherosclerosis. *Arteriosclerosis, Thrombosis, and Vascular Biology*. 2007;27(11):2292–2301.

4. Hajra L, Evans AI, Chen M, Hyduk SJ, Collins T, Cybulsky MI. The NF-κB signal transduction pathway in aortic endothelial cells is primed for activation in regions predisposed to atherosclerotic lesion formation. *Proceedings of the National Academy of Sciences of the United States of America*. 2000;97(16):9052–9057.

5. Cybulsky MI, Iiyama K, Li H, Zhu S, Chen M, Iiyama M, Davis V, Gutierrez-Ramos JC, Connelly PW, Milstone DS. A major role for VCAM-1, but not ICAM-1, in early atherosclerosis. *Journal of Clinical Investigation*. 2001;107(10):1255–1262.

6. Ley K, Huo Y. VCAM-1 is critical in atherosclerosis. *Journal of Clinical Investigation*. 2001;107(10):1209–1210.

7. Bentzon JF, Otsuka F, Virmani R, Falk E. Mechanisms of plaque formation and rupture. *Circulation Research*. 2014;114(12):1852–1866.

8. Leys D. Atherothrombosis: A major health burden. In: *Cerebrovascular Diseases*.Vol 11.; 2001:1–4.

9. Whitman SC. A Practical Approach to Using Mice in Atherosclerosis Research. *The Clinical Biochemist Reviews*. 2004;25(1):81–93.

10. Zhang SH, Reddick RL, Piedrahita JA, Maeda N. Spontaneous hypercholesterolemia and arterial lesions in mice lacking apolipoprotein E. *Science (New York, N.Y.)*. 1992;258(5081):468–471.
11. Plump AS, Smith JD, Hayek T, Aalto-Setälä K, Walsh A, Verstuyft JG, Rubin EM, Breslow JL. Severe hypercholesterolemia and atherosclerosis in apolipoprotein E-deficient mice created by homologous recombination in ES cells. *Cell*. 1992;71(2):343–353.
12. Ishibashi S, Brown MS, Goldstein JL, Gerard RD, Hammer RE, Herz J. Hypercholesterolemia in low density lipoprotein receptor knockout mice and its reversal by adenovirus-mediated gene delivery. *Journal of Clinical Investigation*. 1993;92(2):883–893.
13. Ishibashi S, Goldstein JL, Brown MS, Herz J, Burns DK. Massive xanthomatosis and atherosclerosis in cholesterol-fed low density lipoprotein receptor-negative mice. *Journal of Clinical Investigation*. 1994;93(5):1885–1893.
14. Moore RE, Kawashiri M, Kitajima K, Secreto A, Millar JS, Pratico D, Rader DJ. Apolipoprotein A-I deficiency results in markedly increased atherosclerosis in mice lacking the LDL receptor. *Arteriosclerosis, Thrombosis, and Vascular Biology*. 2003;23(10):1914–1920.
15. Dorighello GG, Paim BA, Leite ACR, Vercesi AE, Oliveira HCF. Spontaneous experimental atherosclerosis in hypercholesterolemic mice

advances with ageing and correlates with mitochondrial reactive oxygen species. *Experimental Gerontology*. 2018;109:47–50.

16. VanderLaan PA, Reardon CA, Getz GS. Site specificity of atherosclerosis: site-selective responses to atherosclerotic modulators. *Arteriosclerosis, Thrombosis, and Vascular Biology*. 2004;24(1):12–22.
17. Braun A, Trigatti BL, Post MJ, Sato K, Simons M, Edelberg JM, Rosenberg RD, Schrenzel M, Krieger M. Loss of SR-BI expression leads to the early onset of occlusive atherosclerotic coronary artery disease, spontaneous myocardial infarctions, severe cardiac dysfunction, and premature death in apolipoprotein E-deficient mice. *Circulation Research*. 2002;90(3):270–276.
18. Zhang S, Picard MH, Vasile E, Zhu Y, Raffai RL, Weisgraber KH, Krieger M. Diet-induced occlusive coronary atherosclerosis, myocardial infarction, cardiac dysfunction, and premature death in scavenger receptor class B type I-deficient, hypomorphic apolipoprotein ER61 mice. *Circulation*. 2005;111(25):3457–3464.
19. Fuller M, Dadoo O, Serkis V, Abutouk D, MacDonald M, Dhingani N, Macri J, Igdoura SA, Trigatti BL. The effects of diet on occlusive coronary artery atherosclerosis and myocardial infarction in scavenger receptor class B, type 1/low-density lipoprotein receptor double knockout mice. *Arteriosclerosis, Thrombosis, and Vascular Biology*. 2014;34(11):2394–2403.

20. Al-Jarallah A, Trigatti BL. A role for the scavenger receptor, class B type I in high density lipoprotein dependent activation of cellular signaling pathways. *Biochimica Et Biophysica Acta*. 2010;1801(12):1239–1248.

21. Saddar S, Mineo C, Shaul PW. Signaling by the High-Affinity HDL Receptor Scavenger Receptor B Type I. *Arteriosclerosis, Thrombosis, and Vascular Biology*. 2010;30(2):144–150.

22. Trigatti B, Rigotti A, Krieger M. The role of the high-density lipoprotein receptor SR-BI in cholesterol metabolism. *Current Opinion in Lipidology*. 2000;11(2):123–131.

23. Rigotti A, Trigatti BL, Penman M, Rayburn H, Herz J, Krieger M. A targeted mutation in the murine gene encoding the high density lipoprotein (HDL) receptor scavenger receptor class B type I reveals its key role in HDL metabolism. *Proceedings of the National Academy of Sciences of the United States of America*. 1997;94(23):12610–12615.

24. Huby T, Doucet C, Dachet C, Ouzilleau B, Ueda Y, Afzal V, Rubin E, Chapman MJ, Lesnik P. Knockdown expression and hepatic deficiency reveal an atheroprotective role for SR-BI in liver and peripheral tissues. *Journal of Clinical Investigation*. 2006;116(10):2767–2776.

25. Harder C, Lau P, Meng A, Whitman SC, McPherson R. Cholesteryl Ester Transfer Protein (CETP) Expression Protects Against Diet Induced Atherosclerosis in SR-BI Deficient Mice. *Arteriosclerosis, Thrombosis, and Vascular Biology*. 2007;27(4):858–864.

26. Van Eck M, Twisk J, Hoekstra M, Van Rij BT, Van der Lans CAC, Bos IST, Kruijt JK, Kuipers F, Van Berkel TJC. Differential effects of scavenger receptor BI deficiency on lipid metabolism in cells of the arterial wall and in the liver. *The Journal of Biological Chemistry*. 2003;278(26):23699–23705.

27. Hildebrand RB, Lammers B, Meurs I, Korporaal SJA, De Haan W, Zhao Y, Kruijt JK, Praticò D, Schimmel AWM, Holleboom AG, Hoekstra M, Kuivenhoven JA, Van Berkel TJC, Rensen PCN, Van Eck M. Restoration of high-density lipoprotein levels by cholesteryl ester transfer protein expression in scavenger receptor class B type I (SR-BI) knockout mice does not normalize pathologies associated with SR-BI deficiency. *Arteriosclerosis, Thrombosis, and Vascular Biology*. 2010;30(7):1439–1445.

28. Li Y, Gilbert TR, Matsumoto AH, Shi W. Effect of Aging on Fatty Streak Formation in a Diet-Induced Mouse Model of Atherosclerosis. *Journal of vascular research*. 2008;45(3):205–210.

29. Paigen B, Morrow A, Brandon C, Mitchell D, Holmes P. Variation in susceptibility to atherosclerosis among inbred strains of mice. *Atherosclerosis*. 1985;57(1):65–73.

30. Yu P, Xiong T, Tenedero CB, Lebeau P, Ni R, Macdonald ME, Gross PL, Austin RC, Trigatti BL. Rosuvastatin Reduces Aortic Sinus and Coronary Artery Atherosclerosis in SR-B1 (Scavenger Receptor Class B Type 1)/ApoE (Apolipoprotein E) Double Knockout Mice Independently of Plasma

Cholesterol Lowering. *Arteriosclerosis, Thrombosis, and Vascular Biology*. 2018;38(1):26–39.

31. Iiyama K, Hajra L, Iiyama M, Li H, DiChiara M, Medoff BD, Cybulsky MI. Patterns of vascular cell adhesion molecule-1 and intercellular adhesion molecule-1 expression in rabbit and mouse atherosclerotic lesions and at sites predisposed to lesion formation. *Circulation Research*. 1999;85(2):199–207.
32. Matsuzawa N, Takamura T, Kurita S, Misu H, Ota T, Ando H, Yokoyama M, Honda M, Zen Y, Nakanuma Y, Miyamoto K-I, Kaneko S. Lipid-induced oxidative stress causes steatohepatitis in mice fed an atherogenic diet. *Hepatology (Baltimore, Md.)*. 2007;46(5):1392–1403.
33. Recena Aydos L, Aparecida do Amaral L, Serafim de Souza R, Jacobowski AC, Freitas dos Santos E, Rodrigues Macedo ML. Nonalcoholic Fatty Liver Disease Induced by High-Fat Diet in C57bl/6 Models. *Nutrients*. 2019;11(12):3067.
34. Hall P, Cash J. What is the Real Function of the Liver 'Function' Tests? *The Ulster Medical Journal*. 2012;81(1):30–36.
35. Bakogiannis C, Sachse M, Stamatelopoulos K, Stellos K. Platelet-derived chemokines in inflammation and atherosclerosis. *Cytokine*. 2019;122:154157.
36. Gawaz M, Langer H, May AE. Platelets in inflammation and atherogenesis. *The Journal of Clinical Investigation*. 2005;115(12):3378–3384.

37. Zernecke A, Weber C. Chemokines in atherosclerosis: proceedings resumed. *Arteriosclerosis, Thrombosis, and Vascular Biology*. 2014;34(4):742–750.

38. Massberg S, Brand K, Grüner S, Page S, Müller E, Müller I, Bergmeier W, Richter T, Lorenz M, Konrad I, Nieswandt B, Gawaz M. A critical role of platelet adhesion in the initiation of atherosclerotic lesion formation. *The Journal of Experimental Medicine*. 2002;196(7):887–896.

4.7 Supplementary Materials

Supplementary Figure 4.7 – Soluble VCAM-1 and ICAM-1 Levels in Mice. (A) Soluble VCAM-1. (B) Soluble ICAM-1. Each data point represents an individual mouse. Bars represent means and error bars represent standard errors of the mean. All data were analyzed by one-way ANOVA and Tukey's post-hoc test. **P <0.01, ***P <0.001.

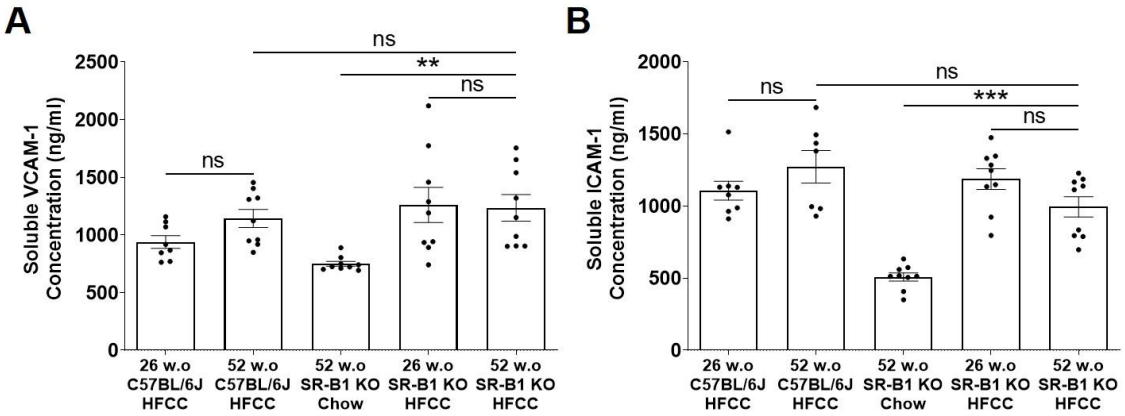

Supplementary Figure 4.8 – Plasma ALT and AST Levels in HFCC Diet-Fed C57BL/6J and SR-B1 KO Mice and Normal Chow-Fed SR-B1 KO Mice. (A) Plasma ALT. (B) Plasma AST. Each data point represents an individual mouse. Bars represent means and error bars represent standard errors of the mean. All data were analyzed by one-way ANOVA and Tukey's post-hoc test. **P <0.01.

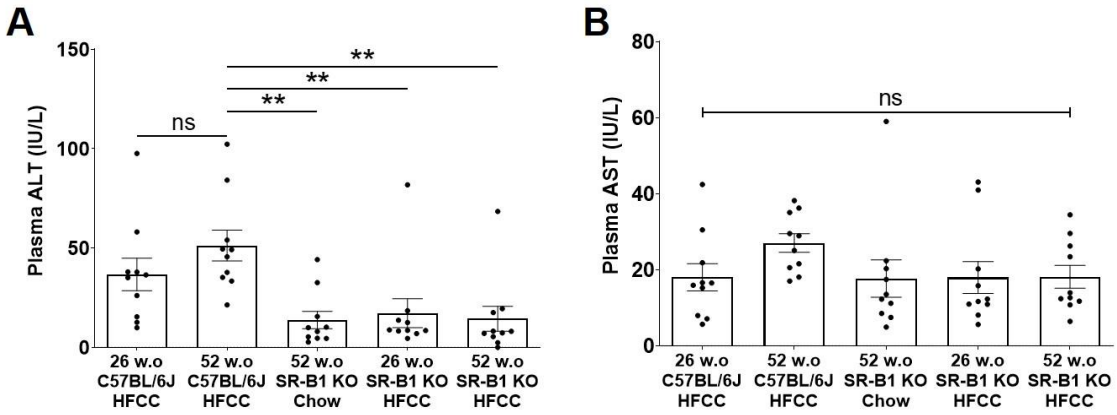

Chapter 5: Discussion

5.1 Summary of Results in Chapters 2-4

The main focus of this thesis is to examine the potential effects of platelet inhibition and aging on CAD development in mice. In chapter 2, the effects of NBEAL2 KO in SR-B1/ApoE DKO mice on CAD were examined. We showed that NBEAL2 deficiency resulted in significantly increased tail bleeding times in mice, consistent with NBEAL2 deficiency inducing thrombocytopenia and platelet dysfunction (Deppermann, Cherpokova, et al., 2013; Guerrero et al., 2014; Kahr et al., 2013). NBEAL2 deficiency in SR-B1/ApoE DKO mice increased plasma total and free cholesterol and PCSK9 levels, independent of hepatic expression levels of PCSK9, SREBP2, LDLR, and HMG-CoAR genes. However, NBEAL2 KO reduced aortic sinus and coronary artery atherosclerosis and platelet accumulation in atherosclerotic coronary arteries in SR-B1/ApoE DKO mice. Despite the reduction in atherosclerosis levels, NBEAL2/SR-B1/ApoE TKO mice exhibited increased myocardial fibrosis levels, which may in part explain the reduced survival compared to SR-B1/ApoE DKO mice. NBEAL2 deficiency in SR-B1/ApoE DKO mice increased circulating neutrophil levels and reduced neutrophil granularity. Moreover, there was a reduction in MPO-positive neutrophils in the myocardium of NBEAL2/SR-B1/ApoE TKO mice compared to SR-B1/ApoE DKO mice. Together, this study suggests that although NBEAL2 deficiency appears to protect against aortic sinus and coronary artery atherosclerosis in mice, whole-body deficiency of

NBEAL2 exerts other effects that worsen myocardial fibrosis and lead to reduced survival.

In chapter 3, we examined the effects of pharmacologically inhibiting PAR4 using a novel pepducin (RAG8) on CAD in HFCC diet-fed SR-B1/LDLR DKO mice. We showed that RAG8-mediated PAR4 inhibition increased tail bleeding times in HFCC diet-fed SR-B1/LDLR DKO mice, consistent with its effects in C57BL/6J mice (Ramachandran et al., 2017). Although RAG8 treatment did not affect aortic sinus atherosclerosis levels, it reduced coronary artery atherosclerosis and myocardial fibrosis, and also reduced VCAM-1 protein levels in non-atherosclerotic coronary arteries and platelet accumulation in atherosclerotic coronary arteries in HFCC diet-fed SR-B1/LDLR DKO mice. These protective effects of RAG8 treatment against CAD development were independent of changes in circulating lipids, cytokines, and immune cells. Overall, RAG8-mediated PAR4 inhibition appears to protect against CAD development in HFCC diet-fed SR-B1/LDLR DKO mice.

In chapter 4, we examined the effects of older age on CAD development in HFCC diet-fed SR-B1 single KO mice. Interestingly, despite having similar levels of aortic sinus atherosclerosis compared to younger-aged HFCC diet-fed SR-B1 KO mice, older-aged HFCC diet-fed SR-B1 KO mice exhibited greater levels of coronary artery atherosclerosis, increased platelet accumulation in atherosclerotic coronary arteries, increased myocardial fibrosis, and reduced survival. The increased susceptibility to diet-induced CAD in older-aged SR-B1 KO mice did not

appear to be driven by age-dependent changes in plasma lipid levels, but rather due to a combination of increased cellular and systemic inflammation and increased VCAM-1 protein levels in coronary arteries. Therefore, older-aged HFCC diet-fed SR-B1 single KO mice develop extensive atherosclerosis in the aortic sinus and coronary arteries along with outcomes of CAD, namely myocardial fibrosis and reduced survival.

5.2 Implications From the Studies Detailed in Chapters 2-4

5.2.1 Role of Platelets in CAD Development

Investigating the role of platelets in CAD development in mice would provide valuable insight since clinically significant cardiac events are typically associated with atherosclerosis and/or thrombosis in coronary arteries. Chapters 2 and 3 of this thesis provide insight into the potential role of platelets in CAD development. Consistent with previous studies (Fuller et al., 2014; Yu et al., 2018), SR-B1/ApoE DKO and HFCC diet-fed SR-B1/LDLR DKO mice in our studies exhibited evidence of platelet accumulation in atherosclerotic coronary arteries. We demonstrated that NBEAL2 KO or PAR4 inhibition in these mouse models, respectively, not only reduced platelet accumulation in atherosclerotic coronary arteries, but reduced coronary artery atherosclerosis. This suggests that NBEAL2 KO and/or PAR4 inhibition may prevent platelets from driving the initiation and progression of coronary artery atherosclerosis development in these mice. Whether the reduced platelet accumulation in atherosclerotic coronary arteries is due to reduced plaque

disruption and subsequent thrombosis, or due to reduced platelet adhesion and accumulation prior to plaque disruption, is unclear.

Interestingly, aspirin treatment in HFCC diet-fed SR-B1 KO/HypoE mice was shown to reduce the number of thrombi and incidence of premature deaths, but did not attenuate coronary artery atherosclerosis development (Hermann et al., 2016). This suggests the likely possibility that NBEAL2 KO and/or PAR4 inhibition are affecting other cell types in addition to platelets such as immune cells and endothelial cells, respectively, that may influence the development of coronary artery atherosclerosis development and/or platelet adhesion and accumulation. Since we showed that NBEAL2 KO had effects on neutrophils in SR-B1/ApoE DKO mice, examining Ly6G (a marker of neutrophils) or CD45 levels (a marker of leukocytes) in plaques may provide valuable information regarding neutrophil and/or leukocyte infiltration. Impaired neutrophil function due to NBEAL2 deficiency might explain the reduced plaque development in both the aortic sinus and coronary arteries in NBEAL2/SR-B1/ApoE TKO mice compared to SR-B1/ApoE DKO mice, since neutrophils contribute to plaque development (Soehnlein, 2012). However, considering the prominent role of NBEAL2 and PAR4 in platelets and the role of platelets in atherosclerosis initiation and progression, it is likely that the effects of NBEAL2 KO and PAR4 inhibition on platelets are, at least in part, directly affecting coronary artery atherosclerosis development, as these interventions resulted in increased tail bleeding times in mice. We also need to consider the possibility that aspirin treatment may not have as profound effects on platelets

compared to NBEAL2 KO and/or PAR4 inhibition, since NBEAL2 KO induces both thrombocytopenia and platelet dysfunction (Deppermann, Cherpokova, et al., 2013; Guerrero et al., 2014; Kahr et al., 2013), while PAR4 is a receptor for thrombin, which is the most potent activator of platelets (Yun et al., 2016). Nonetheless, whether the reduced coronary artery atherosclerosis seen in chapters 2 and 3 are from the effects of NBEAL2 KO and/or PAR4 inhibition on platelets versus other cell types is unclear and requires further investigation.

Interestingly, NBEAL2 KO reduced both aortic sinus and coronary artery atherosclerosis in SR-B1/ApoE DKO mice, whereas RAG8-mediated PAR4 inhibition reduced only coronary artery atherosclerosis in HFCC diet-fed SR-B1/LDLR DKO mice. This suggests the possibility that platelet inhibition alone may not reduce aortic sinus atherosclerosis, and that NBEAL2 inactivation may have other effects such as reduced leukocyte infiltration and/or neutrophil function that allows it to reduce aortic sinus atherosclerosis whereas PAR4 inhibition cannot. However, despite the reduced aortic sinus and coronary artery atherosclerosis, NBEAL2/SR-B1/ApoE TKO mice had increased myocardial fibrosis levels compared to SR-B1/ApoE DKO mice, suggesting that NBEAL2 KO is exerting effects on other cell types, particularly in the heart, that outweigh the benefits to the vasculature. On the other hand, PAR4 inhibition in HFCC diet-fed SR-B1/LDLR DKO mice reduced myocardial fibrosis, and aspirin treatment in HFCC diet-fed SR-B1 KO/HypoE mice delayed and reduced myocardial infarct sizes (Hermann et al., 2016), suggesting that platelet inhibition may have protective effects against

myocardial fibrosis. Overall, our work demonstrated the potential effects of platelet inhibition in reducing platelet accumulation in atherosclerotic coronary arteries and myocardial fibrosis in mice, consistent with previous findings (Hermann et al., 2016), and demonstrated for the first time the potential effects of platelet inhibition in reducing coronary artery atherosclerosis burden in mice.

5.2.2 SR-B1 Single KO Mice as a Versatile Diet-Inducible Mouse Model of Atherosclerosis

Chapter 4 of this thesis demonstrated the versatility of SR-B1 single KO mice as a potentially useful diet-inducible mouse model of aortic sinus and coronary artery atherosclerosis. Although SR-B1 single KO mice have been shown to develop diet-induced aortic sinus atherosclerosis (Harder et al., 2007; Hildebrand et al., 2010; Huby et al., 2006; Van Eck et al., 2003), coronary artery atherosclerosis development in these mice has been less well-studied. We demonstrated in chapter 4 that younger-aged SR-B1 KO mice develop extensive diet-induced aortic sinus atherosclerosis, consistent with published studies (Harder et al., 2007; Hildebrand et al., 2010; Huby et al., 2006; Van Eck et al., 2003). Interestingly, younger-aged HFCC diet-fed SR-B1 KO mice in our study also exhibited significantly greater levels of coronary artery atherosclerosis compared to younger and older-aged HFCC diet-fed C57BL/6J mice. Compared to younger HFCC diet-fed SR-B1 KO mice, older-aged HFCC diet-fed SR-B1 KO mice exhibited extensive coronary artery atherosclerosis, increased VCAM-1 protein

levels in non-atherosclerotic coronary arteries, and increased circulating cytokines and neutrophils, suggesting an increased inflammatory state. Moreover, older-aged SR-B1 KO mice exhibited HFCC diet-induced myocardial fibrosis, reduced survival, and a large proportion of atherosclerotic coronary arteries exhibiting platelet accumulation, making it a potentially useful diet-inducible mouse model of CAD.

We demonstrated that normal chow-fed SR-B1 single KO mice did not develop much detectable atherosclerosis, at least up to 52 weeks of age, suggesting that SR-B1 KO mice do not develop atherosclerosis spontaneously on a normal chow diet. This provides an advantage to using SR-B1 single KO mice when elucidating age-related factors that contribute to atherosclerosis development. This is in contrast to ApoE KO (Plump et al., 1992; Zhang et al., 1992) and LDLR KO mice (Dorighello et al., 2018; Moore et al., 2003) which develop atherosclerosis spontaneously on a normal chow diet, making it difficult to distinguish between the effects of mouse age and the length of time over which atherosclerosis develops. As previously mentioned, aging is an independent risk factor for CAD development in humans, and CAD is more prevalent in older-aged individuals. However, most basic research studies utilize young mice to study atherosclerosis and therefore, do not take into account age-related factors that may contribute to the susceptibility of atherosclerosis development. Chapter 4 of this thesis demonstrated that key factors known to drive atherosclerosis development may be exacerbated by increased age, such as circulating cytokines, immune cells,

and susceptibility to the level of adhesion molecule expression in endothelial cells, particularly in the coronary arteries.

Overall, SR-B1 single KO mice may prove to be a useful, versatile diet-inducible mouse model to study experimental atherosclerosis. Unlike ApoE KO or LDLR KO mice, SR-B1 KO mice possess intact mechanisms for LDL and VLDL clearance from the blood. Moreover, the use of HFCC diet-fed SR-B1 single KO mice may prevent the need to generate DKO mice to study CAD, making it a simpler model to utilize. Aged HFCC diet-fed SR-B1 single KO mice develop extensive atherosclerosis in both the aortic sinus and coronary arteries and therefore, may prove to be a suitable model for testing therapeutic agents such as statins and PCSK9 inhibitors on atherosclerosis development. Moreover, since they also exhibit platelet accumulation in a large proportion of atherosclerotic coronary arteries, they may be useful for testing the effects of platelet inhibition on CAD development. It would be interesting to examine whether extending the age of SR-B1 KO mice past 40 weeks of age prior to HFCC diet feeding would result in more extensive CAD phenotypes. Nonetheless, HFCC diet-fed SR-B1 single KO mice, particularly those of older age, may be a useful mouse model to study experimental atherosclerosis and identify age-related factors that contribute to the predisposition to atherosclerosis.

5.2.3 Importance of Analyzing Atherosclerosis in Multiple Sites

The vast majority of published studies that have utilized mice to study atherosclerosis have only analyzed atherosclerosis at one site, most commonly the aortic root, although many other published studies analyzed atherosclerosis at either the ascending aorta, aortic arch, descending aorta, brachiocephalic arteries, or carotid arteries. However, lesion development at one site is not always reflective of atherogenesis at other sites (Getz, 2000). A number of studies using different interventions in mice have shown site-specific differences in atherosclerosis. For example, probucol reduces aortic arch and descending aorta atherosclerosis (Witting et al., 2000) but increases aortic root atherosclerosis in ApoE KO mice (Witting et al., 2000; Zhang et al., 1997), IL-4-deficient bone marrow transplantation in LDLR KO mice does not affect aortic root atherosclerosis but reduces aortic arch and thoracic aorta atherosclerosis (King et al., 2002), fractalkine (a chemokine) deficiency has mild effects on aortic root atherosclerosis but dramatically reduces brachiocephalic artery atherosclerosis in ApoE KO mice (Teupser et al., 2004), and recombination activating gene deficiency reduces aortic root atherosclerosis but does not affect brachiocephalic artery atherosclerosis in ApoE KO (Reardon et al., 2001) and LDLR KO mice (Reardon et al., 2003). These studies suggest that there are local factors that contribute to atherosclerosis pathogenesis and/or protection at different sites. In humans, regional differences in atherosclerosis in response to different risk factors was exemplified by an autopsy-based study. For example, among the subjects analyzed for each respective risk factor, smoking resulted in

increased lesions in the abdominal aorta while not affecting atherosclerosis in the right coronary artery (McGill & McMahan, 1998), whereas elevated serum glycohemoglobin had no significant impact on abdominal aortic atherosclerotic lesions, but was associated with extensive lesions in the right coronary artery (McGill et al., 2000).

The site specificity of atherosclerosis development is further exemplified by chapters 3 and 4 of this thesis. In chapter 3, RAG8 treatment in HFCC diet-fed SR-B1/LDLR DKO mice reduced coronary artery atherosclerosis, but did not affect aortic sinus atherosclerosis levels. On the other hand, chapter 4 demonstrated that older age increased diet-induced coronary artery atherosclerosis in SR-B1 single KO mice, but did not affect aortic sinus atherosclerosis levels. These findings demonstrate the importance of analyzing atherosclerosis in not only the aortic sinus, but also the coronary arteries, especially since the coronary arteries are among the most important sites of atherosclerosis development for clinically significant cardiovascular events in humans (VanderLaan et al., 2004). If we had only analyzed aortic sinus atherosclerosis levels for these studies, we may have concluded that neither RAG8-mediated PAR4 inhibition nor advanced age in the respective mouse groups impacted atherosclerosis.

Although multiple murine studies have observed a correlated reduction or increase between aortic sinus and coronary artery atherosclerosis (Al-Jarallah et al., 2013; Gonzalez et al., 2018; Yu et al., 2018), our studies demonstrate that this is not always the case. Therefore, our studies suggest that the factors that trigger

coronary artery atherosclerosis are not necessarily identical to those that trigger aortic sinus atherosclerosis, which calls into question the relevance of a lot of the literature that focused only on atherosclerosis in the aortic sinus. For example, one study observed similar levels of aortic sinus atherosclerosis between high-fat diet-fed PAR4/ApoE DKO mice and control ApoE KO mice, and concluded that thrombin-mediated platelet activation is therefore not required for early development of atherosclerotic plaques in ApoE KO mice (Hamilton et al., 2009). However, we have shown in chapter 3 that PAR4 inhibition via RAG8 treatment reduced coronary artery atherosclerosis in HFCC diet-fed SR-B1/LDLR DKO mice compared to SRQ8-treated mice, despite the two groups exhibiting similar levels of aortic sinus atherosclerosis. One study from our lab also showed a disconnect between the levels of aortic sinus and coronary artery atherosclerosis, where SR-B1/LDLR DKO mice fed a Western-type diet for 12 weeks had more than a 2-fold increase in aortic sinus atherosclerosis levels compared to SR-B1/LDLR DKO mice fed a HFCC diet for 3.5 weeks, but yet had significantly lower levels of coronary artery atherosclerosis (Fuller et al., 2014).

Therefore, this thesis demonstrates the importance of analyzing atherosclerosis in multiple sites and clinically relevant sites – namely the coronary arteries. This is important to do in mice since there is typically limited information on the extent of atherosclerosis in different regions in patients, since patients generally exhibit clinically significant lesions at one specific vascular site and as a result, lesions in other vascular sites are not fully explored (VanderLaan et al.,

2004). The ability to examine multiple vascular sites in mice allows us to obtain more valuable information regarding atherosclerosis development.

5.2.4 Importance of Utilizing Mouse Models that Develop Myocardial Fibrosis for Atherosclerosis Research

Occlusive coronary artery atherosclerosis development typically results in cardiac ischemia and subsequent myocardial fibrosis that can lead to heart failure (Tabas et al., 2015). Therefore, it is intuitive to assume that a reduction in coronary artery atherosclerosis would result in reduced myocardial fibrosis levels. This was the instance in multiple murine studies that analyzed both coronary artery atherosclerosis and myocardial fibrosis when investigating the effects of different interventions and/or elucidating mechanisms driving CAD (Al-Jarallah et al., 2013; Braun et al., 2003; Braun, Yesilaltay, et al., 2008; Fuller et al., 2014; Gonzalez et al., 2018; Karackattu et al., 2006; Yu et al., 2018). However, the relationship between coronary artery atherosclerosis and myocardial fibrosis may not always be straight forward, as exemplified by chapter 2 of this thesis.

We showed that NBEAL2 KO in SR-B1/ApoE DKO mice reduced both aortic sinus and coronary artery atherosclerosis, but counter-intuitively increased myocardial fibrosis, thereby disproving our hypothesis that NBEAL2 KO in SR-B1/ApoE DKO mice would result in reduced myocardial fibrosis levels. As discussed in chapter 2, the increased myocardial fibrosis levels in NBEAL2/SR-B1/ApoE TKO mice compared to SR-B1/ApoE DKO mice despite the reduced

coronary artery atherosclerosis may be due to dysfunctional neutrophils, direct effects from increased circulating PCSK9 levels, or possibly other unanticipated effects on the myocardium caused by NBEAL2 deficiency. Nonetheless, it appears that the myocardium of NBEAL2/SR-B1/ApoE TKO mice are more sensitive to the development of myocardial fibrosis even with reduced coronary artery atherosclerosis levels. Moreover, NBEAL2 deficiency reduced the survival of SR-B1/ApoE DKO mice, despite reducing both aortic sinus and coronary artery atherosclerosis levels, presumably due to the increased myocardial fibrosis. To our knowledge, chapter 2 of this thesis is the first study demonstrating increased myocardial fibrosis despite reduced coronary artery atherosclerosis in mice. Therefore, when examining the effects of interventions on atherosclerosis and/or investigating mechanisms driving CAD development, it may be imperative to examine myocardial fibrosis levels in addition to analyzing atherosclerosis, since there may be unanticipated effects that may prove to be more detrimental.

5.3 Limitations and Future Directions

The primary aims of chapters 2 and 3 were to examine the effects of platelet inhibition via NBEAL2 KO and PAR4 inhibition, respectively, on CAD phenotypes in mice. However, since we utilized mice with whole-body deficiency of NBEAL2 and a PAR4 inhibitor that targets cells in a non-selective manner, it is difficult to interpret how much of our findings are due to the effects of NBEAL2 KO and/or PAR4 inhibition on platelets alone. This adds complexity to our studies, and the

extent to which the effects of NBEAL2 deficiency or PAR4 inhibition in other cell types are contributing to our findings is unclear. For example, NBEAL2 KO has been shown to have effects on multiple hematopoietic cells that are implicated in atherosclerosis development such as neutrophils (Claushuis et al., 2018; Sowerby et al., 2017), monocytes (Claushuis et al., 2018), NK cells (Sowerby et al., 2017), and mast cells (Drube et al., 2017). Moreover, it is possible that NBEAL2 deficiency affects secretory pathways in other cell types that have not yet been elucidated, such as hepatocytes which may result in increased PCSK9 secretion, which in turn may affect myocardial fibrosis levels. PAR4 is also expressed in key blood and vascular cell types other than platelets, such as leukocytes (Vergnolle et al., 2002), endothelial cells (Kataoka et al., 2003), smooth muscle cells (Vidwan et al., 2010), and cardiomyocytes (Kolpakov et al., 2020). Therefore, it is possible that our results reflect contributions of PAR4 inhibition in these cell types. Nonetheless, NBEAL2 and PAR4 both play important roles in platelet function and the common result of their inhibition, reduced coronary artery atherosclerosis development, suggests that their roles in platelets influences CAD development.

Rather than whole-body deficiency, the effects of NBEAL2 and/or PAR4 deficiency can be narrowed down to hematopoietic cells by performing bone marrow transplantation experiments, without affecting their expression in other cell types. In brief, bone marrow from mice deficient in NBEAL2 or PAR4 can be transplanted into mouse models of CAD. Since SR-B1/ApoE DKO mice have a 50% mortality at 6 weeks of age (Braun et al., 2002) and develop spontaneous

atherosclerosis rapidly, utilizing SR-B1/LDLR DKO recipient mice for these experiments would be more suitable. Therefore, future studies can aim to examine the effects of NBEAL2 or PAR4 deficiency in hematopoietic cells on CAD development in mice. This will further elucidate the role of NBEAL2 and/or PAR4 in CAD development. For example, if NBEAL2 deficiency in only hematopoietic cells does not cause increased myocardial fibrosis levels in a mouse model of CAD, then it is likely that the increased fibrosis seen in our NBEAL2/SR-B1/ApoE TKO mice compared to SR-B1/ApoE DKO mice is due to the effects of NBEAL2 deficiency in non-hematopoietic cells. It would also be interesting to examine the effects of treating SR-B1/ApoE DKO and/or SR-B1/LDLR DKO mice with an established anti-thrombotic agent such as $\alpha_{IIb}\beta_3$ inhibitors on CAD phenotypes, since these mice exhibit evidence of platelet accumulation in atherosclerotic coronary arteries. Moreover, since we demonstrated in chapter 4 that aged HFCC diet-fed SR-B1 single KO mice exhibit CAD phenotypes, including platelet accumulation in atherosclerotic coronary arteries, utilizing this mouse model to examine the effects of platelet inhibition on CAD may be a useful approach without having to generate DKO or TKO mice.

A major caveat of chapters 2 and 3 was the utilization of mice that are deficient in SR-B1, particularly since we aimed to examine the effects of platelet inhibition on CAD via NBEAL2 KO and PAR4 inhibition, respectively. SR-B1 single KO mice have been shown to exhibit thrombocytopenia (Dole et al., 2008; Korporaal et al., 2011; Ma et al., 2010; Yu et al., 2018), their platelets appear to

circulate in an activated state (Korporaal et al., 2011; Yu et al., 2018), and exhibit increased susceptibility to experimental $FeCl_3$-induced thrombosis (Korporaal et al., 2011). Thrombocytopenia and increased basal activation of circulating platelets has also been reported in SR-B1/ApoE DKO mice (Yu et al., 2018). Whether these characteristics are seen in SR-B1/LDLR DKO mice have not yet been determined. By utilizing mice deficient in SR-B1, it is difficult to separate the effects of NBEAL2 KO and/or PAR4 inhibition on platelets from the effects due to thrombocytopenia and/or platelet dysfunction that already exist in SR-B1 deficient mice. However, considering that we observed significant increases in tail bleeding times in NBEAL2/SR-B1/ApoE TKO and RAG8-treated SR-B1/LDLR DKO mice compared to SR-B1/ApoE DKO and SRQ8 control-treated SR-B1/LDLR DKO mice, respectively, it is likely that NBEAL2 KO and PAR4 inhibition still exerted effects on platelets. Nonetheless, it would be useful to evaluate platelet counts and platelet activation markers in the mice utilized in chapters 2 and 3 to determine the effects of NBEAL2 KO and PAR4 inhibition directly on platelets. Future studies that seek to examine the effects of platelet inhibition on CAD development in mice should utilize mouse models with normal levels of SR-B1 to avoid the issue of pre-existing platelet abnormalities. Potential mouse models that can be used that develop coronary artery atherosclerosis and myocardial fibrosis are diet-induced PDZK1/ApoE DKO (Yesilaltay et al., 2009) and eNOS/ApoE DKO mice (Kuhlencordt et al., 2001). However, whether these mice exhibit platelet

abnormalities or exhibit platelet accumulation in their coronary arteries have yet to be determined.

Chapter 4 also presents with a couple notable caveats and/or limitations. Female mice generally reach menopause between 9-12 months of age (Brinton, 2012). Estrogen is considered to be protective against atherosclerosis, but the protective effects of estrogen against atherosclerosis in women during menopause is significantly diminished due to lower levels, resulting in a significantly increased risk of cardiovascular disease in menopausal women (Zhao et al., 2018). One study demonstrated that estrogen supplementation in ovariectomized ApoE KO mice (to mimic a post-menopausal state) significantly reduced aortic sinus atherosclerosis levels compared to ovariectomized ApoE KO mice without any supplementation (Meng et al., 2021). Since our study analyzed female mice at 52 weeks of age, it is possible that the mice reached menopause, resulting in reduced estrogen levels and perhaps contributing to the increased atherosclerosis levels seen in 52 w.o HFCC diet-fed SR-B1 KO mice compared to 26 w.o HFCC diet-fed SR-B1 KO mice. Therefore, we cannot rule out the possibility that menopause may be contributing to the worsened CAD phenotypes seen in older-aged HFCC diet-fed SR-B1 KO mice. A PhD candidate in our lab, Ting Xiong, is currently investigating the effects of older age on CAD phenotypes in male HFCC diet-fed SR-B1 KO mice. Another caveat of the study presented in chapter 4 is the 12 week feeding period of the HFCC diet. Cholate is known to have toxic metabolic effects such as inducing gallstone formation and hepatic steatosis that may lead to

cirrhosis, which may be accompanied by other physiological changes that may alter the pathogenesis of atherosclerosis development (Lichtman et al., 1999; Nishina et al., 1990; Tepperman et al., 1964) and therefore, interfere with the interpretation of our study. However, a non-cholate-containing diet that is potent enough to induce coronary artery atherosclerosis and myocardial fibrosis in SR-B1 single KO mice has yet to be demonstrated.

It will be useful for future studies to examine the cardiac function of mouse groups used in this thesis by performing left ventricular pressure-volume loop measurements (Durham et al., 2019). This will provide valuable information such as cardiac output and ejection fraction, and allows the assessment of the extent to which protection or worsening of myocardial fibrosis affects cardiac function. Additionally, future studies can aim to extensively characterize atherosclerotic coronary arteries that have evidence of platelet accumulation. Although mice in this thesis, as well as previous studies (Fuller et al., 2014; Hermann et al., 2016; Yu et al., 2018), exhibited evidence of platelet accumulation in atherosclerotic coronary arteries, it is unclear whether the platelet accumulation is due to thrombosis post-plaque disruption, or whether it precedes plaque rupture and is contributing directly to atherogenesis. This may be addressed by examining the coronary artery plaques for markers of plaque instability such as large necrotic cores, thin fibrous caps, and extracellular proteases such as matrix metalloproteinases, or markers of plaque disruption and thrombosis such as tissue factor and fibrin. Although the small size of coronary arteries and lesions in mice may pose limitations for

extensive analysis, it would be interesting to examine the proportion of coronary arteries that have thrombosis formation. This may help identify which mouse model develops CAD that is most reflective of human CAD and therefore, most suitable for testing interventions against atherothrombosis.

In humans, older age has been associated with alterations in platelet function that may contribute to the increased incidence of CAD (Jones, 2016; Mohebali et al., 2014). Since chapter 4 of this thesis demonstrated that older-aged HFCC diet-fed SR-B1 single KO mice can be used as a novel mouse model of CAD and for age-related studies, it would be interesting to assess the effects of impaired NBEAL2 or PAR4 function in these mice. This will allow us to evaluate the effects of older age on these platelet signaling pathways on CAD development, at least in mice.

5.4 Conclusions

Altogether, the results presented in this thesis demonstrate the potential role of platelets and aging in CAD development in mice. This thesis also demonstrates SR-B1 single KO mice as a potentially useful diet-inducible mouse model that can be utilized to study mechanisms underlying CAD development. Moreover, this thesis highlights the importance of analyzing atherosclerosis in multiple sites as well as myocardial fibrosis when investigating novel pathways/mechanisms involved in CAD development and/or effects of interventions on CAD development in mice. This would provide a more whole and clearer picture, and may prove to be

an effective approach for discovering novel therapeutics to treating atherothrombotic disease in patients.

References

Aarts, C. E. M., Downes, K., Hoogendijk, A. J., Sprenkeler, E. G. G., Gazendam, R. P., Favier, R., Favier, M., Tool, A. T. J., van Hamme, J. L., Kostadima, M. A., Waller, K., Zieger, B., van Bergen, M. G. J. M., Langemeijer, S. M. C., van der Reijden, B. A., Janssen, H., van den Berg, T. K., van Bruggen, R., Meijer, A. B., … Kuijpers, T. W. (2021). Neutrophil specific granule and NETosis defects in gray platelet syndrome. *Blood Advances*, *5*(2), 549–564. https://doi.org/10.1182/bloodadvances.2020002442

Acton, S. L., Scherer, P. E., Lodish, H. F., & Krieger, M. (1994). Expression cloning of SR-BI, a CD36-related class B scavenger receptor. *The Journal of Biological Chemistry*, *269*(33), 21003–21009.

Adams, M. N., Ramachandran, R., Yau, M.-K., Suen, J. Y., Fairlie, D. P., Hollenberg, M. D., & Hooper, J. D. (2011). Structure, function and pathophysiology of protease activated receptors. *Pharmacology & Therapeutics*, *130*(3), 248–282. https://doi.org/10.1016/j.pharmthera.2011.01.003

Albers, C. A., Cvejic, A., Favier, R., Bouwmans, E. E., Alessi, M.-C., Bertone, P., Jordan, G., Kettleborough, R. N., Kiddle, G., Kostadima, M., Read, R. J., Sipos, B., Sivapalaratnam, S., Smethurst, P. A., Stephens, J., Voss, K., Nurden, A., Rendon, A., Nurden, P., & Ouwehand, W. H. (2011). Exome sequencing identifies NBEAL2 as the causative gene for Gray Platelet

Syndrome. *Nature Genetics*, *43*(8), 735–737. https://doi.org/10.1038/ng.885

Al-Jarallah, A., Igdoura, F., Zhang, Y., Tenedero, C. B., White, E. J., MacDonald, M. E., Igdoura, S. A., & Trigatti, B. L. (2013). The effect of pomegranate extract on coronary artery atherosclerosis in SR-BI/APOE double knockout mice. *Atherosclerosis*, *228*(1), 80–89. https://doi.org/10.1016/j.atherosclerosis.2013.02.025

Arai, T., Wang, N., Bezouevski, M., Welch, C., & Tall, A. R. (1999). Decreased atherosclerosis in heterozygous low density lipoprotein receptor-deficient mice expressing the scavenger receptor BI transgene. *The Journal of Biological Chemistry*, *274*(4), 2366–2371. https://doi.org/10.1074/jbc.274.4.2366

Armstrong, S. M., Sugiyama, M. G., Fung, K. Y. Y., Gao, Y., Wang, C., Levy, A. S., Azizi, P., Roufaiel, M., Zhu, S.-N., Neculai, D., Yin, C., Bolz, S.-S., Seidah, N. G., Cybulsky, M. I., Heit, B., & Lee, W. L. (2015). A novel assay uncovers an unexpected role for SR-BI in LDL transcytosis. *Cardiovascular Research*, *108*(2), 268–277. https://doi.org/10.1093/cvr/cvv218

Assmann, G., & Gotto, A. M. (2004). HDL Cholesterol and Protective Factors in Atherosclerosis. *Circulation*, *109*(23_suppl_1), III–8. https://doi.org/10.1161/01.CIR.0000131512.50667.46

Badimon, L., & Vilahur, G. (2014). Thrombosis formation on atherosclerotic lesions and plaque rupture. *Journal of Internal Medicine*, *276*(6), 618–632. https://doi.org/10.1111/joim.12296

Bakogiannis, C., Sachse, M., Stamatelopoulos, K., & Stellos, K. (2019). Platelet-derived chemokines in inflammation and atherosclerosis. *Cytokine*, *122*, 154157. https://doi.org/10.1016/j.cyto.2017.09.013

Bennett, M. R., Sinha, S., & Owens, G. K. (2016). Vascular smooth muscle cells in atherosclerosis. *Circulation Research*, *118*(4), 692–702. https://doi.org/10.1161/CIRCRESAHA.115.306361

Blair, P., & Flaumenhaft, R. (2009). Platelet α–granules: Basic biology and clinical correlates. *Blood Reviews*, *23*(4), 177–189. https://doi.org/10.1016/j.blre.2009.04.001

Bombeli, T., Schwartz, B. R., & Harlan, J. M. (1998). Adhesion of activated platelets to endothelial cells: Evidence for a GPIIbIIIa-dependent bridging mechanism and novel roles for endothelial intercellular adhesion molecule 1 (ICAM-1), alphavbeta3 integrin, and GPIbalpha. *The Journal of Experimental Medicine*, *187*(3), 329–339. https://doi.org/10.1084/jem.187.3.329

Braun, A., Rigotti, A., & Trigatti, B. L. (2008). Myocardial infarction following atherosclerosis in murine models. *Current Drug Targets*, *9*(3), 217–223. https://doi.org/10.2174/138945008783755566

Braun, A., Trigatti, B. L., Post, M. J., Sato, K., Simons, M., Edelberg, J. M., Rosenberg, R. D., Schrenzel, M., & Krieger, M. (2002). Loss of SR-BI Expression Leads to the Early Onset of Occlusive Atherosclerotic Coronary Artery Disease, Spontaneous Myocardial Infarctions, Severe Cardiac Dysfunction, and Premature Death in Apolipoprotein E–Deficient Mice. *Circulation Research*, *90*(3), 270–276. https://doi.org/10.1161/hh0302.104462

Braun, A., Yesilaltay, A., Acton, S., Broschat, K. O., Krul, E. S., Napawan, N., Stagliano, N., & Krieger, M. (2008). Inhibition of intestinal absorption of cholesterol by ezetimibe or bile acids by SC-435 alters lipoprotein metabolism and extends the lifespan of SR-BI/apoE double knockout mice. *Atherosclerosis*, *198*(1), 77–84. https://doi.org/10.1016/j.atherosclerosis.2007.10.012

Braun, A., Zhang, S., Miettinen, H. E., Ebrahim, S., Holm, T. M., Vasile, E., Post, M. J., Yoerger, D. M., Picard, M. H., Krieger, J. L., Andrews, N. C., Simons, M., & Krieger, M. (2003). Probucol prevents early coronary heart disease and death in the high-density lipoprotein receptor SR-BI/apolipoprotein E double knockout mouse. *Proceedings of the National Academy of Sciences of the United States of America*, *100*(12), 7283–7288. https://doi.org/10.1073/pnas.1237725100

Breton-Gorius, J., Vainchenker, W., Nurden, A., Levy-Toledano, S., & Caen, J. (1981). Defective alpha-granule production in megakaryocytes from gray

platelet syndrome: Ultrastructural studies of bone marrow cells and megakaryocytes growing in culture from blood precursors. *The American Journal of Pathology*, *102*(1), 10–19.

Chatzizisis, Y. S., Coskun, A. U., Jonas, M., Edelman, E. R., Feldman, C. L., & Stone, P. H. (2007). Role of Endothelial Shear Stress in the Natural History of Coronary Atherosclerosis and Vascular Remodeling: Molecular, Cellular, and Vascular Behavior. *Journal of the American College of Cardiology*, *49*(25), 2379–2393. https://doi.org/10.1016/j.jacc.2007.02.059

Claushuis, T. A. M., de Stoppelaar, S. F., de Vos, A. F., Grootemaat, A. E., van der Wel, N. N., Roelofs, J. J. T. H., Ware, J., van't Veer, C., & van der Poll, T. (2018). Nbeal2 Deficiency Increases Organ Damage but Does Not Affect Host Defense During Gram-Negative Pneumonia-Derived Sepsis. *Arteriosclerosis, Thrombosis, and Vascular Biology*, *38*(8), 1772–1784. https://doi.org/10.1161/ATVBAHA.118.311332

Coughlin, S. R. (2000). Thrombin signalling and protease-activated receptors. *Nature*, *407*(6801), 258–264. https://doi.org/10.1038/35025229

Coughlin, S. R. (2005). Protease-activated receptors in hemostasis, thrombosis and vascular biology. *Journal of Thrombosis and Haemostasis: JTH*, *3*(8), 1800–1814. https://doi.org/10.1111/j.1538-7836.2005.01377.x

Covey, S. D., Krieger, M., Wang, W., Penman, M., & Trigatti, B. L. (2003). Scavenger Receptor Class B Type I–Mediated Protection Against Atherosclerosis in LDL Receptor–Negative Mice Involves Its Expression in

Bone Marrow–Derived Cells. *Arteriosclerosis, Thrombosis, and Vascular Biology*, *23*(9), 1589–1594. https://doi.org/10.1161/01.ATV.0000083343.19940.A0

Covic, L., Gresser, A. L., Talavera, J., Swift, S., & Kuliopulos, A. (2002). Activation and inhibition of G protein-coupled receptors by cell-penetrating membrane-tethered peptides. *Proceedings of the National Academy of Sciences of the United States of America*, *99*(2), 643–648. https://doi.org/10.1073/pnas.022460899

Covic, L., Misra, M., Badar, J., Singh, C., & Kuliopulos, A. (2002). Pepducin-based intervention of thrombin-receptor signaling and systemic platelet activation. *Nature Medicine*, *8*(10), 1161–1165. https://doi.org/10.1038/nm760

Cramer, E. M., Vainchenker, W., Vinci, G., Guichard, J., & Breton-Gorius, J. (1985). Gray Platelet Syndrome: Immunoelectron Microscopic Localization of Fibrinogen and von Willebrand Factor in Platelets and Megakaryocytes. *Blood*, *66*(6), 1309–1316. https://doi.org/10.1182/blood.V66.6.1309.1309

Crowther, M. A. (2005). Pathogenesis of Atherosclerosis. *Hematology*, *2005*(1), 436–441. https://doi.org/10.1182/asheducation-2005.1.436

Daugherty, A. (2002). Mouse models of atherosclerosis. *The American Journal of the Medical Sciences*, *323*(1), 3–10. https://doi.org/10.1097/00000441-200201000-00002

Davignon, J., & Ganz, P. (2004). Role of Endothelial Dysfunction in Atherosclerosis. *Circulation*, *109*(23_suppl_1), III–27. https://doi.org/10.1161/01.CIR.0000131515.03336.f8

Debreczeni, M. L., Németh, Z., Kajdácsi, E., Farkas, H., & Cervenak, L. (2021). Molecular Dambusters: What Is Behind Hyperpermeability in Bradykinin-Mediated Angioedema? *Clinical Reviews in Allergy & Immunology*, *60*(3), 318–347. https://doi.org/10.1007/s12016-021-08851-8

Denorme, F., Vanhoorelbeke, K., & De Meyer, S. F. (2019). von Willebrand Factor and Platelet Glycoprotein Ib: A Thromboinflammatory Axis in Stroke. *Frontiers in Immunology*, *10*. https://www.frontiersin.org/article/10.3389/fimmu.2019.02884

Deppermann, C., Cherpokova, D., Nurden, P., Schulz, J.-N., Thielmann, I., Kraft, P., Vögtle, T., Kleinschnitz, C., Dütting, S., Krohne, G., Eming, S. A., Nurden, A. T., Eckes, B., Stoll, G., Stegner, D., & Nieswandt, B. (2013). Gray platelet syndrome and defective thrombo-inflammation in Nbeal2-deficient mice. *The Journal of Clinical Investigation*, 69210. https://doi.org/10.1172/JCI69210

Deppermann, C., Nurden, P., Nurden, A. T., Nieswandt, B., & Stegner, D. (2013). The Nbeal2−/− mouse as a model for the gray platelet syndrome. *Rare Diseases*, *1*, e26561. https://doi.org/10.4161/rdis.26561

Brinton, R. D. (2012). Minireview: Translational Animal Models of Human Menopause: Challenges and Emerging Opportunities. *Endocrinology*, *153*(8), 3571–3578. https://doi.org/10.1210/en.2012-1340

Dole, V. S., Matuskova, J., Vasile, E., Yesilaltay, A., Bergmeier, W., Bernimoulin, M., Wagner, D. D., & Krieger, M. (2008). Thrombocytopenia and platelet abnormalities in high-density lipoprotein receptor-deficient mice. *Arteriosclerosis, Thrombosis, and Vascular Biology*, *28*(6), 1111–1116. https://doi.org/10.1161/ATVBAHA.108.162347

Dorighello, G. G., Paim, B. A., Leite, A. C. R., Vercesi, A. E., & Oliveira, H. C. F. (2018). Spontaneous experimental atherosclerosis in hypercholesterolemic mice advances with ageing and correlates with mitochondrial reactive oxygen species. *Experimental Gerontology*, *109*, 47–50. https://doi.org/10.1016/j.exger.2017.02.010

Drouin, A., Favier, R., Massé, J. M., Debili, N., Schmitt, A., Elbim, C., Guichard, J., Adam, M., Gougerot-Pocidalo, M. A., & Cramer, E. M. (2001). Newly recognized cellular abnormalities in the gray platelet syndrome. *Blood*, *98*(5), 1382–1391. https://doi.org/10.1182/blood.v98.5.1382

Drube, S., Grimlowski, R., Deppermann, C., Fröbel, J., Kraft, F., Andreas, N., Stegner, D., Dudeck, J., Weber, F., Rödiger, M., Göpfert, C., Drube, J., Reich, D., Nieswandt, B., Dudeck, A., & Kamradt, T. (2017). The Neurobeachin-like 2 Protein Regulates Mast Cell Homeostasis. *The Journal*

of Immunology, *199*(8), 2948–2957. https://doi.org/10.4049/jimmunol.1700556

Duncan, S. E., Gao, S., Sarhene, M., Coffie, J. W., Linhua, D., Bao, X., Jing, Z., Li, S., Guo, R., Su, J., & Fan, G. (2020). Macrophage Activities in Myocardial Infarction and Heart Failure. *Cardiology Research and Practice*, *2020*, 4375127. https://doi.org/10.1155/2020/4375127

Durham, K. K., Kluck, G., Mak, K. C., Deng, Y. D., & Trigatti, B. L. (2019). Treatment with apolipoprotein A1 protects mice against doxorubicin-induced cardiotoxicity in a scavenger receptor class B, type I-dependent manner. *American Journal of Physiology. Heart and Circulatory Physiology*, *316*(6), H1447–H1457. https://doi.org/10.1152/ajpheart.00432.2018

Fatkhullina, A. R., Peshkova, I. O., & Koltsova, E. K. (2016). The Role of Cytokines in the Development of Atherosclerosis. *Biochemistry. Biokhimiia*, *81*(11), 1358–1370. https://doi.org/10.1134/S0006297916110134

French, S. L., & Hamilton, J. R. (2016). Protease-activated receptor 4: From structure to function and back again. *British Journal of Pharmacology*, *173*(20), 2952–2965. https://doi.org/10.1111/bph.13455

Fuller, M., Dadoo, O., Serkis, V., Abutouk, D., MacDonald, M., Dhingani, N., Macri, J., Igdoura, S. A., & Trigatti, B. L. (2014). The Effects of Diet on Occlusive Coronary Artery Atherosclerosis and Myocardial Infarction in Scavenger Receptor Class B, Type 1/Low-Density Lipoprotein Receptor

Double Knockout Mice. *Arteriosclerosis, Thrombosis, and Vascular Biology*, *34*(11), 2394–2403. https://doi.org/10.1161/ATVBAHA.114.304200

Galkina, E., & Ley, K. (2007). Vascular adhesion molecules in atherosclerosis. *Arteriosclerosis, Thrombosis, and Vascular Biology*, *27*(11), 2292–2301. https://doi.org/10.1161/ATVBAHA.107.149179

Gawaz, M., Langer, H., & May, A. E. (2005). Platelets in inflammation and atherogenesis. *Journal of Clinical Investigation*, *115*(12), 3378–3384. https://doi.org/10.1172/JCI27196

Gawaz, M., Neumann, F. J., Dickfeld, T., Reininger, A., Adelsberger, H., Gebhardt, A., & Schömig, A. (1997). Vitronectin receptor (alpha(v)beta3) mediates platelet adhesion to the luminal aspect of endothelial cells: Implications for reperfusion in acute myocardial infarction. *Circulation*, *96*(6), 1809–1818. https://doi.org/10.1161/01.cir.96.6.1809

Gerrard, J. M., Phillips, D. R., Rao, G. H., Plow, E. F., Walz, D. A., Ross, R., Harker, L. A., & White, J. G. (1980). Biochemical studies of two patients with the gray platelet syndrome. Selective deficiency of platelet alpha granules. *The Journal of Clinical Investigation*, *66*(1), 102–109. https://doi.org/10.1172/JCI109823

Getz, G. S. (2000). Mouse Model of Unstable Atherosclerotic Plaque? *Arteriosclerosis, Thrombosis, and Vascular Biology*, *20*(12), 2503–2505. https://doi.org/10.1161/01.ATV.20.12.2503

Getz, G. S., & Reardon, C. A. (2012). Animal Models of Atherosclerosis. *Arteriosclerosis, Thrombosis, and Vascular Biology*, *32*(5), 1104–1115. https://doi.org/10.1161/ATVBAHA.111.237693

Glembotsky, A. C., De Luca, G., & Heller, P. G. (2021). A Deep Dive into the Pathology of Gray Platelet Syndrome: New Insights on Immune Dysregulation. *Journal of Blood Medicine*, *12*, 719–732. https://doi.org/10.2147/JBM.S270018

Gonzalez, L., MacDonald, M. E., Deng, Y. D., & Trigatti, B. L. (2018). Hyperglycemia Aggravates Diet-Induced Coronary Artery Disease and Myocardial Infarction in SR-B1-Knockout/ApoE-Hypomorphic Mice. *Frontiers in Physiology*, *9*. https://www.frontiersin.org/article/10.3389/fphys.2018.01398

Gonzalez, L., & Trigatti, B. (2016). Mouse Models of Coronary Artery Atherosclerosis. *Journal of Cardiovascular Disorders*, *3*(1), 10.

Grimsey, N. J., & Trejo, J. (2016). Integration of Endothelial Protease-activated Receptor-1 Inflammatory Signaling by Ubiquitin. *Current Opinion in Hematology*, *23*(3), 274–279. https://doi.org/10.1097/MOH.0000000000000232

Guerrero, J. A., Bennett, C., van der Weyden, L., McKinney, H., Chin, M., Nurden, P., McIntyre, Z., Cambridge, E. L., Estabel, J., Wardle-Jones, H., Speak, A. O., Erber, W. N., Rendon, A., Ouwehand, W. H., & Ghevaert, C. (2014). Gray platelet syndrome: Proinflammatory megakaryocytes and α-

granule loss cause myelofibrosis and confer metastasis resistance in mice. *Blood*, *124*(24), 3624–3635. https://doi.org/10.1182/blood-2014-04-566760

Gunay-Aygun, M., Falik-Zaccai, T. C., Vilboux, T., Zivony-Elboum, Y., Gumruk, F., Cetin, M., Khayat, M., Boerkoel, C. F., Kfir, N., Huang, Y., Maynard, D., Dorward, H., Berger, K., Kleta, R., Anikster, Y., Arat, M., Freiberg, A. S., Kehrel, B. E., Jurk, K., … Gahl, W. A. (2011). NBEAL2 is mutated in Gray Platelet Syndrome and is required for biogenesis of platelet alpha-granules. *Nature Genetics*, *43*(8), 732–734. https://doi.org/10.1038/ng.883

Hajar, R. (2017). Risk Factors for Coronary Artery Disease: Historical Perspectives. *Heart Views : The Official Journal of the Gulf Heart Association*, *18*(3), 109–114. https://doi.org/10.4103/HEARTVIEWS.HEARTVIEWS_106_17

Hamilton, J. R., Cornelissen, I., & Coughlin, S. R. (2004). Impaired hemostasis and protection against thrombosis in protease-activated receptor 4-deficient mice is due to lack of thrombin signaling in platelets. *Journal of Thrombosis and Haemostasis: JTH*, *2*(8), 1429–1435. https://doi.org/10.1111/j.1538-7836.2004.00783.x

Hamilton, J. R., Cornelissen, I., Mountford, J. K., & Coughlin, S. R. (2009). Atherosclerosis proceeds independently of thrombin-induced platelet activation in ApoE-/- mice. *Atherosclerosis*, *205*(2), 427–432. https://doi.org/10.1016/j.atherosclerosis.2009.01.018

Hamilton, J. R., Frauman, A. G., & Cocks, T. M. (2001). Increased expression of protease-activated receptor-2 (PAR2) and PAR4 in human coronary artery by inflammatory stimuli unveils endothelium-dependent relaxations to PAR2 and PAR4 agonists. *Circulation Research*, *89*(1), 92–98. https://doi.org/10.1161/hh1301.092661

Hansson, G. K., & Hermansson, A. (2011). The immune system in atherosclerosis. *Nature Immunology*, *12*(3), 204–212. https://doi.org/10.1038/ni.2001

Hansson, G. K., & Libby, P. (2006). The immune response in atherosclerosis: A double-edged sword. *Nature Reviews Immunology*, *6*(7), 508–519. https://doi.org/10.1038/nri1882

Harder, C., Lau, P., Meng, A., Whitman, S. C., & McPherson, R. (2007). Cholesteryl Ester Transfer Protein (CETP) Expression Protects Against Diet Induced Atherosclerosis in SR-BI Deficient Mice. *Arteriosclerosis, Thrombosis, and Vascular Biology*, *27*(4), 858–864. https://doi.org/10.1161/01.ATV.0000259357.42089.dc

Head, T., Daunert, S., & Goldschmidt-Clermont, P. J. (2017). The Aging Risk and Atherosclerosis: A Fresh Look at Arterial Homeostasis. *Frontiers in Genetics*, *8*, 216. https://doi.org/10.3389/fgene.2017.00216

Heestermans, M., Naudin, C., Mailer, R. K., Konrath, S., Klaetschke, K., Jämsä, A., Frye, M., Deppermann, C., Pula, G., Kuta, P., Friese, M. A., Gelderblom, M., Sickmann, A., Preston, R. J. S., Nofer, J.-R., Rose-John,

S., Butler, L. M., Salomon, O., Stavrou, E. X., & Renné, T. (2021). Identification of the factor XII contact activation site enables sensitive coagulation diagnostics. *Nature Communications*, *12*(1), 5596. https://doi.org/10.1038/s41467-021-25888-7

Henn, V., Slupsky, J. R., Gräfe, M., Anagnostopoulos, I., Förster, R., Müller-Berghaus, G., & Kroczek, R. A. (1998). CD40 ligand on activated platelets triggers an inflammatory reaction of endothelial cells. *Nature*, *391*(6667), 591–594. https://doi.org/10.1038/35393

Hermann, S., Kuhlmann, M. T., Starsichova, A., Eligehausen, S., Schäfers, K., Stypmann, J., Tiemann, K., Levkau, B., & Schäfers, M. (2016). Imaging Reveals the Connection Between Spontaneous Coronary Plaque Ruptures, Atherothrombosis, and Myocardial Infarctions in HypoE/SRBI−/− Mice. *Journal of Nuclear Medicine*, *57*(9), 1420–1427. https://doi.org/10.2967/jnumed.115.171132

Heuberger, D. M., & Schuepbach, R. A. (2019). Protease-activated receptors (PARs): Mechanisms of action and potential therapeutic modulators in PAR-driven inflammatory diseases. *Thrombosis Journal*, *17*(1), 4. https://doi.org/10.1186/s12959-019-0194-8

Hildebrand, R. B., Lammers, B., Meurs, I., Korporaal, S. J. A., De Haan, W., Zhao, Y., Kruijt, J. K., Praticò, D., Schimmel, A. W. M., Holleboom, A. G., Hoekstra, M., Kuivenhoven, J. A., Van Berkel, T. J. C., Rensen, P. C. N., & Van Eck, M. (2010). Restoration of high-density lipoprotein levels by

cholesteryl ester transfer protein expression in scavenger receptor class B type I (SR-BI) knockout mice does not normalize pathologies associated with SR-BI deficiency. *Arteriosclerosis, Thrombosis, and Vascular Biology*, *30*(7), 1439–1445. https://doi.org/10.1161/ATVBAHA.110.205153

Hinderer, S., & Schenke-Layland, K. (2019). Cardiac fibrosis – A short review of causes and therapeutic strategies. *Advanced Drug Delivery Reviews*, *146*, 77–82. https://doi.org/10.1016/j.addr.2019.05.011

Huang, L., Chambliss, K. L., Gao, X., Yuhanna, I. S., Behling-Kelly, E., Bergaya, S., Ahmed, M., Michaely, P., Luby-Phelps, K., Darehshouri, A., Xu, L., Fisher, E. A., Ge, W.-P., Mineo, C., & Shaul, P. W. (2019). SR-B1 Drives Endothelial Cell LDL Transcytosis via DOCK4 to Promote Atherosclerosis. *Nature*, *569*(7757), 565–569. https://doi.org/10.1038/s41586-019-1140-4

Huby, T., Doucet, C., Dachet, C., Ouzilleau, B., Ueda, Y., Afzal, V., Rubin, E., Chapman, M. J., & Lesnik, P. (2006). Knockdown expression and hepatic deficiency reveal an atheroprotective role for SR-BI in liver and peripheral tissues. *Journal of Clinical Investigation*, *116*(10), 2767–2776. https://doi.org/10.1172/JCI26893

Huilcaman, R., Venturini, W., Fuenzalida, L., Cayo, A., Segovia, R., Valenzuela, C., Brown, N., & Moore-Carrasco, R. (2022). Platelets, a Key Cell in Inflammation and Atherosclerosis Progression. *Cells*, *11*(6), 1014. https://doi.org/10.3390/cells11061014

Huo, Y., Schober, A., Forlow, S. B., Smith, D. F., Hyman, M. C., Jung, S., Littman, D. R., Weber, C., & Ley, K. (2003). Circulating activated platelets exacerbate atherosclerosis in mice deficient in apolipoprotein E. *Nature Medicine*, *9*(1), 61–67. https://doi.org/10.1038/nm810

Ishibashi, S., Brown, M. S., Goldstein, J. L., Gerard, R. D., Hammer, R. E., & Herz, J. (1993). Hypercholesterolemia in low density lipoprotein receptor knockout mice and its reversal by adenovirus-mediated gene delivery. *Journal of Clinical Investigation*, *92*(2), 883–893. https://www.ncbi.nlm.nih.gov/pmc/articles/PMC294927/

Ishibashi, S., Goldstein, J. L., Brown, M. S., Herz, J., & Burns, D. K. (1994). Massive xanthomatosis and atherosclerosis in cholesterol-fed low density lipoprotein receptor-negative mice. *Journal of Clinical Investigation*, *93*(5), 1885–1893. https://doi.org/10.1172/JCI117179

Jacques, S. L., & Kuliopulos, A. (2003). Protease-activated receptor-4 uses dual prolines and an anionic retention motif for thrombin recognition and cleavage. *The Biochemical Journal*, *376*(Pt 3), 733–740. https://doi.org/10.1042/BJ20030954

Jogl, G., Shen, Y., Gebauer, D., Li, J., Wiegmann, K., Kashkar, H., Krönke, M., & Tong, L. (2002). Crystal structure of the BEACH domain reveals an unusual fold and extensive association with a novel PH domain. *The EMBO Journal*, *21*(18), 4785–4795. https://doi.org/10.1093/emboj/cdf502

Jones, C. I. (2016). Platelet function and ageing. *Mammalian Genome*, *27*, 358–366. https://doi.org/10.1007/s00335-016-9629-8

Kahn, M. L., Zheng, Y.-W., Huang, W., Bigornia, V., Zeng, D., Moff, S., Farese, R. V., Tam, C., & Coughlin, S. R. (1998). A dual thrombin receptor system for platelet activation. *Nature*, *394*(6694), 690–694. https://doi.org/10.1038/29325

Kahr, W. H. A., Hinckley, J., Li, L., Schwertz, H., Christensen, H., Rowley, J. W., Pluthero, F. G., Urban, D., Fabbro, S., Nixon, B., Gadzinski, R., Storck, M., Wang, K., Ryu, G.-Y., Jobe, S. M., Schutte, B. C., Moseley, J., Loughran, N. B., Parkinson, J., … Di Paola, J. (2011). Mutations in NBEAL2, encoding a BEACH protein, cause gray platelet syndrome. *Nature Genetics*, *43*(8), 738–740. https://doi.org/10.1038/ng.884

Kahr, W. H. A., Lo, R. W., Li, L., Pluthero, F. G., Christensen, H., Ni, R., Vaezzadeh, N., Hawkins, C. E., Weyrich, A. S., Di Paola, J., Landolt-Marticorena, C., & Gross, P. L. (2013). Abnormal megakaryocyte development and platelet function in Nbeal2−/− mice. *Blood*, *122*(19), 3349–3358. https://doi.org/10.1182/blood-2013-04-499491

Karackattu, S. L., Trigatti, B., & Krieger, M. (2006). Hepatic Lipase Deficiency Delays Atherosclerosis, Myocardial Infarction, and Cardiac Dysfunction and Extends Lifespan in SR-BI/Apolipoprotein E Double Knockout Mice. *Arteriosclerosis, Thrombosis, and Vascular Biology*, *26*(3), 548–554. https://doi.org/10.1161/01.ATV.0000202662.63876.02

Kataoka, H., Hamilton, J. R., McKemy, D. D., Camerer, E., Zheng, Y.-W., Cheng, A., Griffin, C., & Coughlin, S. R. (2003). Protease-activated receptors 1 and 4 mediate thrombin signaling in endothelial cells. *Blood*, *102*(9), 3224–3231. https://doi.org/10.1182/blood-2003-04-1130

King, V. L., Szilvassy, S. J., & Daugherty, A. (2002). Interleukin-4 deficiency decreases atherosclerotic lesion formation in a site-specific manner in female LDL receptor-/- mice. *Arteriosclerosis, Thrombosis, and Vascular Biology*, *22*(3), 456–461. https://doi.org/10.1161/hq0302.104905

Kolpakov, M. A., Guo, X., Rafiq, K., Vlasenko, L., Hooshdaran, B., Seqqat, R., Wang, T., Fan, X., Tilley, D. G., Kostyak, J. C., Kunapuli, S. P., Houser, S. R., & Sabri, A. (2020). Loss of Protease-Activated Receptor 4 Prevents Inflammation Resolution and Predisposes the Heart to Cardiac Rupture After Myocardial Infarction. *Circulation*, *142*(8), 758–775. https://doi.org/10.1161/CIRCULATIONAHA.119.044340

Kolpakov, M. A., Rafiq, K., Guo, X., Hooshdaran, B., Wang, T., Vlasenko, L., Bashkirova, Y. V., Zhang, X., Chen, X., Iftikhar, S., Libonati, J. R., Kunapuli, S. P., & Sabri, A. (2016). Protease-activated receptor 4 deficiency offers cardioprotection after acute ischemia reperfusion injury. *Journal of Molecular and Cellular Cardiology*, *90*, 21–29. https://doi.org/10.1016/j.yjmcc.2015.11.030

Korporaal, S. J. A., Meurs, I., Hauer, A. D., Hildebrand, R. B., Hoekstra, M., Cate, H. T., Praticò, D., Akkerman, J.-W. N., Van Berkel, T. J. C., Kuiper, J., &

Van Eck, M. (2011). Deletion of the high-density lipoprotein receptor scavenger receptor BI in mice modulates thrombosis susceptibility and indirectly affects platelet function by elevation of plasma free cholesterol. *Arteriosclerosis, Thrombosis, and Vascular Biology*, *31*(1), 34–42. https://doi.org/10.1161/ATVBAHA.110.210252

Kozarsky, K. F., Donahee, M. H., Rigotti, A., Iqbal, S. N., Edelman, E. R., & Krieger, M. (1997). Overexpression of the HDL receptor SR-BI alters plasma HDL and bile cholesterol levels. *Nature*, *387*(6631), 414–417. https://doi.org/10.1038/387414a0

Krieger, M. (1999). Charting the fate of the “good cholesterol”: Identification and characterization of the high-density lipoprotein receptor SR-BI. *Annual Review of Biochemistry*, *68*, 523–558. https://doi.org/10.1146/annurev.biochem.68.1.523

Krishnaswamy, S. (2013). The Transition of Prothrombin to Thrombin. *Journal of Thrombosis and Haemostasis : JTH*, *11*(0 1), 265–276. https://doi.org/10.1111/jth.12217

Kuhlencordt, P. J., Gyurko, R., Han, F., Scherrer-Crosbie, M., Aretz, T. H., Hajjar, R., Picard, M. H., & Huang, P. L. (2001). Accelerated Atherosclerosis, Aortic Aneurysm Formation, and Ischemic Heart Disease in Apolipoprotein E/Endothelial Nitric Oxide Synthase Double-Knockout Mice. *Circulation*, *104*(4), 448–454. https://doi.org/10.1161/hc2901.091399

Kzhyshkowska, J., Neyen, C., & Gordon, S. (2012). Role of macrophage scavenger receptors in atherosclerosis. *Immunobiology*, *217*(5), 492–502. https://doi.org/10.1016/j.imbio.2012.02.015

Lagace, T. A. (2014). PCSK9 and LDLR degradation: Regulatory mechanisms in circulation and in cells. *Current Opinion in Lipidology*, *25*(5), 387–393. https://doi.org/10.1097/MOL.0000000000000114

Lee, H., Sturgeon, S. A., Jackson, S. P., & Hamilton, J. R. (2012). The contribution of thrombin-induced platelet activation to thrombus growth is diminished under pathological blood shear conditions. *Thrombosis and Haemostasis*, *107*(2), 328–337. https://doi.org/10.1160/TH11-06-0418

Lee, Y. T., Lin, H. Y., Chan, Y. W. F., Li, K. H. C., To, O. T. L., Yan, B. P., Liu, T., Li, G., Wong, W. T., Keung, W., & Tse, G. (2017). Mouse models of atherosclerosis: A historical perspective and recent advances. *Lipids in Health and Disease*, *16*, 12. https://doi.org/10.1186/s12944-016-0402-5

Li, D., D'Angelo, L., Chavez, M., & Woulfe, D. S. (2011). Arrestin-2 Differentially Regulates PAR4 and ADP Receptor Signaling in Platelets. *The Journal of Biological Chemistry*, *286*(5), 3805–3814. https://doi.org/10.1074/jbc.M110.118018

Libby, P. (2002). Inflammation in atherosclerosis. *Nature*, *420*(6917), 868–874. https://doi.org/10.1038/nature01323

Libby, P. (2009). Molecular and cellular mechanisms of the thrombotic complications of atherosclerosis. *Journal of Lipid Research*, *50*(Suppl), S352–S357. https://doi.org/10.1194/jlr.R800099-JLR200

Libby, P., Ridker, P. M., & Hansson, G. K. (2011). Progress and challenges in translating the biology of atherosclerosis. *Nature*, *473*(7347), 317–325. https://doi.org/10.1038/nature10146

Lichtman, A. H., Clinton, S. K., Iiyama, K., Connelly, P. W., Libby, P., & Cybulsky, M. I. (1999). Hyperlipidemia and atherosclerotic lesion development in LDL receptor-deficient mice fed defined semipurified diets with and without cholate. *Arteriosclerosis, Thrombosis, and Vascular Biology*, *19*(8), 1938–1944. https://doi.org/10.1161/01.atv.19.8.1938

Lo, R. W., Li, L., Leung, R., Pluthero, F. G., & Kahr, W. H. A. (2018). NBEAL2 (Neurobeachin-Like 2) Is Required for Retention of Cargo Proteins by α-Granules During Their Production by Megakaryocytes. *Arteriosclerosis, Thrombosis, and Vascular Biology*, *38*(10), 2435–2447. https://doi.org/10.1161/ATVBAHA.118.311270

Luo, X., Lv, Y., Bai, X., Qi, J., Weng, X., Liu, S., Bao, X., Jia, H., & Yu, B. (2021). Plaque Erosion: A Distinctive Pathological Mechanism of Acute Coronary Syndrome. *Frontiers in Cardiovascular Medicine*, *8*. https://www.frontiersin.org/article/10.3389/fcvm.2021.711453

Lusis, A. J. (2000). Atherosclerosis. *Nature*, *407*(6801), 233–241. https://doi.org/10.1038/35025203

Ma, Y. (2021). Role of Neutrophils in Cardiac Injury and Repair Following Myocardial Infarction. *Cells*, *10*(7), 1676. https://doi.org/10.3390/cells10071676

Ma, Y., Ashraf, M. Z., & Podrez, E. A. (2010). Scavenger receptor BI modulates platelet reactivity and thrombosis in dyslipidemia. *Blood*, *116*(11), 1932–1941. https://doi.org/10.1182/blood-2010-02-268508

Madamanchi, N. R., Vendrov, A., & Runge, M. S. (2005). Oxidative Stress and Vascular Disease. *Arteriosclerosis, Thrombosis, and Vascular Biology*, *25*(1), 29–38. https://doi.org/10.1161/01.ATV.0000150649.39934.13

Massberg, S., Brand, K., Grüner, S., Page, S., Müller, E., Müller, I., Bergmeier, W., Richter, T., Lorenz, M., Konrad, I., Nieswandt, B., & Gawaz, M. (2002). A critical role of platelet adhesion in the initiation of atherosclerotic lesion formation. *The Journal of Experimental Medicine*, *196*(7), 887–896. https://doi.org/10.1084/jem.20012044

Maxwell, M. J., Westein, E., Nesbitt, W. S., Giuliano, S., Dopheide, S. M., & Jackson, S. P. (2007). Identification of a 2-stage platelet aggregation process mediating shear-dependent thrombus formation. *Blood*, *109*(2), 566–576. https://doi.org/10.1182/blood-2006-07-028282

Maynard, D. M., Heijnen, H. F. G., Gahl, W. A., & Gunay-Aygun, M. (2010). The Alpha Granule Proteome: Novel Proteins in Normal and Ghost Granules in Gray Platelet Syndrome. *Journal of Thrombosis and Haemostasis : JTH*, *8*(8), 1786–1796. https://doi.org/10.1111/j.1538-7836.2010.03932.x

McGill, H. C., & McMahan, C. A. (1998). Determinants of atherosclerosis in the young. Pathobiological Determinants of Atherosclerosis in Youth (PDAY) Research Group. *The American Journal of Cardiology*, *82*(10B), 30T-36T. https://doi.org/10.1016/s0002-9149(98)00720-6

McGill, H. C., McMahan, C. A., Herderick, E. E., Tracy, R. E., Malcom, G. T., Zieske, A. W., & Strong, J. P. (2000). Effects of Coronary Heart Disease Risk Factors on Atherosclerosis of Selected Regions of the Aorta and Right Coronary Artery. *Arteriosclerosis, Thrombosis, and Vascular Biology*, *20*(3), 836–845. https://doi.org/10.1161/01.ATV.20.3.836

Meng, Q., Li, Y., Ji, T., Chao, Y., Li, J., Fu, Y., Wang, S., Chen, Q., Chen, W., Huang, F., Wang, Y., Zhang, Q., Wang, X., & Bian, H. (2021). Estrogen prevent atherosclerosis by attenuating endothelial cell pyroptosis via activation of estrogen receptor α-mediated autophagy. *Journal of Advanced Research*, *28*, 149–164. https://doi.org/10.1016/j.jare.2020.08.010

Mineo, C., & Shaul, P. W. (2007). Role of High-Density Lipoprotein and Scavenger Receptor B Type I in the Promotion of Endothelial Repair. *Trends in Cardiovascular Medicine*, *17*(5), 156–161. https://doi.org/10.1016/j.tcm.2007.03.005

Mohebali, D., Kaplan, D., Carlisle, M., Supiano, M. A., & Rondina, M. T. (2014). Alterations in Platelet Functions During Aging: Clinical Correlations with Thrombo-Inflammatory Disease in Older Adults. *Journal of the American Geriatrics Society*, *62*(3), 529–535. https://doi.org/10.1111/jgs.12700

Moore, R. E., Kawashiri, M., Kitajima, K., Secreto, A., Millar, J. S., Pratico, D., & Rader, D. J. (2003). Apolipoprotein A-I deficiency results in markedly increased atherosclerosis in mice lacking the LDL receptor. *Arteriosclerosis, Thrombosis, and Vascular Biology*, *23*(10), 1914–1920. https://doi.org/10.1161/01.ATV.0000092328.66882.F5

Mori, K., Suzuki, S., & Sugai, K. (1984). Electron microscopic and functional studies on platelets in gray platelet syndrome. *The Tohoku Journal of Experimental Medicine*, *143*(3), 261–287. https://doi.org/10.1620/tjem.143.261

Nakashima, Y., Plump, A. S., Raines, E. W., Breslow, J. L., & Ross, R. (1994). ApoE-deficient mice develop lesions of all phases of atherosclerosis throughout the arterial tree. *Arteriosclerosis and Thrombosis: A Journal of Vascular Biology*, *14*(1), 133–140. https://doi.org/10.1161/01.atv.14.1.133

Neculai, D., Schwake, M., Ravichandran, M., Zunke, F., Collins, R. F., Peters, J., Neculai, M., Plumb, J., Loppnau, P., Pizarro, J. C., Seitova, A., Trimble, W. S., Saftig, P., Grinstein, S., & Dhe-Paganon, S. (2013). Structure of LIMP-2 provides functional insights with implications for SR-BI and CD36. *Nature*, *504*(7478), 172–176. https://doi.org/10.1038/nature12684

Nishina, P. M., Verstuyft, J., & Paigen, B. (1990). Synthetic low and high fat diets for the study of atherosclerosis in the mouse. *Journal of Lipid Research*, *31*(5), 859–869.

Nurden, A. T., & Nurden, P. (2007). The gray platelet syndrome: Clinical spectrum of the disease. *Blood Reviews*, *21*(1), 21–36. https://doi.org/10.1016/j.blre.2005.12.003

Nurden, A. T., & Nurden, P. (2016). Should any genetic defect affecting α-granules in platelets be classified as gray platelet syndrome? *American Journal of Hematology*, *91*(7), 714–718. https://doi.org/10.1002/ajh.24359

Owens, A. P., Howatt, D. A., Daugherty, A., & Mackman, N. (2014). Abstract 20120: Protease-activated Receptor 4 Deficiency Reduces Atherosclerosis. *Circulation*, *130*(suppl_2), A20120–A20120. https://doi.org/10.1161/circ.130.suppl_2.20120

Owens, A. P., Howatt, D. A., Daugherty, A., & Mackman, N. (2018). Abstract 20120: Protease-activated Receptor 4 Deficiency Reduces Atherosclerosis. *Circulation*, *130*(suppl_2), A20120–A20120. https://doi.org/10.1161/circ.130.suppl_2.20120

Paigen, B., Morrow, A., Brandon, C., Mitchell, D., & Holmes, P. (1985). Variation in susceptibility to atherosclerosis among inbred strains of mice. *Atherosclerosis*, *57*(1), 65–73. https://doi.org/10.1016/0021-9150(85)90138-8

Periayah, M. H., Halim, A. S., & Mat Saad, A. Z. (2017). Mechanism Action of Platelets and Crucial Blood Coagulation Pathways in Hemostasis. *International Journal of Hematology-Oncology and Stem Cell Research*, *11*(4), 319–327. https://www.ncbi.nlm.nih.gov/pmc/articles/PMC5767294/

Phillips, M. C. (2014). Molecular mechanisms of cellular cholesterol efflux. *The Journal of Biological Chemistry*, *289*(35), 24020–24029. https://doi.org/10.1074/jbc.R114.583658

Plump, A. S., Smith, J. D., Hayek, T., Aalto-Setälä, K., Walsh, A., Verstuyft, J. G., Rubin, E. M., & Breslow, J. L. (1992). Severe hypercholesterolemia and atherosclerosis in apolipoprotein E-deficient mice created by homologous recombination in ES cells. *Cell*, *71*(2), 343–353. https://doi.org/10.1016/0092-8674(92)90362-g

PrabhuDas, M. R., Baldwin, C. L., Bollyky, P. L., Bowdish, D. M. E., Drickamer, K., Febbraio, M., Herz, J., Kobzik, L., Krieger, M., Loike, J., McVicker, B., Means, T. K., Moestrup, S. K., Post, S. R., Sawamura, T., Silverstein, S., Speth, R. C., Telfer, J. C., Thiele, G. M., … El Khoury, J. (2017). A Consensus Definitive Classification of Scavenger Receptors and Their Roles in Health and Disease. *Journal of Immunology (Baltimore, Md.: 1950)*, *198*(10), 3775–3789. https://doi.org/10.4049/jimmunol.1700373

Qanbar, R., & Bouvier, M. (2003). Role of palmitoylation/depalmitoylation reactions in G-protein-coupled receptor function. *Pharmacology & Therapeutics*, *97*(1), 1–33. https://doi.org/10.1016/s0163-7258(02)00300-5

Ramachandran, R., Mihara, K., Thibeault, P., Vanderboor, C. M., Petri, B., Saifeddine, M., Bouvier, M., & Hollenberg, M. D. (2017). Targeting a Proteinase-Activated Receptor 4 (PAR4) Carboxyl Terminal Motif to

Regulate Platelet Function. *Molecular Pharmacology*, *91*(4), 287–295. https://doi.org/10.1124/mol.116.106526

Reardon, C. A., Blachowicz, L., Lukens, J., Nissenbaum, M., & Getz, G. S. (2003). Genetic background selectively influences innominate artery atherosclerosis: Immune system deficiency as a probe. *Arteriosclerosis, Thrombosis, and Vascular Biology*, *23*(8), 1449–1454. https://doi.org/10.1161/01.ATV.0000079793.58054.2E

Reardon, C. A., Blachowicz, L., White, T., Cabana, V., Wang, Y., Lukens, J., Bluestone, J., & Getz, G. S. (2001). Effect of immune deficiency on lipoproteins and atherosclerosis in male apolipoprotein E-deficient mice. *Arteriosclerosis, Thrombosis, and Vascular Biology*, *21*(6), 1011–1016. https://doi.org/10.1161/01.atv.21.6.1011

Rendu, F., & Brohard-Bohn, B. (2001). The platelet release reaction: Granules' constituents, secretion and functions. *Platelets*, *12*(5), 261–273. https://doi.org/10.1080/09537100120068170

Rigotti, A., Trigatti, B. L., Penman, M., Rayburn, H., Herz, J., & Krieger, M. (1997). A targeted mutation in the murine gene encoding the high density lipoprotein (HDL) receptor scavenger receptor class B type I reveals its key role in HDL metabolism. *Proceedings of the National Academy of Sciences of the United States of America*, *94*(23), 12610–12615. https://www.ncbi.nlm.nih.gov/pmc/articles/PMC25055/

Rodrigueza, W. V., Thuahnai, S. T., Temel, R. E., Lund-Katz, S., Phillips, M. C., & Williams, D. L. (1999). Mechanism of scavenger receptor class B type I-mediated selective uptake of cholesteryl esters from high density lipoprotein to adrenal cells. *The Journal of Biological Chemistry*, *274*(29), 20344–20350. https://doi.org/10.1074/jbc.274.29.20344

Sambrano, G. R., Weiss, E. J., Zheng, Y.-W., Huang, W., & Coughlin, S. R. (2001). Role of thrombin signalling in platelets in haemostasis and thrombosis. *Nature*, *413*(6851), 74–78. https://doi.org/10.1038/35092573

Sharda, A., & Flaumenhaft, R. (2018). The life cycle of platelet granules. *F1000Research*, *7*, 236. https://doi.org/10.12688/f1000research.13283.1

Shen, W.-J., Azhar, S., & Kraemer, F. B. (2018). SR-B1: A Unique Multifunctional Receptor for Cholesterol Influx and Efflux. *Annual Review of Physiology*, *80*, 95–116. https://doi.org/10.1146/annurev-physiol-021317-121550

Sims, M. C., Mayer, L., Collins, J. H., Bariana, T. K., Megy, K., Lavenu-Bombled, C., Seyres, D., Kollipara, L., Burden, F. S., Greene, D., Lee, D., Rodriguez-Romera, A., Alessi, M.-C., Astle, W. J., Bahou, W. F., Bury, L., Chalmers, E., Da Silva, R., De Candia, E., … Guerrero, J. A. (2020). Novel manifestations of immune dysregulation and granule defects in gray platelet syndrome. *Blood*, *136*(17), 1956–1967. https://doi.org/10.1182/blood.2019004776

Soehnlein, O. (2012). Multiple Roles for Neutrophils in Atherosclerosis. *Circulation Research*, *110*(6), 875–888. https://doi.org/10.1161/CIRCRESAHA.111.257535

Sowerby, J. M., Thomas, D. C., Clare, S., Espéli, M., Guerrero, J. A., Hoenderdos, K., Harcourt, K., Marsden, M., Abdul-Karim, J., Clement, M., Antrobus, R., Umrania, Y., Barton, P. R., Flint, S. M., Juss, J. K., Condliffe, A. M., Lyons, P. A., Humphreys, I. R., Chilvers, E. R., … Smith, K. G. C. (2017). NBEAL2 is required for neutrophil and NK cell function and pathogen defense. *The Journal of Clinical Investigation*, *127*(9), 3521–3526. https://doi.org/10.1172/JCI91684

Tabas, I. (2010). Macrophage death and defective inflammation resolution in atherosclerosis. *Nature Reviews. Immunology*, *10*(1), 36–46. https://doi.org/10.1038/nri2675

Tabas, I., García-Cardeña, G., & Owens, G. K. (2015). Recent insights into the cellular biology of atherosclerosis. *The Journal of Cell Biology*, *209*(1), 13–22. https://doi.org/10.1083/jcb.201412052

Tangirala, R. K., Rubin, E. M., & Palinski, W. (1995). Quantitation of atherosclerosis in murine models: Correlation between lesions in the aortic origin and in the entire aorta, and differences in the extent of lesions between sexes in LDL receptor-deficient and apolipoprotein E-deficient mice. *Journal of Lipid Research*, *36*(11), 2320–2328.

Tepperman, J., Caldwell, F. T., & Tepperman, H. M. (1964). INDUCTION OF GALLSTONES IN MICE BY FEEDING A CHOLESTEROL-CHOLIC ACID CONTAINING DIET. *The American Journal of Physiology*, *206*, 628–634. https://doi.org/10.1152/ajplegacy.1964.206.3.628

Teupser, D., Pavlides, S., Tan, M., Gutierrez-Ramos, J.-C., Kolbeck, R., & Breslow, J. L. (2004). Major reduction of atherosclerosis in fractalkine (CX3CL1)-deficient mice is at the brachiocephalic artery, not the aortic root. *Proceedings of the National Academy of Sciences of the United States of America*, *101*(51), 17795–17800. https://doi.org/10.1073/pnas.0408096101

Trigatti, B. L., & Fuller, M. (2016). HDL signaling and protection against coronary artery atherosclerosis in mice. *Journal of Biomedical Research*, *30*(2), 94–100. https://doi.org/10.7555/JBR.30.20150079

Trigatti, B., Rayburn, H., Viñals, M., Braun, A., Miettinen, H., Penman, M., Hertz, M., Schrenzel, M., Amigo, L., Rigotti, A., & Krieger, M. (1999). Influence of the high density lipoprotein receptor SR-BI on reproductive and cardiovascular pathophysiology. *Proceedings of the National Academy of Sciences of the United States of America*, *96*(16), 9322–9327. https://doi.org/10.1073/pnas.96.16.9322

Tryfonos, A., Green, D. J., & Dawson, E. A. (2019). Effects of Catheterization on Artery Function and Health: When Should Patients Start Exercising Following Their Coronary Intervention? *Sports Medicine (Auckland, N.Z.)*, *49*(3), 397–416. https://doi.org/10.1007/s40279-019-01055-3

Tyrrell, D. J., & Goldstein, D. R. (2021). Ageing and atherosclerosis: Vascular intrinsic and extrinsic factors and potential role of IL-6. *Nature Reviews Cardiology*, *18*(1), 58–68. https://doi.org/10.1038/s41569-020-0431-7

Ueda, Y., Gong, E., Royer, L., Cooper, P. N., Francone, O. L., & Rubin, E. M. (2000). Relationship between expression levels and atherogenesis in scavenger receptor class B, type I transgenics. *The Journal of Biological Chemistry*, *275*(27), 20368–20373. https://doi.org/10.1074/jbc.M000730200

Van Eck, M., Twisk, J., Hoekstra, M., Van Rij, B. T., Van der Lans, C. A. C., Bos, I. S. T., Kruijt, J. K., Kuipers, F., & Van Berkel, T. J. C. (2003). Differential effects of scavenger receptor BI deficiency on lipid metabolism in cells of the arterial wall and in the liver. *The Journal of Biological Chemistry*, *278*(26), 23699–23705. https://doi.org/10.1074/jbc.M211233200

Vandendries, E. R., Hamilton, J. R., Coughlin, S. R., Furie, B., & Furie, B. C. (2007). Par4 is required for platelet thrombus propagation but not fibrin generation in a mouse model of thrombosis. *Proceedings of the National Academy of Sciences of the United States of America*, *104*(1), 288–292. https://doi.org/10.1073/pnas.0610188104

VanderLaan, P. A., Reardon, C. A., & Getz, G. S. (2004). Site Specificity of Atherosclerosis. *Arteriosclerosis, Thrombosis, and Vascular Biology*, *24*(1), 12–22. https://doi.org/10.1161/01.ATV.0000105054.43931.f0

Varga-Szabo, D., Pleines, I., & Nieswandt, B. (2008). Cell adhesion mechanisms in platelets. *Arteriosclerosis, Thrombosis, and Vascular Biology*, *28*(3), 403–412. https://doi.org/10.1161/ATVBAHA.107.150474

Vergnolle, N., Derian, C. K., D'Andrea, M. R., Steinhoff, M., & Andrade-Gordon, P. (2002). Characterization of thrombin-induced leukocyte rolling and adherence: A potential proinflammatory role for proteinase-activated receptor-4. *Journal of Immunology (Baltimore, Md.: 1950)*, *169*(3), 1467–1473. https://doi.org/10.4049/jimmunol.169.3.1467

Vidwan, P., Pathak, A., Sheth, S., Huang, J., Monroe, D. M., & Stouffer, G. A. (2010). Activation of Protease-Activated Receptors 3 and 4 Accelerates Tissue Factor–Induced Thrombin Generation on the Surface of Vascular Smooth Muscle Cells. *Arteriosclerosis, Thrombosis, and Vascular Biology*, *30*(12), 2587–2596. https://doi.org/10.1161/ATVBAHA.110.211177

Vos, D., Kuivenhoven, J. A., & van de Sluis, B. (2018). Recycling the LDL receptor to combat atherosclerosis. *Aging (Albany NY)*, *10*(12), 3638–3640. https://doi.org/10.18632/aging.101681

Wang, J. C., & Bennett, M. (2012). Aging and Atherosclerosis. *Circulation Research*, *111*(2), 245–259. https://doi.org/10.1161/CIRCRESAHA.111.261388

Weber, C., Zernecke, A., & Libby, P. (2008). The multifaceted contributions of leukocyte subsets to atherosclerosis: Lessons from mouse models. *Nature Reviews Immunology*, *8*(10), 802–815. https://doi.org/10.1038/nri2415

Weinberger, T., & Schulz, C. (2015). Myocardial infarction: A critical role of macrophages in cardiac remodeling. *Frontiers in Physiology*, *6*, 107. https://doi.org/10.3389/fphys.2015.00107

Whitman, S. C. (2004). A Practical Approach to Using Mice in Atherosclerosis Research. *The Clinical Biochemist Reviews*, *25*(1), 81–93. https://www.ncbi.nlm.nih.gov/pmc/articles/PMC1853358/

Williams, D. L., de La Llera-Moya, M., Thuahnai, S. T., Lund-Katz, S., Connelly, M. A., Azhar, S., Anantharamaiah, G. M., & Phillips, M. C. (2000). Binding and cross-linking studies show that scavenger receptor BI interacts with multiple sites in apolipoprotein A-I and identify the class A amphipathic alpha-helix as a recognition motif. *The Journal of Biological Chemistry*, *275*(25), 18897–18904. https://doi.org/10.1074/jbc.M002411200

Wilson, S. J., Ismat, F. A., Wang, Z., Cerra, M., Narayan, H., Raftis, J., Gray, T. J., Connell, S., Garonzik, S., Ma, X., Yang, J., & Newby, D. E. (2018). PAR4 (Protease-Activated Receptor 4) Antagonism With BMS-986120 Inhibits Human Ex Vivo Thrombus Formation. *Arteriosclerosis, Thrombosis, and Vascular Biology*, *38*(2), 448–456. https://doi.org/10.1161/ATVBAHA.117.310104

Witting, P. K., Pettersson, K., Letters, J., & Stocker, R. (2000). Site-Specific Antiatherogenic Effect of Probucol in Apolipoprotein E–Deficient Mice. *Arteriosclerosis, Thrombosis, and Vascular Biology*, *20*(8), e26–e33. https://doi.org/10.1161/01.ATV.20.8.e26

Wouters, K., Shiri-Sverdlov, R., van Gorp, P. J., van Bilsen, M., & Hofker, M. H. (2005). Understanding hyperlipidemia and atherosclerosis: Lessons from genetically modified apoe and ldlr mice. *Clinical Chemistry and Laboratory Medicine*, *43*(5), 470–479. https://doi.org/10.1515/CCLM.2005.085

Xu, W., Andersen, H., Whitmore, T. E., Presnell, S. R., Yee, D. P., Ching, A., Gilbert, T., Davie, E. W., & Foster, D. C. (1998). Cloning and characterization of human protease-activated receptor 4. *Proceedings of the National Academy of Sciences of the United States of America*, *95*(12), 6642–6646. https://www.ncbi.nlm.nih.gov/pmc/articles/PMC22580/

Yesilaltay, A., Daniels, K., Pal, R., Krieger, M., & Kocher, O. (2009). Loss of PDZK1 Causes Coronary Artery Occlusion and Myocardial Infarction in Paigen Diet-Fed Apolipoprotein E Deficient Mice. *PLoS ONE*, *4*(12), e8103. https://doi.org/10.1371/journal.pone.0008103

Yu, P., Xiong, T., Tenedero, C. B., Lebeau, P., Ni, R., Macdonald, M. E., Gross, P. L., Austin, R. C., & Trigatti, B. L. (2018). Rosuvastatin Reduces Aortic Sinus and Coronary Artery Atherosclerosis in SR-B1 (Scavenger Receptor Class B Type 1)/ApoE (Apolipoprotein E) Double Knockout Mice Independently of Plasma Cholesterol Lowering. *Arteriosclerosis, Thrombosis, and Vascular Biology*, *38*(1), 26–39. https://doi.org/10.1161/ATVBAHA.117.305140

Yun, S.-H., Sim, E.-H., Goh, R.-Y., Park, J.-I., & Han, J.-Y. (2016). Platelet Activation: The Mechanisms and Potential Biomarkers. *BioMed Research International*, *2016*, 9060143. https://doi.org/10.1155/2016/9060143

Zhang, S. H., Reddick, R. L., Avdievich, E., Surles, L. K., Jones, R. G., Reynolds, J. B., Quarfordt, S. H., & Maeda, N. (1997). Paradoxical enhancement of atherosclerosis by probucol treatment in apolipoprotein E-deficient mice. *The Journal of Clinical Investigation*, *99*(12), 2858–2866. https://doi.org/10.1172/JCI119479

Zhang, S. H., Reddick, R. L., Piedrahita, J. A., & Maeda, N. (1992). Spontaneous hypercholesterolemia and arterial lesions in mice lacking apolipoprotein E. *Science (New York, N.Y.)*, *258*(5081), 468–471. https://doi.org/10.1126/science.1411543

Zhang, S., Picard, M. H., Vasile, E., Zhu, Y., Raffai, R. L., Weisgraber, K. H., & Krieger, M. (2005). Diet-induced occlusive coronary atherosclerosis, myocardial infarction, cardiac dysfunction, and premature death in scavenger receptor class B type I-deficient, hypomorphic apolipoprotein ER61 mice. *Circulation*, *111*(25), 3457–3464. https://doi.org/10.1161/CIRCULATIONAHA.104.523563

Zhao, D., Guallar, E., Ouyang, P., Subramanya, V., Vaidya, D., Ndumele, C. E., Lima, J. A., Allison, M. A., Shah, S. J., Bertoni, A. G., Budoff, M. J., Post, W. S., & Michos, E. D. (2018). Endogenous Sex Hormones and Incident Cardiovascular Disease in Post-Menopausal Women. *Journal of*

the American College of Cardiology, *71*(22), 2555–2566.

https://doi.org/10.1016/j.jacc.2018.01.083